STRUCTURAL AND ENZYMATIC CHARACTERIZATION OF BACTERIAL CELL WALL ENZYMES: FOCUS ON PENICILLIN-BINDING PROTEINS

A DISSERTATION IN

Pharmaceutical Sciences

and Chemistry

Presented to the Faculty of University

of Missouri-Kansas City in partial fulfillment of

the requirements for the degree

DOCTOR OF PHILOSOPHY

by

SUDHEER BOBBA

B. Pharm., Nagarjuna University, 2007

Kansas City, Missouri

2013

STRUCTURAL AND ENZYMATIC CHARACTERIZATION OF BACTERIAL CELL WALL ENZYMES: FOCUS ON PENICILLIN BINDING-PROTEINS

Sudheer Bobba, Candidate for the Doctor of Philosophy Degree

University of Missouri-Kansas City, 2013

ABSTRACT

The research presented in this dissertation was aimed at understanding several structural and biochemical features underlying the bacterial cell wall biosynthetic process using statistical, biochemical and analytical tools. Penicillin-binding proteins (PBPs) are ubiquitous and essential enzymes necessary for cell wall biosynthesis. PBPs are broadly classified as low molecular mass (LMM) and high molecular mass (HMM) based on their molecular weight. Although all PBPs share a set of highly conserved active site residues, different PBPs have different propensities for catalyzing reactions.

To understand the structural differences among PBPs, a global catalytic residue comparison was performed for all the PBPs available in the protein data bank. This dataset was analyzed using univariate and multivariate statistical methods, revealing several interesting relationships such as: (1) Distribution of the dihedral angle for the SXXK-motif Lys side chain was bimodal, and strongly correlated with HMM/transpeptidase vs LMM/hydrolase activity; (2) Distance between the SXXK-motif Lys-NZ atom and the Lys/His-nitrogen atom of the (K/H)T(S)G-motif was highly conserved.

Unlike LMM PBPs, HMM PBPs when purified, give undetectable or weak enzyme activity that has impeded efforts to develop new inhibitors. In the next section of this dissertation, we described a fluorescently detected microtiter plate-based assay for HMM PBPs. Purified PBPs were immobilized onto microtiter plate wells and labeled with biotinylated-ampicillin (Bio–Amp). Treatment of Bio–Amp-labeled PBPs with a streptavidin–horseradish peroxidase conjugate followed by a fluorogenic HRP substrate allowed the detection of PBPs. The HMM PBP assay was extended to penicillin-binding protein 2a, the molecular determinant of high-level β-lactam resistance in methicillin-resistant *Staphylococcus aureus* using Bio-Amp and biotinylated-cephalexin as tagging reagents. This assay was then demonstrated for use in competition assays for screening and characterizing both β-lactam and non β-lactam inhibitors.

The cytoplasmic steps of cell wall biosynthesis involve a series of UDP-linked intermediates whose synthesis is catalyzed by Mur enzymes. The final section of the dissertation deals with developing an LC-MS/MS detection and quantification of UDP-peptidoglycan intermediates in the bacterial cell wall biosynthetic pathway. The assay was validated and then used to quantitate the *in vivo* levels of UDP-intermediates in *S. aureus* treated with different antibiotics acting at various stages of cell wall biosynthesis.

APPROVAL PAGE

The faculty listed below, appointed by the Dean of School of Graduate Studies have examined the dissertation titled "Structural and Enzymatic Characterization of Bacterial Cell Wall Enzymes: Focus on Penicillin-Binding Proteins" presented by Sudheer Bobba, candidate for the Doctor of Philosophy degree, and certify that in their opinion it is worthy of acceptance.

Supervisory Committee

William G. Gutheil, Ph.D., Committee Chair

Department of Pharmaceutical Sciences

Simon H. Friedman, Ph.D.

Department of Pharmaceutical Sciences

Kun Cheng, Ph.D.

Department of Pharmaceutical Sciences

Santosh Kumar, Ph.D.

Department of Pharmacology and Toxicology

Nathan A. Oyler, Ph.D.

Department of Chemistry

CONTENTS

PART II

LIST OF ILLUSTRATIONS

Figure Page

LIST OF TABLES

Table Page

ACKNOWLEDGEMENTS

First, I would like to thank my advisor William Gutheil for his constant support and advice. He has been very patient and helpful in teaching me all the techniques and knowledge. He personally taught many of the experimental techniques. He has been supportive of all my endeavors. During my stay at UMKC, I not only matured as a scientist but also as a person. I also thank my supervisory committee members Drs. Simon Friedman, Kun Cheng, Santosh Kumar, and Nathan Oyler for their help and guidance throughout my thesis work.

I would also like to thank my current and former lab mates Sandeep Putty, Harika Shetty Vemula and Darshan Jamindar for their help in my research. I would like to thank Chaithanya Ponnaluri and his mentor Mridul Mukherji for their help in cloning and expressing GST-PBP2a. I also would like to extend my thanks to Sharon Self, Joyce Johnson, Connie Mahone, and Nancy Hoover and for their constant help with the administrative work. I want to thank Patricia Hovis-French for letting me be a part of the Preparing Future Fellowship program, which has been very helpful in my graduate career. I also heart fully thank our collaborators Drs. Garth Resch (UMKC), Rob Nicholas (UNC), Eric Sauvage, and Paulette Charlier (Université de Liège). I want to extend my gratitude to Joanna Barbara (Xenotech LLC) for her help in analyzing samples by HRMS.

Finally, I would like to express my sincere gratitude to my dad, mom and sister. Without their constant support and encouragement, I would not have completed my degree. They helped me immensely to stay focused during my difficult times. I would like to extend my sincere appreciation towards my long list of friends, especially Suneetha Kambampati for sharing my joys and sorrows and for believing in me all the time.

DEDICATED TO MY LOVING FAMILY

CHAPTER 1

INTRODUCTION AND LITERATURE REVIEW

Peptidoglycan

Bacterial peptidoglycan (murein) is a complex macro-molecular structure that forms the cell wall and protects the bacteria from lysis due to its internal osmatic pressure[1]. It is also responsible for maintaining definite cell shape and is closely involved in cell growth and division. Murein is a complex yet flexible macro-molecular structure that can expand and shrink up to three-fold without rupture[2]. The biosynthesis of peptidoglycan is an intricate and multi-step process that can be divided in to three stages. In Gram-positive bacteria, the first stage involves the formation of UDP-Mur-L-Ala-D-Glu-L-Lys-D-Ala-D-Ala (UDP-Penta) through a series of steps starting from UDP-*N*-acetylglucosamine (UDP-NAG) in cytoplasm. Enzymes MurA to MurF catalyze these reactions. The second stage enzymatic reactions are catalyzed by enzymes MraY and MurG on the inner leaflet of the cell membrane. MraY catalyzes the addition of an undecaprenol-phosphate, a 55-carbond containing compound to UDP-Penta leading to formation of lipid I intermediate. In the later step MurF catalyzes the transfer of *N*-acetylglucosamine (NAM) to lipid I to form β-(1→4) linked NAG-NAM-pentapeptide (lipid II)[3]. The peptide unit, which forms the bridge between two crosslinks of this lipid intermediate can undergo various modifications such as amidation or addition of extra amino acids. The peptidoglycan polymer (lipid II) formed from second stage is trans-located across the membrane and is incorporated into the growing peptidoglycan layer by penicillin-binding proteins (PBPs) (Figure 1)[3,4]. PBPs catalyze the final step of cell wall biosynthesis.

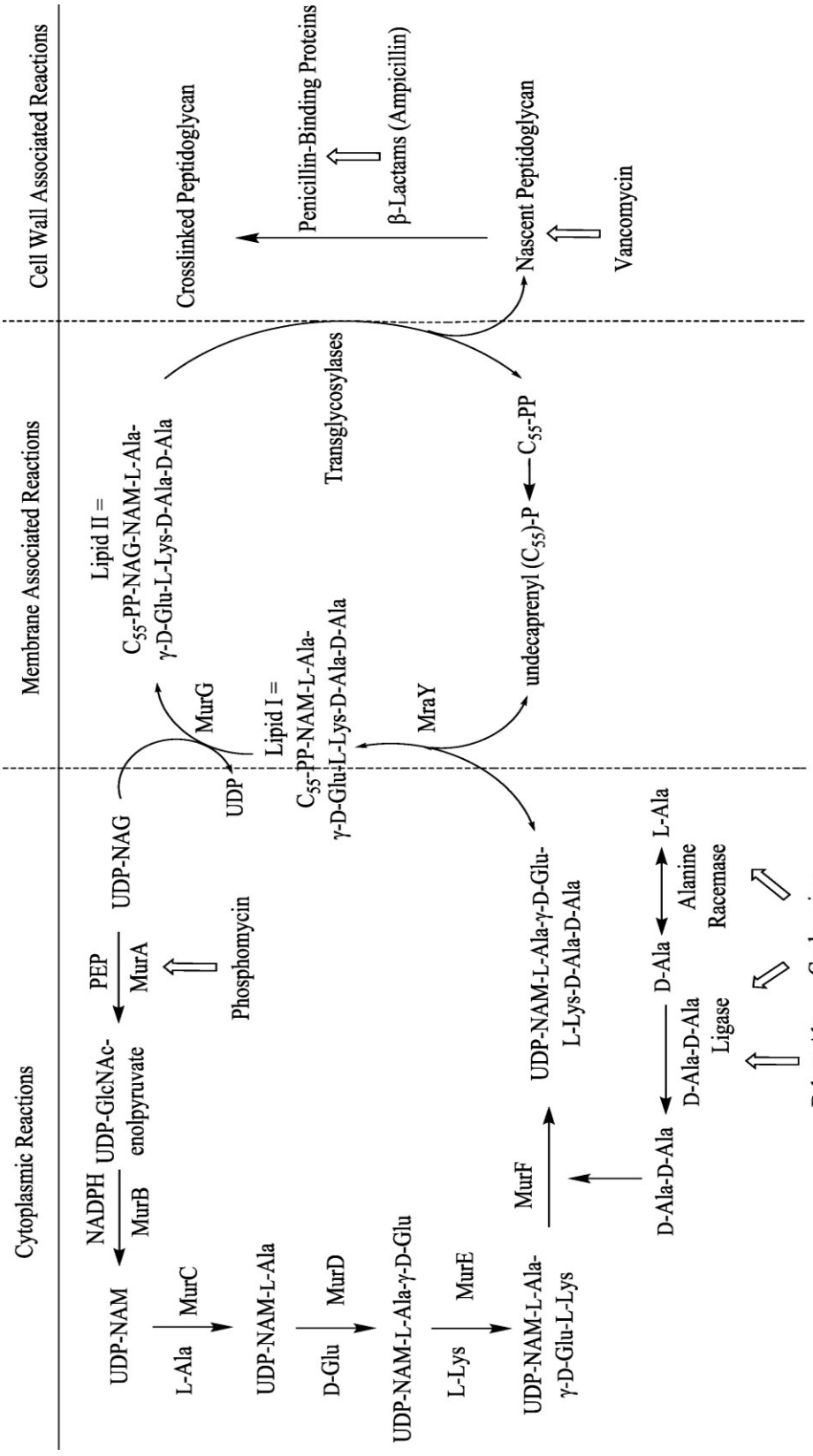

Figure 1: Bacterial cell wall biosynthetic pathway in *S. aureus* showing different antibiotics and their targets.

The peptidoglycan backbone is a chain of two alternating glycan chains interlinked by short peptides[1,5]. The glycan chains are composed of alternating units of *N*-acetylglucosamine (NAG) and *N*-acetylmuramic acid (NAM) connected by β-(1→4) linkage (Figure 2). Two types of enzyme reactions are involved in the polymerization of peptidoglycan, glycosyltransferases that catalyze the formation of the linear glycan chains and transpeptidases that catalyze the formation of peptide cross bridges[5]. The glycan chain synthesis is catalyzed by glycosyltransferase domain of class A high molecular mass penicillin-binding proteins and by non-penicillin-binding monofunctional glycosyltransferases, whereas the peptide cross-linking reaction is catalyzed by transpeptidation domain of penicillin-binding proteins. The carboxy terminal of each NAM is substituted by a stem peptide subunit, which is L-Ala-γ-D-Glu-*meso*-diaminopimelicacid-D-Ala-D-Ala in Gram-negative bacteria or L-Ala-γ-D-Glu-L-Lys-D-Ala-D-Ala in Gram-positive bacteria. As the peptidoglycan matures, it loses one or both of the C-terminal D-Ala residues[5]. A peptide bridge links the adjacent glycan chains together through the stem peptide subunits. The interpeptide bridge usually extends from the ω-amino group of the diamino acid of one peptide subunit to the D-Ala carboxy group of another peptide subunit. The interpeptide bridge can show great variation in their chemical composition from one species to another. For example, in *E. coli* the peptide subunits are directly cross-linked, whereas in *S. aureus* they are connected by a pentaglycine bridge. Variations in the peptide subunit are depicted in Figure 3. The bacterial cell wall biosynthetic pathway being unique to bacteria, is the target for many commercially available antibiotics including phosphomycin, cycloserine, the glycopeptides, and the β-lactams.

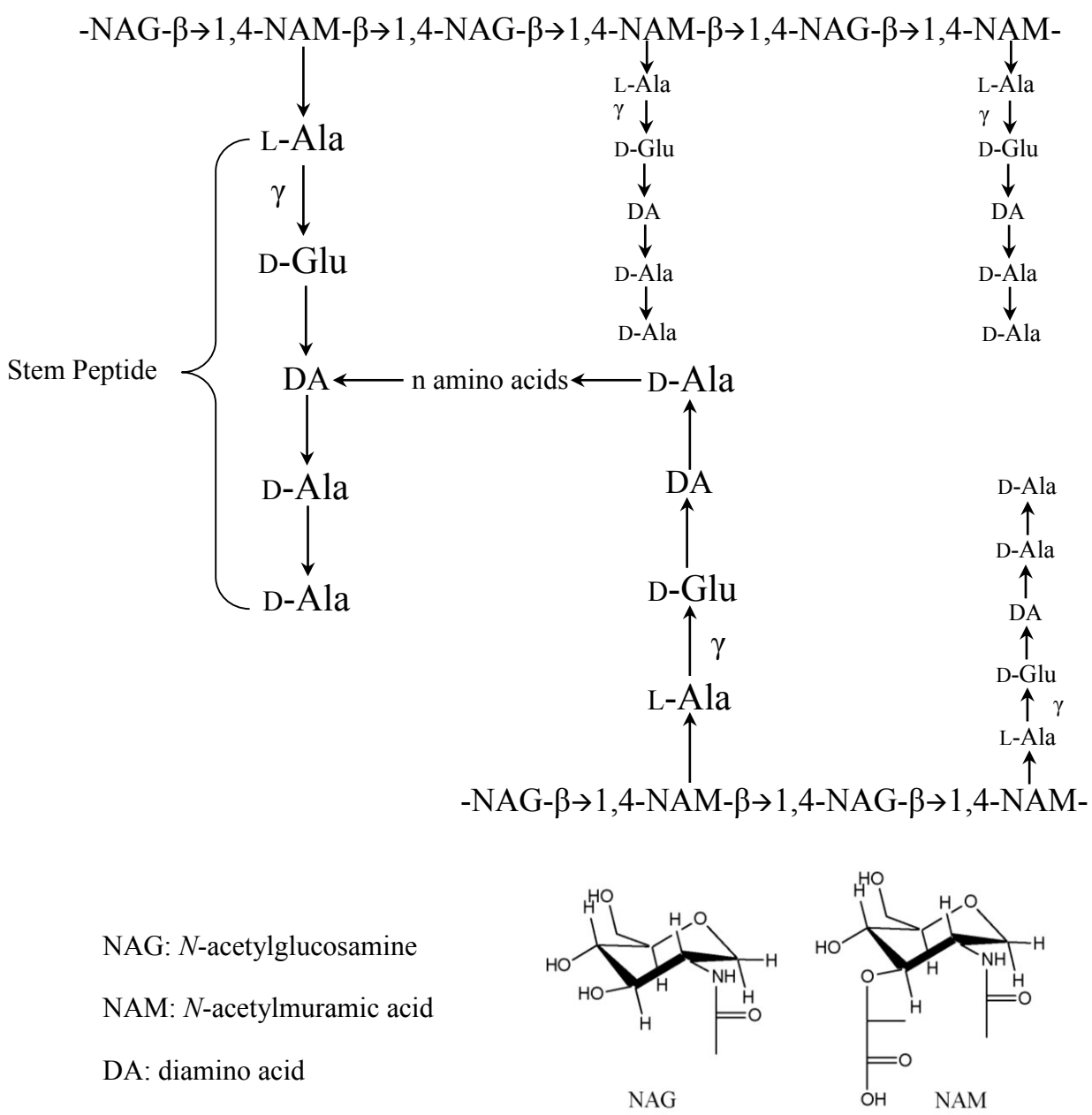

Figure 2: Bacterial peptidoglycan structure showing a representative linkage between glycan strands and the crosslinking stem peptide.

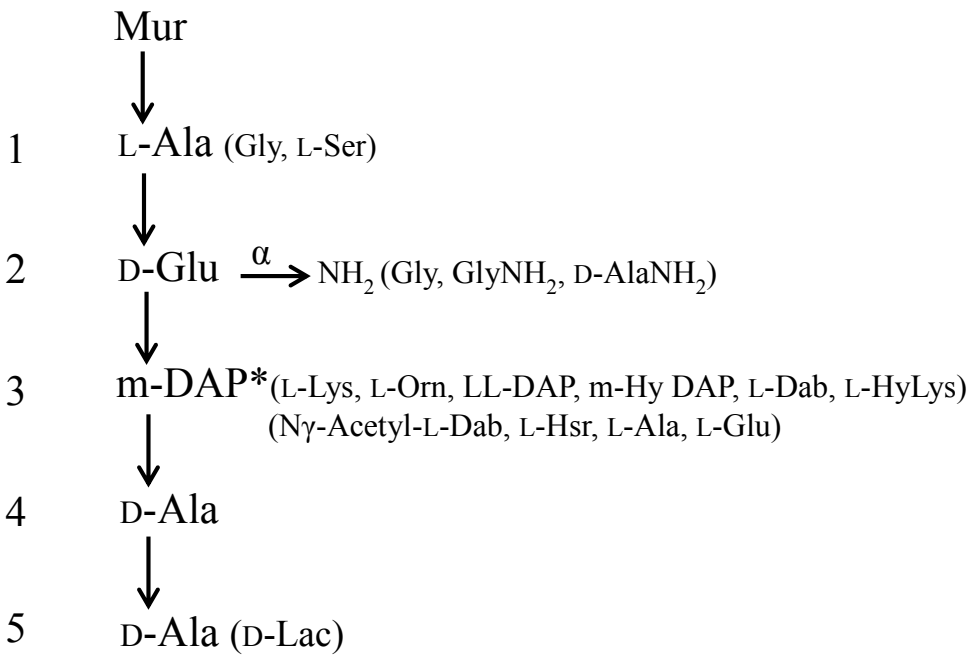

Figure 3: Variations of the peptide subunit found in crosslinking stem peptide of bacterial peptidoglycan. Amino acids in the parentheses may replace the corresponding amino acid. Adapted from Schleifer et.,al 1972.

Abbreviations: m-DAP: *meso*-diaminopimelic acid, Orn: ornithine, m-Hy DAP: *meso*-2, 6-diamino-3-hydroxy-β-pimelic acid, Dab: diaminobutyric acid, HyLys: hydroxy lysine, Hsr: homoserine, Lac: lactate

Penicillin-Binding Proteins

Penicillin-binding proteins (PBPs) are ubiquitous and essential bacterial enzymes necessary for bacteria survival that catalyze the final steps in cell wall biosynthesis[6-9]. As their name implies, PBPs are the targets of β-lactam antibiotics. PBPs modulate the crosslinks important to bacterial cell wall integrity. Each bacterial species has multiple PBPs, which are generally labeled in order of their decreasing molecular mass. An idealized autoradiogram showing different bacterial species with different PBPs is given in Figure 4.

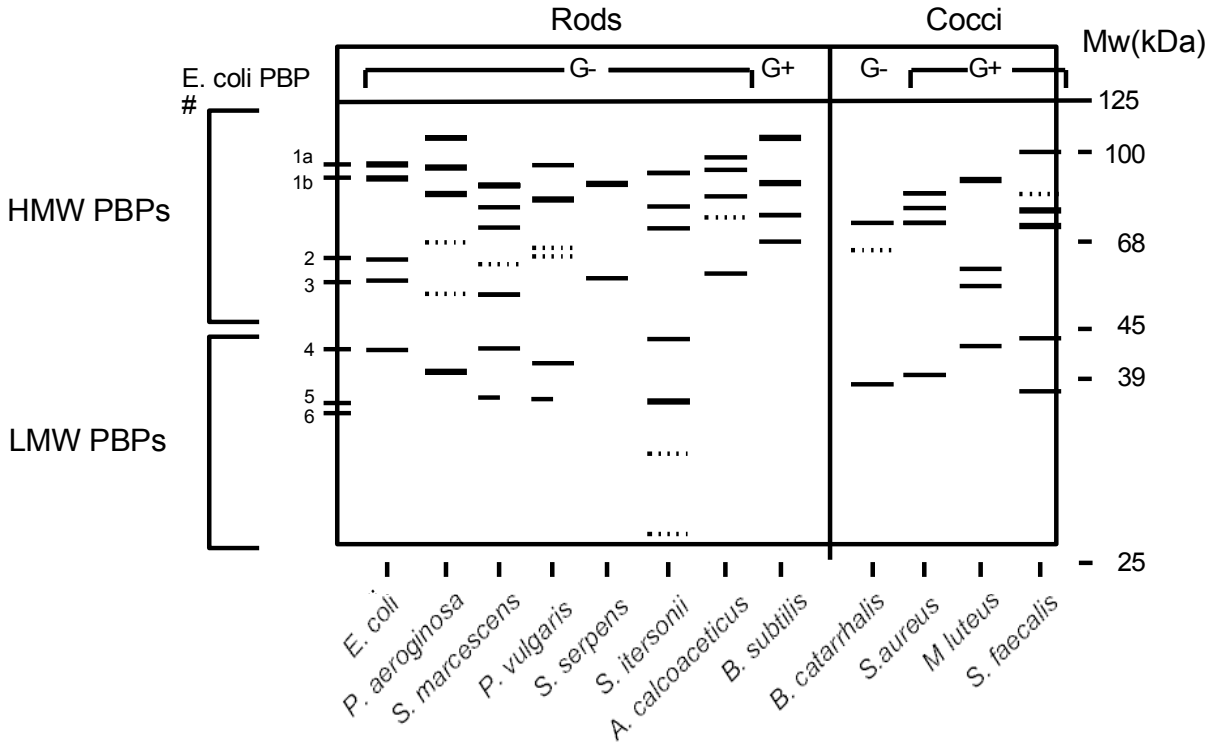

Figure 4: Idealized radiolabeled penicillin SDS-PAGE autoradiogram showing different bacterial species and different PBPs. Adapted from Georgopapadkou et.,al 1983.

PBP Classification and β-lactam Antibiotics

PBPs have molecular masses of 20−120 kDa and can be broadly divided into two groups, the low molecular mass (LMM) PBPs ranging from 20-50 kDa and the high molecular mass (HMM) PBPs ranging from 50-120 kDa. Each of these groups can be further subdivided into three classes, A, B, and C, based on sequence analysis[10,11]. LMM PBPs are monofunctional enzymes, whereas HMM PBPs possess an additional N-terminal domain that in HMM class A enzymes is a penicillin-insensitive transglycosylase involved in glycan polymerization of the cell wall. Table 1 shows different PBP classes and their functions. Different bacteria have different PBPs, for example, *E. coli* has twelve classically known PBPs, three HMM class A PBPs labeled 1A, 1B, and 1C, two HMM class B PBPs (PBP2 and PBP3) and seven LMM PBPs[12,13].

Table 1:
Classification of bacterial DD-peptidases on the basis of amino acid sequence and function (Adapted from Goffin et.,al, 2002).

DD-peptidases class	**Function *in vivo***
High molecular mass A (HMMA)	Transglycosylase, transpeptidases (bifunctional)
High molecular mass B (HMMB)	Transpeptidases
Low molecular mass A (LMMA)	Carboxypeptidase
Low molecular mass B (HMMB)	Carboxypeptidase
Low molecular mass C (HMMC)	Carboxypeptidase/endopeptidase

HMM class A and B enzymes, as well as LMM class A, and C enzymes, all possess three highly conserved active site sequence motifs (SXXK, SXN, and K(T/S)G) (where X resembles any variable amino acid), while LMM class B enzymes have a YXN in place of the SXN motif. The serine residue of the motif SXXK is central to catalysis and involves in enzyme acylation and deacylation steps[14].

The discovery of β-lactams led to a revolution in the treatment of bacterial infections. Penicillins and cephalosporins belong to the β-lactam class antibiotics and act by covalently inhibiting PBPs. It has been hypothesized that β-lactam antibiotics are suicide substrates and inhibit the PBPs by acting as substrate analogs of ~D-Ala-D-Ala to form an acyl enzyme intermediate with the serine residue of the PBP active site[6,15]. The mechanism of β-lactams involves forming an acyl-enzyme complex similar to substrates, with the cleavage of the amide bond of β-lactam ring. The deacylation step is very slow leading to the formation of stable penicilloyl enzyme and inactivation of PBPs[16]. There are a wide variety of penicillins and cephalosporins available with variations at the -R position. Figure 5 shows the general structure of penicillin and cephalosporin along with the D-Ala-D-Ala backbone.

LMM vs HMM PBPs

Different PBPs have different propensities for catalyzing the transpeptidase, hydrolase (DD-carboxypeptidase), and endopeptidase reactions required for cell wall biosynthesis and modulation (Figure 6). The catalysis reaction by PBPs involve the attack of active serine on the carboxy terminal of D-Ala-D-Ala peptide, leading to the formation of acyl-enzyme complex and the release of the C-terminal D-Ala. The acyl-enzyme complex can then undergo hydrolysis to form shortened peptide (carboxypeptidation), or form a cross-link

with other peptidoglycan stem peptide (transpeptidation) (Figure 6). HMM PBPs catalyze exclusively transpeptidation reactions, whereas LMM PBPs catalyze carboxypeptidase (e.g., NG PBP3, *Actinomadura* R39)[10,17-21]and endopeptidase (e.g., EC PBP4)[22-25] reactions, with the exception of *Streptomyces* K15 being a LMM PBP strictly catalyzes transpeptidase reactions[26]. HMM PBPs are essential for bacterial viability and are the lethal targets for β-lactam antibiotics, whereas LMM PBPs are nonessential for cell viability. A particularly enigmatic feature of the PBPs is that LMM PBPs have readily detectable activity against peptide substrates, whereas purified HMM PBPs have either low or undetectable activity against natural or synthetic cell wall-related peptide substrates[27]. Recent studies have made progress in detecting and characterizing the transpeptidase activities of a few HMM PBPs, such as *E. coli* PBPs 1A and 1B[28,29], but these activities were still much lower than those observed with LMM PBPs. The low or undetectable activity of purified HMM PBPs has partly been attributed to the regulation of HMM PBP activity through interactions in macromolecular complexes within the cell wall environment[29-32].

The roles of individual PBPs in bacterial cell wall biosynthesis from a number of bacterial species have been elucidated by mutagenesis and knockout studies[18,20,33]. These studies have revealed that HMM PBPs are involved in cell elongation, cell morphology, and cell division[34]. While these studies also show that LMM PBPs are not essential for cell viability, these PBPs often play important roles in normal bacterial cell morphology[18,33]. For example in *E. coli,* the loss of PBP1a or PBPlb (HMM A) is tolerated, but the loss of both is lethal to bacteria[15]. On the other hand, LMM PBPs are generally dispensable for cell survival. For example the loss of PBP5 results in aberrant morphology[24] and the loss of either PBP4 or PBP7 results in no significant morphological change[24,35]. Examples of LMM PBPs

important for cell morphology include *Streptococcus pneumoniae* (SP) PBP3[36,37], *Staphylococcus aureus* (SA) PBP4[38], *E. coli* (EC) PBP5[39-42], and *N. gonorrhoeae* (NG) PBPs 3 and 4[43]. Despite these advances, there remains a significant knowledge gap in understanding the role of individual PBPs in the cell wall biosynthetic process.

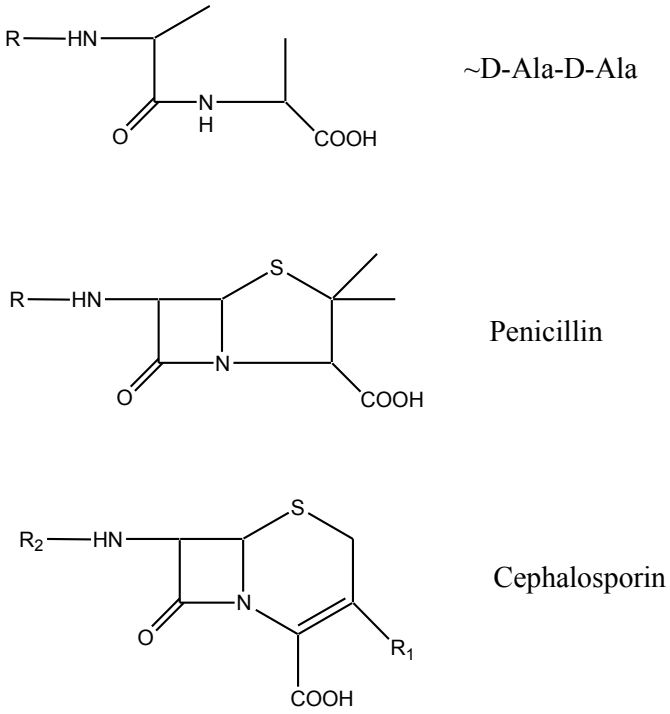

Figure 5: General structure of PBPs substrates, penicillins and cephalosporins.

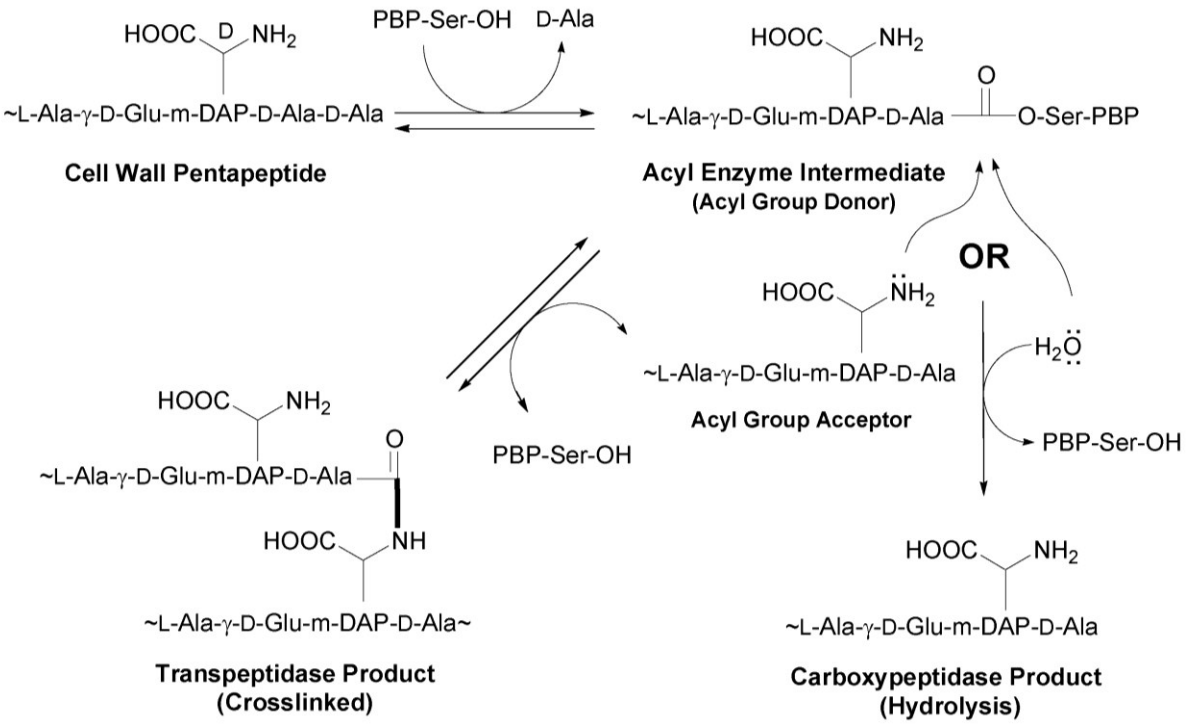

Figure 6: Bacterial cell wall biosynthesis reactions catalyzed by the PBPs in most Gram-negative bacteria (Transpeptidation vs Carboxypeptidation).

Substrates for PBPs

Given their readily detectable activity, most *in vitro* studies have focused on LMM PBPs. Different LMM PBPs show a large range of intrinsic activities against natural and synthetic cell wall-related substrates[21], with activities ranging from very weak to nearing the diffusion limit. Despite extensive study, features required for substrate specificity have been identified only for a few LMM PBPs.

The substrate specificity of several LMM PBPs has been investigated[7,19,44,45] concentrating primarily on the C-terminal and penultimate D-Ala of the natural ~D-Ala-D-Ala substrate (Figure 3). The standard substrate used for most of the studies was Ac_2-L-Lys-D-Ala-D-Ala[19]. Some of the noteworthy points in terms of substrate specificity are[46]:

- Presence of D-isomer at C-terminal is necessary as substitution with L-Ala makes the peptide to a weaker or nonsubstrate but it can be replaced with other D-amino acid with little change in the substrate activity
- Specificity for the terminal D-Ala residue is lower, and it is substituted with D-Lac in some vancomycin resistant bacterial strains[44]. (Vancomycin exerts its antibacterial effect by sequestering the D-Ala-D-Ala terminus of the pentapeptide precursor (Figure 3)
- PBPs are very specific for the penultimate D-Ala and the substitution with L-Ala or any other D-amino acid resulted in peptide with no activity
- Replacement of L-Lys (the third amino acid from C-terminal) with L-A_2bu or L-Hse causes decrease in substrate specificity, whereas substitution with pimelic acid or diamino pimelic acid representing natural cell wall stem peptide can result

in increased substrate activity as is the case with *Actinomadura* R39 and *Streptomyces* R61

- Depsipeptides, peptides with α-amino and α-hydroxy carboxylic acids linked by either an amide or an ester bonds, generally give higher turnover

The substrate interaction with PBP enzymes is given in Eq. 1.

$$E + S \underset{k_{-1}}{\overset{k_1}{\rightleftharpoons}} E\text{-}S \xrightarrow{k_2} E\text{-}P \xrightarrow{k_3} E + P \quad \text{..... Eq. 1}$$

With peptide substrates, acylation (k_1) is the rate limiting step, even with the best substrates studied so far[47-49]. Substrates of depsipeptide and thio-ester have high turnover and is due to an increase in k_2, which makes deacylation (k_3) as the rate limiting step[50]. This suggests that the presence of a good substrate increases the k_{cat} (k_2) in concentration dependent manner. Peptides based on the backbone ~D-Ala-D-Ala were widely used, but thiol ester substrates which can be monitored continuously were also used to characterize PBP substrate specificity[51].

HMM PBP Characterization

Purified LMM PBPs give readily detectable enzyme activity and are easily characterized, whereas HMM PBPs when purified give low or undetectable enzyme activity, which presents something of a mystery[8,27,52]. This has greatly impeded studies of the enzymes. In chapters 4 and 5, we described the first microtiter plate based assay for HMM

PBP characterization and inhibitor screening. HMM PBPs being transmembrane proteins require detergents for solubilization and makes characterization difficult. In *E. coli* five HMM PBPs have been identified: EC PBP 1a, 1b, 1c, 2, and 3. Transpeptidase activity has been observed for *E. coli* PBP 1a and 1b against complex substrates such as Lipid II[53,54]. Other HMM PBPs have exhibited no detectible activity against even complex substrates, for example EC PBP3, and the peptidoglycan transglycosylase PBP domain from *Bacillus megaterium*[55,56]. The very weak activity of EC PBP 1b or other HMM PBPs when purified is inconsistent with their role in cell wall biosynthesis[27]. The observation that EC PBP 1b transpeptidase activity is greatly stimulated by addition of membrane extracts[57] indicates that HMM PBPs may be (fully) active only within protein complexes where their enzymatic activity is tightly regulated[27]. Crystal structures of HMM PBPs either showed 'closed' active site conformation (*S. pneumonia* PBP1b)[58,59] or distorted active site (*S. aureus* PBP2a)[60], which hinder access to substrates or β-lactam antibiotics. This suggests that the binding of substrate or β-lactam might require a conformational change, which may be externally controlled to regulate enzyme activity[21]. Frere and coworkers have attempted to solve the assay problem for HMM PBPs by developing highly reactive thiolester substrates[51,56,57]. These substrates gave activity with some HMM PBPs but not all, and have allowed the basic enzymatic properties of these HMM PBPs to be assessed[51,56,57,61]. However, these thiolester substrates bear little similarity to natural cell wall substrates[62], give high background hydrolysis rates, and do not give turnover with all HMM PBPs.

Historically detection and characterization of HMM PBPs had been done with ^{3}H, ^{14}C, or ^{125}I- radiolabeled penicillin, separating the proteins by SDS-PAGE gel followed by autoradiogram[63,64]. The major limitation is that it can take hours to days to complete the

whole experiment and involves handling of radioactive substances. Recent advances to detect and study PBPs for their role in bacterial cell wall synthesis led to the discovery of several florescent probes[65-69]. Some of the widely used probes are BOCILLIN FL, Biotin-Ampicillin, Cephalosporin C-fluorescein, Vancomycin-FL, and Boronic acid-FL.

BOCILLIN FL is a widely used derivative of penicillin V and is commercially available from Molecular Probes®. It is synthesized from penicillin V and BODIPY FL dye and has an extinction coefficient of 68,000 and a maximal absorption at 504 nm. Detection of various PBPs in membrane extracts was similar to that of PBPs detected using radiolabeled penicillins. BOCILLIN FL was used as a fluorogenic probe to characterize PBPs and their inhibitors using competitive binding assays[66,68,70-73], and affinities measured were similar to that of what had been observed with radiolabel assays[65]. BOCILLIN FL has also used in fluorescence polarization based assays[65,66]. The advantage of fluorescence polarization (FP) is that it can be expanded to microtiter plate based assays for use in high throughput screening (HTS) of potential inhibitors[66], while the drawback is that, the affinities of the measured β-lactams were far off from the values observed with membrane extractions and solubilized enzymes using radio-label technique[65].

Biotinylated β-lactams (biotin conjugated to free side chain amino group of β-lactams) could also be used as probes to label PBPs. β-lactams by virtue of their nature bind to PBPs and the complex formed with biotinylated β-lactam (PBP-Bio-Amp) can be used for detection and characterization of PBPs[74-76]. The complex could be subjected to SDS-PAGE, transferred to a nitrocellulose paper and detected by treating with streptavidin-horseradish peroxidase conjugate, which can be developed by using colorimetric or chemiluminescence method. Biotinylated β-lactams were used in PBP detection in bacterial extracts and were

used in determining affinities of different β-lactams in competitive binding assay setting. The affinities obtained were similar to those obtained from traditional radiolabeling. This probe was also used in purification of PBPs from bacterial extracts[74].

Some less widely used but still useful probes are Cephalosporin C-fluorescein[68], Vancomycin-FL[77], boronic acid-FL[67] and nitrocefin[60]. Due to the selective nature of different antibiotics (penicillin, cephalosporin) and their different affinities towards PBPs, probes such as Ceph C-fluorescein and boronic acid FL can be used to study particular enzyme reactions[68]. The cephalosporin C FL derivatives were synthesized with selective scaffolds that interact with a subset of PBPs instead of all the PBPs as is the case with BOCILLIN FL. These probes were used to visualize and study PBPs using microscopy, SDS-PAGE and mass spectrometry[68]. Vancomycin binds to the ~D-Ala-D-Ala terminus of the nascent peptidoglycan and halts the crosslinking of growing peptidoglycan[78]. Van-FL can be an especially useful tool in studying the peptidoglycan synthesis as it acts on a different target and has different mechanism of action than β-lactams[69]. Van-FL was used to visualize the nascent cell wall insertion pattern by using fluorescence microscopy[69]. The boronic acid-FL was used as a tracer in fluorescence polarization assay. The assay was used to measure the binding constants of β-lactams and boronic acids. Boronic acid inhibitors are transitional state analogs and are designed based on the enzyme-substrate tetrahedral intermediate. The advantage of the boronic acid FL probe over other β-lactam based probes is that, this probe serves as reversible binding tracer, whereas β-lactam based probes are irreversible in nature. β-lactams and other boronic acids were able to displace the tracer in competitive assays[67].

CHAPTER 2

MULTIVARIATE GEOMETRICAL ANALYSIS OF CATALYTIC RESIDUES IN THE PENICILLIN-BINDING PROTEINS[79]

INTRODUCTION AND RATIONALE

Although all PBPs share a set of highly conserved active site residues, different PBPs have different propensities for catalyzing the transpeptidase and hydrolase (DD-carboxypeptidase and endopeptidase) reactions required for cell wall biosynthesis and modulation. HMM PBPs catalyze transpeptidation reactions[8,28,80-83], whereas LMM PBPs generally catalyze carboxypeptidase[10,17-21] and endopeptidase[22-25,84] reactions. The *Streptomyces* K15 enzyme is a notable exception to this general pattern in that – even though it is a LMM PBP– it acts as strict transpeptidase[26]. Since all PBPs share the same or nearly the same set of conserved active site residues (Table 2), a significant question is: Are there specific and identifiable structural features associated with PBPs, which catalyze different reaction paths (e.g. transpeptidase vs hydrolase activity)? Another point of interest is that HMM PBPs are essential for bacterial viability and are the lethal targets for β-lactam antibiotics, whereas LMM PBPs are non-essential for cell viability. In view of this distinction, a further particularly enigmatic difference between HMM PBPs and LMM PBPs is that LMM PBPs have readily detectible activity against peptide substrates, whereas purified HMM PBPs have either low or undetectable activity against natural or synthetic cell wall-related peptide substrates[27]. An obvious question in this context is: Is this difference in activity between the purified LMM and HMM PBPs due to a difference in the alignment of their core catalytic residues, or some other feature of their respective active sites? The

identification of key similarities within and differences between the active site of different subclasses of PBPs would be an important step towards understanding to functional role of different PBPs in the cell wall biosynthesis process. The PBPs are of high interest for their important role in bacterial cell wall biosynthesis, and are mechanistically interesting enzymes that can catalyze alternative reaction pathways using the same catalytic machinery.

A substantial database of PBP structures (>90) now exists, and a global analysis of these structures could provide insight into fundamental features of the PBPs, including catalytic mechanism, how different PBPs select for a particular reaction pathway (transpeptidase, carboxypeptidase, or endopeptidase), and insight into similarities and differences between LMM PBPs and the essential and the enigmatic HMM PBPs. The visual comparison of such a large number of structures seems impractical. However, such a large number of structures are suitable for the application of univariate and multivariate statistical methods. Therefore, we have undertaken an analysis to assess the feasibility of a such statistically based approach, and its potential to provide insight into PBP structure, function, and mechanism.

Table 2:
Structurally-based catalytic residue sequence alignment of the PBPs used in this study.

	SXXK	**SXN**	**KT(S)G**
	* *	* *	* * *
LMM Class A and C PBPs			
AM_R39	44-QLLPA**S**NM**K**LFTAA-57	293-PFMKF**S**N**N**GHAEM-305	405-GVVEA**KTG**TMSGV-417
BS_4a	47-RMRPA**S**SL**K**LLTAA-60	294-PFMKL**S**N**N**GHAEV-306	406-GKVRA**KTG**SLSTV-418
EC_4	57-MALPA**S**TQ**K**VITAL-70	301-IMLKK**S**D**N**MIADT-313	412-GKVSA**KTG**SLQGV-424
EC_5	39-RRDPA**S**LT**K**MMTSY-52	105-GINLQ**S**G**N**DACVA-117	208-NVDGI**KTG**HTDKA-220
EC_6	35-KLDPA**S**LT**K**IMTSY-48	101-GVIIQ**S**G**N**DACIA-113	204-NVDGM**KTG**TTAGA-216
HI_4	64-FMLPA**S**TQ**K**VFTAV-77	305-KMMKK**S**D**N**QIADS-317	415-KNVIA**KTG**SLKGV-427
HI_5	60-RQYPA**S**LT**K**MMTSY-73	123-GVIVV**S**G**N**DATVA-135	226-NVDGM**KTG**HTSQA-238
MTb_DacB2	64-AHPPA**S**TI**K**VLLAL-77	119-GLLLV**S**G**N**DAANT-131	225-GAIGG**KTG**YTNAA-237
SA_4	70-KWNPA**S**MT**K**LMTMY-83	134-ITVSN**S**S**N**AAALI-146	254-GTDGL**KTG**SSDTA-266
SM_K15	30-RRSTG**S**TT**K**IMTAK-43	91-GLMLP**S**G**C**DAAYA-103	209-GAIGV**KTG**SGPEA-221
HMM Class A and B PBPs			
EC_1b	505-RRSIG**S**LA**K**PATYL-518	567-DALTR**S**M**N**VPTVN-579	693-LHLAG**KTG**TTNNN-705
NG_2	305-MIEPG**S**AI**K**PFVIA-318	357-GIMQK**S**S**N**VGTSK-369	492-FDVGA**KTG**TAKHV-515
SA_2	393-PHPTG**S**SL**K**PFLAY-406	449-DALRQ**S**F**N**IPALK-461	578-VNMGA**KTG**TGTYG-590
SA_2a	398-TTSPG**S**TQ**K**ILTAM-411	457-QAIES**S**D**N**IFFAR-469	592-ANLIG**KSG**TAELK-604
SP_1a	365-NRDWG**S**TM**K**PITDY-378	423-YALQQ**S**R**N**VPAVE-435	552-LPQAG**KTG**TSNYT-564
SP_1b	455-KRSPA**S**TT**K**PLLAY-468	511-EALNY**S**W**N**IPAYW-523	646-ADWIG**KTG**TTNQD-658
SP_2b	381-VFVPG**S**VV**K**AATIS-394	438-QALEY**S**S**N**TYMVQ-450	610-VSISG**KTG**TAESY-622
SP_2x	332-NYEPG**S**TM**K**VMMLA-345	390-QGFAH**S**S**N**VGMTL-402	542-QNVAL**KSG**TAQIA-554
LMM R61 Class B PBP		**YXN**	**HXG**
SM_R61	57-RFRVG**S**VT**K**SFSAV-70	154-GAAYS**Y**S**N**TNFVV-166	293-ISVYG**HTG**TVQGY-305

Abbreviations: AM_R39, *Actinomadura* R39 PBP; BS_4a, *Bacillus subtilis* PBP4a; EC_1b, *Escherichia coli* PBP1b; EC_4, *Escherichia coli* PBP4; EC_5,*Escherichia coli* PBP5; EC_6, *Escherichia coli* PBP6; HI_4, *Haemophilus influenza* PBP4; HI_5,*Haemophilus influenza* PBP5; MTb_DacB2, *Mycobacterium tuberculosis* PBPDacB2; SA_2,*Staphylococcus aureus* PBP2; SA_2a, Methicillin resistant *Staphylococcus aureus* PBP2a; SA_4,*Staphylococcus aureus* PBP4; SM_K15, *Streptomyces* K15 PBP; SM_R61, *Streptomyces* R61 PBP; SP_1a, *Streptococcus pneumonia* PBP1a; SP_1b, *Streptococcus pneumonia* PBP1b; SP_2b,*Streptococcus pneumonia* PBP2b; SP_2x, *Streptococcus pneumonia* PBP2X

MATERIALS AND METHODS

Structures for analysis

Structures for analysis were downloaded from the RCSB protein data bank. A complete list of structures and their features is given in Tables 3 and 4.

Table 3:
Summary of PBP Structures, Characteristics, and References

PBP	PDB ID	Class	Active Site Ligand	Complex	Mutant	Activity	Res (Å)	Ref
AM_R39	1W79	LMM C	None	None	No	Active	1.80	[85]
	1W8Q	LMM C	None	None	No	Active	2.85	[85]
	1W8Y	LMM C	Nitrocefin	Acyl	No	Active	2.40	[85]
	2VGJ	LMM C	Ceph C	Acyl	No	Active	2.40	[86]
	2VGK	LMM C	Peptide Substrate	Non-Covalent	No	Active	2.25	[86]
	2WKE	LMM C	6-β-Iodopenicillinate	Acyl	No	Active	2.20	[87]
BS_4a	1W5D	LMM C	None	None	No	Active	2.10	[88]
	2J9P	LMM C	Product complex	Acyl	No	Active	2.80	[88]
EC_4	2EX2_A	LMM C	None	None	No	Active	1.55	[25]
	2EX2_B	LMM C	None	None	No	Active	1.55	[25]
	2EX6	LMM C	Amp	Acyl	No	Active	1.60	[25]
	2EX8	LMM C	PenG	Acyl	No	Active	1.60	[25]
	2EX9	LMM C	PenV	Acyl	No	Active	1.65	[25]
	2EXA	LMM C	Farom	Acyl	No	Active	1.70	[25]
	2EXB	LMM C	Flomox	Acyl	No	Active	1.75	[25]
EC_5	1HD8	LMM A	None	None	Yes	DD	2.30	[89]
	1NJ4	LMM A	None	None	Yes	DD	1.90	[90]
	1NZO	LMM A	None	None	No	Active	1.85	[90]
	1NZU	LMM A	β-Mercaptoethanol	None	No	Inactive	2.00	[91]
	1SDN	LMM A	Hg	None	Yes	DD	2.50	[91]
	1Z6F	LMM A	Peptide boronate	TS	No	Active	1.60	[92]
	3BEB	LMM A	Peptide mimetic Pen	Acyl	No	Active	2.00	[86]
	3BEC	LMM A	Peptide mimetic Ceph	Acyl	No	Active	1.60	[86]

EC_6	3IT9	LMM A	None	None	No	Active	2.10	[93]
	3ITA	LMM A	Amp	Acyl	No	Active	1.80	[93]
	3ITB	LMM A	Peptide Fragment	Acyl	No	Active	1.80	[93]
HI_4	3A3D	LMM C	None	None	No	Active	1.60	[94]
	3A3E	LMM C	Amp Analog	None	No	Active	2.40	[94]
	3A3F	LMM C	Amp	None	No	Active	2.10	[94]
	3A3I	LMM C	Amp Analog	None	No	Active	2.00	[94]
HI_5	3A3J	LMM A	None	None	No	Active	2.15	[94]
MTb_DacB2	2BCF	LMM	None	None	No	Unknown	2.30	UP
SA_4	1TVF	LMM A	None	None	No	Active	2.00	UP
	3HUM	LMM A	Cefotaxime	Acyl	No	Active	2.30	[95]
	3HUN	LMM A	Amp	Acyl	No	Active	2.00	[95]
SM_K15	1ES3	LMM A	None	None	Yes	Active	2.20	[96]
	1ES4	LMM A	None	None	Yes	Active	1.90	[96]
	1ES5	LMM A	None	None	Yes	Unknown	1.40	UP
	1ESI	LMM A	None	None	Yes	Unknown	1.80	UP
	1SKF	LMM A	None	None	No	Active	2.00	[97]
EC_1b	3FWL	HMM A	Moenomycin (TG site)	None	No	Active	3.09	[98]
	3FWM	HMM A	Moenomycin (TG site)	None	No	Active	2.16	[98]
NG_2	3EQU	HMM B	None	None	No	Active	2.40	[99]
	3EQV	HMM B	None	None	Res	Active	2.40	[99]
SA_2	2OLU	HMM A	None	None	No	Active	2.90	[100]
	2OLV	HMM A	None	None	No	Active	2.80	[100]
	3DWK	HMM A	None	None	No	Active	3.10	[101]
SA_2a	1MWR	HMM B	None	None	No	Active	2.45	[60]

	1MWS	HMM B	Nitrocefin	Acyl	No	Active	2.00	[60]
	1MWT	HMM B	Pen G	Acyl	No	Active	2.45	[60]
	1MWU	HMM B	Methicillin	Acyl	No	Active	2.60	[60]
	1VQQ	HMM B	None	None	No	Active	1.80	[60]
SP_1a	2C5W	HMM A	Cefotaxime	Acyl	No	Active	2.55	[102]
	2C6W	HMM A	None	None	No	Active	2.61	[102]
	2V2F	HMM A	None	None	Res	Active	1.90	[103]
	2ZC5	HMM A	Biapenem	Acyl	No	Active	3.00	[104]
	2ZC6	HMM A	Tebipenem	Acyl	No	Active	2.70	[104]
SP_1b	2JCH	HMM A	Lactivicin	Acyl	No	Active	2.40	[58]
	2JCI	HMM A	Acyl_Ala	Acyl	No	Active	2.50	[105]
	2JE5	HMM A	Lactivicin	Acyl	No	Active	2.60	[58]
	2UWX	HMM A	Nitrocefin	Acyl	Yes	Active	2.39	[59]
	2UWY	HMM A	Cefotaxime	Acyl	Yes	Active	3.00	[59]
SP_2b	2WAD	HMM B	None	None	Res	Active	2.18	[106]
	2WAE	HMM B	None	None	Res	Active	2.26	[106]
	2WAF	HMM B	None	None	No	Active	3.29	[106]
SP_2x	1K25	HMM B	None	None	Res	Active	3.20	[107]
	1PYY	HMM B	Glycoside	None	Res	Active	2.42	[108]
	1QME	HMM B	None	None	No	Active	2.40	[109]
	1QMF	HMM B	Cefuroxime	Acyl	No	Active	2.80	[109]
	1RP5	HMM B	None	None	Res	Active	3.00	[110]
	2Z2L	HMM B	None	None	No	Active	2.85	[111]
	2Z2M	HMM B	Cefditoren	Acyl	No	Active	2.60	[111]
	2ZC3	HMM B	Biapenem	Acyl	No	Active	2.50	[104]
	2ZC4	HMM B	Tebipenem	Acyl	No	Active	2.80	[104]
SM_R61	3PTE_AA	LMM B	None	None	No	Active	1.60	[112]
	3PTE_AB	LMM B	None	None	No	Active	1.60	[112]
	3PTE_BA	LMM B	None	None	No	Active	1.60	[112]
	3PTE_BB	LMM B	None	None	No	Active	1.60	[112]
	1CEF	LMM B	Cefotaxime	Acyl	No	Active	2.04	[113]

1CEG	LMM B	Cephalothin	Acyl	No	Active	1.80	[113]
1HVB_A	LMM B	Cephalosporin	Acyl	No	Active	1.17	[114]
1HVB_B	LMM B	None	None	No	Active	1.17	[114]
1IKG	LMM B	Peptidoglycan Fragment	Non-Covalent	No	Active	1.90	[115]
1IKI_A	LMM B	Peptide	Non-Covalent	No	Active	1.25	[115]
1IKI_B	LMM B	Peptide	Non-Covalent	No	Active	1.25	[115]
1MPL	LMM B	Peptide phosphonate	TS	No	Active	1.12	[116]
1PW1_A	LMM B	Pencillin	Acyl	CM	Inactive	1.20	[117]
1PW1_B	LMM B	None	None	CM	Inactive	1.20	[117]
1PW8	LMM B	Cephalosporin	Acyl	No	Active	1.30	[117]
1PWC	LMM B	PenG	Acyl	No	Active	1.10	[117]
1PWD	LMM B	Cephalosporin C	Acyl	No	Active	1.20	[117]
1PWG	LMM B	Pencillin	Acyl	No	Active	1.07	[117]
1SCW	LMM B	Monocyclic Phosphate	TS-Like	No	Active	1.13	[118]
1SDE	LMM B	Bicyclic Phosphate	TS-Like	No	Active	1.15	[118]

[a] Abbreviations: CM = Chemically modified, DD = deacylation defective, Res = β-lactam resistant, TG=Transglycolase, TS = transition-state, UP = unpublished.

Table 4:
Summary of hydrolase (carboxypeptidase (CPase), endopeptidase (EPase)), and transpeptidase (TPase) activities observed for the LMM PBPs included in this study.

PBP	Activity	Ref
AM_R39	CPase TPase	[119] [120]
BS_4a	CPase	[35]
EC_4	CPase and EPase from *in vivo* studies. CPase activity from *in vitro* study.	[23,24] [121]
EC_5	CPase, weak TPase.	[22,122,123]
EC_6	CPase No detectible activity	[122] [124]
HI_4	ND	
HI_5	ND	
SA_4	Readily detectible CPase activity, which transitions to TPase activity at low acceptor concentrations	[125]
SM_K15	Strict TPase	[26]
SM_R61	CPase TPase	[126] [127]

Nomenclature

The definition of the geometrical parameters extracted in this study is provided in Table 5.

Table 5:
Definition of terms[a]. Figure 18 shows Lys1, Ser2, Ser3 and Lys4.

Distances	
D_12'	Distance between N1 and O2'.
D_2'3	Distance between O2' and O3.
D_34	Distance between O3 and N4.
D_13	Distance between N1 and O3.
D_14	Distance between N1 and N4.
D_2'4	Distance between O2' and N4.
D_22'	Distance between O2 and O2'.
Oh-N1	Distance between Oh and N1.
Oh-O3	Distance between Oh and O3.
Oh-N4	Distance between Oh and N4.

Angles	
CN1Oh	Angle between Lys1-CE, N1, and Oh.
CO3Oh	Angle between Ser3-CB (or Try3-CZ in the SM_R61 enzyme), O3, and Oh.
CN4Oh	Angle between Lys4-CE (or His4-CE1 in the R61 enzyme), N4, and Oh .
BOhN1	Angle between B, Oh, and N1.
BOhO3	Angle between B, Oh, and O3.
BOhN4	Angle between B, Oh, and N4.
A_12'3	Angle between O3, O2', and N1.
A_2'34	Angle between O2', O3, and N4.
A_12'4	Angle between N4, O2', and N1.
A_134	Angle between N1, O3, and N4.
A_132'	Angle between N1, O3, and O2'.
A_142'	Angle between N1, N4, and O2'.
A_143	Angle between N1, N4, and O3.
A_2'13	Angle between O2', N1, and O3.
A_2'14	Angle between O2', N1, and N4.
A_2'43	Angle between O2', N4, and O3.
A_32'4	Angle between O3, O2' N4.
A_314	Angle between O3, N1, and N4.
CN1O2'	Angle between Lys1-CE, N1 and O2'.
CO2'N1	Angle between Ser2-CB, O2', and N1.
CO2'O3	Angle between Ser2-CB, O2', and N1.
CO3O2'	Angle between Ser3-CB (or Try3-CZ in the SM_R61 enzyme), O3, O2'.
CO3N4	Angle between Ser3-CB (or Try3-CZ in the SM_R61 enzyme), O3, and N4.
CN4O3	Angle between Lys4-CE (or His4-CE1 in the R61 enzyme), N4, and O3.

Dihedral Angles	
DA_1	Dihedral angle between Lys1-CG, CD, CE, and N1 (NZ).
DA_2	Dihedral angle between Ser2-C, CA, CB, and O2 (OG).
DA_2'	Dihedral angle between Ser2-C, CA, CB, and O2’ (OG’).
DA_3	Dihedral angle between Ser3-C, CA, CB, and O3 (OG). NA to the SM_R61
DA_4	Dihedral angle between Lys4-CG, CD, CE, and N4 (NZ). NA to the
DA_12'34	Dihedral angle between N1, O2’, O3, and N4.

[a] Lys1 refers to the Lys of the SXXK motif. Ser2 refers to the Ser of SXXK motif. Ser3/Tyr3 refers to the Ser/Tyr of (S/Y)XN motif. Lys4/His4 refers to the Lys/His of the (K/H)TG motif. N1 refers to the Lys1-NZ atom, O2 refers to the Ser2-OG atom, O3 refers to the Ser3-OG or Tyr3-OH atom, and N4 refers to the Lys4-NZ or the His4-NE2 atom. O2’ and 2' refer to the Ser2-OG atom from the superpositioned boronate complex. This is used since in all catalytic intermediate (acylated or transition-state analog) complexes the Ser2-OG atom is in this position (Figure 7), regardless of its position in apo complexes. Finally, Oh refers to the hydrolytic (nucleophilic) water atom from the superpositioned boronate complex, and B refers to the boron atom in the super positioned boronate complex, which is positioned very close to the carbonyl-carbon atom in overlaid acyl-complexes (Figure 7).

Initial processing

Downloaded structures were processed using UCSF Chimera[128]. In structures with multiple protein molecules in the unit cell, redundant chains were removed, and the resulting pared structures saved as PDB files. In the 1HVB and 1IKI structures for SM_R61, two conformations for the Ser of the SXXK motif are given - one ligated and one not, and a file for each conformation was saved and processed separately (1HVB_A and 1HVB_B, and 1IKI_A and 1IKI_B respectively). In the case of EC_4 2EX2 and SM_R61 1PW1, the Ser of their SXXK motifs was in two conformations and each of these was saved and processed separately (2EX2_A and 2EX2_B, and 1PW1_A and 1PW1_B respectively). Finally, in the SM_R61 3PTE structure, both the Lys of the SXXK motif and the Tyr of the YXN motif were in two alternate conformations, and all four combinations were saved and processed separately (3PTE_AA, 3PTE_AB, 3PTE_BA, and 3PTE_BB respectively, where the first A/B refers to the alternate conformation of the Lys residue and the second of the Tyr residue). A complete list of processed structures is given in Table 3.

Structure alignment

To align the active sites of these structures, our previously reported structure of *E. coli* PBP 5 complexed with a peptide boronic acid transition-state analog inhibitor[84,91] (EC_5 structure 1Z6F) was used as the reference (aligned to) structure. Alignments were performed using the UCSF Chimera "Match" function. Initial alignment was performed using all of the atoms of the active site Ser of the SXXK motif. However, inspection of these initial aligned structures revealed that the side chain of this Ser residue could be found (predominantly) in two conformations (Figure 7). Structures were therefore realigned using the four backbone

atoms (N, CA, C, O) of the Ser of the SXXK motif (Figure 7). Aligned structures were saved into new PDB files for further analysis.

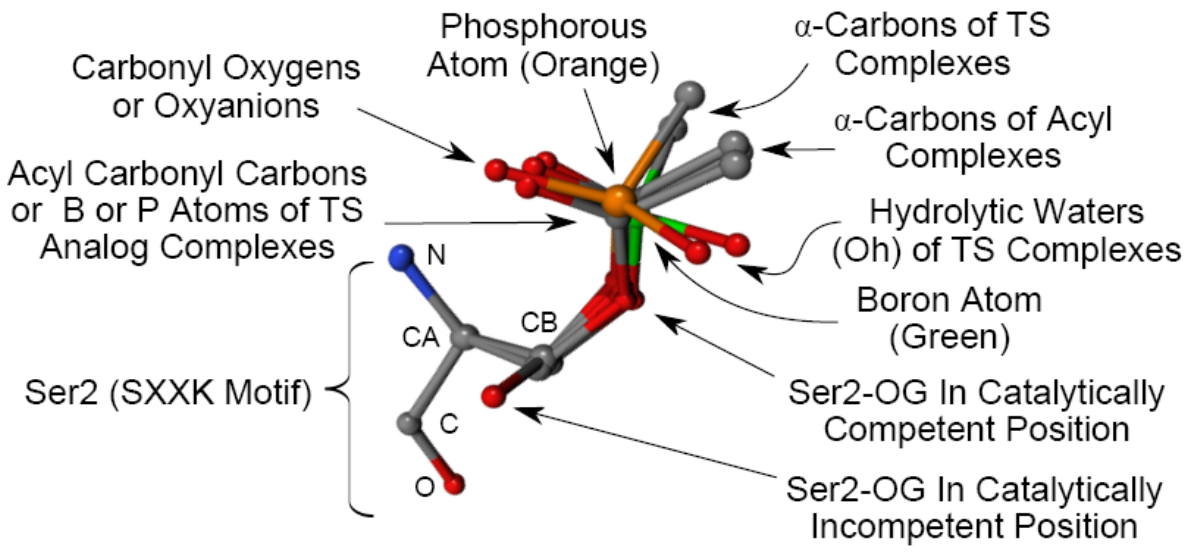

Figure 7: Overlay of the aligned SXXK motif Ser residue (Ser2) atoms from 6 PBP structures – EC 5 1Z6F, EC 5 3BEB, SM R61 1MPL, SM R61 1PW8, SA 2a 1MWR, and SA 2a 1MWS. Also included are several attached atoms from ligands from the two structures with transition-state (TS) analogs bound – 1Z6F (peptide boronic acid) and 1MPL (peptide phosphonate), and from three acylated structures – 1PW8, 3BEB, and 1MWS. Atoms from one unacylated structure (1MWR) with Ser2-OG in the down (catalytically incompetent) position are also shown. This figure illustrates that the backbone atoms of the Ser2 residues (N, CA, C, and O), upon which the alignments in this study are based, are very well aligned and essentially indistinguishable. This figure also illustrates the close alignment of the Ser2-OG atom in all acylated and transition-state analog ligated complexes. It is also notable that the acyl oxygens from acylated intermediates, and the oxyanions from transition-state analog complexes, are also very closely aligned, which in turn indicates that the transition-state analog complex during catalysis among all the PBPs is likely to be very similar to the transition-state analog structures (EC 5 1Z6F and SM 61 1MPL) shown here. This is the basis of the superpositioning approach used in this study.

Superpositioning and geometric parameter extraction

Geometric parameters (Table 5) were calculated using UCSF Chimera distance and angle functions. Since Ser2-OG was always found in a specific position in acylated and transition-state analog inhibited structures (Figure 7), it was desirable to use the active conformation position in this analysis. This was accomplished by overlaying (superpositioning) three atoms from the EC_5 1Z6F boronic acid reference structure[91] onto all analyzed structures – the Ser2-OG atom, the boron atom (which corresponding to the acyl carbon atom in the acylated enzyme intermediates and enzyme transition-state analog complexes), and the Oh atom (which corresponds to the nucleophilic water atom in the deacylation reaction[91]) (Figure 7). Distances and angles with the superpositioned atoms were included to provide insight into conserved features related to the catalytic complex among all of the assembled structures. In total 39 parameters were extracted from each structure (Table 6). Microsoft excel scripts were written to automate the superimposition and geometric parameter extraction and used in chimera.

Data analysis

Basic data analysis and plotting were performed using Microsoft Excel (Redmond, WA). The collected data were analyzed for summary statistics such as average, range, and standard deviation (Table 6). An additional Table segregating the SM_R61 values and all other PBP values is given in Table 7. Plots and histograms were prepared for each parameter (examples given in Figures 8-14). Normalized root mean square distances for each PBP were calculated as described in the discussion. Principal Components Analysis (PCA) was performed using SPSS statistical software (Chicago, IL) using the Factor Analysis method

with extraction set to principal components, and with analysis performed on the correlation matrix (appropriate for variables with substantially different ranges, such as the distance and angle variables used in this study). The statistical significance of the association of DA_1 values with hydrolase/LMM vs transpeptidase/HMM classification (Figure 8) was tested using three non-parametric tests of variance implemented in the SPSS software package: the Kruskal-Wallis test, the Mann-Whitney U test, and the Kolmogorov-Smirnov test.

Table 6:
Summary statistics of extracted geometric parameter values for the PBPs -all PBPs together.

	Count	Ave	Min	Max	Range	SD	% SD[a]
Distances							
D_12'	96	2.92	2.29	5.46	3.17	0.54	18%
D_2'3	96	3.47	2.65	8.43	5.78	0.99	29%
D_34	96	3.54	2.30	9.56	7.26	1.37	39%
D_13	96	3.46	1.91	7.34	5.43	1.02	30%
D_14	96	5.44	4.37	7.39	3.02	0.63	11%
D_2'4	96	5.11	3.74	7.43	3.69	0.85	17%
D_22'	96	0.90	0.00	2.68	2.68	0.81	90%
Oh-N1	96	4.29	3.13	6.56	3.43	0.51	12%
Oh-O3	96	3.51	1.75	8.05	6.30	0.98	28%
Oh-N4	96	5.86	3.81	8.66	4.85	1.04	18%
Two Party Angles							
CN1Oh	96	125	56	171	116	22	
CO3Oh	96	103	32	140	108	21	
CN4Oh	96	106	22	172	150	46	
BOhN1	96	70	40	100	60	11	
BOhO3	96	103	89	135	46	8	
BOhN4	96	90	82	107	25	4	
CN1O2'	96	111	36	164	128	34	
CO2'N1	96	122	79	158	79	12	
CO2'O3	96	90	67	144	77	16	
CO3O2'	96	136	36	176	140	34	

CO3N4	96	105	53	180	126	20
CN4O3	96	98	42	142	100	29
Three Party Angles						
A_12'3	96	64	24	118	94	15
A_2'34	96	98	20	147	127	21
A_12'4	96	81	48	115	68	12
A_134	96	108	32	149	118	25
A_132'	96	52	20	116	97	15
A_142'	96	32	22	62	40	7
A_143	96	34	15	94	79	12
A_2'13	96	64	38	102	64	11
A_2'14	96	67	42	99	57	11
A_2'43	96	40	21	131	110	14
A_32'4	96	42	13	103	90	18
A_314	96	38	14	120	107	23
Dihedral Angles						
DA_1	96	129	40	334	293	59
DA_2	96	183	119	313	194	50
DA_2'	96	145	131	227	95	9
DA_3	76	101	26	270	244	44
DA_4	76	125	46	296	250	77
DA_12'34	96	253	205	342	137	25

[a] %SD = SD * 100/Avg. %SD is only calculated for distances, since for distance relative error has physically significant meaning. In the case of angles, it is possible for an angle to have a mean of zero, and a significant SD, and %SD therefore lacks significance for angle values. In the case of angles, the SD itself is the most meaningful measure of dispersion.

Table 7:
Summary statistics on extracted geometric parameter values for the PBPs – R61 only and all other PBPs separately.

	R61 Only							All PBPs without R61						
	Count	Ave	Min	Max	Range	SD	%SD[a]	Count	Ave	Min	Max	Range	SD	%SD[a]
D_12'	20	3.04	2.33	4.44	2.11	0.54	18%	76	2.89	2.29	5.46	3.17	0.47	16%
D_2'3	20	2.94	2.65	3.10	0.45	0.99	34%	76	3.60	2.65	8.43	5.78	1.07	30%
D_34	20	5.08	4.01	7.01	3.00	1.37	27%	76	3.14	2.30	9.56	7.26	1.11	35%
D_13	20	2.85	1.91	3.47	1.56	1.02	36%	76	3.62	2.55	7.34	4.79	1.08	30%
D_14	20	5.51	4.37	6.00	1.63	0.63	11%	76	5.43	4.50	7.39	2.89	0.65	12%
D_2'4	20	5.87	5.29	6.12	0.83	0.85	15%	76	4.91	3.74	7.43	3.69	0.84	17%
D_22'	20	0.80	0.10	2.07	1.97	0.81	101%	76	0.92	0.00	2.68	2.68	0.85	92%
Oh-N1	20	4.35	3.68	5.04	1.36	0.51	12%	76	4.28	3.13	6.56	3.43	0.52	12%
Oh-O3	20	2.96	1.75	3.93	2.18	0.98	33%	76	3.66	2.21	8.05	5.84	1.01	28%
Oh-N4	20	6.93	6.29	7.24	0.95	1.04	15%	76	5.58	3.81	8.66	4.85	0.99	18%
CN1Oh	20	125	80	145	65	22		76	125	56	171	116	22	
CO3Oh	20	107	95	140	44	21		76	102	32	136	104	23	
CN4Oh	20	29	22	33	12	46		76	126	67	172	105	26	
BOhN1	20	75	61	100	39	11		76	69	40	87	47	10	
BOhO3	20	99	89	119	30	8		76	104	92	135	42	8	
BOhN4	20	86	85	87	2	4		76	91	82	107	25	4	
CN1O2'	20	126	52	156	104	34		76	107	36	164	128	32	
CO2'N1	20	115	87	131	43	12		76	124	79	158	79	11	
CO2'O3	20	101	81	144	63	16		76	87	67	140	73	14	
CO3O2'	20	143	129	158	29	34		76	135	36	176	140	38	
CO3N4	20	103	83	115	32	20		76	105	53	180	126	22	
CN4O3	20	49	42	54	12	29		76	111	64	142	78	16	
A_12'3	20	56	24	75	51	15		76	66	38	118	80	15	
A_2'34	20	92	50	111	61	21		76	99	20	147	127	21	
A_12'4	20	70	48	85	37	12		76	84	55	115	61	11	
A_134	20	88	35	117	82	25		76	114	32	149	118	21	
A_132'	20	64	47	116	70	15		76	49	20	74	55	12	
A_142'	20	31	23	49	25	7		76	32	22	62	40	7	
A_143	20	26	22	30	7	12		76	36	15	94	79	13	
A_2'13	20	59	40	71	32	11		76	65	38	102	64	11	
A_2'14	20	79	70	84	13	11		76	64	42	99	57	10	
A_2'43	20	28	25	30	5	14		76	44	21	131	110	14	
A_32'4	20	60	40	103	62	18		76	37	13	98	85	13	
A_314	20	66	38	120	82	23		76	31	14	105	92	13	
DA_1	20	94	58	185	127	59		76	139	40	334	293	58	
DA_2	20	164	142	230	87	50		76	189	119	313	194	53	
DA_2'	20	146	142	154	12	9		76	145	131	227	95	10	
DA_3		--	NA	--				76	101	26	270	244	44	
DA_4		--	NA	--				76	125	46	296	250	77	
DA_12'34	20	277	249	342	93	25		76	247	205	295	90	18	

[a] %SD = SD * 100/Avg. %SD is only calculated for distances, since for distance relative error has physically significant meaning. In the case of angles, it is possible for an angle to have a mean of zero, and a significant SD, and %SD therefore lacks significance for angle values. In the case of angles, the SD itself is the most meaningful measure of dispersion.

RESULTS

Summary statistics, parameter plots, and histograms

Summary statistics for the extracted parameters are given in Table 6. Since the SM_R61 enzyme is a LMM Class B PBP with a distinct active site from the other PBPs, summary statistics were segregated into two groups – those for the SM_R61 enzyme and those for all of the other PBPs, and are given in Table 7. Plots of parameter values vs PBP ID, and corresponding histograms, are given in Figures 8-14. Two parameter plots and histograms, which stood out as particularly informative, are shown in Figure 8 and Figure 9, and their significance will be discussed further below.

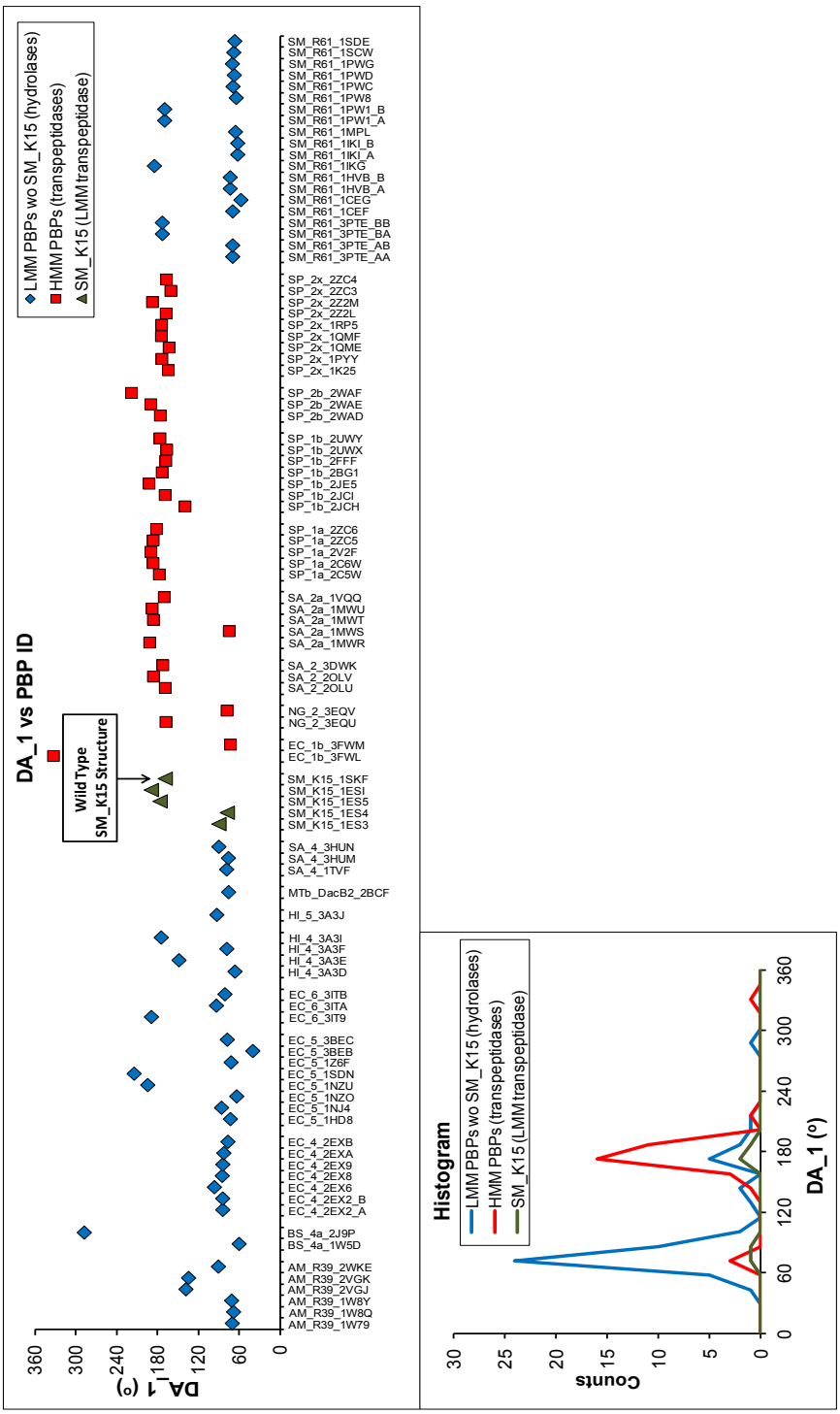

Figure 8: (Top) Plot of DA 1 vs PBP ID as a function of LMM/hydrolase (i.e., without the SM K15 enzyme), HMM/transpeptidase, and for the SM K15 enzyme (a LMM transpeptidase). (Bottom) Corresponding histograms. Note that some of the LMM PBPs included in this study have not been characterized enzymatically (e.g., HI 4 and HI 5) (Table 4), and their classification as hydrolases is based on their classification as LMM PBPs.

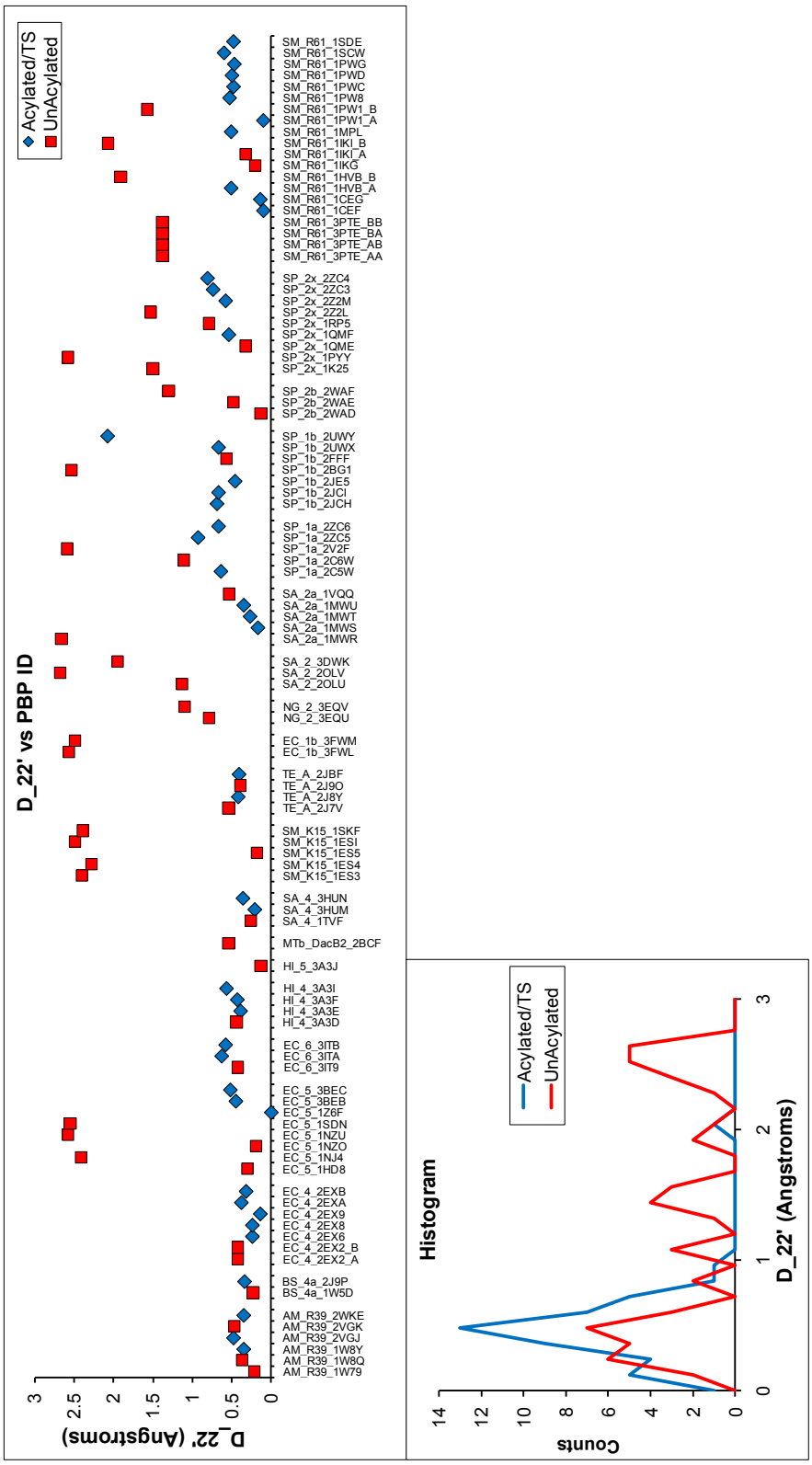

Figure 9: Top: Plot of D_22' as a function of PBP ID and acylation/TS status (blue diamonds) or unacylated status (red boxes). Bottom: Corresponding histogram.

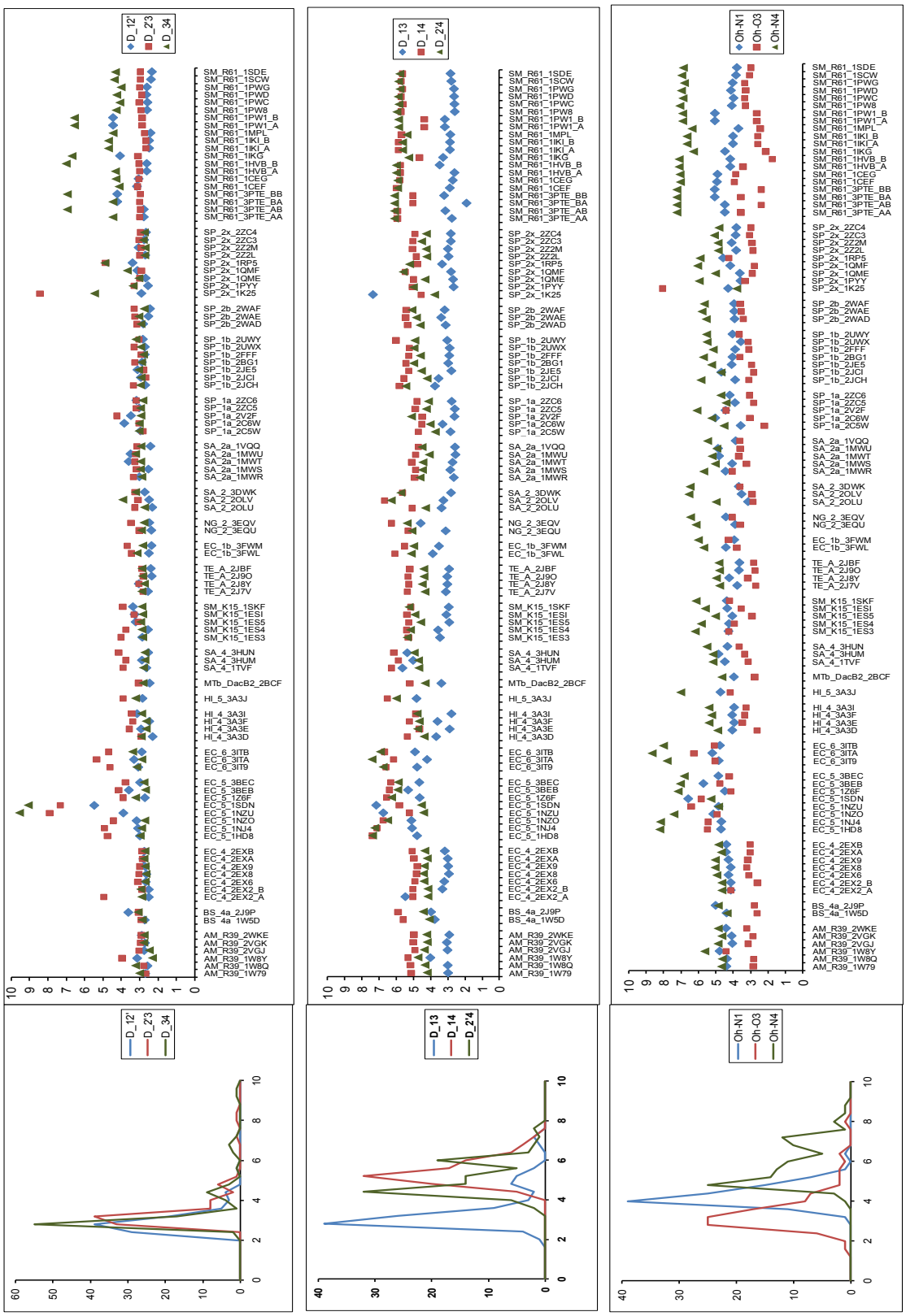

Figure 10: Plots of parameter values vs PBP ID, and histograms

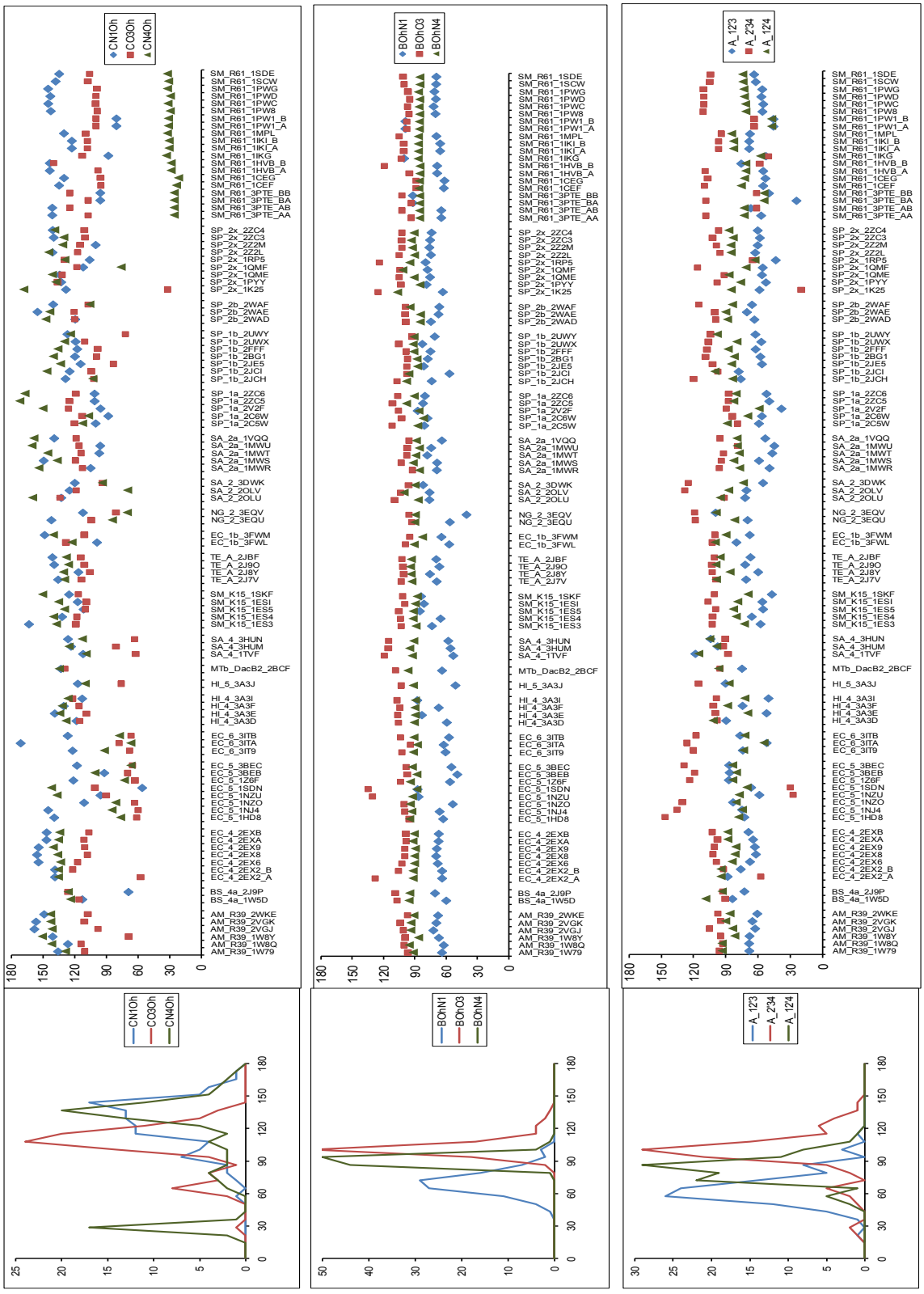

Figure 11: Plots of parameter values vs PBP ID, and histograms

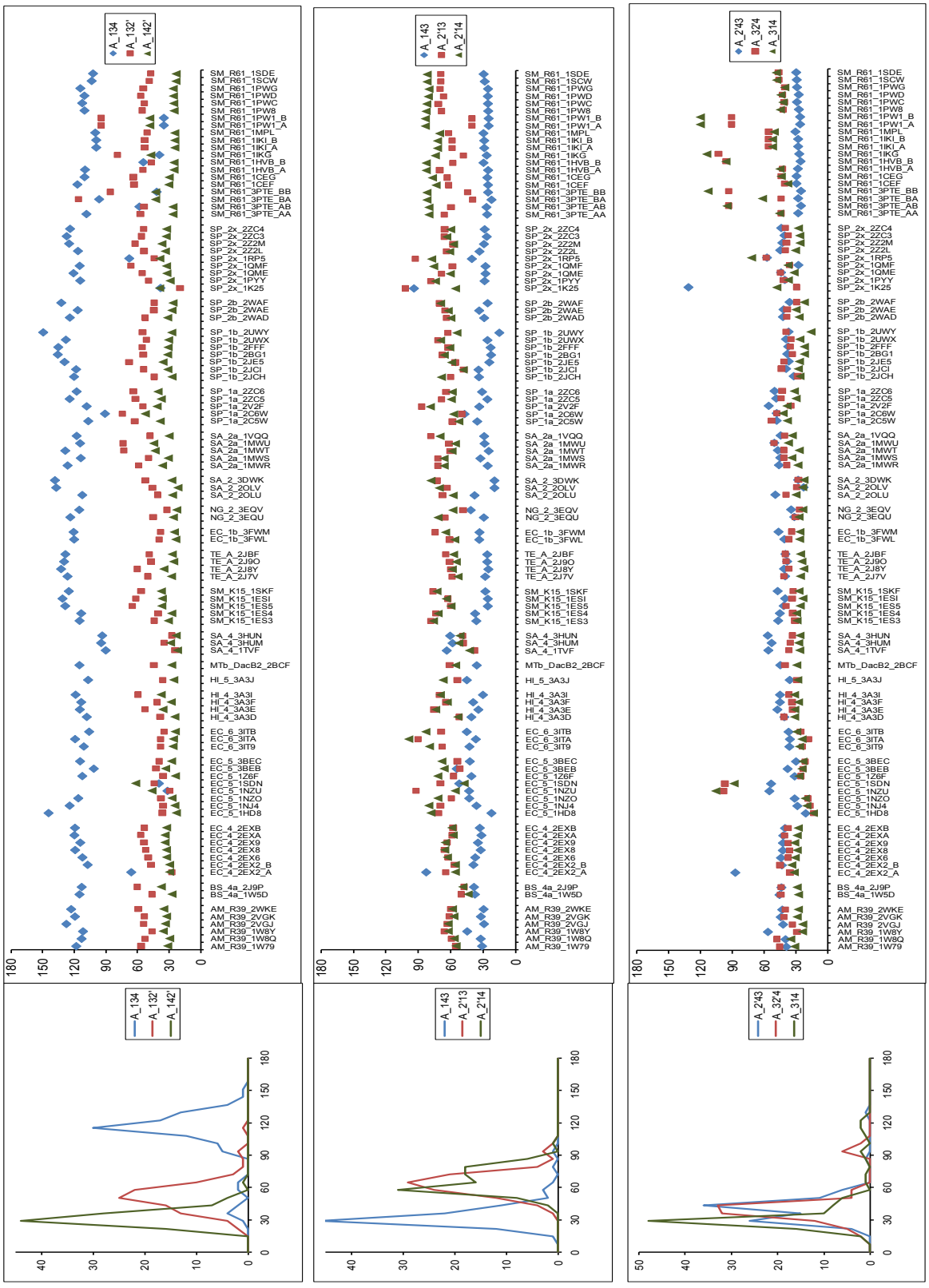

Figure 12: Plots of parameter values vs PBP ID, and histograms

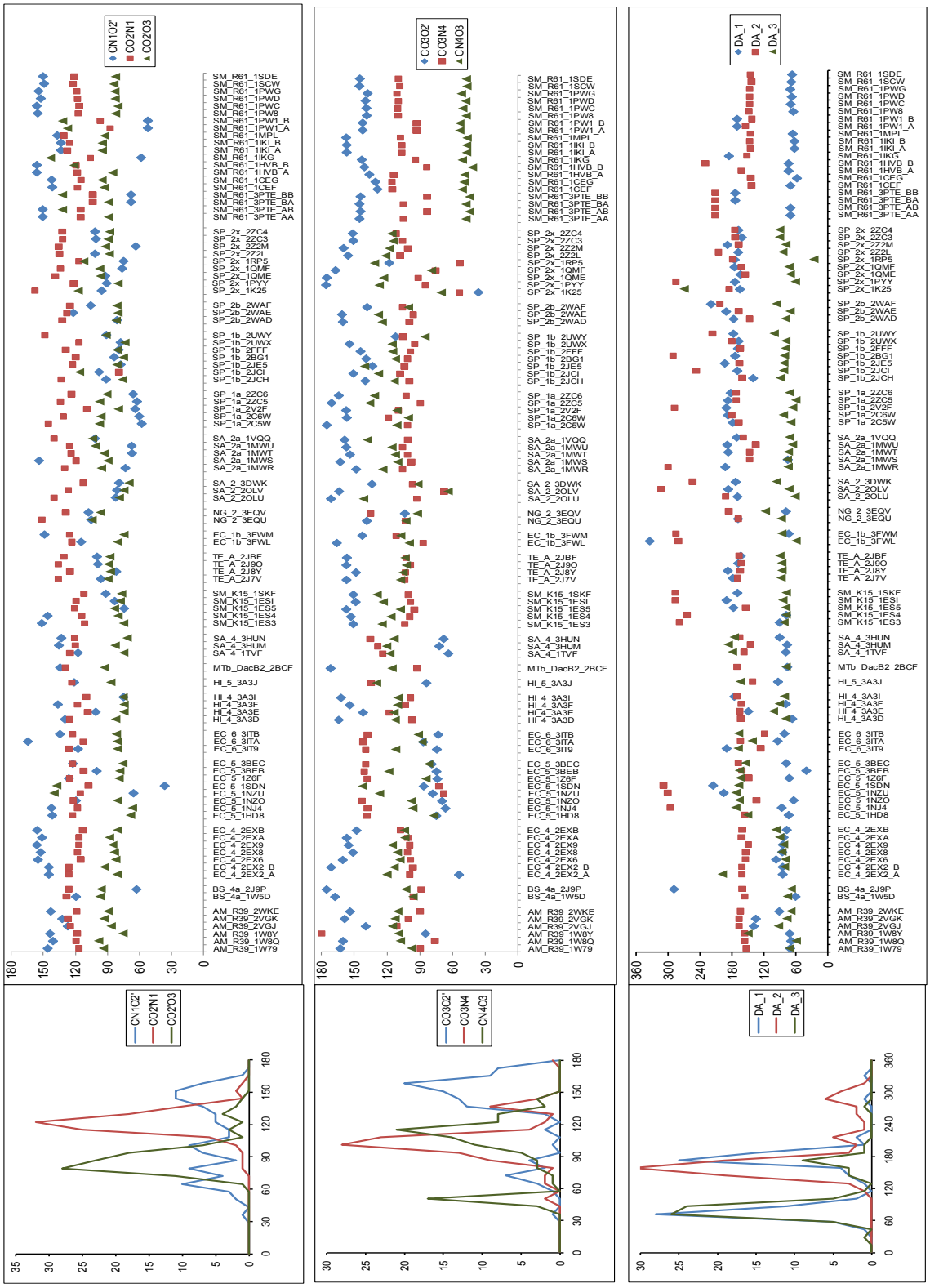

Figure 13: Plots of parameter values vs PBP ID, and histograms

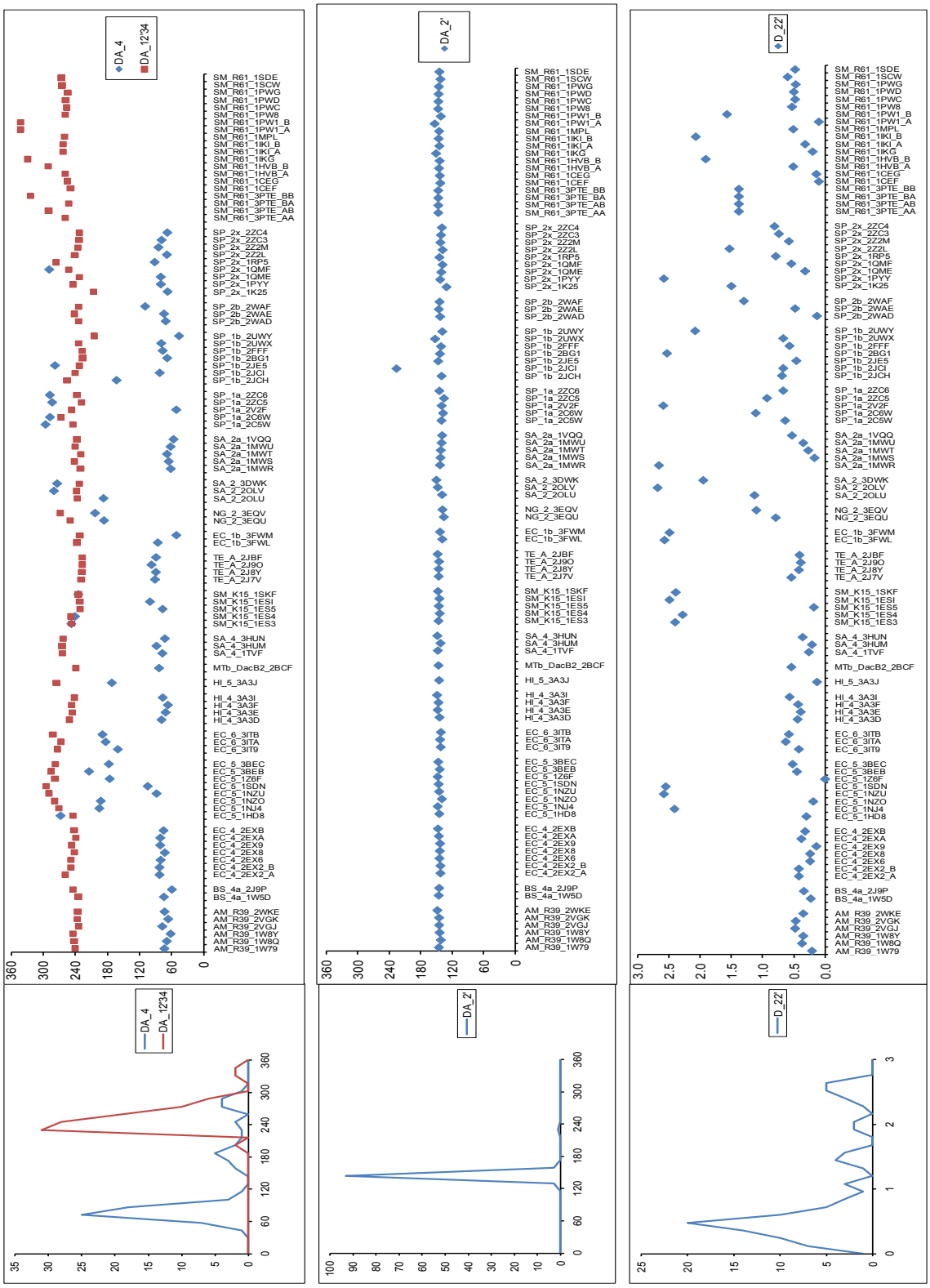

Figure 14: Plots of parameter values vs PBP ID, and histograms

Normalized root mean square deviation (NRMSD) calculation and identification of outliers

In any large data set there are likely to be outliers, which need to be identified, and possibly removed for some statistical analyses. Several possible outliers in the present data set could be identified by examining parameter plots (Figures 8-14), but a more rigorous numerical measure of distance from the mean (center) of parameter values was desired. Since distance measurements in angstroms are on a substantially different scale that angle measurements in degrees, it was necessary to use normalized parameters for this calculation. The normalized RMS deviation (distance) (NRMSD) was used in this case, based on the global average and global standard deviations (SDs) for all the parameters used in this study. For each PBP;

$$\text{NRMSD} = \sqrt{\frac{1}{n}\sum_{i=1}^{n}\left(\frac{X_i-\overline{X}}{\sigma}\right)^2}$$

Where n is the total number of parameters used in this calculation (n = 39), X_i is the i^{th} parameter value for the PBP in question, $\overline{X}$ is the mean of the parameter overall PBPs, and σ is the standard deviation of the parameter over all PBPs. All parameters except the test parameter D_22' (which was used as measure of catalytically competent vs catalytically incompetent positioning of the Ser2-OG atom) were used in this calculation. NRMSD provides an estimate of the normalized average deviation (distance) from the mean for all PBPs included in this study. A plot of NRMSD vs PBP ID is shown in Figure 15, along with a histogram. Several PBP structures were flagged as outliers, and several others as possible outliers, as indicated in Figure 15 by solid and dashed circles respectively. Outliers identified in these way included two *E. coli* structures (1NZU, 1SND), one SP_1b structure (2JCI), and

four SM_R61 structures (3PTE_BB, 1IKG, 1PW1_A, and 1PW1_B). The outlying *E. coli* structures were from covalently modified enzymes with known active site perturbations[91,92].

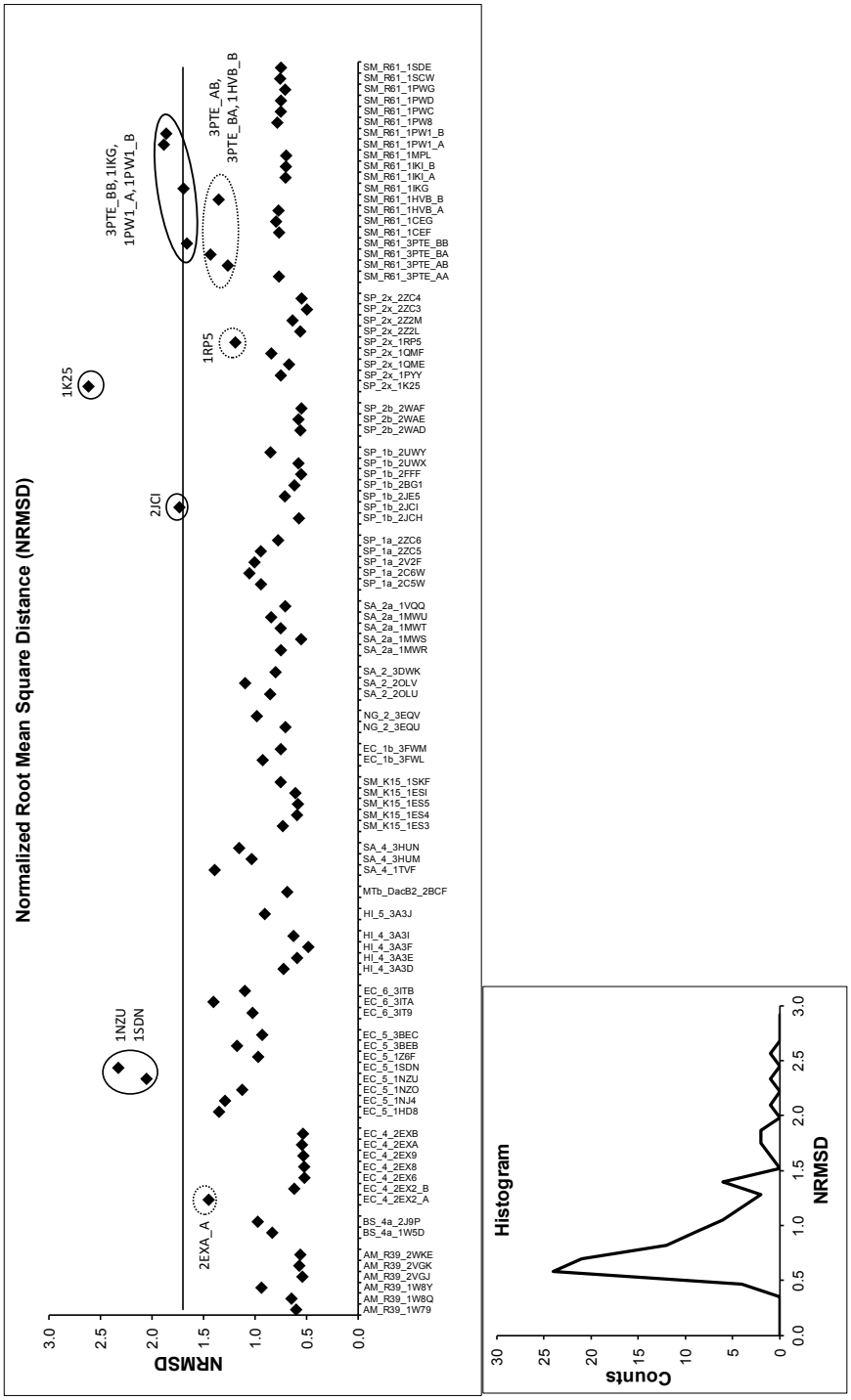

Figure 15: Top: Plot of NRMSD vs PBP ID. Clear outliers are denoted by solid circles, and intermediate outliers by dashed circles. Bottom: Corresponding histogram.

Principal components analysis (PCA)

PCA is a powerful method for the dimensional reduction and analysis of large multivariate data sets[129]. PCA recasts high dimensional data onto a new set of coordinates (axes, components) with lower dimensionality by selecting a new set of orthogonal axes comprised of linear combinations of the original variables. The first axis is selected to account for as much of the original variation in the data as possible; the second (orthogonal) axis is then selected to account for as much of the remaining variation in the data as possible, etc. Generally, PCA greatly reduces the number of axes (dimensions, components) required to explain variation in the data.

PCA was first applied to all of the PBPs in this data set, including the SM_R61 structures and the outliers identified using the NRMSD approach. Since the SM_R61 structures did not provide DA_3 and DA_4 angles (the SM_R61 enzyme does not have DA_3 and DA_4 angles since residue 3 is a Tyr and residue 4 is a His in SM_R61), these two parameters were excluded from this initial PCA analysis. The result of this analysis was a series of eigenvalues – which reflect how much of variation in the original data is accounted for by each component, eigenvectors – which are the new set of orthogonal axes vectors (components), and a set of new coordinates – which define the location of each PBP on the new set of orthogonal axes. The numerical results of this analysis for the full data set are given in Table 8. A plot of the location of all the PBPs included in this study is shown in Figure 16 panels A-C.

These PCA plots reveal the global relationships among all the PBPs based on active site residue geometry parameters, and allow similarities and differences between PBPs to be assessed (Figure 16A-C). *Note that some of the clustering indicated in the F1 vs F2 plot is*

only clear from also viewing the F1 vs F3 and F2 vs F3 plots. Plots from this first round PCA analysis confirm that two EC_5 structures (1NZU and 1SDN) and one SP_2x structure (1K25) are significant outliers. While the SP_1b 2JCI structure lies within the Main Cluster of PBPs, examination of other plots (e.g. the NRMSD plot in Fig. 15) suggests it is highly unusual, and comparison of its structure with other PBPs reveals that the Ser2-CB atom of its SXXK motif is in an unusual position. Several PBPs were isolated away from all other PBPs in PCA plots, and these are also labeled in the first round PCA plots shown in Figure 16A and Table 8.

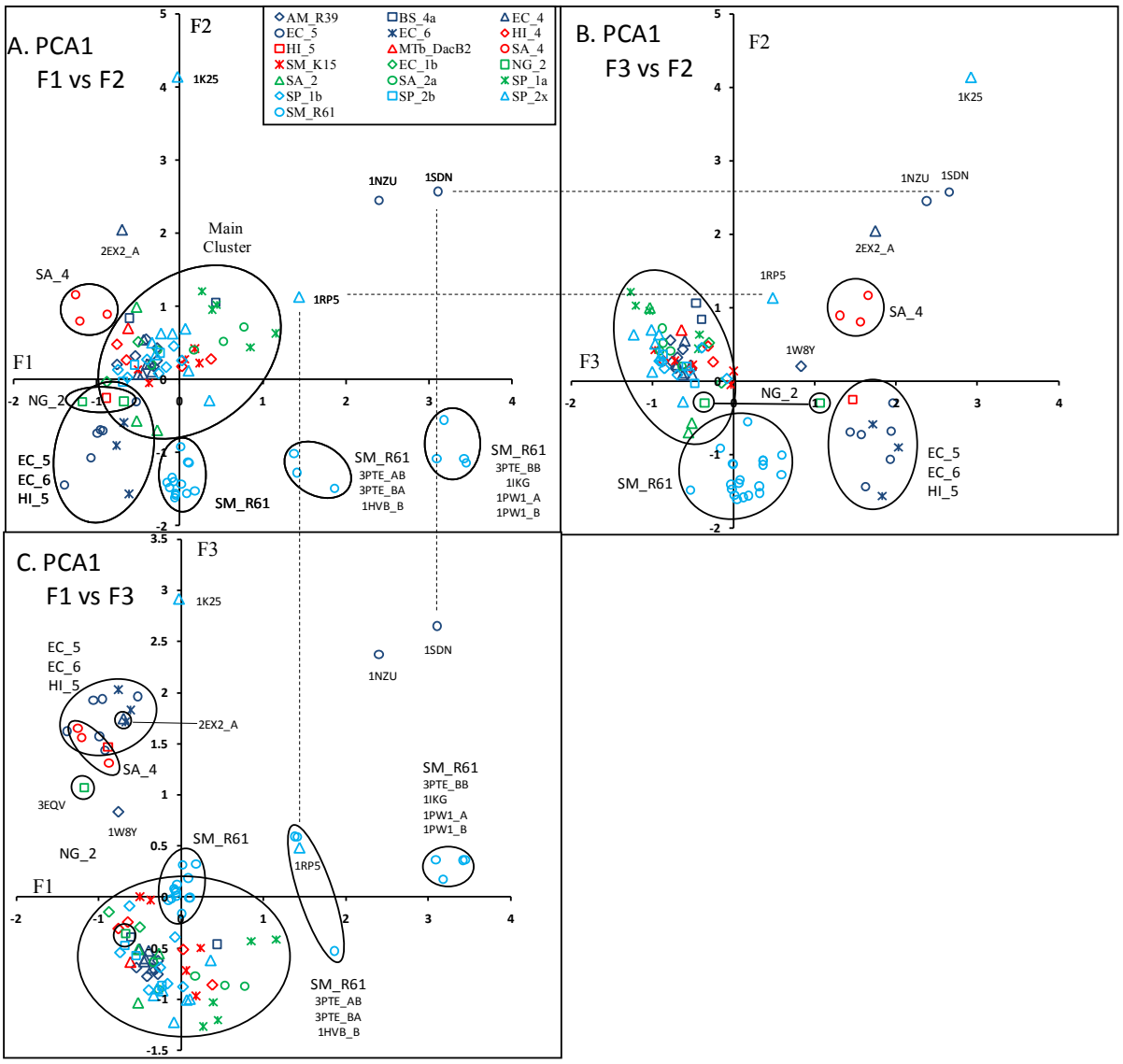

Figure 16: Panel A: PCA plot of the location of all the PBPs in this study on the F1 vs F2 axes from the first round PCA (PCA1). Corresponding plots on the F2 vs F3 and F1 vs F3 axes are given in panels B and C respectively. A legend is given in panel A. Apparent associations/clusters are circled. Structures which lie outside of identified clusters have been labeled with their structure ID. As indicated by dashed lines for the PCA1 plots, individual points are aligned in adjacent panels for a given PCA.

Table 8: Results from first round PCA (PCA1) including all PBPs, omitting DA_3 and DA_4.

Component	Eigenvalues		
	Total	% of Variance	Cumulative %
1	9.292	25.114	25.114
2	7.221	19.517	44.631
3	6.900	18.649	63.280
4	3.183	8.602	71.882
5	2.693	7.278	79.161
6	1.634	4.416	83.576
7	1.557	4.208	87.784
8	.941	2.543	90.327
Extraction Method: Principal Component Analysis.			

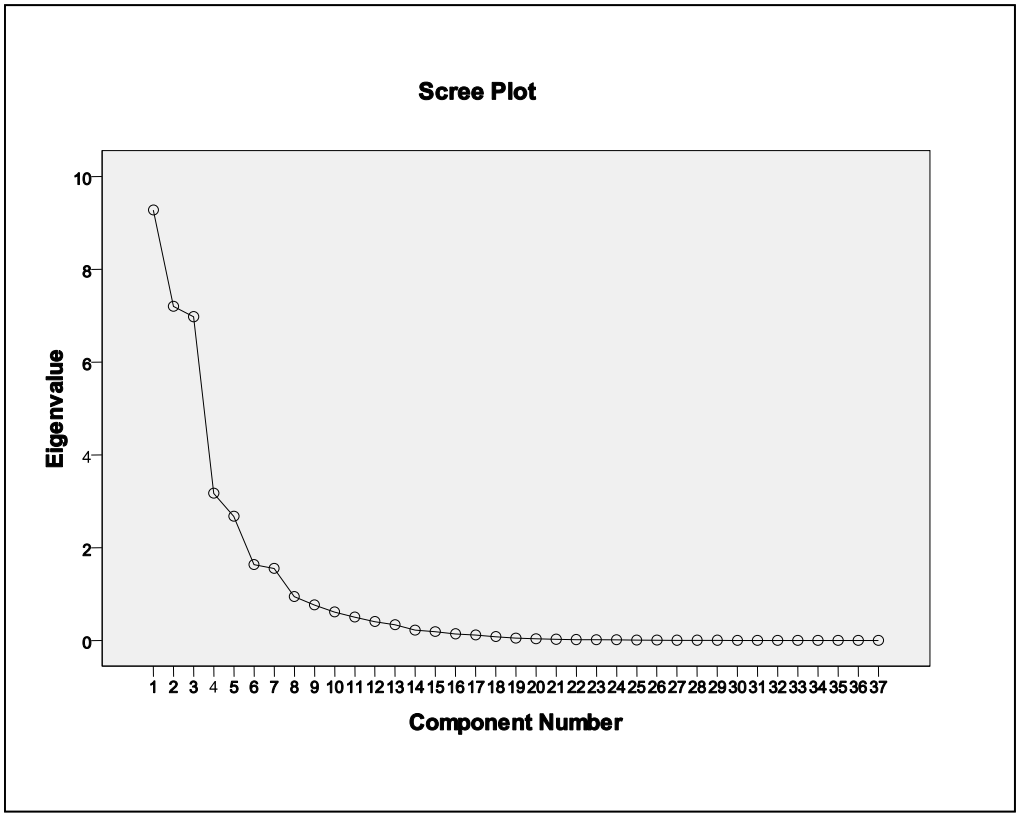

Component Matrix[a]							
	Component						
	1	2	3	4	5	6	7
D_12'	.779	.104	.260	.285	-.427	-.092	.016
D_2'3	.086	.471	.753	.371	.196	.061	.034
D_34	.795	-.069	.383	-.155	.286	.208	-.063
D_13	-.092	.432	.868	-.046	-.089	.117	-.031
D_14	-.450	-.411	.574	-.006	-.190	.401	-.197
D_2'4	.006	-.777	.504	.247	.031	.188	-.121
Oh-N1	.377	-.014	.609	.104	-.483	-.130	.162
Oh-O3	-.146	.239	.699	.592	.105	-.045	.067
Oh-N4	.066	-.817	.467	.239	.027	.103	-.096
CN1Oh	-.587	-.263	-.109	-.047	.536	-.133	.344
CO3Oh	.327	.011	-.763	-.115	.197	.227	.070
CN4Oh	-.267	.809	-.296	.223	-.118	-.020	.206
BOhN1	.749	.068	-.374	.323	.040	-.015	-.028
BOhO3	.216	.692	.367	-.195	.224	.151	-.053
BOhN4	-.315	.466	.141	-.012	-.029	.243	-.182
A_12'3	-.563	.142	.454	-.561	-.223	.201	-.059
A_2'34	-.678	-.569	-.133	.272	-.270	.092	-.074
A_12'4	-.668	.454	-.107	-.475	-.148	.194	-.057
A_134	-.731	-.154	-.504	.322	-.206	.091	-.028
A_132'	.652	-.301	-.510	.087	-.295	-.234	-.043
A_142'	.767	.409	-.082	.240	-.269	-.253	.076
A_143	-.191	.577	.644	-.193	.035	-.235	.060
A_2'13	-.128	.211	.082	.615	.680	.047	.134
A_2'14	.220	-.774	.173	.362	.344	-.043	.012
A_2'43	-.094	.854	.181	.090	.210	-.280	.096
A_32'4	.871	.020	.018	-.389	.159	.105	.015
A_314	.899	-.130	.220	-.253	.207	.022	.000
CN1O2'	-.547	-.398	.196	-.316	.397	-.168	.347
CO2'N1	-.441	.350	-.133	-.007	.272	-.108	-.683
CO2'O3	.797	.169	.139	-.303	.099	.061	-.042
CO3O2'	.185	-.072	-.913	-.120	.101	.114	.027
CO3N4	-.475	-.398	.346	.096	-.416	-.334	.098
CN4O3	-.274	.702	-.189	.227	-.262	.055	.195
DA_1	.372	.417	-.315	.404	-.229	.300	-.274
DA_2	.159	.196	-.006	.401	.088	.644	.226
DA_2'	.063	-.096	-.027	-.179	-.318	.385	.663
DA_12'34	.597	-.362	.526	-.274	-.108	-.026	.000

Extraction Method: Principal Component Analysis.

a. 7 components extracted.

Factor loadings on first three components (axes) for PCA1

PBP	F1	F2	F3	PBP	F1	F2	F3
AM_R39_1W79	-0.31	0.18	-0.72	SA_2_3DWK	-0.27	-0.70	-0.55
AM_R39_1W8Q	-0.28	0.43	-0.63	SA_2_2OLV	-0.52	-0.57	-0.51
AM_R39_1W8Y	-0.76	0.20	0.83	SA_2a_1MWR	0.17	0.41	-0.77
AM_R39_2VGJ	-0.54	0.32	-0.69	SA_2a_1MWS	-0.34	0.20	-0.64
AM_R39_2VGK	-0.41	0.55	-0.78	SA_2a_1MWT	0.53	0.52	-0.87
AM_R39_2WKE	-0.28	0.26	-0.76	SA_2a_1MWU	0.77	0.72	-0.87
BS_4a_1W5D	-0.61	0.84	-0.39	SA_2a_1VQQ	-0.27	0.41	-0.90
BS_4a_2J9P	0.44	1.06	-0.46	SP_1a_2C5W	0.45	1.02	-1.20
EC_4_2EX2_A	-0.70	2.05	1.74	SP_1a_2C6W	1.16	0.63	-0.42
EC_4_2EX2_B	-0.43	0.55	-0.60	SP_1a_2V2F	0.85	0.44	-0.43
EC_4_2EX6	-0.39	0.22	-0.52	SP_1a_2ZC5	0.27	1.21	-1.27
EC_4_2EX8	-0.45	0.08	-0.63	SP_1a_2ZC6	0.39	0.96	-1.03
EC_4_2EX9	-0.33	0.11	-0.61	SP_1b_2JCH	-0.63	0.03	-0.09
EC_4_2EXA	-0.35	0.22	-0.69	SP_1b_2JCI	-0.07	0.45	-0.39
EC_4_2EXB	-0.50	0.08	-0.51	SP_1b_2JE5	0.02	0.26	-0.88
EC_5_1HD8	-1.38	-1.44	1.62	SP_1b_2BG1	-0.25	0.08	-0.69
EC_5_1NJ4	-1.06	-1.07	1.93	SP_1b_2FFF	-0.39	0.27	-0.91
EC_5_1NZO	-0.96	-0.68	1.94	SP_1b_2UWX	-0.16	0.17	-0.85
EC_5_1NZU	2.40	2.45	2.37	SP_1b_2UWY	-0.74	0.13	-0.54
EC_5_1SDN	3.11	2.58	2.65	SP_2b_2WAD	-0.23	0.37	-0.87
EC_5_1Z6F	-0.99	-0.73	1.57	SP_2b_2WAE	-0.55	0.20	-0.58
EC_5_3BEB	-0.53	-0.30	1.96	SP_2b_2WAF	-0.68	-0.03	-0.47
EC_5_3BEC	-0.92	-0.70	1.44	SP_2x_1K25	-0.03	4.14	2.92
EC_6_3IT9	-0.67	-0.59	1.71	SP_2x_1PYY	0.11	0.12	-1.00
EC_6_3ITA	-0.61	-1.56	1.83	SP_2x_1QME	-0.09	0.63	-1.22
EC_6_3ITB	-0.76	-0.90	2.03	SP_2x_1QMF	0.36	-0.29	-0.62
HI_4_3A3D	-0.76	0.48	-0.31	SP_2x_1RP5	1.44	1.13	0.48
HI_4_3A3E	0.03	0.17	-0.52	SP_2x_2Z2L	-0.23	0.63	-0.91
HI_4_3A3F	-0.64	0.26	-0.25	SP_2x_2Z2M	0.07	0.69	-1.00
HI_4_3A3I	0.38	0.28	-0.86	SP_2x_2ZC3	-0.29	0.34	-0.89
HI_5_3A3J	-0.89	-0.25	1.47	SP_2x_2ZC4	-0.33	0.50	-0.96
MTb_DacB2_2BCF	-0.62	0.70	-0.64	SM_R61_3PTE_AA	0.09	-1.56	0.19
SA_4_1TVF	-1.25	1.16	1.65	SM_R61_3PTE_AB	1.41	-1.27	0.59
SA_4_3HUM	-0.88	0.89	1.31	SM_R61_3PTE_BA	1.86	-1.49	-0.53
SA_4_3HUN	-1.20	0.80	1.56	SM_R61_3PTE_BB	3.09	-1.08	0.37
SM_K15_1ES3	-0.37	-0.05	-0.03	SM_R61_1CEF	0.02	-1.43	0.32
SM_K15_1ES4	-0.50	0.14	0.00	SM_R61_1CEG	0.18	-1.53	0.32
SM_K15_1ES5	0.18	0.42	-0.97	SM_R61_1HVB_A	-0.05	-1.58	0.12
SM_K15_1ESI	0.06	0.28	-0.72	SM_R61_1HVB_B	1.38	-1.01	0.59
SM_K15_1SKF	0.24	0.23	-0.50	SM_R61_1IKG	3.18	-0.55	0.17
EC_1b_3FWL	-0.50	0.52	-0.30	SM_R61_1IKI_A	0.10	-1.13	-0.01
EC_1b_3FWM	-0.87	-0.03	-0.15	SM_R61_1IKI_B	0.11	-1.14	-0.01
NG_2_3EQU	-0.67	-0.30	-0.36	SM_R61_1MPL	0.01	-0.92	-0.16
NG_2_3EQV	-1.17	-0.30	1.07	SM_R61_1PW1_A	3.45	-1.14	0.36
SA_2_2OLU	-0.52	1.00	-1.03	SM_R61_1PW1_B	3.42	-1.09	0.36

SM_R61_1PW8	-0.06	-1.62	0.05	SM_R61_1SDE	-0.09	-1.34	0.08
SM_R61_1PWC	-0.12	-1.48	-0.02	AM_R39_1W79	-0.31	0.18	-0.72
SM_R61_1PWD	-0.05	-1.56	0.01	AM_R39_1W8Q	-0.28	0.43	-0.63
SM_R61_1PWG	-0.15	-1.41	-0.03	AM_R39_1W8Y	-0.76	0.20	0.83
SM_R61_1SCW	-0.07	-1.39	0.06	AM_R39_2VGJ	-0.54	0.32	-0.69

Second Round PCA

A second round PCA (PCA2) was performed after excluding the SM_R61 enzyme, a LMM Class B PBP with a significantly different set of active site residues than the other PBPs included in this study (Table 2). Exclusion of the SM_R61 enzyme also allowed the DA_3 and DA_4 parameters, which are undefined for SM_R61, to be included in this second round analysis, which was desirable in order to be able assess similarities and differences in these two key parameters among the PBPs to which they pertain. Four outliers identified above (1NZU, 1SDN, 1K25, and 2JCI) were also excluded from the second round PCA. Results are summarized in Figure 17 and Table 9. The F1 vs F2 plot, and the corresponding F1 vs F3 and F2 vs F3 plots are shown in Figure 17. The pattern of association is very similar to that seen in the first round PCA. The majority of structures again fell within the Main Cluster. EC_5, EC_6, and HI_5 again form a distinct cluster, as does SA_4. For the two NG_2 structures, one is close to the EC_5/EC_6/HI_5 cluster and one is embedded in the Main Cluster. The AM_R39 2EX2_A and SP_2x 1RP5 structures are isolated from other PBPs, and appear to be outliers (1RP5 as an outlier is only apparent in the F1 vs F3 and F2 vs F3 plots in Figure 17). The SP_2b 2C6W and SP_2b 2V2F structures lie on the outer fringe of the Main Cluster (only visible in the F1 vs F3 and F2 vs F3 plots in Figure 17).

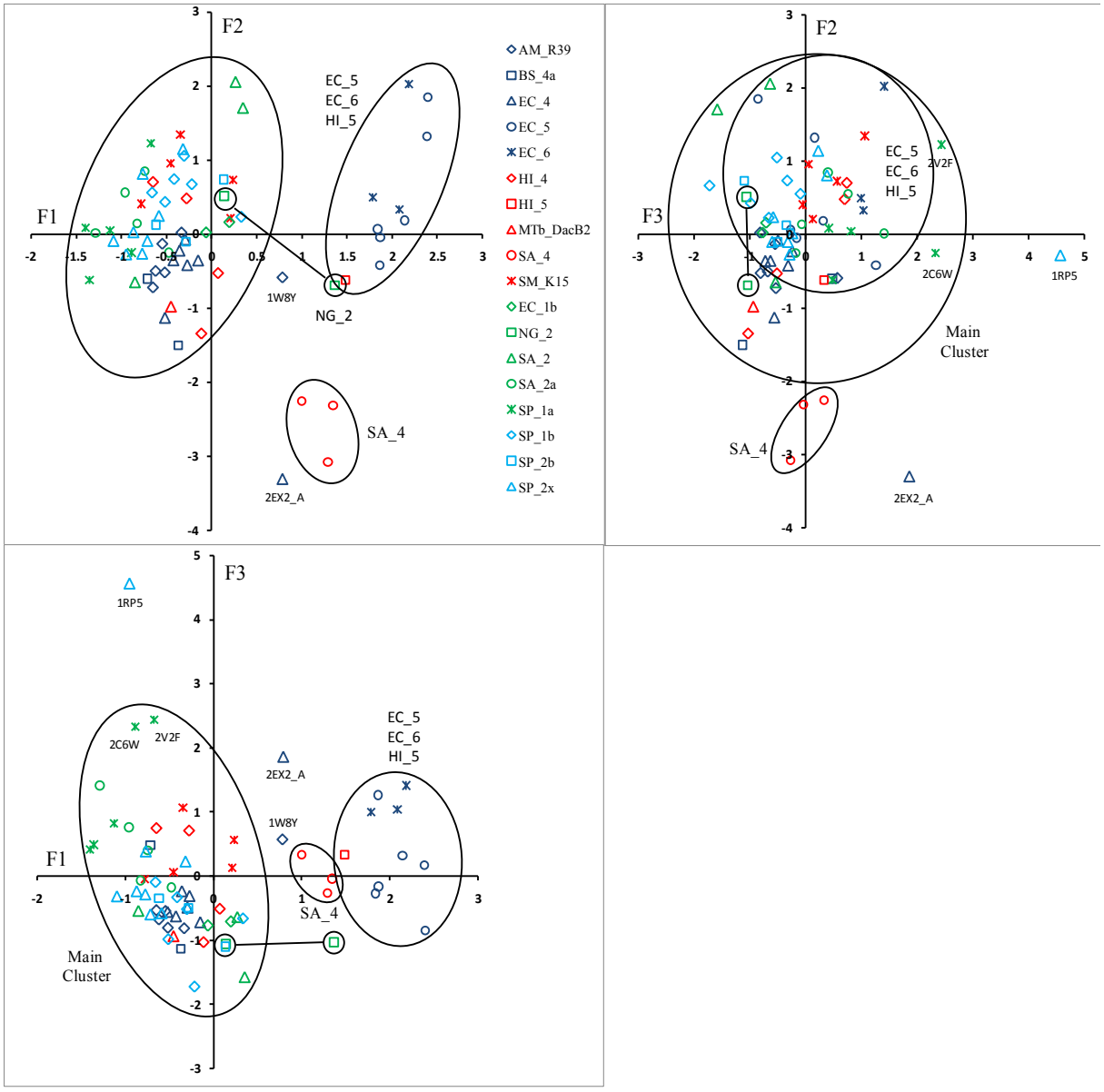

Figure 17: PCA Plot of the location of the PBPs from the second round PCA analysis on the F1 vs F2 axes (top left), F1 vs F3 axis (lower left), and F2 vs F3 axes (top right). A legend is given in the top right panel. Associations apparent in all three PCA1 plots are circled. Structures which lie outside of the main cluster for each group have been labeled with their structure ID. Note that individual PBPs and groups in adjacent plots will be horizontally and vertically aligned.

Table 9: Results from second round PCA (PCA2) omitting SM_R61, and several outlying PBPs, and including DA_3 and DA_4 parameters.

Component	Eigenvalues		
	Total	% of Variance	Cumulative %
1	13.095	33.577	33.577
2	6.361	16.311	49.888
3	4.727	12.120	62.008
4	3.307	8.479	70.487
5	2.744	7.035	77.522
6	1.870	4.794	82.315
7	1.713	4.392	86.707
8	1.100	2.821	89.528
9	.904	2.318	91.846
Extraction Method: Principal Component Analysis.			

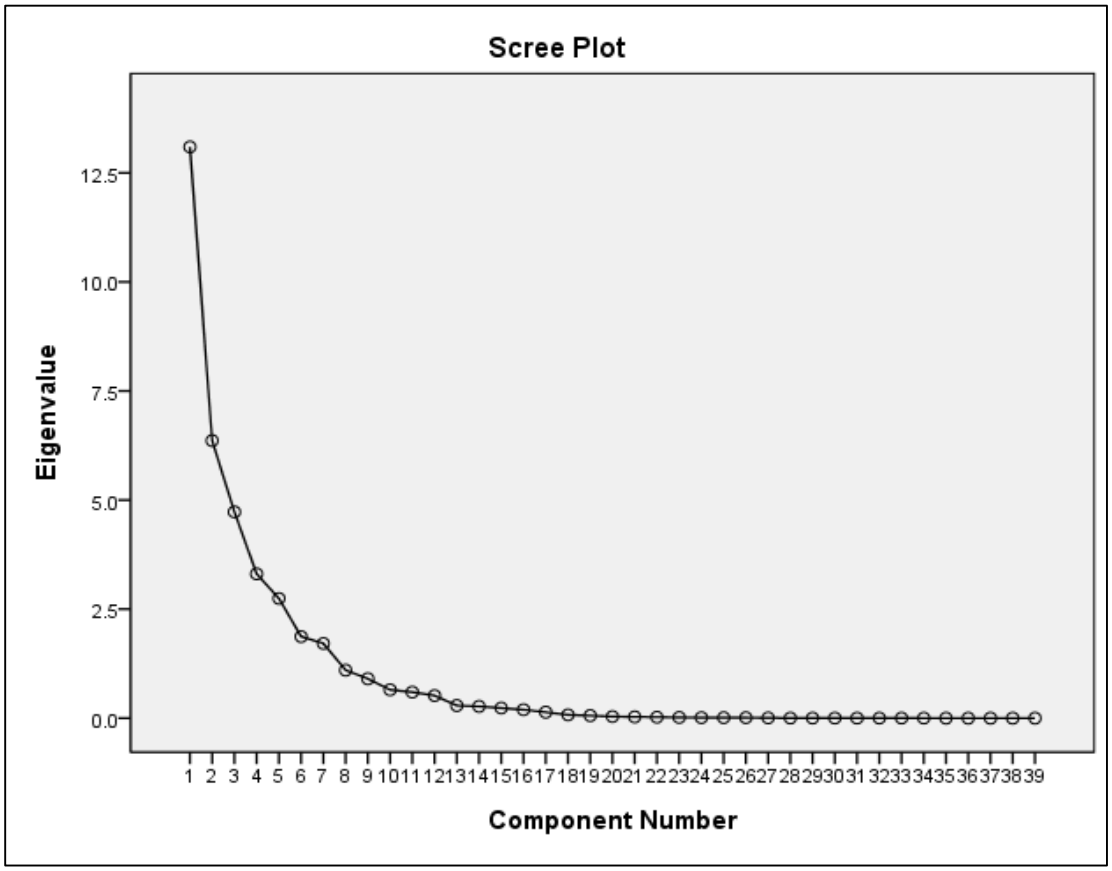

Component Matrix[a]							
	Component						
	1	2	3	4	5	6	7
D_12'	.779	.104	.260	.285	-.427	-.092	.016
D_2'3	.086	.471	.753	.371	.196	.061	.034
D_34	.795	-.069	.383	-.155	.286	.208	-.063
D_13	-.092	.432	.868	-.046	-.089	.117	-.031
D_14	-.450	-.411	.574	-.006	-.190	.401	-.197
D_2'4	.006	-.777	.504	.247	.031	.188	-.121
Oh-N1	.377	-.014	.609	.104	-.483	-.130	.162
Oh-O3	-.146	.239	.699	.592	.105	-.045	.067
Oh-N4	.066	-.817	.467	.239	.027	.103	-.096
CN1Oh	-.587	-.263	-.109	-.047	.536	-.133	.344
CO3Oh	.327	.011	-.763	-.115	.197	.227	.070
CN4Oh	-.267	.809	-.296	.223	-.118	-.020	.206
BOhN1	.749	.068	-.374	.323	.040	-.015	-.028
BOhO3	.216	.692	.367	-.195	.224	.151	-.053
BOhN4	-.315	.466	.141	-.012	-.029	.243	-.182
A_12'3	-.563	.142	.454	-.561	-.223	.201	-.059
A_2'34	-.678	-.569	-.133	.272	-.270	.092	-.074
A_12'4	-.668	.454	-.107	-.475	-.148	.194	-.057
A_134	-.731	-.154	-.504	.322	-.206	.091	-.028
A_132'	.652	-.301	-.510	.087	-.295	-.234	-.043
A_142'	.767	.409	-.082	.240	-.269	-.253	.076
A_143	-.191	.577	.644	-.193	.035	-.235	.060
A_2'13	-.128	.211	.082	.615	.680	.047	.134
A_2'14	.220	-.774	.173	.362	.344	-.043	.012
A_2'43	-.094	.854	.181	.090	.210	-.280	.096
A_32'4	.871	.020	.018	-.389	.159	.105	.015
A_314	.899	-.130	.220	-.253	.207	.022	.000
CN1O2'	-.547	-.398	.196	-.316	.397	-.168	.347
CO2'N1	-.441	.350	-.133	-.007	.272	-.108	-.683
CO2'O3	.797	.169	.139	-.303	.099	.061	-.042
CO3O2'	.185	-.072	-.913	-.120	.101	.114	.027
CO3N4	-.475	-.398	.346	.096	-.416	-.334	.098
CN4O3	-.274	.702	-.189	.227	-.262	.055	.195
DA_1	.372	.417	-.315	.404	-.229	.300	-.274
DA_2	.159	.196	-.006	.401	.088	.644	.226
DA_2'	.063	-.096	-.027	-.179	-.318	.385	.663
DA_12'34	.597	-.362	.526	-.274	-.108	-.026	.000

Extraction Method: Principal Component Analysis.

a. 7 components extracted.

Factor loadings on first three components (axes) for PCA2

PBP	F1	F2	F3	PBP	F1	F2	F3
AM_R39_1W79	-0.52	-0.52	-0.81	SM_K15_1ESI	-0.45	0.96	0.06
AM_R39_1W8Q	-0.65	-0.73	-0.53	SM_K15_1SKF	-0.35	1.35	1.07
AM_R39_1W8Y	0.78	-0.59	0.57	EC_1b_3FWL	-0.06	0.02	-0.77
AM_R39_2VGJ	-0.33	0.02	-0.82	EC_1b_3FWM	0.20	0.16	-0.71
AM_R39_2VGK	-0.62	-0.50	-0.68	NG_2_3EQU	0.14	0.52	-1.06
AM_R39_2WKE	-0.55	-0.13	-0.55	NG_2_3EQV	1.37	-0.69	-1.03
BS_4a_1W5D	-0.37	-1.50	-1.13	SA_2_2OLU	-0.85	-0.65	-0.54
BS_4a_2J9P	-0.71	-0.60	0.48	SA_2_2OLV	0.35	1.71	-1.58
EC_4_2EX2_A	0.79	-3.30	1.86	SA_2_3DWK	0.27	2.06	-0.64
EC_4_2EX2_B	-0.52	-1.13	-0.55	SA_2a_1MWR	-0.74	0.85	0.40
EC_4_2EX6	-0.27	-0.42	-0.31	SA_2a_1MWS	-0.47	-0.25	-0.17
EC_4_2EX8	-0.29	-0.08	-0.49	SA_2a_1MWT	-0.96	0.56	0.76
EC_4_2EX9	-0.36	-0.23	-0.23	SA_2a_1MWU	-1.29	0.02	1.42
EC_4_2EXA	-0.42	-0.36	-0.62	SA_2a_1VQQ	-0.82	0.14	-0.07
EC_4_2EXB	-0.15	-0.36	-0.72	SP_1a_2C5W	-1.36	-0.62	0.49
EC_5_1HD8	2.40	1.85	-0.85	SP_1a_2C6W	-0.89	-0.25	2.33
EC_5_1NJ4	2.39	1.32	0.17	SP_1a_2V2F	-0.67	1.23	2.44
EC_5_1NZO	2.14	0.19	0.32	SP_1a_2ZC5	-1.40	0.09	0.42
EC_5_1Z6F	1.87	-0.04	-0.16	SP_1a_2ZC6	-1.13	0.05	0.82
EC_5_3BEB	1.86	-0.42	1.26	SP_1b_2JCH	0.33	0.23	-0.66
EC_5_3BEC	1.84	0.07	-0.27	SP_1b_2JE5	-0.66	0.56	-0.09
EC_6_3IT9	1.79	0.50	1.00	SP_1b_2BG1	-0.30	1.05	-0.51
EC_6_3ITA	2.18	2.02	1.42	SP_1b_2FFF	-0.52	0.43	-0.98
EC_6_3ITB	2.08	0.33	1.04	SP_1b_2UWX	-0.41	0.74	-0.33
HI_4_3A3D	-0.12	-1.35	-1.03	SP_1b_2UWY	-0.22	0.67	-1.72
HI_4_3A3E	-0.28	0.48	0.71	SP_2b_2WAD	-0.62	0.13	-0.35
HI_4_3A3F	0.07	-0.53	-0.51	SP_2b_2WAE	-0.29	-0.10	-0.50
HI_4_3A3I	-0.65	0.70	0.75	SP_2b_2WAF	0.14	0.74	-1.10
HI_5_3A3J	1.49	-0.62	0.34	SP_2x_1PYY	-0.77	0.81	0.38
MTb_DacB2_2BCF	-0.45	-0.98	-0.94	SP_2x_1QME	-1.09	-0.09	-0.32
SA_4_1TVF	1.29	-3.08	-0.26	SP_2x_1QMF	-0.32	1.15	0.23
SA_4_3HUM	1.00	-2.26	0.33	SP_2x_1RP5	-0.95	-0.28	4.57
SA_4_3HUN	1.34	-2.32	-0.04	SP_2x_2Z2L	-0.77	-0.27	-0.29
SM_K15_1ES3	0.24	0.73	0.57	SP_2x_2Z2M	-0.87	0.02	-0.24
SM_K15_1ES4	0.21	0.21	0.13	SP_2x_2ZC3	-0.59	0.24	-0.58
SM_K15_1ES5	-0.78	0.41	-0.05	SP_2x_2ZC4	-0.71	-0.09	-0.60

Statistical tests of differences in DA_1 distribution

The DA_1 parameter value distribution was bimodal, with values associated with different subsets of PBP classification (Figures 8 and 18). Three non-parametric statistical tests of the significance of the association of DA_1 values with 1) either carboxypeptidase or transpeptidase classification, or 2) HMM vs LMM classification were performed with and without the SM_K15 values included (Mann-Whitney U test, Kruskal-Wallis test, and Kolmogorov-Smirnov test). All gave $P<0.001$, demonstrating a highly significant association between the DA_1 value and LMM/carboxypeptidase or HMM/transpeptidase classification.

DISCUSSION

Alignment

The first issue was how to align these structures. Our initial effort was based on all of the atoms of the Ser2 residue (the Ser residue in the SXXK motif). However, it was observed that Ser2 is found (predominantly) in two alternative side chain conformations (Figure 7), and using all the Ser2 atoms for alignment was therefore not a very good approach for those PBP structures with the alternate conformation. The backbone atoms of Ser2 (N, CA, C, O) were very closely aligned in all PBP structures (Figure 7), and this provided a convenient and reliable basis for aligning these structures.

Superpositioning of key catalytic complex atoms

During the initial structure alignment effort, we observed that the position of the Ser2-OG atom was virtually identical in acylated and transition-state analog complex structures, and this position is referred to as the catalytically competent or “up” position

(Figure 7). In contrast, in unacylated complexes the Ser2-OG atom was found in two alternative conformations: about 50% of the time in the up (catalytically competent) position and the other 50% in the down (catalytically incompetent) position.

To provide the best possible basis for comparison of PBP active site geometry, it was desirable to minimize the variability of the Ser2-OG atom position, which was clearly not associated with catalysis. This was accomplished by using an overlay of each PBP with the reference structure – *E. coli* PBP 5 with a peptide boronic acid transition-state analog (the EC_5 1Z6F structure). These overlays provided the position of the Ser2-OG atom in the catalytically competent (corrected) position. This superpositioning also provided the position for the acyl carbon atom (equivalent to the position of the boron atom in the 1Z6F structure, denoted as B) and the position of the hydrolytic water for deacylation (denoted as Oh)[92] (Figure 7). To identify the superpositioned Ser2-OG atom as from the superpositioned structure, it is designated with a prime (e.g., O2') in parameters depended on this atom location (Table 5).

To verify this approach, one of the calculated parameters included in this effort was the D_22' parameter, which is the distance between the actual Ser2-OG atom of the structure in question and the superpositioned Ser2-OG atom. A plot of D_22' as a function of PBP ID and of acylated/transition-state analog ligated or unacylated status is given in Figure 9. D_22' was less than 1.0 Å for 46 structures out of 47 acylated/transition-state analog ligated structures (the one outlier is the SP_1b 2UWY structure). Out of 53 unacylated structures, the value of D_22' was less than 1.0 Å for 25 structures, and greater than 1.0 for 28 structures. D_22' was essentially uncorrelated with all of the other parameters included in this study except DA_2 (the uncorrected dihedral angle for Ser2 - correlation coefficient of 0.89). The

correlation of D_22' with DA_2 is expected, since DA_2 determines the (uncorrected) orientation of Ser2-OG. The lack of correlation with all of the other positionally corrected parameters included in this study (absolute correlation coefficients all <0.33, with an average absolute correlation coefficient of 0.11) demonstrates that the correct or incorrect placement of Ser2-OG does not have an effect on any other parameter in this system, and thus on the location of other atoms within the active site of the PBPs.

Parameter extraction and preliminary analysis

A number of geometrical parameters were then extracted from these aligned PBP structures, including distances, angles, and dihedral angles (Table 5). Summary statistics were calculated (Table 6), and plots prepared to visualize the results (Figure 8-14). Examination of these plots revealed that a number of structures had parameter values which deviated substantially from the norm, and appeared to be outliers. In order to assess outliers, a measure of distance to the global center (average) of all parameter values was used; the NRMSD.

A plot of NRMSD vs PBP ID, and the corresponding histogram, are shown in Figure 15. Examination of this plot in conjunction with plots of individual parameters, and the features of each structure as given in Table 3, led to the assessment that the EC_5 1NZU and 1SDN structures are outliers, and this observation is supported by the observation that the 1NZU enzyme is catalytically inactive, and that the 1SDN enzyme is deacylation defective [89,92]. The SP_1b 2JCI structure also was identified as an outlier. Examination of the 2JCI structure and parameter plots reveals that the anomaly in this structure is an unusual positioning of the Ser2-CB atom (Figure 14 plot for DA_2').

Several separate clusters of NRMSD values seemed apparent for the SM_R61 structures, with several seeming to deviate substantially from the main group of SM_R61 structures and other PBPs (3PTE_BB, 1IKG, 1PW1A, and 1PW1_B) (Figure 15). The SM_R61 enzyme is a Class B LMM PBP, with a significant difference in its active site residues (YXN and HTG motifs in place of SXN and KTG motifs in all other PBP classes – Table 2). There were also several PBPs, which demonstrate an intermediate level of variation from the norm, including the EC_4 2EXA_A structure, the SP_2x 1RP5 structure, and several SM_R61 structures (3PTE_AB, 3PTE_BA, and 1HVB_B). It is notable in regard to the SP_2x 1RP5 and 1K25 structures that both of these are β-lactam resistant enzymes, and that their deviation from the norm may be related to their β-lactam resistance.

First round PCA

In order to get a global (all parameters) assessment of similarities and differences among the geometrical parameters included in this study, PCA was applied to this data set. The numerical results are included in the Tables 8 and 9. Plots of the location of each PBP from the first round PCA (PCA1) on the first three factor axes (principal components) are given in Figure 16 A-C. As illustrated by the ellipses drawn in these PCA plots, the PBPs can be segregated into several clusters (note that some of the clusters are only revealed by examining all three PCA1 plots in Figure 16 panels A, B, and C). Among the SM_R61 enzymes three subclusters were observed (corresponding to the three groups observed in the NRMSD plot in Figure 15); one with SM_R61 structures which appear normal relative to all other PBPs (left SM_R61 cluster in Figure 16 A), one with SM_R61 structures of

intermediate deviation from the norm (middle SM_R61 cluster in Figure 16 A), and one with SM_R61 structures of high deviation from the norm (right SM_R61 cluster in Figure 16 A).

Outliers identified based on the NRMSD plot also appear as outliers in the PCA1 plots, including the EC_5 1NZU and 1SDN structures, and the intermediate case SP_2x 1RP5 structure. The AM_R39 2EXA_A and AM_R39 1W8Y structures only appear as outliers in F1 vs F3 and F2 vs F3 plots (Figure 16 panels C and B respectively). The three SA_4 structures also appear as a separate cluster, which is only clearly visible in the F1 vs F3 and F2 vs F3 plots. For the two NG_2 structures, one was grouped with the Main Cluster (3EQU) and the other (3EQV) was clustered with the EC_5/EC_6/HI_5 cluster.

Second round PCA

Since the SM_R61 enzyme has a substantially different constellation of active site residues than other PBPs (Table 2), the DA_3 and DA_4 parameters are undefined for SM_R61, and it seemed reasonable to exclude the SM_R61 structures from a second PCA to allow the DA_3 and DA_4 parameters to be included. It is also well known that outliers can adversely affect any statistical analysis, and for this reason it seemed reasonable to remove the EC_5 1NZU and 1SDN structures, since are both have drastically altered catalytic properties[91]. Finally, the SP_2x 1K25 structure appears as the worst outlier among all of the PBPs in the first round PCA, and – even though this structure corresponded to an active enzyme – it seemed reasonable to exclude this structure from the second round PCA. (Examination of an overlay of all the SP_2x structures reveals that the 1K25 structure deviates substantially from the other SP_2x structures.)

The numerical results from this second round PCA (PCA2) are given in Table 9, as are plots of location on the first three factor axes (Figure 17). The PBPs included in PCA2 segregate essentially the same as in PCA1, but in an expanded format since outliers have been omitted. The SP_2x 1RP5 structure still appears as a moderate outlier, as does EC_4 2EX2_A. The AM_R39 1W8Y structure also seems to be on outlier - it is located in a region between other clusters and well away from other AM_R39 structures. Overall, the same general pattern of clustering was observed in PCA2 as in PCA1. Of particular interest is that in both PCA1 and PCA2 the HMM Class A and B PBPs, the LMM Class C PBPs, and the SM_K15 LMM Class A PBPs cluster together in a Main Cluster. Outside of the main cluster are two LMM PBP Class A subclusters, the EC_5/EC_6/HI_5 subcluster and the SA_4 subcluster, and as noted above in first round PCA, several SM_R61 LMM Class B subclusters. The observation that the HMM Class A and B PBPs and the LMM Class C PBPs cluster together in the Main Cluster is particularly notable, since it indicates that these PBPs share a similar overall global catalytic residue geometry. This observation indicates that the enigmatic lack of activity observed in the HMM PBPs does not appear to be associated with some global misalignment of the catalytic residues. The observation that separate subclusters are observed for several of the LMM Class A PBPs indicates that the LMM Class A demonstrate a greater degree of variability in their catalytic residue geometry than the HMM Class A and B and LMM Class C PBPs. This observation may be relevant to assessing mechanistic similarities and differences between different PBPs.

Identification of two parameters of interest

After completing the PCA, summary statistics, plots, and histograms of individual parameters were reexamined to look for easily identifiable structural and functional correlations. An examination of the summary statistics in Tables 6 and 7 and the plots shown in Figures 8-14 revealed the following observations. First, among the distances included in this study, D_14 was particularly highly conserved among all the PBPs included in this study, including the R61 enzyme (Table 6, average distance of 5.44 Å, with a SD of 0.63 Å, for a relative SD of 11%) (Figure 18). This is therefore one of the longest distances among highly conserved key atoms in the PBP active site, and the least (in %SD terms) variable distances in the PBPs. This distance is also conserved between the SM_R61 PBP structures and all other PBP structures (see Table 7). This observation suggests that the distance between the Lys-NZ of the SXXK motif and the Lys-NZ or His-NE2 of the K(H)TG motif is somehow important for the function of the PBPs. While the role of Lys1 in catalysis seems generally agreed upon (reviewed in[21]), at the present time the role of the Lys4/His4 residue in PBP catalysis is uncertain, but numerous studies have implicated this residue as important in either catalysis or substrate binding[21,92,130-132]. The observation that the D_14 distance is highly conserved may be useful in assessing alternative possibilities for the role of the Lys4/His4 residue in substrate binding and/or catalysis. One possibility, which can be suggested, is that this distance is important in controlling the protonation state of these (and other nearby) residues during the catalytic cycle, such that both residues would prefer to not be simultaneously protonated during the catalytic cycle.

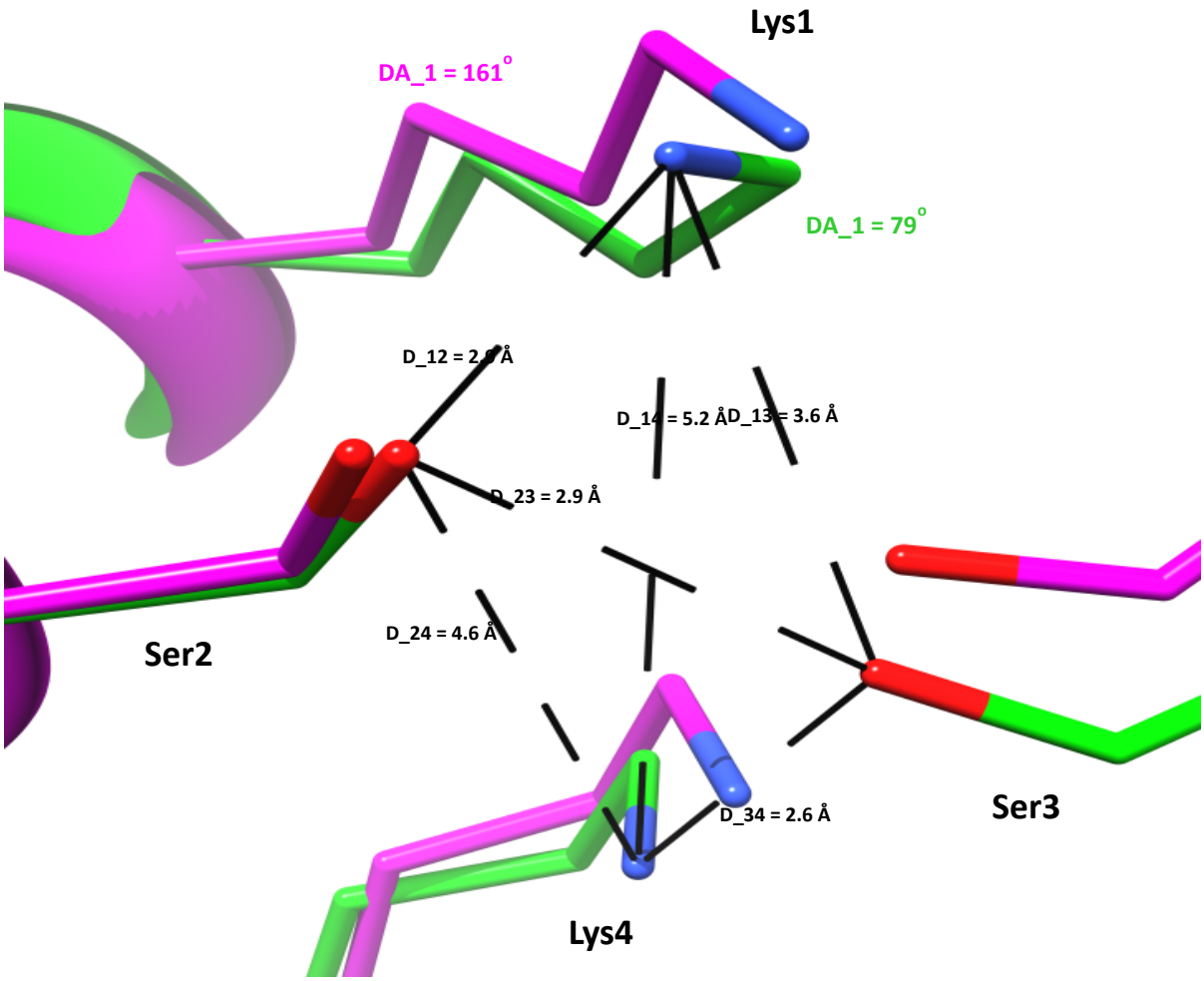

Figure 18: Overlay of the four key catalytic residues from a Main Cluster LMM/hydrolase (AM R39 1W79, green) and a Main Cluster HMM/transpeptidase (SA 2a 1VQQ, magenta). Also indicated in this figure are distance designators and values between key atoms for the AM R39 enzyme, and the DA 1 values for the two enzymes illustrating the difference in geometry between low and high DA 1 value.

A second noteworthy parameter is the DA_1 dihedral angle – the dihedral angle among terminal side chain atoms of the Lys1 residue (of the SXXK motif). This parameter shows a pronounced two-peak profile in its histogram (Figure 8). Further inspection reveals that DA_1 has one value in very nearly all of the HMM PBPs, and a different value for nearly all of the LMM PBPs (Figure 18). The LMM PBPs nearly always have hydrolase activity [10,17-21], whereas the HMM PBPs – while often devoid of activity when purified – are associated with transpeptidase activity *in vivo*[8,28,80-83]. As noted in the introduction, the SM_K15 enzyme is a notable exception to this general pattern in that it is a LMM PBP with strict transpeptidase activity [26]. As can be seen in Figure 8, The SM_K15 structures give DA_1 values in both groupings, with the wild type SM_K15_1SKF structure having A DA_1 value associated with a HMM/transpeptidase grouping. However, these few LMM/transpeptidase structures are insufficient to determine if DA_1 value is associated with LMM vs HMM classification, or hydrolase vs transpeptidase activity. In addition, several of the LMM PBPs included in this study, notably the HI_4 and HI_5 structures, have not yet been characterized enzymatically (Table 4) and their classification as hydrolases is as yet uncertain.

The correlation between DA_1 and LMM/hydrolase vs HMM/transpeptidase activity (excluding the SM_K15 enzyme) is quite strong, with 76% of LMM/hydrolases having DA_1 values <125º, and with 92% of HMM/transpeptidase having DA_1 values >125º. Three non-parametric test of significance of this difference in distribution were performed for both LMM vs HMM and hydrolase vs transpeptidase activity (Mann-Whitney U test, Kruskal-Wallis test, and Kolmogorov-Smirnov test), and all three test for both associations gave P-values<0.001, including or excluding the SM_K15 enzyme, demonstrating that this

difference is clearly unlikely to be due to random chance. This observation clearly indicates that DA_1 is either strongly associated with LMM vs HMM classification, or with alternative reaction path between transpeptidase vs hydrolase activity.

In summary, this study demonstrates a novel multivariate global comparison of geometrical relationships between key active site residues in the PBPs of known structure. One of the first observations was that a number of PBP structures show substantial variation from the norm (i.e., are outliers). Some of these were from inactive mutants, which was expected, but some were from active enzymes. This indicates that some care must be used in interpreting the results from individual structures. The use of PCA as a data reduction technique to provides a very convenient overview of the interrelationships between global active site residue geometries. However, the careful examination of individual parameter plots was key to revealing structural/functional correlations for individual parameters, which were not apparent in the PCA analysis (e.g., the D_14 distance conservation and the DA_1 correlation with HMM/transpeptidase or LMM/hydrolase classification. A number of significant observations were made in this study. 1) The distance between the SXXK-motif Lys-NZ atom and the Lys/His-nitrogen atom of the (K/H)T(S)G-motif was highly conserved, suggesting importance for PBP function. 2) Distribution of the dihedral angle for the SXXK-motif Lys side chain was bimodal, and strongly correlated with HMM/transpeptidase vs LMM/hydrolase classification ($P<0.001$). 3) Principal components-based cluster analysis revealed several distinct clusters, with the HMM Class A and B, the SM_K15 LMM Class A, and the LMM Class C PBPs forming one “Main” cluster, and demonstrating a globally similar arrangement of catalytic residues within this group. The third observation suggests

that the lack of activity observed in purified HMM PBPs is not due to misalignment of their catalytic machinery in their purified state. Observation 2 indicates that the geometry of the Lys residue of SXXK motif is associated with a key classification and/or reaction pathway distinction among the PBPs. The analysis demonstrated in this study provides a very convenient "map" of active site geometrical relationships within the PBPs, and is expected to be of utility for further exploration of PBP structure, function, and mechanism. This approach also allows outlying structures to be identified, which is likely to facilitate future structural analyses. Extension of this effort to related members of this enzyme family, namely the β-lactamases and the HMM Class C PBPs, could provide further insight into this groups of enzymes.

CHAPTER 3

SUBSTRATE SPECIFICITY STUDIES OF LOW MOLECULAR MASS PBP ACTINOMADURA R39

Note: Some of the procedures (substrate synthesis, CPase assay, pH dependence and stability), presented in this chapter have been very well established in our lab for other LMM enzymes (NG PBP3, NG PBP4, and EC 5) and are adapted[43,92,133-135].

INTRODUCTION AND RATIONALE

Actinomadura is a Gram-positive organism that uses the stem peptide L-Ala-D-iGln-*meso*-DAP-D-Ala-D-Ala in cell wall crosslinking reactions[21,45] (Figure 19). The *Actinomadura* R39 is a LMM class C PBP that catalyzes transpeptidase, carboxypeptidase and endopeptidase activities and helps to catalyze the formation and regulation of crosslinking in peptidoglycan biosynthesis[45,73]. This LMM class C PBP is loosely associated with the cell membrane and is a soluble protein unlike other PBPs, which are strongly anchored in the membrane.

Given the importance of PBPs, one would imagine these enzymes would exhibit high substrate specificity, but elucidation of their specificity has been elusive[21]. LMM B and LMM C enzymes are quite well characterized for the substrate specificity, whereas LMM A and HMM class enzymes still remain a mystery[21,45,73] (please refer to chapter 1 - introduction and literature review for background on peptidoglycan substrates and general specificity of PBPs). Substrate specificity has been studied on different LMM PBPs such as *Streptomyces* R61 (LMM B), *E. coli* (EC) PBP5 (LMM A), *Neisseria gonorrhoeae* (NG) PBP3 (LMM C),

Neisseria gonorrhoeae PBP4 (LMM A), and *Bacillus subtilis* (BS) PBP4a (LMM C)[35,43,45,49,86,92,121,133,134,136-139]. Different PBPs showed different substrate specificities, for e.g., *Streptomyces* R61 LMM PBP has shown a high degree of specificity for a glycine-substituted pimelic acid side chain, analogous to that found in its natural diaminopimelic acid (DAP)-containing substrates[21,48,139](Figure 19), NG PBP4 has specificity for N^{ε}-acylated substrates[133], whereas EC PBP5 did not show any substrate specificity[134].

Even though NG PBP3, *Actinomadura* R39, and BS PBP4a belong to the same group of classification (LMM C); these enzymes have different substrate specificities as demonstrated in our previous studies[43,49,133,134]. NG PBP3 shows pronounced substrate specificity towards acylated N^{ε}-amino acid side chain whereas *Actinomadura* R39 has the opposite substrate specificity to that of NG PBP3, where it shows specificity toward unacylated N^{ε}-amino acid side chains, *Bacillus subtilis* (BS) PBP4a shows no such substrate specificity in particular. Structural studies of R39 with a peptidoglycan like substrate also revealed a binding site for the side chain α-aminopimelyl moiety (unacylated)[86], which made more interactions that are favorable over acylated side chain. (Figure 19 shows the stem peptide of *Actinomadura* R39 and substrates used in this study).

It is evident from the substrate specificity studies on different LMM PBPs that they do not share the same affinity towards different substrates[45]. Even though studies have identified the substrate specificity profile for *Actinomadura* R39[73,136,140], there has not been a methodical approach to probe the specificity of the reaction with particular elements of peptidoglycan peptide. We sought out to identify the key elements of substrate specificity for *Actinomadura* R39 by using tripeptide (L-Lys-D-Ala-D-Ala) substrates having different modification of the Lys side chain. Knowledge of the substrate specificity of *Actinomadura*

R39 could provide valuable insight for its role in cell wall biosynthesis and of the specificity and role of LMM PBPs in general. The specificity for peptide chain length was also evaluated with pentapeptide substrates (L-Ala-γ-D-Glu-L-Lys-D-Ala-D-Ala) similar to that of tripeptide studies. pH profile was established along with pH stability to determine the optimum enzyme activity at different pHs using the standard substrates Ac-L-Lys (Ac)-D-Ala-D-Ala **(7)** and Ac-L-Lys-D-Ala-D-Ala **(10)**.

Transition state analogs (TSAs) are compounds that mimic the transition state of an enzyme-catalyzed reaction, and are often potent inhibitors of the respective enzyme[141-143]. TSAs are powerful probes of the enzyme structure, function, mechanism, as well as potent inhibitors. The peptide boronic acid inhibitors were found to be the most effective transition state PBP inhibitors found in our own laboratory and have subsequently been used by several other researchers[73,84,92,143,144]. The specificity studies on tripeptides against R39 yielded good saturating substrates with specificity for unacylated N^{ε} amino acid side chain. From the substrate specificity data, peptide boronic acid inhibitors corresponding to the best substrates were evaluated for inhibition against R39. Transition state inhibitors that mimic the best substrates of an enzyme should in principle are the best inhibitors for the particular enzyme. The substrate specificity was then correlated with analogous peptide boronic transition state inhibitors.

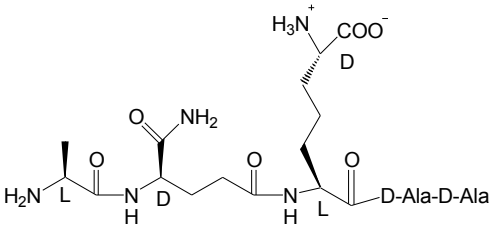

L-Ala-D-iGln-*meso*-DAP-D-Ala-D-Ala

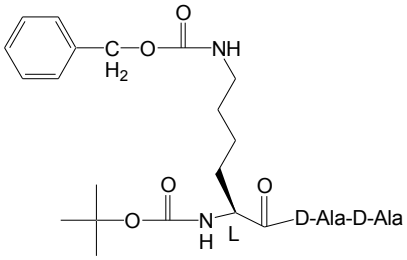

Boc-L-Lys(Cbz)-D-Ala-D-Ala (3)

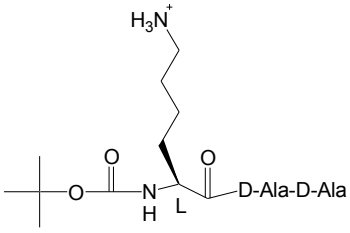

Boc-L-Lys-D-Ala-D-Ala (4)

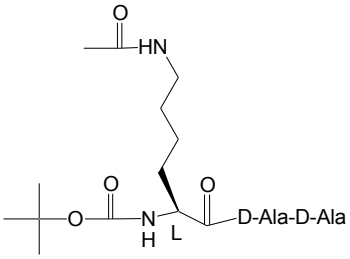

Boc-L-Lys(Ac)-D-Ala-D-Ala (5)

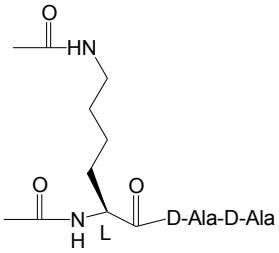

Ac-L-Lys(Ac)-D-Ala-D-Ala (7)

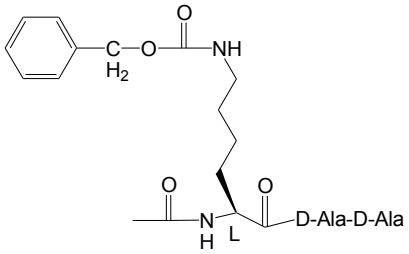

Ac-L-Lys(Cbz)-D-Ala-D-Ala (9)

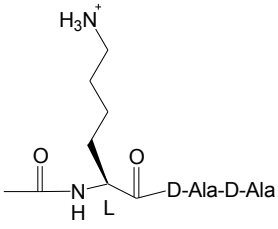

Ac-L-Lys-D-Ala-D-Ala (10)

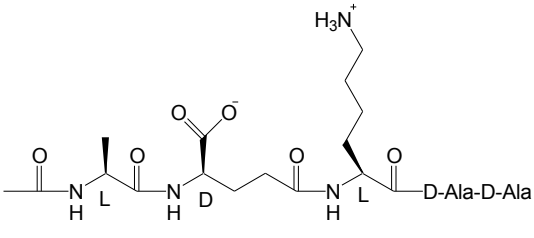

Ac-L-Ala-r-D-Glu-L-Lys-D-Ala-D-Ala (17)

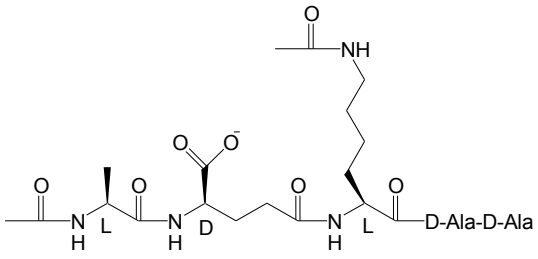

Ac-L-Ala-r-D-Glu-L-Lys(Ac)-D-Ala-D-Ala (18)

Figure 19: Structure of stem peptide in *Actinomadura* R39 (shown at the top) and substrates used in this study.

MATERIALS AND METHODS

General materials and reagents

Tris, D-Ala, horse-radish peroxidase (HRP, Type X, 21 mg/ml as an ammonium sulfate suspension, 291 units/mg), ampicillin, and FAD were from Sigma-Aldrich (St. Louis, MO). Pig kidney D-aminoacid oxidase prepared as an ammonium sulfate suspension (DAO; 5 mg/ml) was from Roche Molecular Biochemicals (Indianapolis, IN). The PBP/CPase substrate diacetyl-L-Lys-D-Ala-D-Ala (Ac-L-Lys (Ac)-D-Ala-D-Ala) and substituted X-K(Y)AA substrates (designated as X on α-position and Y on γ-position) were purchased from Sigma-Aldrich or synthesized using solution-phase peptide synthesis. Amplex Red (AR) (10-acetyl-3, 7-dihydroxyphenoxazine) was from Molecular Probes (Eugene, OR). Protein concentrations were determined by Micro Bradford assays (Sigma-Aldrich) following the manufacturer's protocol.

Synthesis of substrates

Peptide substrates were synthesized as described previously and are outlined in Figures 20 and 21[49,84]. Boc-L-Lys(Cbz) and other protected amino acids were from Sigma-Aldrich (Saint Louis, MO) or Bachem (King of Prussia, PA). General reagents and solvents, were from Sigma-Aldrich (St. Louis, MO). LC-MS was performed on an Applied Biosystems Sciex 3200 QTrap mass spectrometer equipped with a Shimadzu UFLC HPLC system using electrospray ionization (ESI) source and run using Analyst® v. 1.4.2. C_{18} or C_8 Nucleodur column 100-5 C18 125 x 3 mm (Macherey–Nagel, Bethlehem, PA) was used with an elution gradient of; solvent A (0.1% FA in water) for 1 min, then 0 to 100% solvent B (0.1% FA in 30% water, 70% acetonitrile) in 10 min, and then 0% to 100% solvent C (0.1% of FA in acetonitrile) in 2 min, and chromatograms monitored at 205 and 260 nm.

Preparative HPLC of final substrates was performed on a preparative C_{18} column (Econosil, 22 x 250 mm, 10 μm particles) at 5 mL/min with an elution gradient of; 100% of solvent A initially, then 10-100% solvent B in 60 min, then 0-100% solvent C in 30 min.

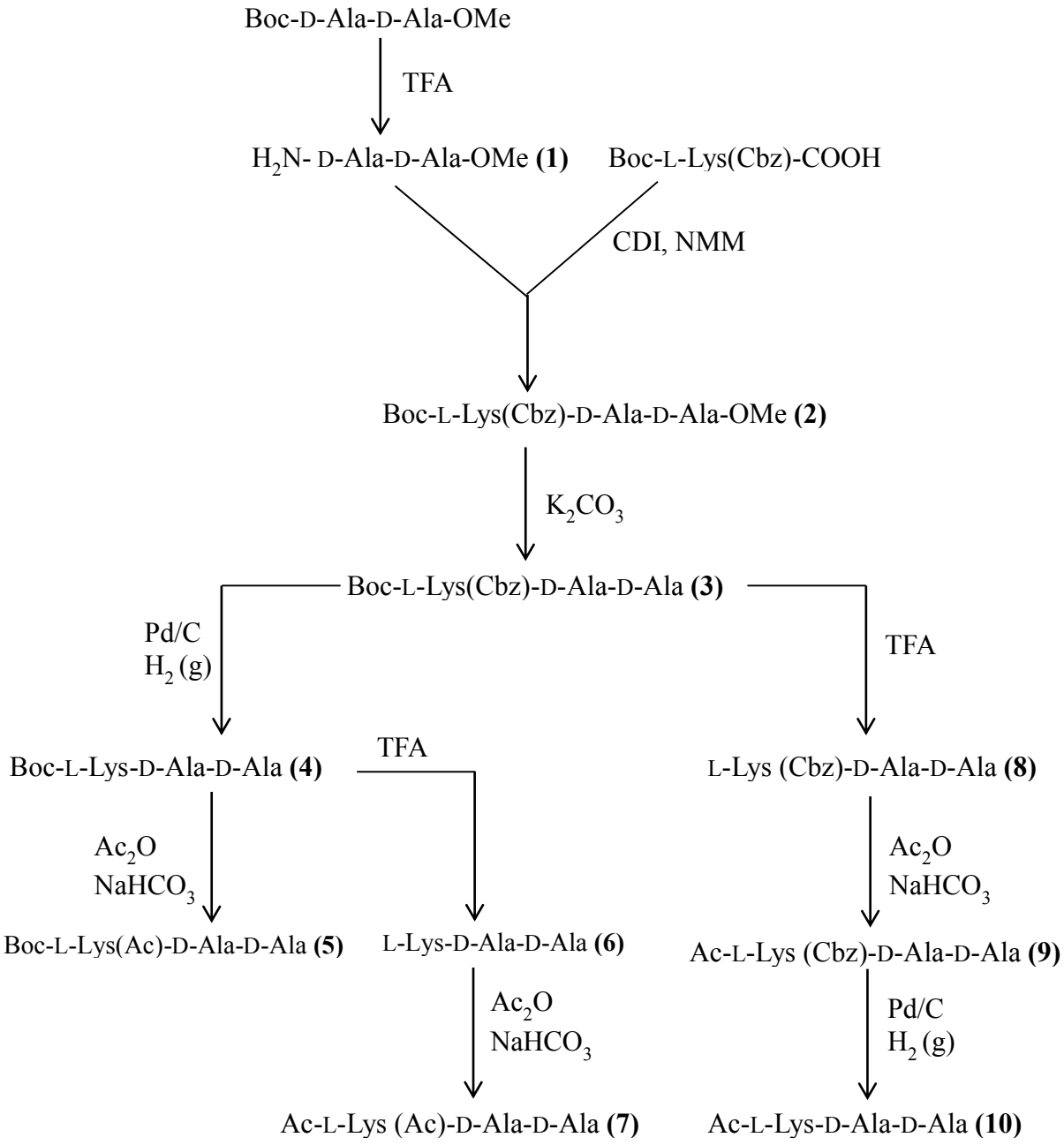

Figure 20: Scheme showing synthesis of tripeptides

Abbreviations: TFA: triflouroacetic acid, CDI: Carbonyldiimidazole, NMM: N-methyl morpholine, Pd/C: palladium on carbon

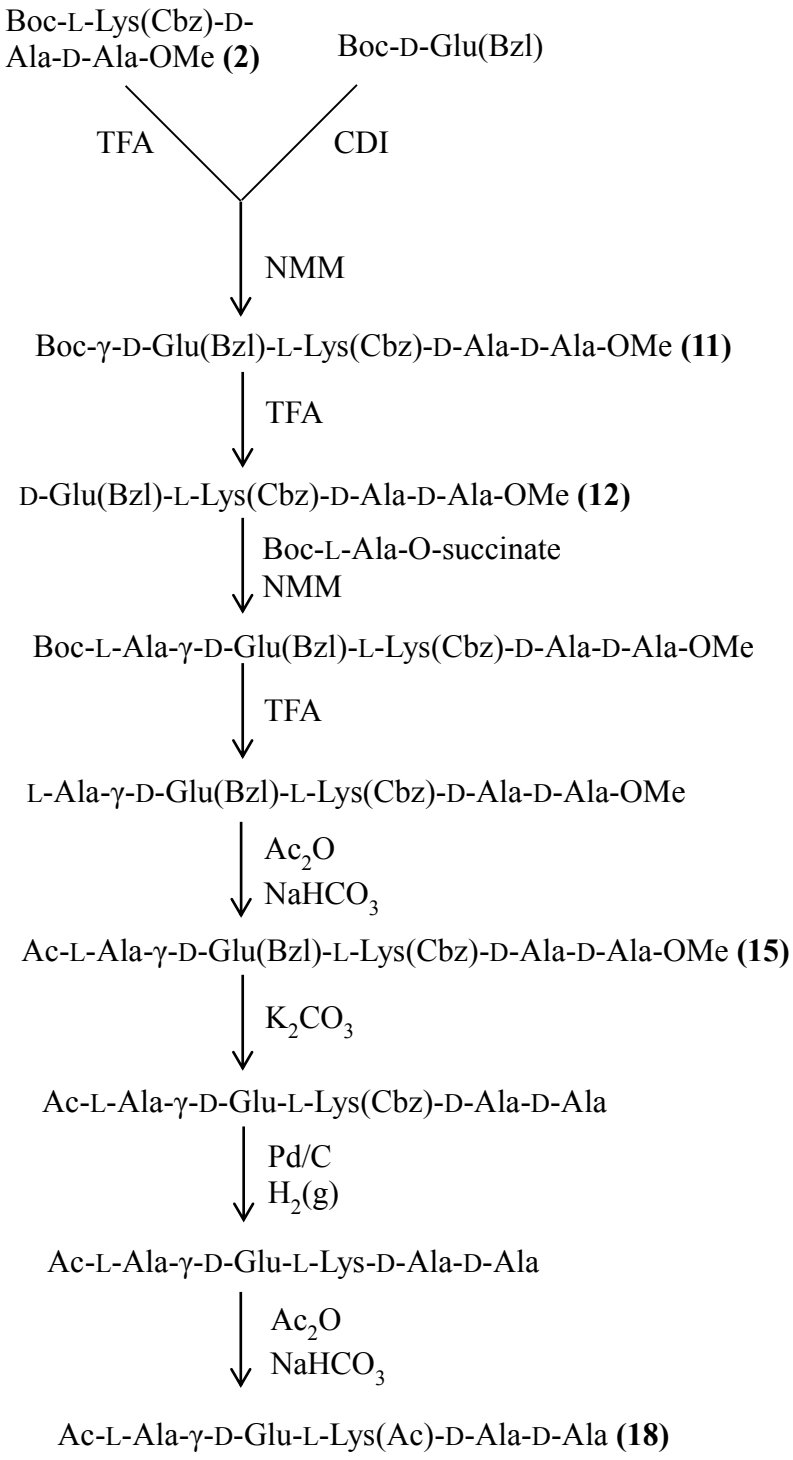

Figure 21: Scheme showing synthesis of pentapeptides

TFA.NH_2-D-Ala-D-Ala-OMe **(1)**[84]. To 14.6 gm of Boc-D-Ala-D-Ala-OMe (53.2 mmol) added 50 ml of ice cold TFA, and the reaction was kept on ice for 15 min and at room temperature for another 60 min. The completed reaction was confirmed by ninhydrin test for the presence of free amino group. The reaction was evaporated and dried under high vacuum. The product was dissolved in THF and used in the next reaction.

Boc-L-Lys(Cbz)-D-Ala-D-Ala-OMe **(2)**[49]. 24.3 gm of Boc-L-Lys(Cbz) (64 mmol) was dissolved in 100 ml THF and added 11 gm of carbonyldiimidazole (CDI) (68mmol). The mixture was added to TFA.NH_2-D-Ala-D-Ala-OMe (1) along with 17.6 ml of N-methyl morpholine (160 mmol). Checked the pH to make sure it was basic and the reaction was kept at room temperature for overnight (~14 hrs) and checked by LC-MS for completion, quenched with 100 ml of 1M $NaHCO_3$ and evaporated at a temperature not exceeding 40ºC. The reaction mixture was extracted with 3 equal volumes of methelene chloride. The combined organic extracts were washed with 1M HCl, 1M $NaHCO_3$, dried over anhydrous $MgSO_4$, and evaporated to dryness. The product was recrystallized from ethyl acetate and hexane mixture, filtered, dried and checked by LC-MS.

Boc-L-Lys(Cbz)-D-Ala-D-Ala **(3)**[49]. Boc-L-Lys(Cbz)-D-Ala-D-Ala-OMe (2) (5.36 gm, 10 mmol) was dissolved in 75 ml of 1:1:1: methanol/acetonitrile/water and cooled to 0ºC followed by the addition of 1.4 gm of K_2CO_3 (10 mmol). Kept the reaction in refrigerator at 4ºC. Additional 1 equivalents of K_2CO_3 were added after 12 hr and 24 hr. The reaction was let go for 72 hrs and checked by LC-MS for completion. The reaction was quenched with 1M HCl and the solvents methanol and acetonitrile were removed under high vacuum. The compound was extracted with one volume of ether to remove any traces of unreacted starting material. The pH of the aqueous layer was adjusted to 2 with 1M HCl, and the product was

extracted with 4 equal volumes of chloroform. The combined organic layers were dried over $MgSO_4$, evaporated and dried under high vacuum. The residue was dissolved in methanol/water and titrated to pH 7 with 1M $NaHCO_3$ and evaporated to dryness. The residue was again dissolved in warm ether and ethyl acetate mixture three times to get a white solid powder. Purity and identity was checked by LC-MS.

Boc-L-Lys-D-Ala-D-Ala **(4)**[49]. To a solution of 1.5 gm of Boc-L-Lys(Cbz)-D-Ala-D-Ala (3) (2.75 mmol) in 15 ml MeOH, added 150 mg 10% activated palladium on carbon in a flask flushed with N_2 gas for 15 min. The reaction mixture was stirred under hydrogen for 4 hrs and checked by LC-MS for completion. The reaction mixture was filtered and evaporated to dryness.

Boc-L-Lys(Ac)-D-Ala-D-Ala **(5)**[49]. 0.916 mmol of Boc-L-Lys-D-Ala-D-Ala (1) was taken in a round bottom flask and dissolved in MeOH. To the solution added 12 equivalents of $NaHCO_3$ (12 ml of 1M $NaHCO_3$) and 5 equivalents of acetic anhydride (471.7 µl). The reaction mixture was stirred for overnight (~14 hrs). The reaction was quenched and neutralized with 12 equivalents of HCl (12 ml of 1M HCl) and checked the pH. Analysis for completion of the reaction was performed by ninhydrin reagent to confirm the absence of free side chain amino group of lysine. The compound was extracted with 4 equal volumes of chloroform and acetonitrile, evaporated to dryness and purified by HPLC. The HPLC purified product was dried and dissolved in water and titrated to pH 7 with 1M $NaHCO_3$.

L-Lys-D-Ala-D-Ala **(6)**[49]. 0.916 mmol of Boc-L-Lys-D-Ala-D-Ala (1) was taken in a round bottom flask, added 6ml TFA and kept the reaction at room temperature for 1 hr. After completion of the reaction, the mixture was evaporated under high vacuum. The residue was dissolved in ethyl acetate and evaporated to dryness.

Ac-L-Lys(Ac)-D-Ala-D-Ala **(7)**[49]. L-Lys-D-Ala-D-Ala (6) (0.916 mmol) was dissolved in MeOH and acylation reaction was performed as described for 5. The compound was extracted with 15 ml warm acetone, filtered the salts and evaporated to dryness. Ether was added to the residue and evaporated to dryness. The final product was dissolved in water and titrated to pH 7 with 1M $NaHCO_3$.

L-Lys(Cbz)-D-Ala-D-Ala **(8)**[49]. 0.5 gm of Boc-L-Lys(Cbz)-D-Ala-D-Ala (3) (0.918 mmol) was taken and dissolved in 5 ml MeOH. Boc deprotection was performed as described for (1).

Ac-L-Lys(Cbz)-D-Ala-D-Ala **(9)**[49]. 0.918 mmol of L-Lys(Cbz)-D-Ala-D-Ala (8) was taken and subjected to acylation as described in 5. The product was extracted with 3 equal volumes of chloroform and evaporated to dryness. The residue was dissolved in warm MeOH/water and dried under high vacuum. The compound was purified by HPLC. The HPLC purified product was dried and dissolved in water and titrated to pH 7 with 1M $NaHCO_3$.

Ac-L-Lys-D-Ala-D-Ala **(10)**[49]. Cbz deprotection by hydrogenation of Ac-L-Lys(Cbz)-D-Ala-D-Ala (9) (0.45 mmol)was performed as described in (4).

Boc-γ-D-Glu(Bzl)-L-Lys(Cbz)-D-Ala-D-Ala-OMe **(11)**[49]. Boc deprotection of Boc-L-Lys(Cbz)-D-Ala-D-Ala-OMe (2) (1.59 gm, 2.96 mmol) was performed as described in (1). Activation of carboxyl group of Boc-D-Glu(Bzl) (1gm, 2.96 mmol) and coupling was performed as described in (2). The product was recrystallized from ethyl acetate, filtered, dried and checked by LC-MS.

D-Glu(Bzl)-L-Lys(Cbz)-D-Ala-D-Ala-OMe **(11)**[49]. Boc deprotection of Boc-γ-D-Glu(Bzl)-L-Lys(Cbz)-D-Ala-D-Ala-OMe (10) (700 mg, 0.92 mmol) was performed as described in (1).

Boc-L-Ala-γ-D-Glu(Bzl)-L-Lys(Cbz)-D-Ala-D-Ala-OMe **(13)**[49]. 0.92 mmol of D-Glu(Bzl)-L-Lys(Cbz)-D-Ala-D-Ala-OMe was dissolved in DMF and the coupling reaction was performed by adding 2 equivalents of Boc-L-Ala-O-succinate (529.6 mg) and 2 equivalents of NMM (203.3 µl). The reaction was performed at room temperature for 3 hours and quenched with 1M $NaHCO_3$ and stirred for 40 min. The desired compound was extracted 3 times with ethyl acetate, washed with 1M HCl and 1M $NaHCO_3$. The ethyl acetate layer was dried over $MgSO_4$, filtered and dried under high vacuum.

L-Ala-γ-D-Glu(Bzl)-L-Lys(Cbz)-D-Ala-D-Ala-OMe **(14)**[49]. Deprotection of Boc group of Boc-L-Ala-γ-D-Glu(Bzl)-L-Lys(Cbz)-D-Ala-D-Ala-OMe (12) was performed as described in (1).

Ac-L-Ala-γ-D-Glu(Bzl)-L-Lys(Cbz)-D-Ala-D-Ala-OMe **(15)**[49]. Acylation of free amine group of L-Ala was performed as described in reaction (5).

Ac-L-Ala-γ-D-Glu-L-Lys(Cbz)-D-Ala-D-Ala **(16)**[49]. Saponification of Ac-L-Ala-γ-D-Glu(Bzl)-L-Lys(Cbz)-D-Ala-D-Ala-OMe (14) was performed as described in reaction (3). The final product was purified by HPLC and checked by LC-MS.

Ac-L-Ala-γ-D-Glu-L-Lys-D-Ala-D-Ala **(17)**[49]. Cbz deprotection by hydrogenation of Ac-L-Ala-γ-D-Glu-L-Lys(Cbz)-D-Ala-D-Ala (15) was performed as described in (4). Half of the compound (23 mg, 0.043 mmoles) was dissolved in water and neutralized to pH 7 with 1M $NaHCO_3$.

Ac-L-Ala-γ-D-Glu-L-Lys(Ac)-D-Ala-D-Ala **(18)**[49]. 23 mg (0.043 mmoles) of Ac-L-Ala-γ-D-Glu-L-Lys-D-Ala-D-Ala (16) was used to acylate the side chain free amine group of Lysine. The reaction was performed as described in (5).

DD-Carboxypeptidase activity

PBP DD-carboxypeptidase activity (CPase) was determined by fluorescence detection of D-Ala using the Amplex Red (AR)-based assay described previously[135]. The assays (50 µL) were performed in 100 mM Tris, 100 mM NaCl, 0.5 mg/mL alkylated BSA, and 0-12 mM X-K(Y) AA substrates at pH 8.5. *Actinomadura* R39 diluted in assay buffer was used to start the assays. PBP reactions were stopped by the addition of the detection reagent (150 µL) containing 66.7µg/ml ampicillin, 13.3 µM AR, 0.5 units of HRP, 1.67 µg/mL FAD, and 0.015 units DAO in 100 mM Tris, pH 8.5. Fluorescence was read in a Tecan SpectraFluor Plus microtiter plate reader (Research Triangle Park, NC) after 30 min development with an excitation wavelength of 546 nm and emission of 595 nm. D-Ala standards were included in each experiment, and blanks were performed with and without substrate, in the absence and presence of PBP.

Data Analysis

Data was processed to obtain v/Et values, and analyzed by fitting with the appropriate equation by non-linear regression using IBM SPSS for Windows (Armonk, NY). The Michaelis-Menten equation shown in Eq. 2 was used to obtain values and Eq. 3 to obtain standard errors (SEs) for k_{cat} and K_m.

$$v/Et = \frac{k_{cat} * [S]}{K_m + [S]} \quad \text{..... Eq. 2}$$

$$v/Et = \frac{(k_{cat} / K_m) * K_m * [S]}{K_m + [S]} \quad \text{..... Eq. 3}$$

For substrates that showed substrate inhibition, only those data points up to the maximally observed velocity were used for analysis. In such cases, the k_{cat}/K_m value will be accurate, but the apparent K_m and k_{cat} values will be less than their true values (Eq. 4).

$$v/Et = (k_{cat} / K_m) * [S] \quad \text{..... Eq. 4}$$

Optimization of enzyme concentration and incubation time

To optimize the concentration of enzyme required for sufficient turnover of the substrate and at the same time conserve the amount of protein, different enzyme concentrations ranging from 0 to 18 ng were tested with assay incubation time of 30 min. The substrate used was Ac-L-Lys(Ac)-D-Ala-D-Ala at a fixed concentration of 75 nmoles. The assay incubation time was also optimized under constant enzyme (1.8ng) and substrate concentration (75 nmoles) and the assay conditions were same as mentioned above.

Substrate specificity

Various L-Lys-D-Ala-D-Ala-containing substrates in which the α- and γ-amino groups of Lys were substituted with functional groups (Acetyl or Boc or Cbz) were incubated with

the enzyme at increasing substrate concentrations (0–12 mM X-K(Y)AA). Assays were performed under standard conditions as described above. Since the activity of enzymes varies from one experiment or experimenter to another, Ac-L-Lys-D-Ala-D-Ala **(10)** was included as a reference substrate standard in all the assays.

pH dependence and pH stability

The effect of pH on enzyme activity was studied with 30 μM Ac-L-Lys-D-Ala-D-Ala **(10)** and 300 μM Ac-L-Lys(Ac)-D-Ala-D-Ala **(7)** (1/4th the K_m, subsaturating conditions) in 50 mM buffer, 100 mM NaCl, 0.5 mg/ml Alk-BSA, and at pHs 3.5–12.75. A control study was also performed to determine the effect of pH on R39 stability. For pH stability studies, the enzyme was preincubated in 20 mM buffer for 60 min at 25ºC, then the pH was shifted to 8.5 with 100 mM pyrophosphate (PP), 100 mM NaCl, 0.5 mg/ml Alk-BSA, 300 μM Ac-L-Lys(Ac)-D-Ala-D-Ala **(7)** and the standard enzyme assay was performed. At subsaturating substrate concentrations the following model equation applies:

$$EH_2 \underset{}{\overset{pK_1\ (acidic)}{\rightleftharpoons}} EH + H^+ \overset{pK_2\ (basic)}{\rightleftharpoons} E + H^+ \qquad \text{..... Eq. 5}$$

$$EH + S \xrightarrow{(k_{cat}/K_m)_{EH}} EH + P$$

The following equation was used to fit the data:

$$k_{cat}/K_m = \frac{[H^+]\,(k_{cat}/K_m)_{EH}}{K_2(1+[H^+]/K_2 + [H^+]^2/(K_1K_2))} \quad \text{..... Eq. 6}$$

where k_{cat}/K_m is the observed enzyme activity, $(k_{cat}/K_m)_{EH}$ represents the activity of the mono protonated enzyme, and $[H^+] = 10^{-pH}$; $k_1 = 10^{-pK1}$; $k_2 = 10^{-pK2}$. Values for $(k_{cat}/K_m)_{EH}$, pK_1, and pK_2 were obtained by fitting the data to equation in Eq. 6 using IBM SPSS Statistical Software (Armonk, NY).

Inhibition of R39 by peptide boronic acids

PBP activity assays were performed by detection of D-Ala, produced by the action of PBP on the substrate as described earlier by using DAO/HRP enzyme coupled assays. PBP inhibition assays to determine K_i values for inhibitors were performed with 0.6mM Ac-L-Lys(Ac)-D-Ala-D-Ala **(7)** as the PBP substrate. The concentration of the substrate used was well below the K_m for R39 in this study (subsaturating conditions). The order of the addition of assay reagents was substrate in buffer, inhibitor followed by the addition of enzyme. Peptide boronic acids are competitive inhibitors of the PBPs[84], so under subsaturating substrate concentration ([S] < K_m), the following equation will generally apply

$$v = v_o/(1+I/K_i) \quad \text{..... Eq. 7}$$

where v is the observed enzyme catalyzed rate, v_o is the uninhibited rate, I is the inhibitor concentration, and K_i is the inhibitor dissociation constant. K_i values were obtained by fitting inhibition data with the above equation by non-linear regression using IBM SPSS software. The activity of enzyme in the absence of inhibitors was taken as 100%.

RESULTS

Substrate synthesis

Tri and pentapeptide substrates were successfully synthesized as per Figures 20 and 21. All the peptides were synthesized by solution phase peptide synthesis and the purity was > 95% for all the substrates. Compounds that were difficult to recrystallize and extract with organic solvents were purified by preparative HPLC. The LC-MS data for eight substrates is shown in Figures 22-29.

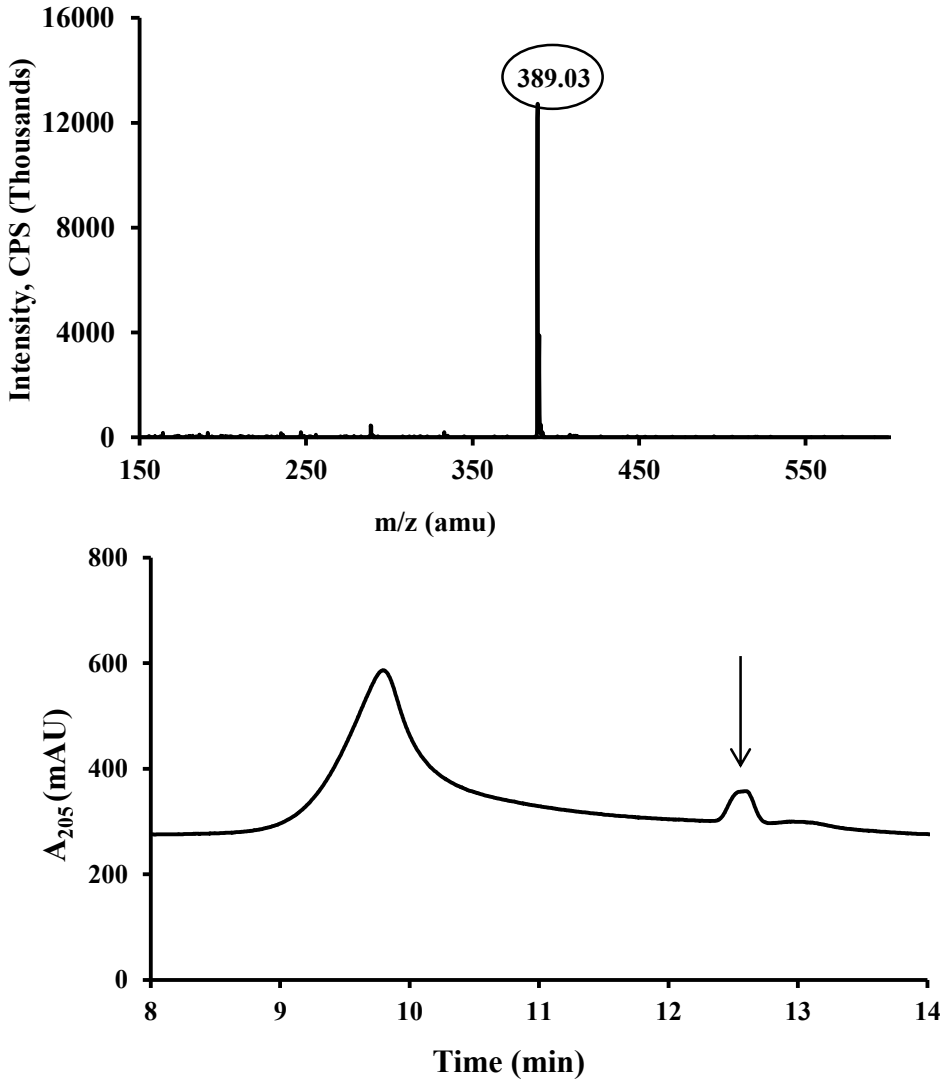

Figure 22: LC-MS spectra of Boc-L-Lys (Cbz)-D-Ala-D-Ala. (Top panel) Mass spectral signal showing $[M+H]^+$ peak for Boc-L-Lys (Cbz)-D-Ala-D-Ala (m/z 389.03). (Bottom panel) UV absorption spectra at 205nm showing the purity of the Boc-L-Lys (Cbz)-D-Ala-D-Ala.

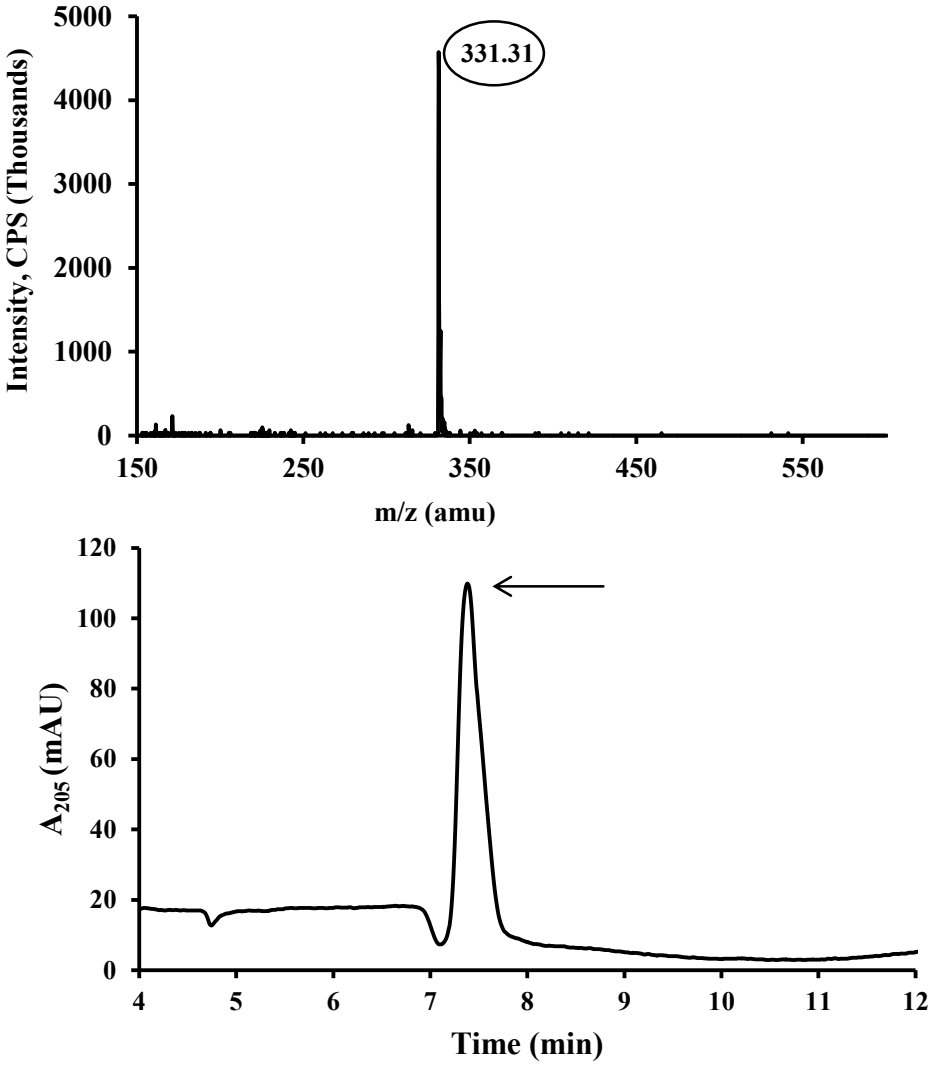

Figure 23: LC-MS spectra of Ac-L-Lys-D-Ala-D-Ala. (Top panel) Mass spectral signal showing $[M+H]^+$ peak for Ac-L-Lys-D-Ala-D-Ala (m/z 331.31). (Bottom panel) UV absorption spectra at 205nm showing the purity of the Ac-L-Lys-D-Ala-D-Ala.

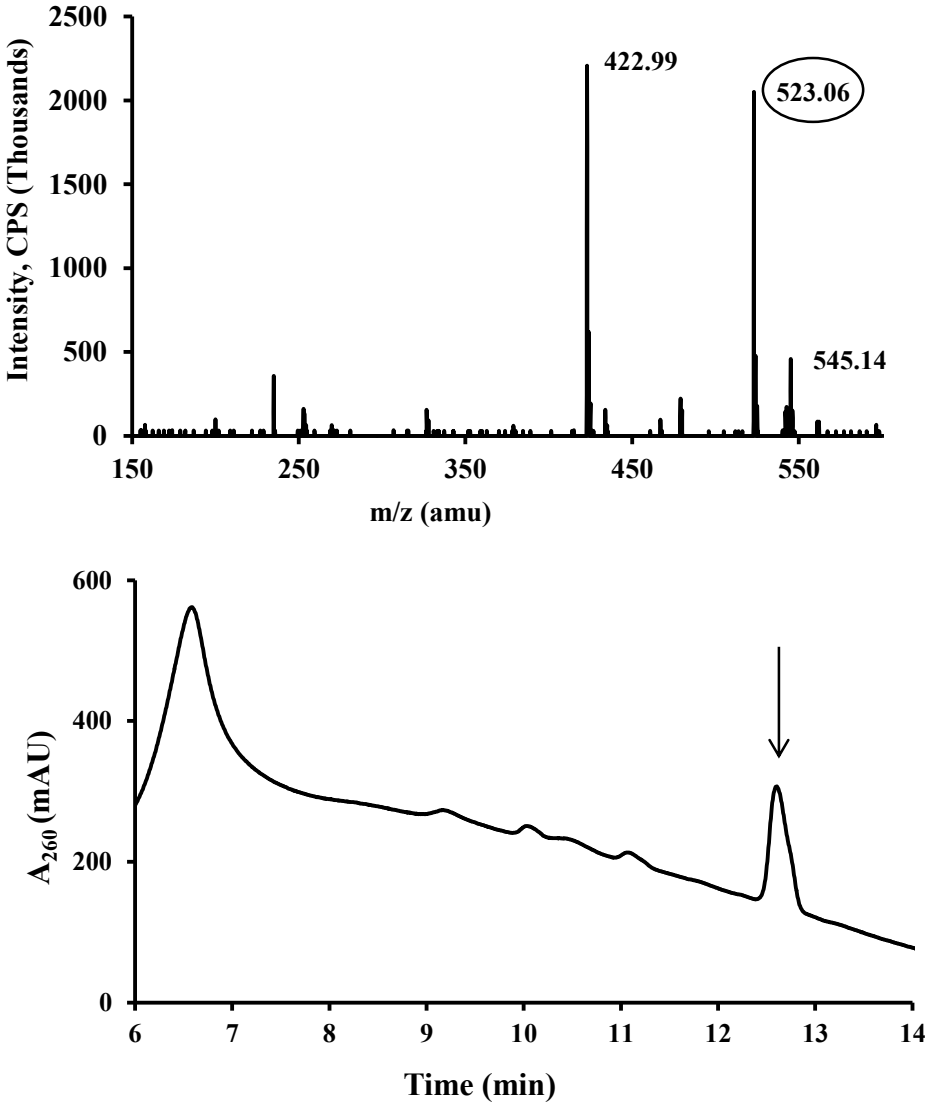

Figure 24: LC-MS spectra of Boc-L-Lys (Cbz)-D-Ala-D-Ala. (Top panel) Mass spectral signal showing $[M+H]^+$ peak for Boc-L-Lys (Cbz)-D-Ala-D-Ala (m/z 523.06). (Bottom panel) UV absorption spectra at 260nm showing the purity of the Boc-L-Lys (Cbz)-D-Ala-D-Ala.

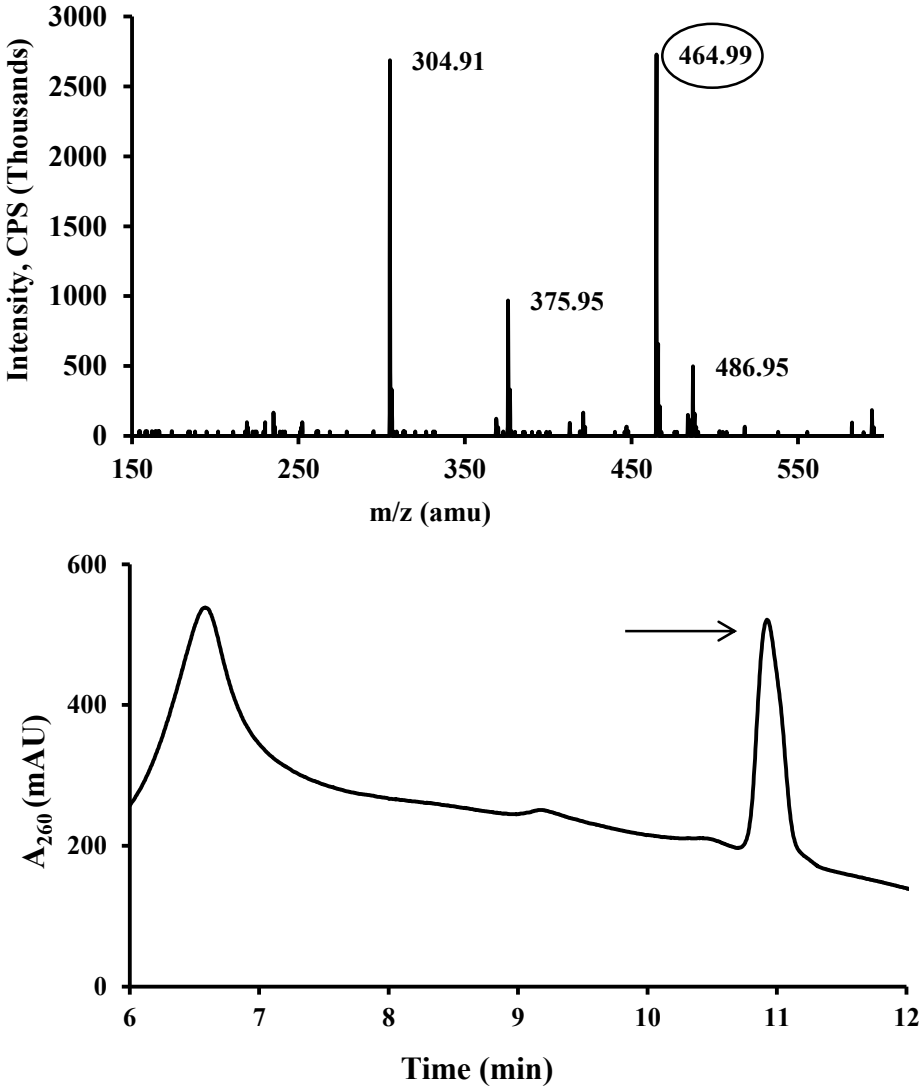

Figure 25: LC-MS spectra of Ac-L-Lys (Cbz)-D-Ala-D-Ala. (Top panel) Mass spectral signal showing $[M+H]^+$ peak for Ac-L-Lys (Cbz)-D-Ala-D-Ala (m/z 464.99). (Bottom panel) UV absorption spectra at 260nm showing the purity of the Ac-L-Lys (Cbz)-D-Ala-D-Ala.

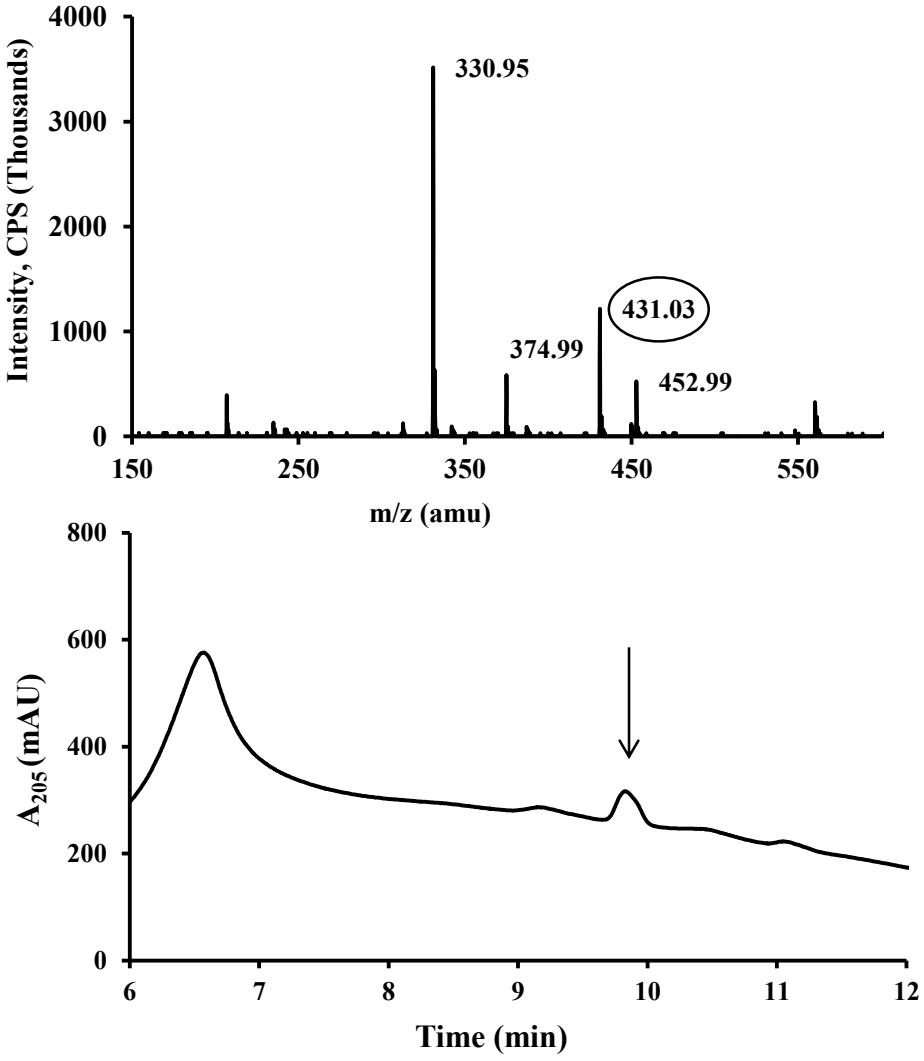

Figure 26: LC-MS spectra of Boc-L-Lys (Ac)-D-Ala-D-Ala. (Top panel) Mass spectral signal showing $[M+H]^+$ peak for Boc-L-Lys (Ac)-D-Ala-D-Ala (m/z 431.03). (Bottom panel) UV absorption spectra at 205nm showing the purity of the Boc-L-Lys (Ac)-D-Ala-D-Ala.

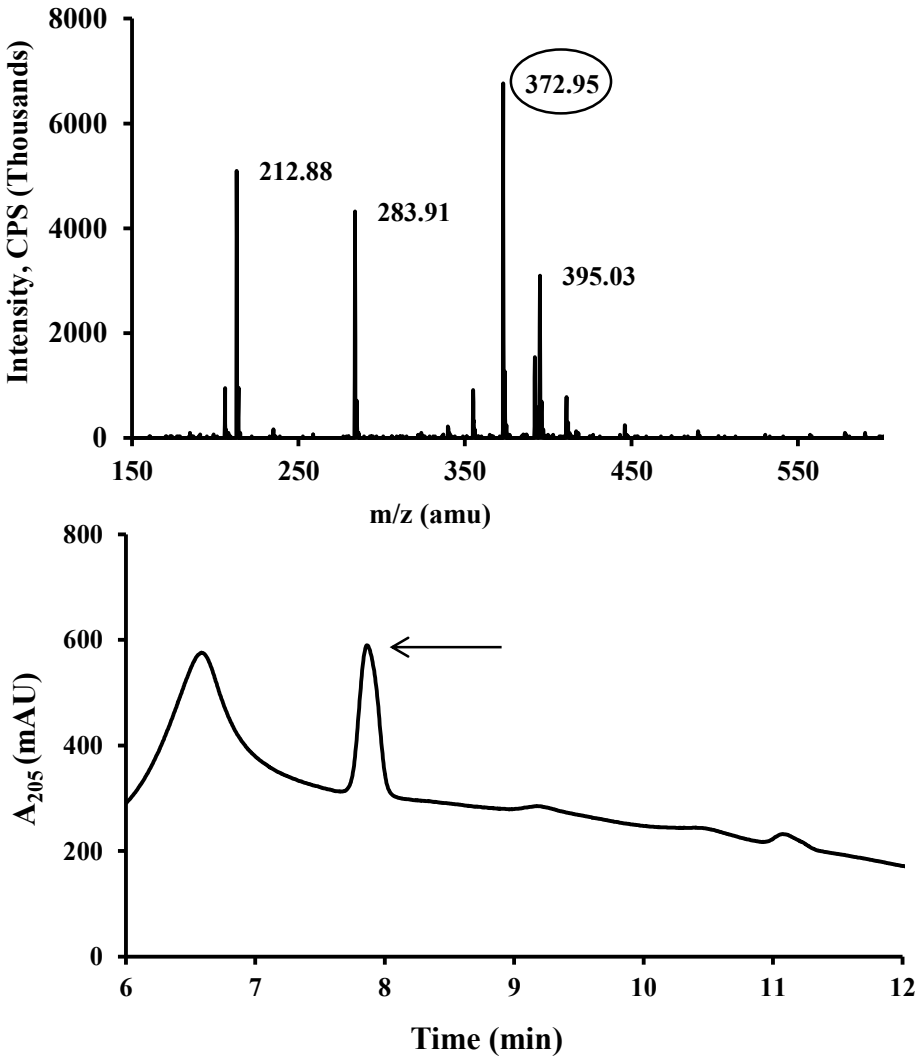

Figure 27: LC-MS spectra of Ac-L-Lys(Ac)-D-Ala-D-Ala. (Top panel) Mass spectral signal showing $[M+H]^+$ peak for Ac-L-Lys(Ac)-D-Ala-D-Ala (m/z 395.03). (Bottom panel) UV absorption spectra at 205nm showing the purity of the Ac-L-Lys(Ac)-D-Ala-D-Ala.

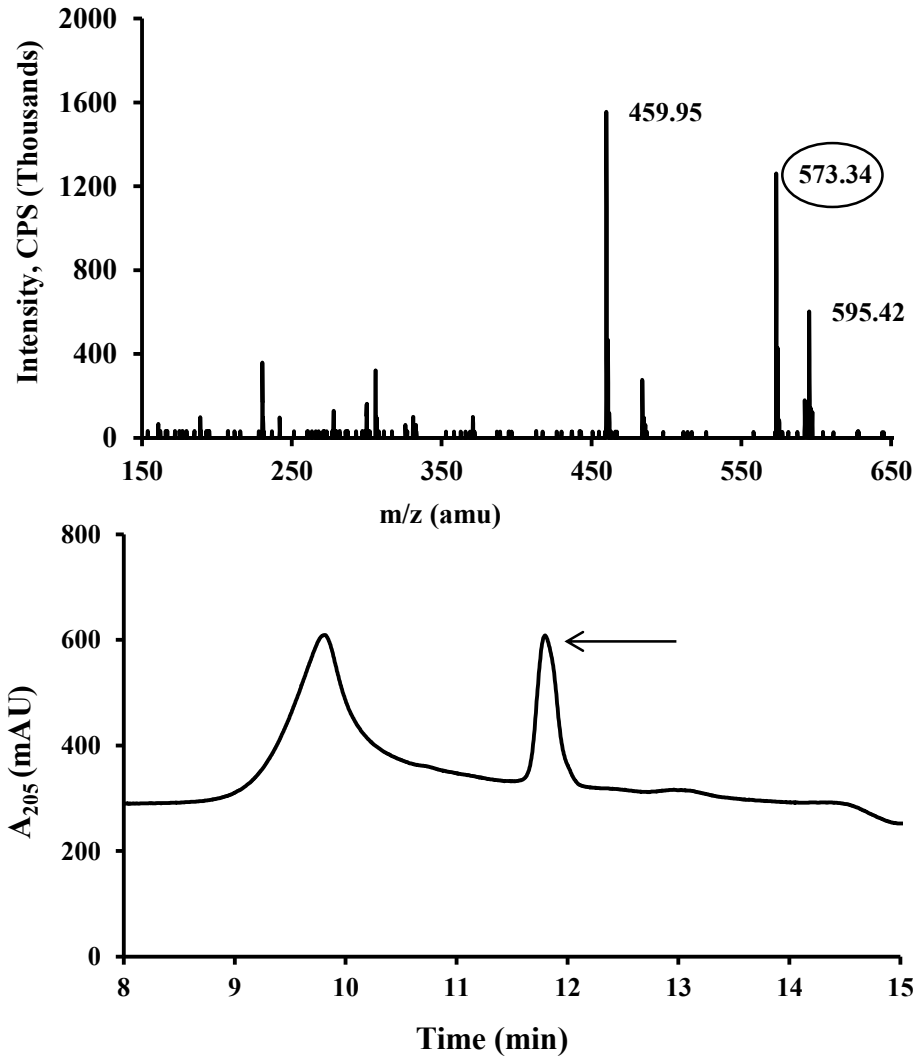

Figure 28: LC-MS spectra of Ac-L-Ala-γ-D-Glu-L-Lys (Ac)-D-Ala-D-Ala. (Top panel) Mass spectral signal showing $[M+H]^+$ peak for Ac-L-Ala-γ-D-Glu-L-Lys (Ac)-D-Ala-D-Ala (m/z 595.42). (Bottom panel) UV absorption spectra at 205nm showing the purity of the Ac-L-Ala-γ-D-Glu-L-Lys (Ac)-D-Ala-D-Ala.

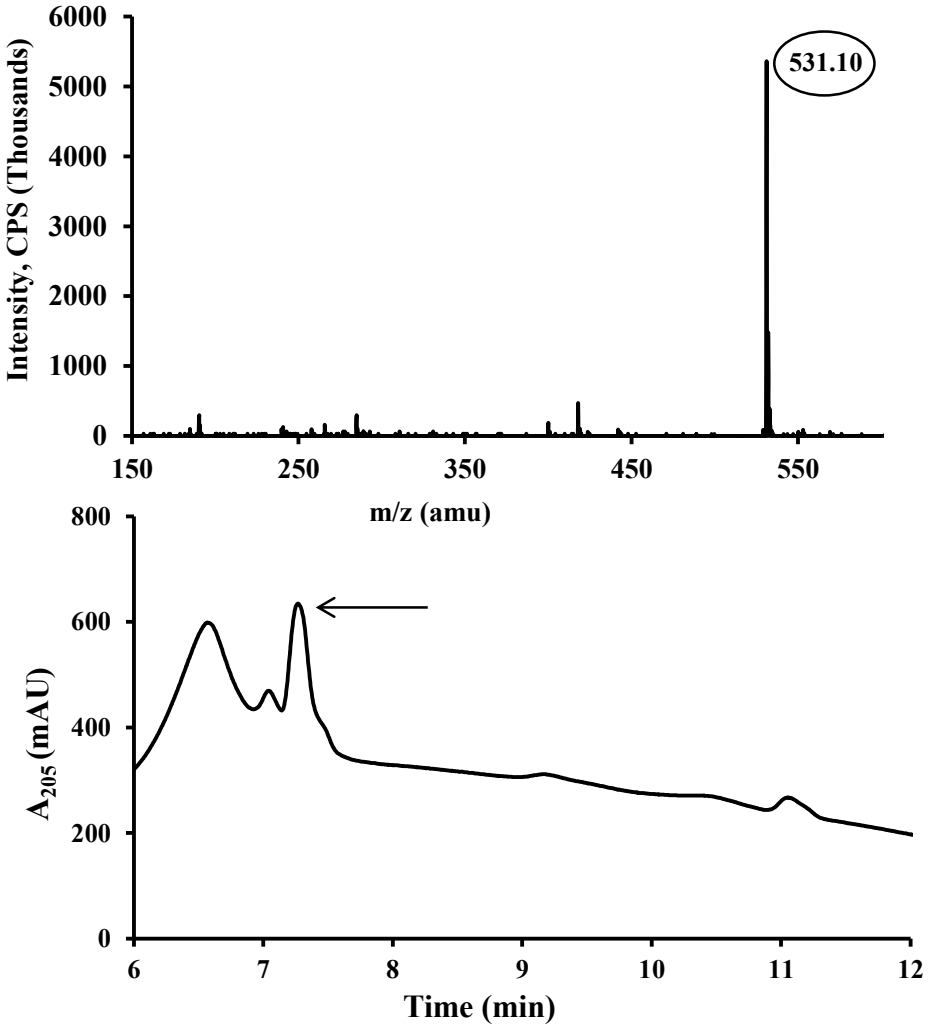

Figure 29: LC-MS spectra of Ac-L-Ala-γ-D-Glu-L-Lys-D-Ala-D-Ala. (Top panel) Mass spectral signal showing $[M+H]^+$ peak for Ac-L-Ala-γ-D-Glu-L-Lys-D-Ala-D-Ala (m/z 531.10). (Bottom panel) UV absorption spectra at 205nm showing the purity of the Ac-L-Ala-γ-D-Glu-L-Lys-D-Ala-D-Ala.

Optimization of enzyme concentration and incubation time

These assays are based on fluorescent D-Ala detection method described previously[135]. Substrate turnover of 5-10% is generally optimal to maximize the signal from an enzyme-catalyzed reaction while remaining under steady-state conditions. It is always advisable in endpoint type of assays to verify linearity. Different enzyme concentrations (0 to 18 ng) were tested and a linear increase in the amount of D-Ala released was observed with increasing enzyme concentration (Figure 30). Based on this data, 1.8 ng of enzyme was used for all the following assays.

Incubation time was then verified from 5 to 60 min and an increase in the turnover, which is measured by the amount of D-Ala released, was observed with increasing incubation time until 50 min at which it reached plateau (Figure 31). A drop in the signal was observed at 60 min, which might correspond to the loss of enzyme activity due to prolonged incubation. Subsequently, based on the data, 30 min was chosen as the optimum time for incubation and used the same for all the assays.

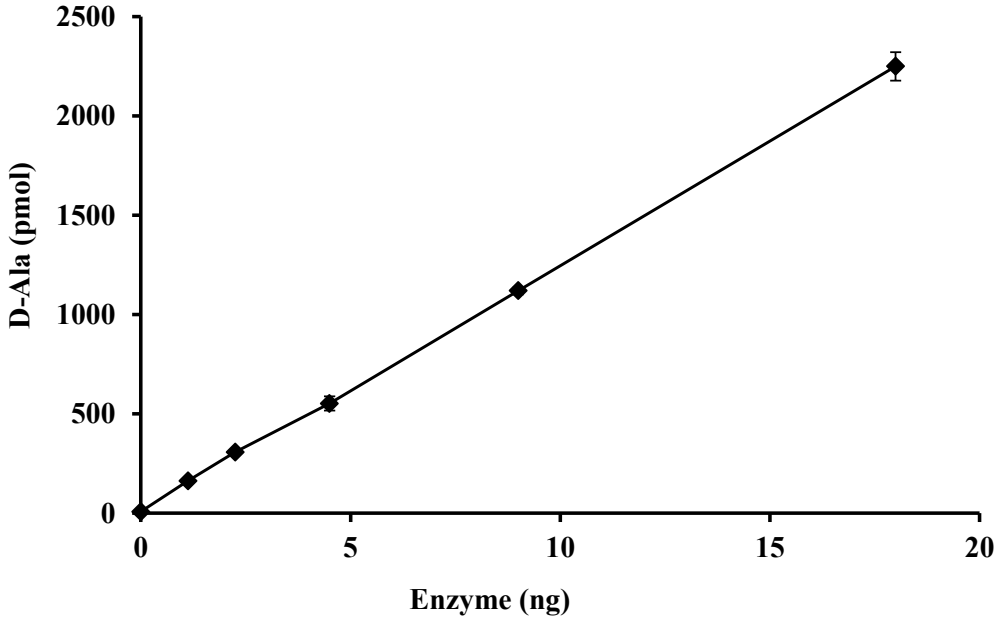

Figure 30: Enzyme concentration dependence on activity expressed as amount of D-Ala produced. Ac-L-Lys (Ac)-D-Ala-D-Ala was used as the substrate (75 nmoles) with assay incubation time of 30 min.

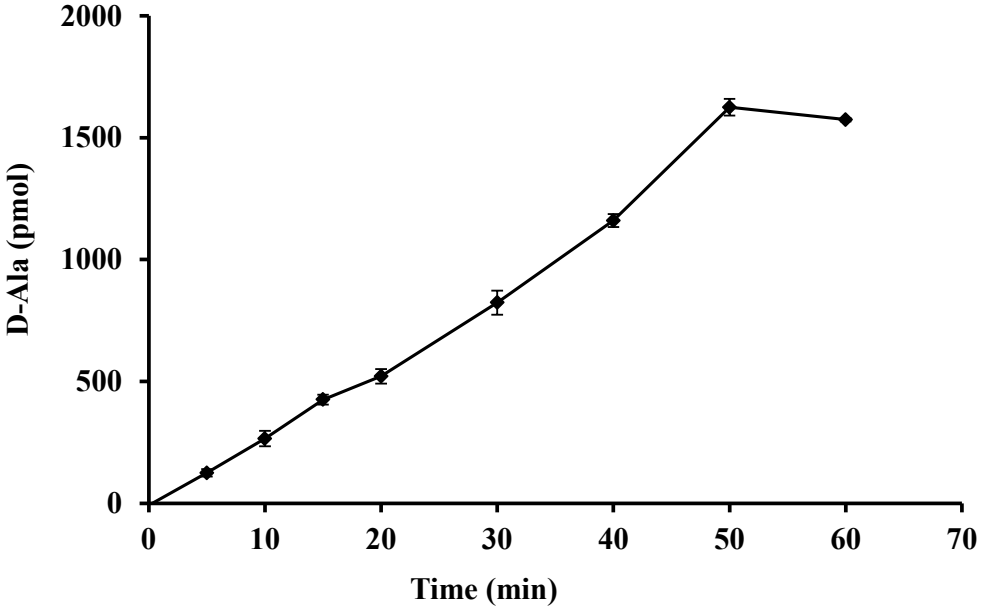

Figure 31: Incubation time dependence on the activity of R39 expressed as amount of D-Ala produced. Ac-L-Lys (Ac)-D-Ala-D-Ala was used as the substrate (75 nmoles) with fixed enzyme concentration (1.8 ng).

Substrate specificity

Actinomadura R39 was characterized against several D-Ala-D-Ala based peptide substrates, as summarized in Figure 32 and Table 10. Enzyme saturation was observed with all the substrates and in the case of Boc-L-Lys (Cbz)-D-Ala-D-Ala (3), Ac-L-Lys (Cbz)-D-Ala-D-Ala (9), Boc-L-Lys (Ac)-D-Ala-D-Ala (5), Ac-L-Ala-γ-D-Glu-L-Lys (Ac)-D-Ala-D-Ala (18), and Ac-L-Ala-γ-D-Glu-L-Lys-D-Ala-D-Ala (17) substrate inhibition was observed at high concentration and only the data points from 0 to peak activity were included in the statistical analysis. k_{cat}/K_m values were obtained for all of the studied substrates. Boc-L-Lys-D-Ala-D-Ala was found out to be the best substrate with k_{cat}/K_m of 580 $mM^{-1}s^{-1}$. *Actinomadura* R39 in general showed highest activity for substrates with no N^{ε}-acetyl substitution. Acylation of N^{ε}-amino group of L-Lys either with acetyl or Cbz group decreased the catalytic efficiency with the enzyme.

pH dependence and pH stability

Our lab has previously reported the pH dependence of several PBPs[43,49,134], such information is useful in assessing the correct pH for enzyme studies and the role of ionizable active site residues in catalysis. The pH dependence of k_{cat}/K_m for *Actinomadura* R39 catalyzed hydrolysis of **(7)** and **(10)** is shown in Figure 33. *Actinomadura* R39 gave a bell-shaped pH profile with an optimum activity in the range of 8-10. Data from citrate buffer were excluded from the analysis for pKa due to inconsistent observations. pKa values obtained were 6.4 and 11.6 with Ac-L-Lys (Ac)-D-Ala-D-Ala and 6.2 and 11.1 with Ac-L-Lys-D-Ala-D-Ala. *Actinomadura* R39 was found to be stable over all the pH ranges tested

(3.5-12.5) for 30 min at room temperature (Figure 34). Control experiments with substrate in the absence of R39 and R39 in the absence of substrate gave no apparent activity.

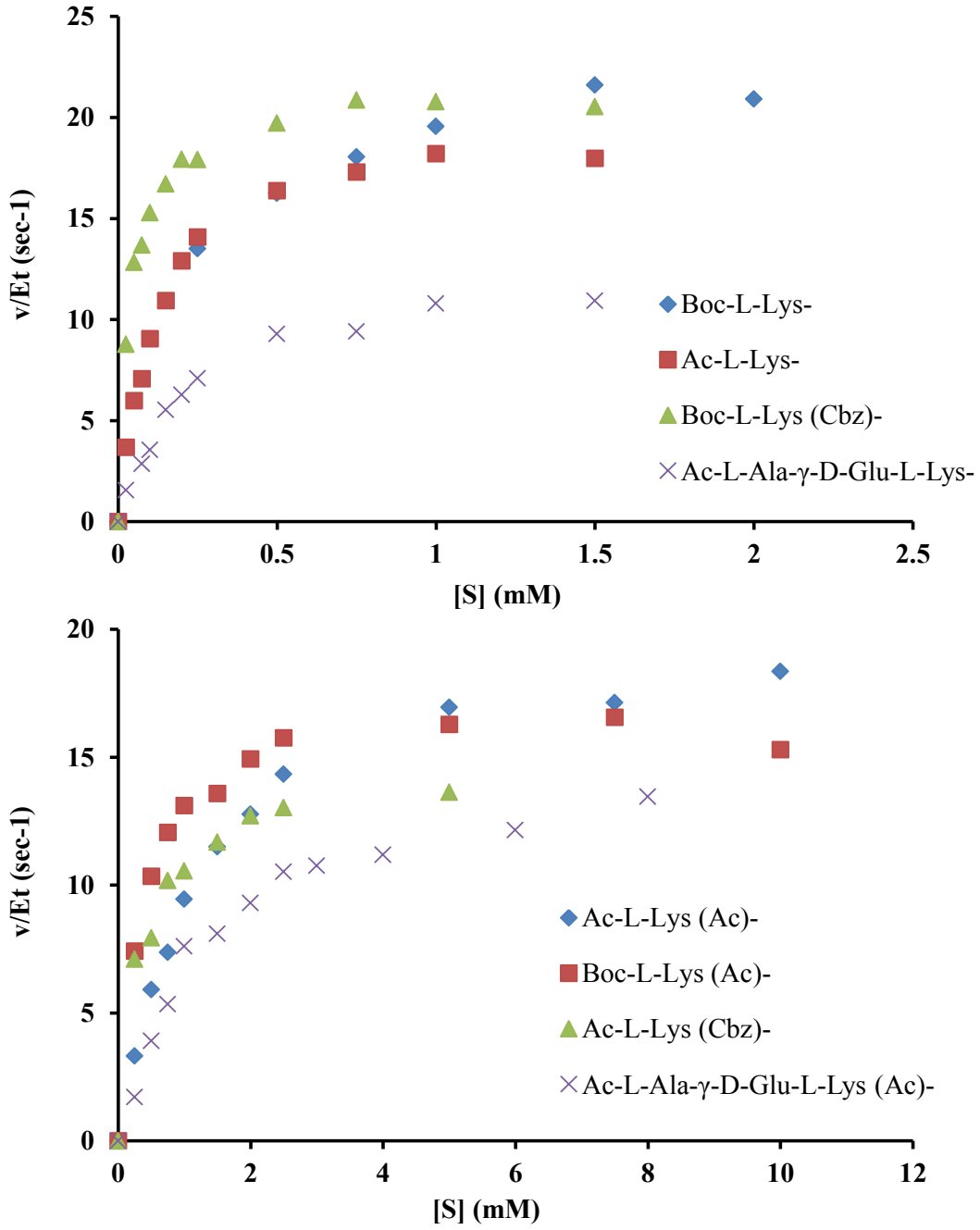

Figure 32: Substrate specificity of R39 towards various tri and penta peptides substrates (0-12 mM). CPase activity was assayed under standard conditions described in materials and methods.

Substrate R group is shown in the labels (R-D-Ala-D-Ala).

Table 10:
Kinetic properties of different substrates against *Actinomadura* R39.

Substrate (R-D-Ala-D-Ala), R=	K_m **(mM)**	k_{cat} **(sec^{-1})**	k_{cat}/K_m **(mM^{-1}sec^{-1})**
Boc-L-Lys-	0.037 ± 0.002	21.2 ± 0.3	580 ± 40
Ac-L-Lys-	0.120 ± 0.006	20.1 ± 0.3	169 ± 6
Boc-L-Lys (Cbz)-	0.20 ± 0.03	23.4 ± 0.6	118 ± 12
Ac-L-Lys (Cbz)-	0.29 ± 0.04	14.0 ± 0.4	48 ± 6
Boc-L-Lys (Ac)-	0.31 ± 0.03	17.0 ± 0.3	55 ± 4
Ac-L-Lys (Ac)-	1.16 ± 0.06	20.2 ± 0.3	17.5 ± 0.7
Ac-L-Ala-γ-D-Glu-L-Lys (Ac)-	1.27 ± 0.14	15.1 ± 0.6	11.9 ± 0.8
Ac-L-Ala-γ-D-Glu-L-Lys-	0.22 ± 0.02	13.0 ± 0.5	57 ± 4

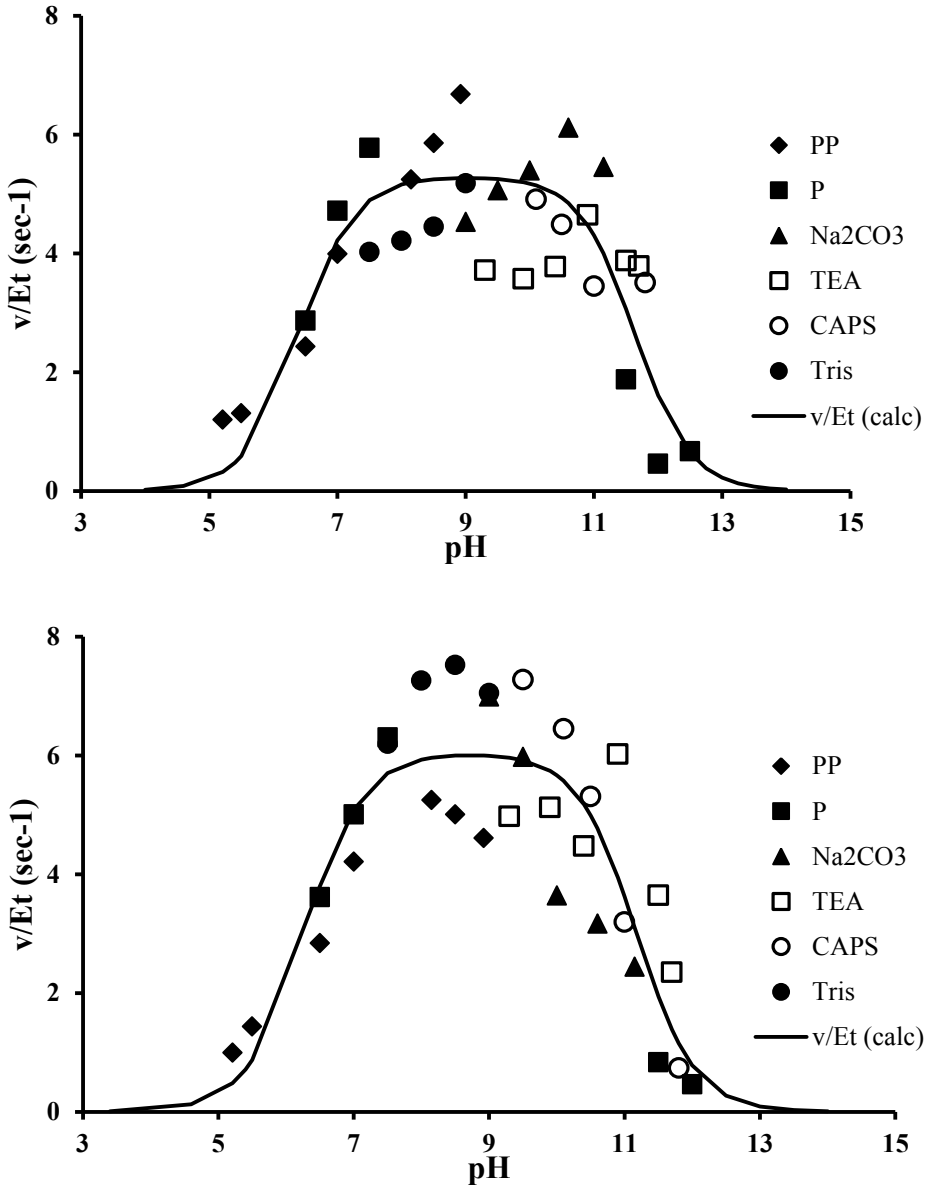

Figure 33: pH optimum of R39. (Top panel) v/Et vs pH profile for hydrolysis of Ac-L-Lys (Ac)-D-Ala-D-Ala (7) (300 μM). (Bottom panel) v/Et vs pH profile for hydrolysis of Ac-L-Lys-D-Ala-D-Ala (10) (30 μM).

Abbreviations of buffers: PP: pyrophosphate, P: phosphate, Na_2CO_3: carbonate, TEA: triethyl amine, CAPS: N-cyclohexyl-3-aminopropanesulfonic acid, Tris: tris(hydroxymethyl)aminomethane.

Inhibition of R39 by peptide boronic acids

Peptide boronic acids similar to the best substrates studied were tested as inhibitors for *Actinomadura* R39. All the three inhibitors (Boc-Lys-D-boroAla-pinanediol (Boc-K-DBA-Pd), Boc-Lys (Ac)-D-boroAla-pinanediol (Boc-K(Ac)-DBA-Pd), and Boc-Lys (Cbz)-D-boroAla-pinanediol (Boc-K(Cbz)-DBA-Pd)) tested inhibited the enzyme activity with K_i's ranging from 2-7 μM. Boc-K-DBA-Pd was found out to be the best inhibitor with K_i of 2.12 μM. This was expected as in accordance with being the mimetic of the best substrate Boc-L-Lys-D-Ala-D-Ala. The presence of acyl group (acetyl or cbz) significantly decreased the inhibition by the peptidomimetics as is evidenced with higher K_i values for Boc-K(Ac)-DBA-Pd (6.97 μM), and Boc-K(Cbz)-DBA-Pd (4.59 μM). The inhibition curves are shown in Figure 35.

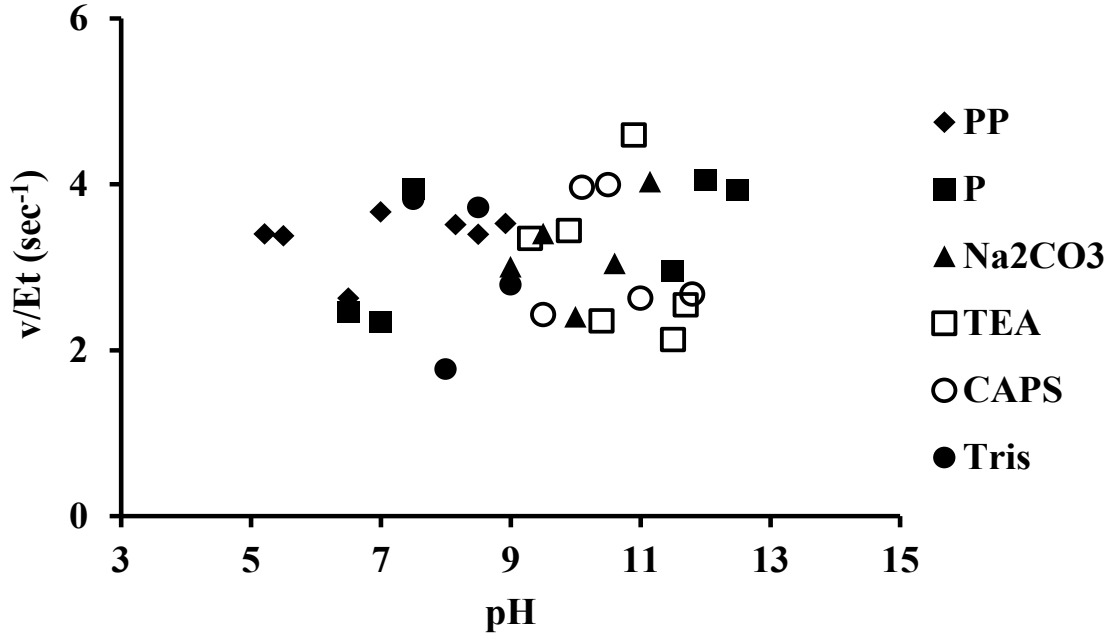

Figure 34: pH stability of R39 expressed as v/Et vs pH profile for hydrolysis of Ac-L-Lys (Ac)-D-Ala-D-Ala (300 μM).

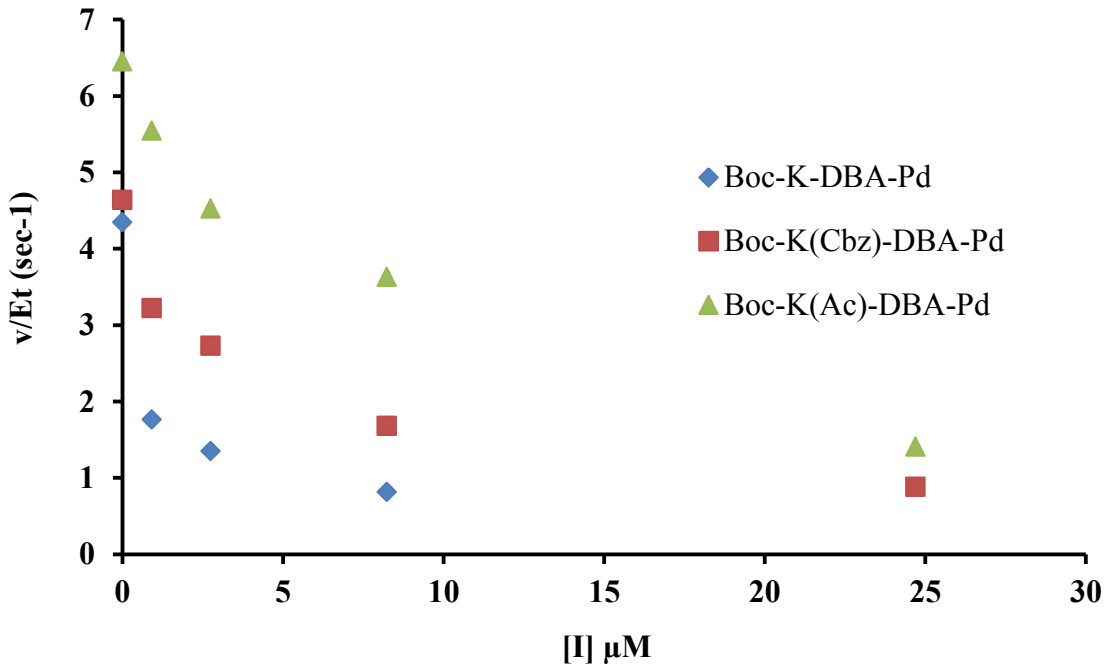

Figure 35: Results of R39 inhibition assays with various D-boroAla inhibitors.

Abbreviations: Boc-K-DBA-Pd: Boc-Lys-D-boroAla-pinanediol, Boc-K(Ac)-DBA-Pd: Boc-Lys (Ac)-D-boroAla-pinanediol, and Boc-K(Cbz)-DBA-Pd: Boc-Lys (Cbz)-D-boroAla-pinanediol.

DISCUSSION

The major aim of this project was to identify good saturating substrates for the *Actinomadura* R39 PBP, determine specificity features of physiologically related substrates, and then test analogous TS analogs for inhibition. In particular, substrates were designed to test whether the presence or absence of an N^{ε}-acyl group on Lys, and the number of residues in the peptide chain length has any effect on substrate specificity. N^{ε}-Acylation is an key point of variation, since within the cell wall a given peptidoglycan chain will either be involved in a cross-link or not, and is a potentially key distinguishing feature of PBP specificity. In a previous study form our lab, NG PBP3 was demonstrated to have a high degree of specificity for acylated vs unacylated substrates[49] and we were hopeful that *Actinomadura* R39 belonging to the same class as NG PBP3 (LMM class C) would exhibit substrate specificity if not similar specificity as NG PBP 3. Another important feature of synthetic substrates is the length of the peptide chain, and therefore both tripeptide and pentapeptide substrates were synthesized and tested.

Table 11:
Kinetic properties of tripeptide substrates against NG PBP3 (Adapted from Stefanova et.al 2003).

Substrate (R-D-Ala-D-Ala), R=	K_m (mM)	k_{cat} (sec^{-1})	k_{cat}/K_m ($mM^{-1}sec^{-1}$)
Boc-L-Lys-	32 ± 3	260 ± 10	8.3 ± 0.4
Ac-L-Lys-	N/A	N/A	N/A
Boc-L-Lys (Cbz)-	3.3 ± 0.8	580 ± 60	180 ± 30
Ac-L-Lys (Cbz)-	3.7 ± 0.2	530 ± 10	142 ± 6
Boc-L-Lys (Ac)-	6.5 ± 0.8	400 ± 10	62 ± 6
Ac-L-Lys (Ac)-	19 ± 2	550 ± 20	29 ± 2

Actinomadura R39 exhibited pronounced preference for N^{ε}-unacylated substrates (free side chain amine group of Lys), in agreement with what others have observed[21,45,86]. Peptides with an N^{ε}-acyl group had substantially less affinity and lower turnover. The preference for unacylation was not only observed with tripeptide substrates but also with pentapeptide substrates. This suggests that the side chain amino group makes favorable interactions with the catalytic active site, consistent with crystallographic studies[86,138]. *Actinomadura* R39 also demonstrated lower K_m and higher k_{cat}/K_m values against tripeptide substrates over pentapeptide substrates, which suggests that R39 does not need full-length peptide chain to achieve maximal activity. The preference for N^{ε}-unacyl group over different acyl groups can be quantified by taking the average of the specificity constant within pairs of homologous substrates.

Effect of acyl (acetyl) group on k_{cat}/K_m (values from Table 10):

$R_{\text{non-acetyl/acetyl}} =$

[(4) / **(5)** + **(10)** / **(7)** + **(17)** / **(18)**] / 3

=> (580/55 + 169/18 + 57/12)/3 = 8.2

Effect of acyl (Cbz) group on k_{cat}/K_m:

$R_{\text{non-cbz/cbz}} =$

[(4) / **(3)** + **(10)** / **(9)]** / 2

=> (580/118 + 169/48)/2 = 4.2

Thus, on average, unacylated substrates show higher catalytic efficiency over acylated substrates by about 4 fold (cbz group) and 8 fold (acetyl). Similarly, ratios for the effect of a longer vs shorter peptide chain (TP vs PP) was $R_{TP/PP} = 2.2$. This confirms the specificity of R39 towards N^{ε}-unacyl side chain. The order of specificity of N^{ε}-side chain amine for R39 was unacyl > cbz > acetyl group. The specificity for unacylated substrates suggests that R39 is selective for un-cross-linked cell wall peptides. Comparison of substrate specificity studies on NG PBP3, which belongs to the same LMM class C yields interesting observations (Table 11). The enzyme specificity of R39 and NG PBP3 appears to be focused on nonacylation or acylation, respectively, of the N^{ε}-amino group of their substrates, which reflects lack of participation or participation in the cross-link reaction. These results suggest that the R39 enzyme acts as carboxypeptidase and/or endopeptidase and specific for substrates that have a free side chain N-terminus.

pH dependence is an important enzyme characteristic relevant to physiological, mechanistic, and kinetic understanding of enzyme catalyzed reactions[145]. The physiological significance of pH dependence is of particular relevance for the PBPs, which are exposed to the extracellular environment. *Actinomadura* species grows best at pH 7-8[146]. In this study, the pH dependence activity of R39 was measured using Ac-L-Lys (Ac)-D-Ala-D-Ala and Ac-L-Lys-D-Ala-D-Ala as substrates with a set of 10 buffers covering the pH range 3.5-12.5 using the general protocol described previously[134]. This pH range allowed both acidic and basic limbs of the pH profile to be observed. The pH profile of R39 was bell-shaped, with pKas 6.4 and 11.6 with Ac-L-Lys (Ac)-D-Ala-D-Ala and 6.2 and 11.1 with Ac-L-Lys-D-Ala-D-Ala (Figure 33). The pKas were similar for both the substrates even though R39 shows specificity towards Ac-L-Lys-D-Ala-D-Ala over Ac-L-Lys (Ac)-D-Ala-D-Ala. The pKa values

R39 6.4 and 11.6 are similar to the pKa values for NG PBP 3 of 6.8 and 9.8[43]. The pH profile was obtained at subsaturating substrate concentration, and represents the pH dependence on k_{cat}/K_m. The pH dependence on k_{cat}/K_m reflects the pKa's of ionizable groups in the free enzyme and/or substrate[134]. In the present case, the observed pKa's are well away from the pKa of the carboxyl terminus of the substrate (Ac-L-Lys (Ac)-D-Ala-D-Ala), the only ionizable group on the substrate, and thus can be attributed to ionizable groups on the enzyme. The pKa's obtained with Ac-L-Lys-D-Ala-D-Ala having a free amine group of Lys were same as that of the pKa's from Ac-L-Lys (Ac)-D-Ala-D-Ala, suggesting that ionization of free amine group has little effect on catalysis. Ionizable residues within the active site of R39 include Lys-52 (from SXXK motif), and Lys-410 (from KTG motif).The possible assignments for the pKa values would be 6.4 for Lys-52 corresponding to low acidic pKa as is required catalysis and the higher pKa 11.4 for Lys-410. This assignment also supports the identification of Lys-52 as the general base during acylation of the active site serine[86].

Transition state analogs of enzymes are often potent enzyme inhibitors, and can also be valuable tools in studying substrate specificity, catalytic mechanism, and structure-function correlations of the target enzyme[84]. Effective inhibitors for the PBPs could also provide a basis for the development of new antibacterial agents. Our own research group first reported peptidomimetics based on boron chemistry as effective PBP inhibitors[70,84,92,138]. The crystal structure of R39 with peptide boronic acids was solved and a mixture of monocovalent and tricovalent boronate adducts were observed with the active site[140]. Both ethylboronic acids, representing transitional state analogs and methylboronic acids, lacking the resemblance to natural substrate were observed to be potent inhibitors and were able to

form adducts with active site[140]. This data supports the fact that these peptidomimetics are potent inhibitors of PBPs.

All the peptide boronic acids tested (Boc-K-DBA-Pd, Boc-K (Ac)-DBA-Pd, and Boc-K(Cbz)-DBA-Pd) showed inhibitory activity against R39. A good correlation was observed between the substrates and corresponding transition state analog inhibitors. For example, Boc-K-DBA-Pd was found to be the best inhibitor corresponding to the best substrate (Boc-L-Lys-D-Ala-D-Ala). The order of inhibitory effects of different boronic acids was Boc-K-DBA-Pd > Boc-K(Cbz)-DBA-Pd > Boc-K(Ac)-DBA-Pd, which is similar to what has been observed with substrate specificity (Boc-L-Lys-D-Ala-D-Ala > Boc-L-Lys (Cbz)-D-Ala-D-Ala > Boc-L-Lys (Ac)-D-Ala-D-Ala). The crystal structure of R39 was also solved with one of the inhibitors (Boc-K-DBA-Pd) with our collaborators Paulette Charlier and Eric Sauvage (Université de Liège, Belgium), but with poorly defined structure of inhibitor in the enzyme binding pocket. In summary, this study demonstrates that identification of best substrates for PBPs can not only help in understanding the basic biochemistry of these enzymes but also lead to identification and development of better inhibitors and may ultimately lead to better antimicrobial agents.

CHAPTER 4

A MICROTITER PLATE-BASED β-LACTAM BINDING ASSAY FOR INHIBITORS OF HIGH-MOLECULAR-MASS PENICILLIN-BINDING PROTEINS[76]

INTRODUCTION AND RATIONALE

Penicillin-binding proteins (PBPs) are bacterial enzymes that catalyze the final steps in cell wall biosynthesis, and are the lethal targets of the β-lactam antibiotics[6-10]. PBPs have molecular masses of 20-120 kDa and can be broadly divided into two groups, the high molecular mass (HMM) PBPs and the low molecular mass (LMM) PBPs[8]. The HMM PBPs are generally responsible for catalysis of crosslinking (transpeptidase) reactions, while the LMM PBPs are generally responsible for carboxypeptidase and endopeptidase reactions [10,17,18,20,21,27]. HMM PBPs are essential for bacterial survival and are the lethal targets for β-lactam antibiotics, whereas LMM PBPs are non-essential for cell viability. A particularly enigmatic feature of the PBPs is that, while LMM PBPs give readily detectible activity against peptide substrates, purified HMM PBPs give either low or undetectable activity against natural or synthetic cell wall-related peptide substrates[21,27]. This may be related to their role in bacterial cell wall biosynthesis, and it has been suggested that HMM PBP activity is regulated within macromolecular complexes which synthesize new and degrade existing peptidoglycan in a coordinated fashion[17]. This feature of the essential HMM PBPs has unfortunately impeded the development of convenient assays for the HMM PBPs. Two approaches which have had some success for demonstrating the activity of the HMM PBPs are the use of thiolester-based substrates[51,57], and assays based on the use of lipid II[53,54,80,147], which is a precursor to the nascent peptidoglycan substrate of the PBPs. However, neither of

these assays appear well suited for microtiter plate based high throughput assays – the thiolesters because of their high background rate of hydrolysis[51], and lipid II because of its difficult isolation[148] and synthesis[54,147]. In an effort to circumvent the limitations of these and other HMM PBP assays, deSousa and coworkers have developed scintillation proximity assays to measure membrane associated peptidoglycan synthesis in *E. coli* membrane preparations[149-151], but these assays also appear difficult and cumbersome.

The lack of a straightforward microtiter plate compatible assay for screening and characterizing inhibitors of the HMM PBPs has greatly hampered efforts to develop new inhibitors and antibacterial agents targeting the PBPs. In this report, we describe a generally applicable, simple, and robust assay for screening and characterizing HMM PBP inhibitors. This approach is based on the fact that the HMM PBPs, essentially by definition, bind β-lactams. This assay uses a β-lactam-biotin conjugate (Bio-Amp) previously described for the detection of PBPs in Western Blots[74,152,153]. In the present study, purified PBPs were immobilized onto microtiter plate wells, and labeled with Bio-Amp. Treatment of the Bio-Amp labeled PBP with a streptavidin-horse radish peroxidase (HRP) conjugate followed by a fluorogenic HRP substrate (Amplex Red) allowed the efficient detection of immobilized PBPs (A pictorial representation is shown in Figure 36). Binding curves for Bio-Amp interaction with PBPs were then measured, and used to calculate apparent K_m's for each PBP's interaction with Bio-Amp. Finally, this assay was demonstrated for use in competition assays for the determination and characterization (K_i) of unlabeled β-lactam PBP inhibitors.

MATERIALS AND METHODS

Preparation of Bio-Amp

Biotin ampicillin conjugate (Bio-Amp) was prepared by a modification of the method of Dargis and Malouin[74]. Ampicillin (sodium salt, Sigma # A-9518) (100 µL of a 50 mM solution, 5 µmol) in 0.1 M phosphate buffer/150 mM NaCl pH 8.0 was treated with of EZ-Link-Sulfo-NHS-LC-Biotin (12.5 mg, 20 µmol) (Pierce) for 30 min. The primary amino group of ampicillin was completely acylated as determined using a ninhydrin spot test for free primary amino groups. Glycine (6 mg, 80 µmol) was then added to consume unreacted biotin conjugating reagent, and after 30 min, the mixture was diluted to 200 µL with water to make a 20 mM stock solution of the Bio-Amp labeling reagent, which was stored frozen at -20ºC. The identity and purity of Bio-Amp was assessed by LC-MS (Figure 37).

PBPs

EC PBP1B[154,155], NG PBP 1[156], NG PBP 2[157], NG PBP3[43], NG PBP 4[133], and EC PBP 5[134,158] were generous gifts from professor Robert Nicholas (University of North Carolina).

Data analysis

Data were fit to the appropriate expressions given below using the non-linear regression function in IBM SPSS for Windows (Armonk, NY).

PBP loading onto microtiter plates, labeling and detection

An ELISA like protocol was used in black-walled Costar microtiter plates (Costar #3631). For PBP attachment, wells were treated with 2 µg of PBP in 50 µL of PBS/20%

glycerol at 25ºC for 30 min. The remaining attachment sites were then blocked by treatment (3x) with 150 µL/well of blocking buffer (PBS/0.2% Tween-20) and then washed (3x) with 200 µL/well of washing buffer (PBS/0.05% Tween-20). To label PBPs in initial proof-of principle experiments, 50 µL of 100 µM Bio-Amp in PBS was added to the wells. After10 min the PBPs were denatured. Denaturation is necessary because PBPs catalyze the slow turnover of their β-lactam adducts, and loss of PBP-bound Bio-Amp would result in loss of signal. A number of denaturing conditions were tested, with heating at 80ºC for 3 min, followed by quick cooling on ice, giving the best results (data not shown). The plates were then washed (3x) with washing buffer (250 µL PBS/0.05% Tween-20). Streptavidin-horse radish peroxidase (HRP) conjugate (Pierce #21126) (50 µL of 0.1 µg/ml) was then added to each well. After 30 min the wells were washed (3x), and 100 µL of a fluorescent HRP substrate mixture (1 mM H_2O_2, 20 µM Amplex Red (Molecular Probes) in 100 mM Tris pH 8.5) was added to each well. After 60 min the fluorescence signal was read (Excitation: 546 nm, Emission: 595 nm) in a Tecan Spectafluor Plus microtiter plate reader. A pictorial representation of the assay principle is shown in Figure 36.

Determination of Bio-Amp K_m for binding vs various PBPs

PBPs turnover β-lactams (albeit very slowly) following the simplified general scheme

$$E + I \xrightarrow{k_1} EI \xrightarrow{k_2} E + P \quad \text{.....Eq. 8}$$

The steady-state equation for product formation is

$$v = \frac{[E]_t * k_{cat} * [I]}{K_m + [I]} \quad \text{..... Eq. 9}$$

Where

$$k_{cat} = k_2 \quad \text{..... Eq. 10}$$

and

$$K_m = \frac{k_2}{k_1} \quad \text{..... Eq. 11}$$

In the present case, we are not measuring product formation, but the fraction of enzyme (PBP) with bound Bio-Amp. The apparent binding isotherm for this system will be

$$[E\text{-}I] = \frac{[I] * [E]_t}{K_m + [I]} \quad \text{..... Eq. 12}$$

The expression for the observed fluorescence (relative fluorescence units, RFU) as a function of added Bio-Amp will be

$$RFU = \frac{RFU_{max} * [I]}{K_m + [I]} \quad \text{..... Eq. 13}$$

To take into account the background (blank) fluorescence, this equation was expanded to

$$RFU = RFU_o + \frac{RFU_{max} * [I]}{K_m + [I]} \quad \text{..... Eq. 14}$$

To assess Bio-Amp binding to a given PBP, the microtiter plate bound PBP was treated with serially diluted (steps of 5) concentrations of Bio-Amp (each concentration tested in quadruplicate), and the remaining steps of the assay performed as described above. Signals were plotted, and the set of 5 data points bracketing the midpoint of the saturation curve were analyzed for the K_m of binding by fitting the data to Eq. 14.

Application to HMM PBP-inhibitor screening and characterization

For inhibitor screening and characterization, the concentration of Bio-Amp was used at a fixed concentration equal to the determined K_m for a PBP. This was selected since it was high enough give 1/2 of the maximum possible signal and low enough to still allow inhibition to be readily detected. To demonstrate this capability, NG PBP2 was characterized for inhibition by ampicillin. NG PBP2 was first attached to the wells of a microtiter plate as described above. Serially (steps of 5) diluted solutions of ampicillin in 50 μL PBS were

added to the wells (each concentration tested in quadruplicate). After 15 minutes 5 µL of a 28 µM solution of Bio-Amp was added (final concentration of 1.1 µM Bio-Amp in assay mixture). After 15 minutes, the binding reactions were stopped by heat denaturation and the plates developed as described above. The general expression for a competitive inhibitor in this assay is

$$RFU = \frac{RFU_{max} * [\text{Bio-Amp}]}{K_m * (1+[I]/K_i) + [\text{Bio-Amp}]} \quad \text{..... Eq. 15}$$

Where K_m is the K_m for Bio-Amp vs the particular PBP, [Bio-Amp] is the concentration of Bio-Amp, K_i is the apparent binding constant for the alternative inhibitors, and [I] is the concentration of the alternative inhibitor. With [Bio-Amp] = K_m this expression reduces to

$$RFU = \frac{RFU_{max}}{[I]/K_i + 2} \quad \text{..... Eq. 16}$$

To take into account the background (blank) fluorescence, this equation was expanded to

$$RFU = RFU_o + \frac{RFU_{max}}{[I]/K_i + 2} \quad \text{..... Eq. 17}$$

Inhibitor binding data were plotted, and the set of 5 data points bracketing the midpoint of the saturation curve were analyzed for the K_i of binding by fitting the data to Eq. 17

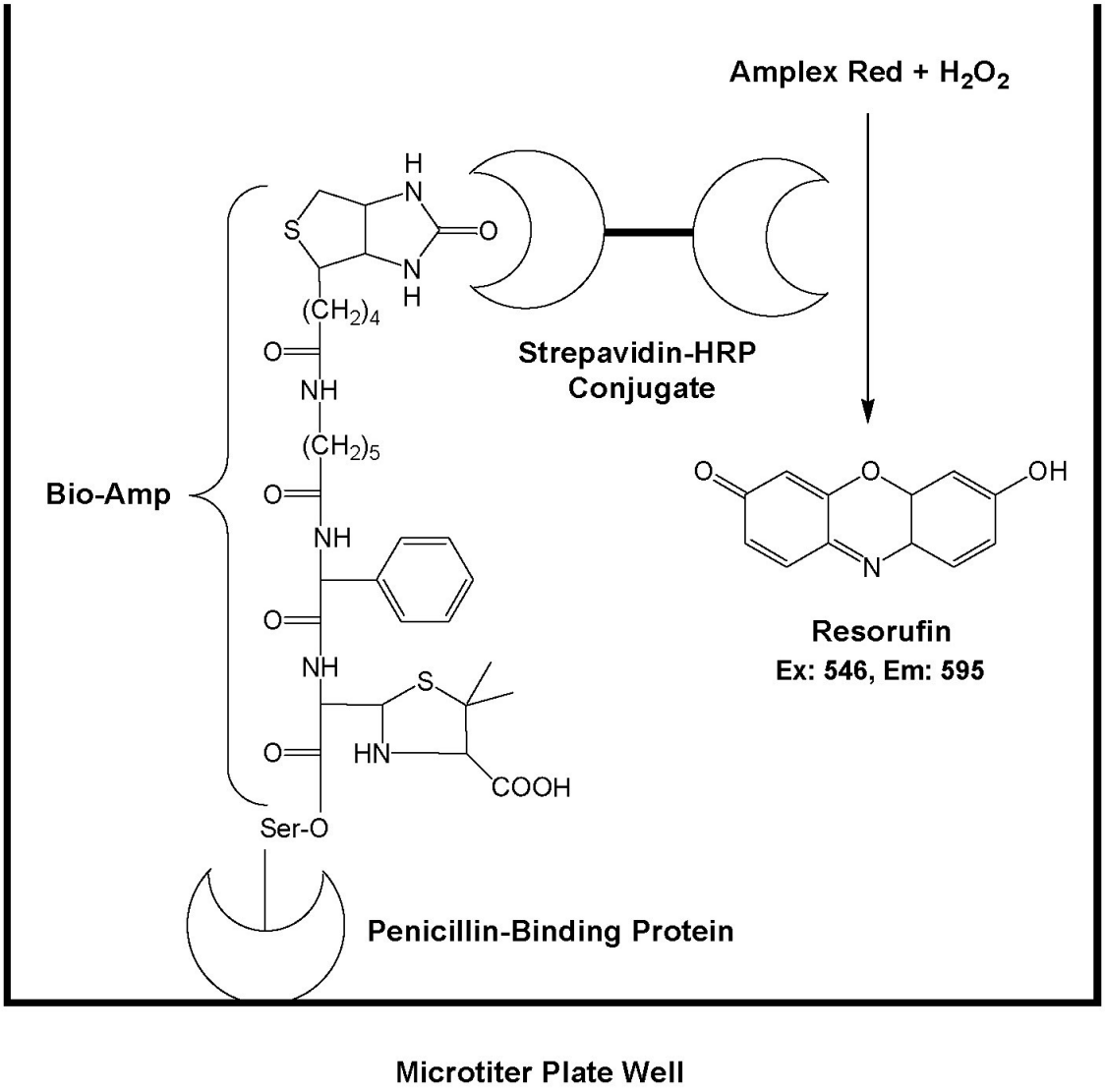

Figure 36: Diagram of the final complex formed in the assay and of the reaction catalyzed by HRP to provide a detectable fluorescent product.

RESULTS

Preparation of Bio-Amp

The conjugation of biotin to ampicillin was straight forward and the conjugate of Bio-Amp was analyzed by LC-MS revealing the identity and purity (Figure 37). The product purity was greater than 95% as determined from the UV absorption spectra.

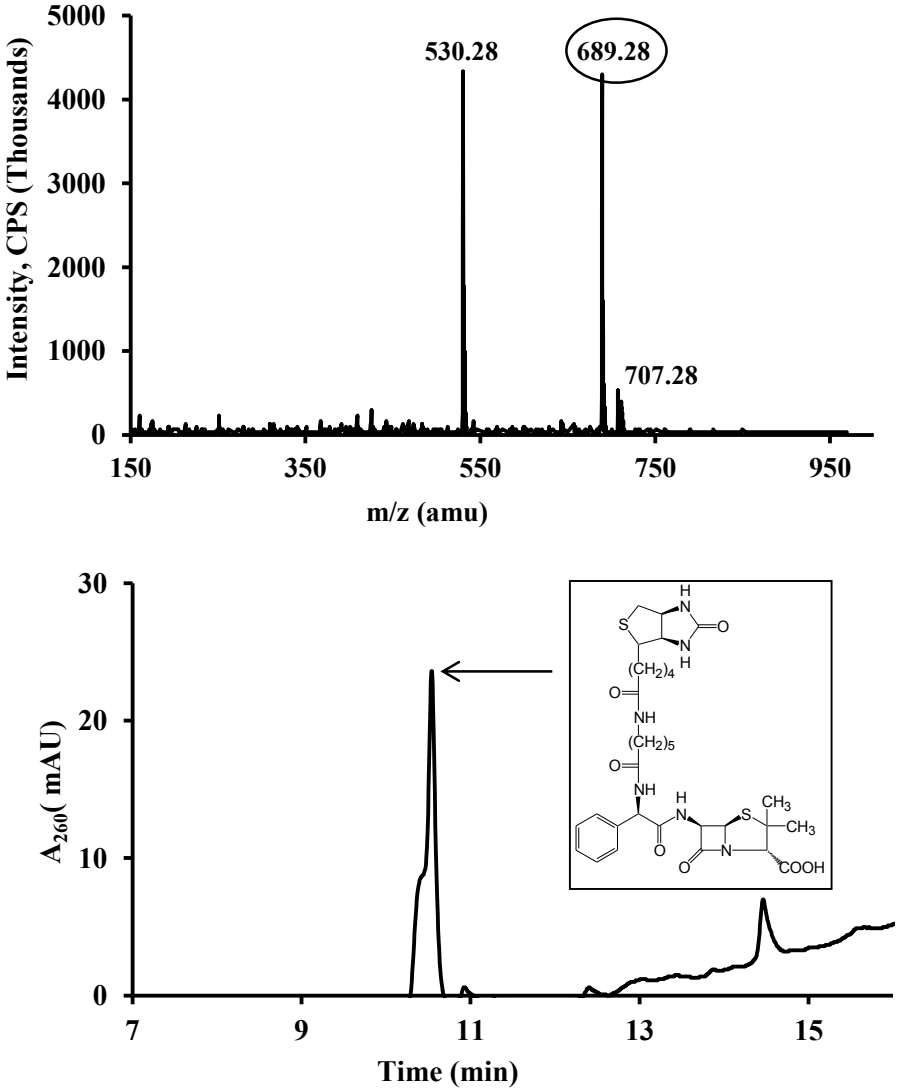

Figure 37: LC-MS spectra of Bio-Amp prepared as described in materials and methods. (Top panel) Mass spectral signal showing $[M+H]^+$ peak for Bio-Amp (m/z 689.28). (Bottom panel) UV absorption spectra at 260nm showing the purity of the Bio-Amp. Structure of Bio-Amp shown in inset.

PBP loading onto microtiter plates, labeling and detection

To demonstrate the application of this microtiter plate based assay, different PBPs were chosen (EC PBP1B, NG PBP1, and NG PBP2, which belong to the class of HMM PBPs, NG PBP3, and EC PBP5, which belong to the class of LMM PBPs). The initial proof of principle experiment with 100 µM of Bio-Amp gave good detectable fluorescence with all the studied PBPs (Figure 38). NG PBP2 gave the highest signal intensity whereas EC PBP5 gave the lowest. Even though the signal intensity was low for EC PBP5, it was strong enough to characterize the protein.

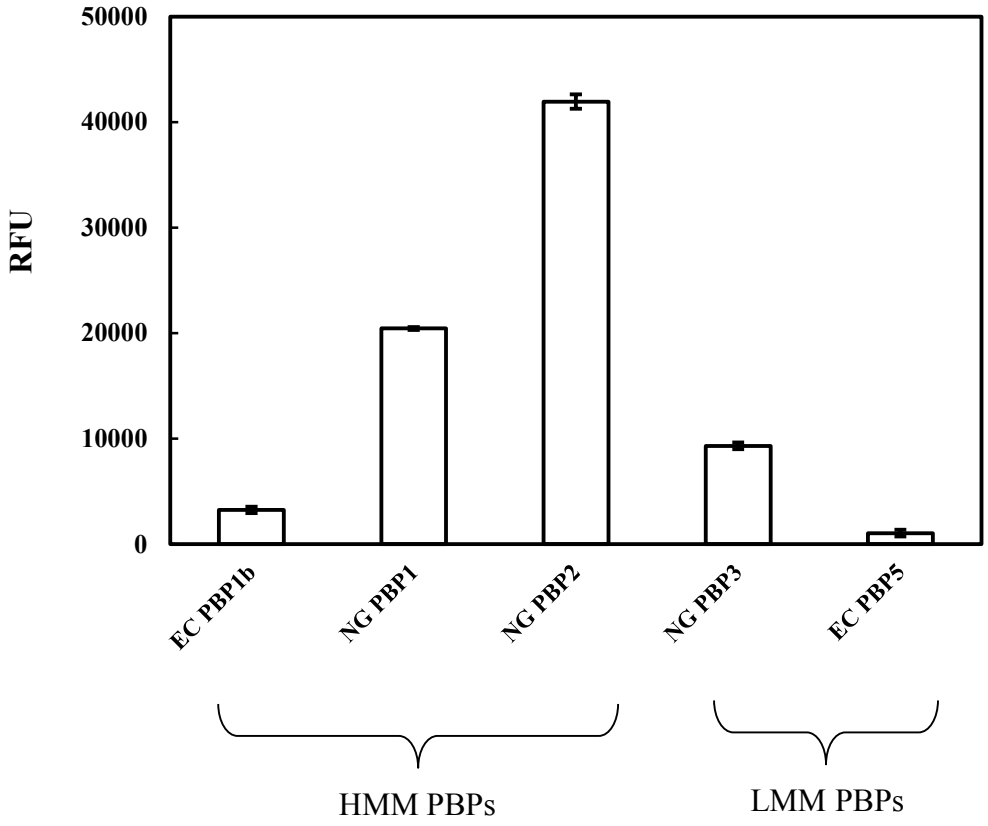

Figure 38: Bar graph of the fluorescence readings (relative fluorescence units [RFU]) obtained from five different PBPs after loading, treatment with 100 µM Bio–Amp, and developed as described in the text (±standard errors [SE], n = 4).

Determination of Bio-Amp K_m for binding vs various PBPs

Bio-Amp was titrated against all the PBPs to determine the concentration at which half of the enzyme was bound (K_m). All the enzymes tested showed good saturation binding curves. A representative binding curve of NG PBP2 is shown in Figure 39. The observed K_ms range from 0.011 μM to 100 μM. NG PBP3 gave the lowest binding constant with 0.011 μM and EC PBP5 gave the highest binding constant with 100 μM (Table 12). The apparent high binding constant for EC PBP5 might be due to the carboxypeptidase activity of the enzyme. Control experiments were conducted without the substrate (Bio-Amp) and without the enzymes and the experimental data were corrected to account for the background fluorescence.

Application to HMM PBP-inhibitor screening and characterization

The developed assay was used for inhibitor screening and characterization. HMM NG PBP2 was used a model enzyme. All the inhibitors tested showed good inhibitory binding curves. A representative binding curve of NG PBP2 with ampicillin is shown in Figure 40. The K_i determined for ampicillin against NG PBP2 was 1 μM, which was close to the K_m observed for Bio-Amp (1.1 μM). Control experiments were conducted without the inhibitor and without the enzyme and the experimental data were corrected to account for the background fluorescence.

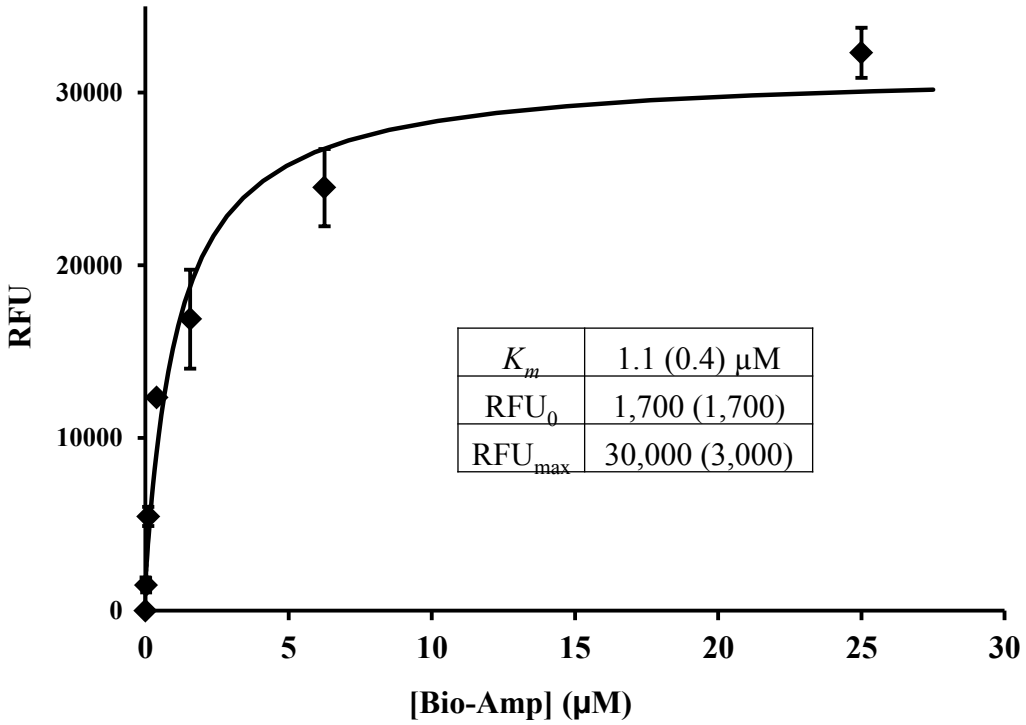

Figure 39: Plot of the RFU for NG PBP2 versus [Bio–Amp] (±SE, n = 4). The best-fit curve (Eq. 14) and parameter values (±SE) are also shown.

Table 12:
Microtiter plate determined K_m values for Bio-Amp with several PBPs.

Enzyme	K_m (μM)
EC PBP1B	1.6 ± 0.2
NG PBP1	0.9 ± 0.2
NG PBP2	1.1 ± 0.4
NG PBP3	0.011 ± 0.003
EC PBP5	100 ± 30

Abbreviations: EC: *E. coli*, NG: *Neisseria gonorrhoeae*

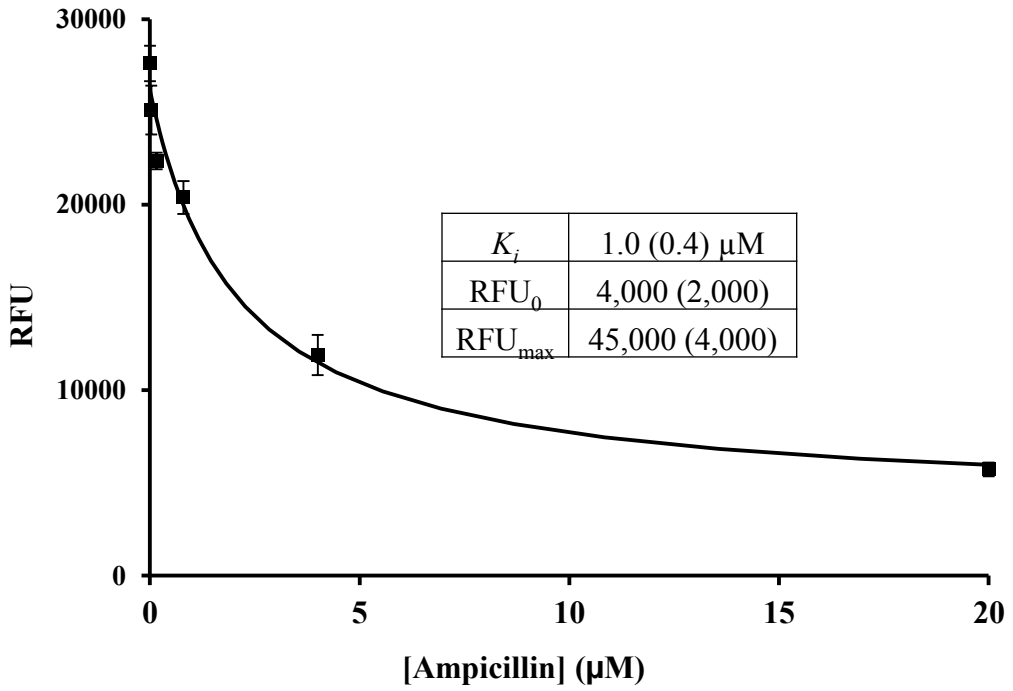

Figure 40: RFU for NG PBP2 versus [AMP] at fixed [Bio–Amp] (equal to its K_m). The best fit curve (Eq. 17) and parameter values are also shown.

DISCUSSION

A straightforward and generally applicable analytical method capable of detecting and screening for HMM PBP inhibitors is expected to be very useful for efforts to develop new and/or improved antibacterial agents. However, purified HMM PBPs generally give low or undetectable activity in enzyme activity based assays, for reasons, which are as yet poorly understood. Since a universal feature of the PBPs – by definition – is β-lactam binding, a β-lactam binding assay appeared to offer the potential for a general assay method, which could be used to screen for and characterize inhibitors of the essential HMM PBPs. Our effort to develop such an assay was based on the Bio-Amp reagent previously described by Dargis and Malouin for the detection of PBPs from membrane extracts[74]. The approach used is derived from a standard immune-capture assay approach, with the major exception that no antibodies are used (Figure 36). Instead, the PBP is bound directly to the microtiter plate by simple incubation, followed by active site labeling using a β-lactam-biotin conjugate which reacts to form a covalent adduct with the microtiter plate attached PBP.

This PBP-(Bio-Amp) conjugate is then detected and quantitated by using a streptavidin horse radish peroxidase conjugate. The key steps to this assay are the binding of the PBP to the microtiter plate, and the Bio-Amp – PBP labeling reaction. The PBPs are generally not stable at room temperature for long periods, and for this reason incubations for loading PBPs onto the wells of microtiter plates were limited to 30 minutes. Also, PBP–β-lactam complexes are turned over (albeit usually very slowly), and it is necessary to "freeze" such a complex in a stable form in order for this assay approach to work. It was therefore necessary to find an approach that could denature the PBP so that it no longer had the catalytic potential to cleave the PBP-β-lactam ester linkage. At the same time, the PBP-β-

lactam ester linkage (Figure 36) is fairly labile, and the denaturation conditions could not be so harsh as to hydrolyze this linkage. A number of alternative methods were tested for this step, with heating at 80°C for three minutes giving the best results (data not shown). A preliminary test of this method, using a relatively high concentration of 100 μM of Bio-Amp, demonstrated readily detectible signals for all of the PBPs tested – both HMM and LMM (Figure 38).

Substantial variation in the signal between PBPs was observed, presumably due to differences between PBPs in the efficiency of binding to the microtiter plates. Next, the dependence on Bio-Amp concentration was determined. An example of the fluorescence signal from NG PBP2 vs [Bio-Amp] is shown in Figure 39, and a summary of K_m values for all of the PBPs included in this study are given in Table 12. This demonstrated a wide range of values for the K_m for individual PBPs, reflecting their affinity for the Bio-Amp reagent. Finally, to demonstrate the potential of this approach for the characterization of active site directed PBPs inhibitors, the competitive inhibition of NG PBP2 by ampicillin was characterized, as illustrated in Figure 40. The K_i obtained for ampicillin of 1.0 μM is very close to the K_m obtained for Bio-Amp of 1.1 μM (K_m and K_i values are equivalent for slowly turned over substrates, as in the present case). These values are both close to the previously reported value of 0.5 μM for NG PBP2 binding to penicillin G determined using a classical approach based on radiolabeled penicillin G[157]. These results indicated that NG PBP2 is relatively insensitive to the differences between these three (ampicillin, Bio-Amp, and penicillin G) β-lactams. The assay developed in this study provides a reliable and general method for quickly screening and characterizing active site directed inhibitors for the lethal

target HMM PBPs. Such a HMM PBP inhibitor assay is essential for the development of new antibacterial agents targeting the HMM PBPs.

CHAPTER 5

A MICROTITER PLATE-BASED ASSAY FOR INHIBITORS OF PENICILLIN-BINDING PROTEIN 2A FROM METHICILLIN-RESISTANT STAPHYLOCOCCUS AUREUS[75]

Note: Some of the work presented in this chapter especially MOE virtual screening and MIC determination has been done in conjugation with Sandeep Putty and presented here through personal communication with Sandeep Putty.

INTRODUCTION AND RATIONALE

Pathogenic bacteria have responded to the widespread use of antibiotics by evolving resistance mechanisms to commonly used antibiotics. Gram-positive bacteria mostly utilize PBP modification (*Streptococcus pneumoniae*)[159], modification of cell wall (VRSA), acquisition of new PBP (MRSA),[160] and β-lactamase production[161]. On the other hand, Gram-negative bacteria combine porins, efflux proteins, and β-lactamase activity to acquire resistance[162-164]. Serine β-lactamases operate on β-lactams in the same fashion as PBPs, by forming an active site serine-acyl enzyme intermediate, except that hydrolysis (deacylation) to release the bound acyl-enzyme inhibitor is relatively fast[165]. This allows the β-lactamases to inactivate β-lactam antibiotics. Considerable research has been devoted to finding compounds, which can inhibit β-lactamases, such as clavulanic acid, so that the traditional β-lactam antibiotics can reach their PBP targets. The development of resistance to this type of therapy demonstrates that this strategy can only provide a temporary solution to β-lactam resistance. The widespread usage of β-lactams has also led to an expansion of the originally

minor β-lactamase family. Metallo-β-lactamases encompass a separate class and uses a metal in its active site for catalysis[166]. Due to their different mechanism, these are not inhibited by normal serine β-lactamase inhibitors such as clavulanic acid[166]. Given the evolutionary mobility of β-lactamases, the prospects for keeping ahead of the evolution of β-lactam resistant bacteria with β-lactamase inhibitors appear dim. In contrast, PBPs are physiologically constrained by their requirement for cell wall biosynthesis. The development of resistance to β-lactam antibiotics has been paralleled by the development of resistance to other antibiotic classes, for example to vancomycin and the aminoglycosides. At present, it seems likely that bacteria resistant to essentially all the commonly used antibiotics will soon emerge.

Bacterial infections were the major cause of death and morbidity prior to the development of modern antibiotics, and the increasing resistance of pathogenic bacteria to commonly used antibacterial agents is of major public health concern. One organism of particular concern is methicillin-resistant *Staphylococcus aureus* (MRSA)[167-169]. The high level of β-lactam resistance seen in MRSA, as compared to methicillin sensitive *S. aureus* (MSSA), is due to the presence of a novel acquired penicillin-binding protein (PBP) - PBP2a[9,170-173]. MRSA is a serious public health threat due to its resistance to nearly all antibiotic classes (including β-lactams), and its continued emerging resistance to agents of last resort such as vancomycin[167,168,174-176]. Originally (at the time the first β-lactams were introduced into clinical practice), *S. aureus* (SA) was very sensitive to all β-lactam antibiotics. However, resistance to β-lactams due to β-lactamase production began to emerge and spread and by the late 1950s β-lactam resistant SA was a serious problem. Methicillin, a

β-lactamase resistant β-lactam, was introduced in 1959 to address this problem. However, with in few years there were reports of methicillin resistance in SA, which continued to spread until the present time. The origin of resistance to methicillin and related β-lactams was eventually determined to be due to horizontal transfer of a gene (*mecA*) for a novel penicillin-binding protein (PBP) – PBP2a[170]. PBP2a is intrinsically resistant to methicillin and other β-lactamase resistant β-lactams. The novel protein PBP2a reacts extremely slow with β-lactams. The presence of β-lactam antibiotics, which can successfully inhibit the essential PBPs in methicillin- sensitive *S. aureus* (MSSA), cannot inhibit PBP2a, which can continue to maintain peptidoglycan integrity in MRSA. Several structures of PBP2a have been reported, both unligated and acylated with different β-lactams[60], and these structures reveal that PBP2a is unusual from most other PBPs in two ways: it has a very narrow active site cleft, and it exhibits a substantial degree of conformation change between its ligated and unligated states. The low acylation efficiency of PBP2a with β-lactams is due to both the poor 'true' affinity, with dissociation constants ((k_d) (k_{-1}/k_1)) of the noncovalent complex EI (Eq. 1), which is in millimolar range and due to extremely slow acylation rate ranging from 0.2 to 0.001 s^{-1} [177,178]. One interesting observation is that the acylation rates of PBP2a increased in the presence of a peptidoglycan surrogate molecule, leading to the speculation that peptidoglycan can stimulate PBP2a allosterically[178,179]. Recently, several new β-lactams designed to target PBP2a have been developed for clinical use against MRSA infections[180,181]. This is encouraging, but these agents will likely only provide a temporary reprieve from the problem of antibiotic resistance in SA and MRSA[181,182].

PBP2a is a high molecular mass class B (HMM B) PBP and is solely responsible for β-lactam resistance in MRSA, which makes it a good target for new antibacterial drug

development efforts[9,170,173]. Assay methods for inhibitor binding to PBP2a have been described based on radiolabeled β-lactam binding[172], or on nitrocefin[183] (a chromogenic cephalosporin derivative) or BOCILIN-FL (a fluorescently tagged penicillin derivative) binding[65,178]. However, these assays are incompatible with a microtiter plate format required for efficient high-throughput inhibitor screening and characterization. The development and characterization of new inhibitors targeting PBP2a would benefit from an effective and convenient assay for inhibitor binding. Given the high intrinsic resistance of PBP2a to β-lactams, it was uncertain whether a microtiter plate β-lactam binding assay of the type we have described in Chapter 4 for other HMM PBPs, e.g., based on biotinylated β-lactams, would work with PBP2a. In this study, we investigated the use of biotinylated β-lactams in microtiter plate assays for PBP2a-inhibitor screening and characterization.

A common approach in determining PBP binding affinities is with a two step assay, where the β-lactam test agent is preincubated with the PBP for a short period (10 - 30 min) to allow complex formation, followed by addition of a saturating concentration of a β-lactam probe agent (such as a radiolabeled, fluorescently labeled, or biotin labeled β-lactam) for a short period (10-30 min), which reacts with and labels the uncomplexed PBP[64,74,184]. This approach is based on relatively slow β-lactam release kinetics from the PBP target, so that addition of probe cannot shift the equilibrium between the test agent-PBP complex substantially in the incubation times used. The slow off-rates observed for β-lactam probes bound to PBP2a indicates that such a kinetic approach is appropriate for measuring β-lactam test agents binding to PBP2a[183], but not for non β-lactam test agents (non covalent inhibitors) (a comparison of covalent vs non-covalent inhibitor binding and catalysis by PBPs is shown in Figure 41). To provide a basis for comparing the one step steady-state approach we

described previously[76] with a classic two step kinetic approach, a microtiter plate-based two step assay was also implemented. To demonstrate the applicability of the easy one step approach for non β-lactam inhibitors, the molecular operating environment program (MOE) was used to virtually screen inhibitors, and the best inhibitors were screened against PBP2a.

The availability of convenient and sensitive microtiter-plate based assays for the screening and characterization of PBP2a inhibitors is expected to facilitate the discovery and development of new PBP2a inhibitors for use in combating the serious public health problem posed by MRSA.

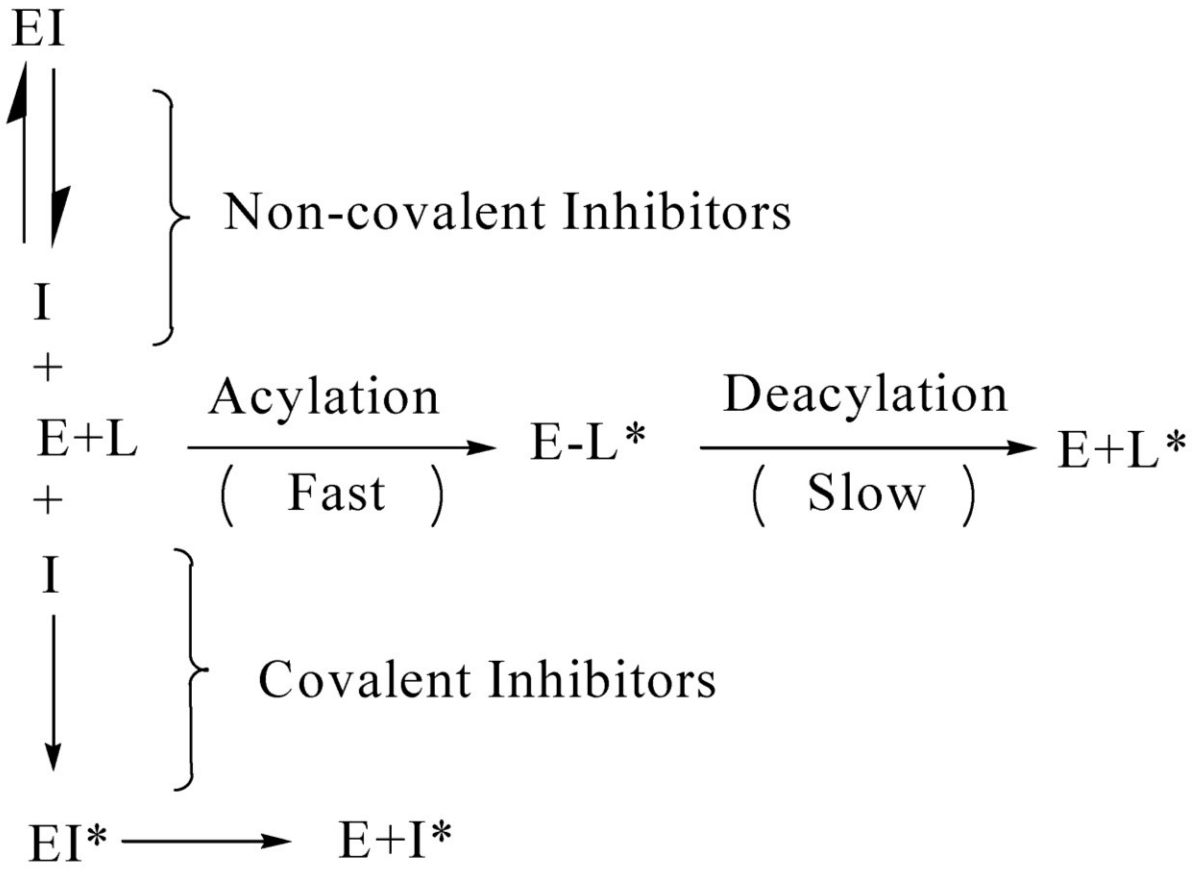

Figure 41: Covalent vs non-covalent inhibitor binding and catalysis by PBPs.

MATERIALS AND METHODS

Cloning of a truncated mecA gene

Chromosomal DNA of MRSA (ATCC 3300) was used as a template for PCR. Primers were designed based on the published *mecA* sequence from NCBI and the primers being a forward primer 5'-PBP2a-*Eco*RI, *Bam*HI: 5'-GGATCCGAATTCCTGGAAGTTCTGTTCCAGGGGCCCATGGCTTCAAAAGATAAA-3' and a reverse primer 3'-PBP2a-*Xho*I, *Hin*dIII: 5'-AAGCTTCTCGAGTTATTCATCTATATCGTA-3'. The primers were designed so that the first 23 amino acids at the N-terminus were deleted. The resulting DNA fragment (~2 kb) was gel purified and then extracted using a gel purification kit (Invitrogen) according to the manufacturer's protocol. The gene was ligated using T4 ligase into the pGEM®-T vector (Promega, Madison, WI), and transformed into competent XL1 Blue cells. The *mecA* gene in the pGEM®-T vector was sequenced using T7 and SP6 promoter primers. The verified insert DNA and the pGEX-4T1 vector (GE Healthcare, Piscataway, NJ) were both digested with same restriction enzymes (*Eco*RI and *Xho*I) and then ligated together to give the expression vector pGEX-PBP2a.

PBP2a expression

The recombinant vector pGEX-PBP2a was transformed into *Escherichia coli* BL21 (DE3) cells (Invitrogen) for protein expression. Cells were grown in Luria–Bertani broth containing 100 μg/mL ampicillin at 37ºC, until the culture reached 0.6 OD_{600}. The culture was chilled in an ice bath for 10 min, then placed in a shaker at 18ºC and protein expression induced by adding 0.5 mM IPTG (initial experiments with these conditions gave soluble

GST-PBP2a). Cells were then grown overnight (16 hrs) at 18ºC with shaking and then harvested by centrifugation at 4ºC. For large scale production, 3 one-liter flasks each containing 350 mL of culture were used.

GST-PBP2a purification

All purification steps were done at 4ºC. The bacterial cell pellet was resuspended in 60 mL cold lysis buffer (40 mM Na_2HPO_4, 10 mM KH_2PO_4, 300 mM NaCl at pH 7.4). Bacterial cells were lysed using a Microfluidizer (model M 100L, Newton, MA). The bacterial extract was centrifuged for 30 min at 30,000g the supernatant was collected, spun for an additional 20 min, and the supernatant was again collected and stored frozen at -80ºC. The GST-PBP2a fusion protein was purified on GST Resin (GenScript Cat. No. L00206) following manufactures (GenScript) instructions and eluted using glutathione. Selected fractions containing the desired protein were concentrated using an Amicon Ultrafiltration stir cell (Millipore, USA). Concentrated protein was dialyzed using 30 kDa cut off dialysis membrane in 100 mM NaCl, 1mM DTT, 50 mM Tris–HCl, pH 8, for 8-10 hrs, to remove glutathione used during elution.

Cleavage of the GST tag

Thrombin (GE Healthcare, Cat. No. 27-0846-01) was reconstituted with PBS to give a final solution of 1 unit/µL. Small aliquots were stored at -80ºC. To cleave the GST tag from purified GST-PBP2a, 35 µg of GST-PBP2a was treated with 70 units of thrombin at 4ºC overnight. SDS-PAGE was used to confirm cleavage. Fractions were collected, analyzed for

purity by SDS-PAGE, and concentrated using an Amicon Ultrafiltration stir cell. The final protein concentration was estimated by Bradford assay.

Biotinylated ampicillin (Bio-Amp) and biotinylated cephalexin (Bio-Ceph) preparation

Bio-Amp was prepared by a modification of the method of Dargis and Malouin[74] as described previously[76]. Bio-Ceph was prepared using the same procedure except that the final stock concentration was 4.2 mM due to the lower solubility of Bio-Ceph.

General procedure for GST-PBP2a loading onto microtiter plates, labeling, and detection

The protocol was similar to that described previously[76]. Briefly, for GST-PBP2a attachment, black walled microtiter plate wells (Costar, product no. 3631) were treated with 0.5-1 μg of GST-PBP2a in 50 μL of PBS/20% glycerol at 25°C for 30 min with gentle rocking, followed by treatment (3x) with 150 μL/well of blocking buffer (PBS/0.2% Tween-20), and then washing (3x) with 200 μL/well of washing buffer (PBS/0.05% Tween-20). To label GST-PBP2a in initial proof-of-principle experiments, 50 μL of 100 μM Bio-Amp or Bio-Ceph in PBS was added to the wells. After 15 min the biotin labeled GST-PBP2a was denatured with heating at 80°C for 3 min in a water bath, followed by quick cooling on ice. The plates were then washed (3x) with washing buffer (250 μL PBS/0.05% Tween-20). Streptavidin-horse radish peroxidase (HRP) conjugate (Pierce #21126) (50 μL of 0.4 μg/mL) was then added to each well. After 30 min the wells were washed (3x) with washing buffer, and 100 μL of a fluorescent HRP substrate mixture (1 mM H_2O_2, 20 μM Amplex Red (Molecular Probes) in 100 mM Tris pH 8.5) was added to each well. After 30-60 min the fluorescence signal was read (Excitation: 546 nm, Emission: 595 nm) in a Tecan Spectrafluor

Plus microtiter plate reader. An identical protocol was also followed using untagged PBP2a for comparison.

Determination of Bio-Amp and Bio-Ceph K_m for binding to PBP2a

To assess Bio-Amp and Bio-Ceph binding to PBP2a, microtiter plate bound PBP2a was treated with serially diluted (steps of 2) concentrations of Bio-Amp or Bio-Ceph (each concentration tested in triplicate), and the remaining steps of the assay performed as described above. To assess the effect of labeling reaction incubation time (in the GST-PBP2a + Bio-Amp reaction) on the detected signal, an alternative incubation time of 30 min for labeling was also tested. Data (relative fluorescence units; RFU) were analyzed for the K_m (the apparent steady-state binding constant to PBP2a, since PBPs turn over β-lactams, albeit generally very slowly) by fitting the data to Eq. 18[76]. No protein blanks were also included in these experiments.

$$RFU = RFU_0 + (RFU_{max} * [I]) / (K_m + [I]) \quad \text{..... Eq. 18}$$

Solution-phase SDS-PAGE-based Bio-Amp binding assay to confirm untagged PBP2a Bio-Amp binding activity, and to provide a solution phase K_m for Bio-Amp

GST-PBP2a and untagged PBP2a were labeled in solution with Bio-Amp, the complex denatured and resolved by SDS-PAGE, and Bio-Amp labeled proteins detected using a procedure similar to that described by Dargis and Malouin[74]. Briefly, to GST-PBP2a

and PBP2a, added the tagging reagent Bio-Amp at varying concentration and incubated for 15 min at room temperature. A range of concentrations of Bio-Amp were used in the labeling reaction to assess affinity (0x K_m, ⅛x K_m, ½x K_m, 2x K_m, 8x K_m). The protein- Bio-Amp complex was denatured by heating to 80^{o}C for 3 min and subjected to SDS-PAGE. The protein complex was then transferred onto nitrocellulose blot membrane. The blot was blocked using blocking buffer (PBS/0.2% Tween-20) (3x) and then washed (3x) with washing buffer (PBS/0.05% Tween-20). Streptavidin-horse radish peroxidase was added (0.4 µg/ml) and incubated for 25 min. This was treated with blocking buffer (3x) and developed using chemiluminescence kit (Pierce # 34078, Rockford, IL).

Characterization of inhibition of PBP2a using a one step approach

For inhibitor screening and characterization the concentration of Bio-Amp was used at a fixed concentration equal to the determined K_m for PBP2a, e.g. 1.6 µM of Bio-Amp. GST-PBP2a was first attached to the wells of a microtiter plate as described above. Serially (steps of 2) diluted solutions of the prospective inhibitor, plus Bio-Amp at a fixed concentration of 1.6 µM, in 100 µL PBS were added to the wells, with each concentration tested in triplicate. Different time points were tested (15 min and 30 min) to determine whether equilibrium was being achieved. After respective time points, the binding reactions were stopped and the plates developed as described above. With [Bio-Amp] = K_m, and taking into account the background (blank) fluorescence, the competitive (with Bio-Amp) inhibitor binding isotherm will be described by Eq. 19[76]

$$RFU = RFU_0 + RFU_{max} / ([I] / K_i + 2) \quad \text{..... Eq. 19}$$

Inhibitor binding data were plotted, and the saturation curves were analyzed for the K_i of binding by fitting the data to Eq. 19.

Screening of potential PBP2a inhibitors using a one step approach

To demonstrate the potential of this assay for inhibitor screening and characterization, a demonstration screening of 13 randomly selected β-lactam antibiotics (Table 13) against GST-PBP2a was performed. Screening was done with a high concentration of each antibiotic (750 μM), with the Bio-Amp concentration fixed at its K_m. Each determination was done in triplicate.

Characterization of inhibition of PBP2a using a two step assay approach

GST-PBP was bound to microtiter plate wells as described above. In the first step, various concentrations of ceftobiprole in 50 μL PBS were added to the wells. For the second step, after 15 min 50 μL of Bio-Amp at 16x the K_m for Bio-Amp (25.6 μM) (final concentration of 8x the K_m) was added to each well. After an additional 15 min the reactions were stopped by heat denaturation and the plates developed as described above. Taking into account the background (blank) fluorescence, the inhibitor binding isotherm in this experimental design will be described by Eq. 20, which can be derived following the same general procedure as previously described for Eq. 19[76]. Date collected using the two step assay were analyzed by fitting with Eq. 20.

$$RFU = RFU_0 + [RFU_{max} * K_i / (K_i + [I])] \quad \text{..... Eq. 20}$$

Structure-based virtual screening for PBP2a inhibitors

A virtual screen for PBP2a inhibitors was conducted in MOE (Molecular Operating Environment) software (Chemical Computing Group, Montreal, Canada). The Sigma-Aldrich 70% coverage library of molecules (~2000 compounds) was downloaded from the Zinc database at UCSF. This library was conformationally imported (i.e., with a substantial number of low energy conformations generated for each structure) into a MOE database to give the SA_70_conf.mdb library of structures. The target structure used for docking was the Protein Data Bank 1MWS structure[160], which is of the acyl enzyme complex of PBP2a and nitrocefin. The structure was prepared, and examined for the appropriate ionization state of residues within the active site pocket. The SA_70_conf.mdb library was then docked against the 1MWS structure using the MOE Dock function. The option to use forcefield refinement of the small molecule docked poses within a rigid target protein framework was selected.

Virtual screening compound selection, PBP2a inhibition assays, and anti-MRSA testing

The set of binding energy ranked SA_70 library compounds were examined in their docked possess within the PBP2a active site. Compounds with a predicted strong interaction with PBP2a near the atom site for the acyl-enzyme carbonyl atom were selected, since this is the catalytic focus of the reactions catalyzed by the PBPs. 10 high ranking compounds which showed favorable interaction with the catalytic core of PBP2a were selected for screening.

Compounds were purchased from Sigma-Aldrich, and screened for activity using our microtiter plate-based PBP2a assay. Compounds I-IV were identified as potential PBP2a inhibitors and were chosen for further characterization. Compounds I-IV (0.75 μmol) were tested by filter disc (0.5 cm) assay for antibacterial activity vs MRSA in the presence and

absence of 16 μg/mL cefoxitin. These four compounds were then tested for MICs against MSSA, MRSA, and MRSA+16 μg/mL cefoxitin, and also for K_is for PBP2a inhibition.

MIC determination

Minimal inhibitory concentrations (MICs) were determined by broth microdilution following CLSI guidelines (Clinical and Laboratory Standards Institute[185]). Two-fold serial dilutions of test agents were prepared in 100 μL of Mueller Hinton Broth (Difco) in the wells of microtiter plates. Wells were inoculated with ~1×10^4 colony forming units (cfu) of the test bacteria, and plates incubated for 16–20 h at 35°C. The plates were read for turbidity either visually or at 600 nm in a Tecan SpectroFluor Plus microtiter plate reader. The MIC was read as the lowest concentration of test compound for which no turbidity is apparent (Transmittance >90% of a media control well). All MIC determinations were performed in triplicate.

RESULTS

Cloning, expression and purification of GST-PBP2a

Truncated PBP2a omitting the first 23 amino acids from the N-terminus was cloned in pGEMT vector and verified using T7 and SP6 promoters (Figure 42). The verified gene was ligated to pGEX-4T1 to give pGEX-PBP2a (Figure 43). The recombinant vector was transformed in to *E. coli* BL21 (DE3) expression system and expressed as GST-fusion protein (GST-PBP2a). The expression of the protein was carried out at 18^{o}C for overnight. The GST-PBP2a was purified (>95% purity) using GST affinity chromatography (Figure 44). The size of the GST-tagged PBP2a was found to be ~100 kDa.

Cleavage of the GST tag

To obtain PBP2a, the GST tag was cleaved from GST-PBP2a using thrombin. The free GST tag and uncleaved GST-PBP2a were removed from the cleaved product PBP2a by passage over the GST resin as described in materials and methods. Purified untagged PBP2a passed though the column in the flow through, whereas GST and GST-PBP2a were retained. Samples at different time points were analyzed by SDS-PAGE (Figure 45). More than 90% of GST was cleaved within 4 hours of incubation and complete cleavage was achieved at 24 hours. The size of the PBP2a was found to be ~76 kDa. Concentration of the protein was determined by Bradford assay.

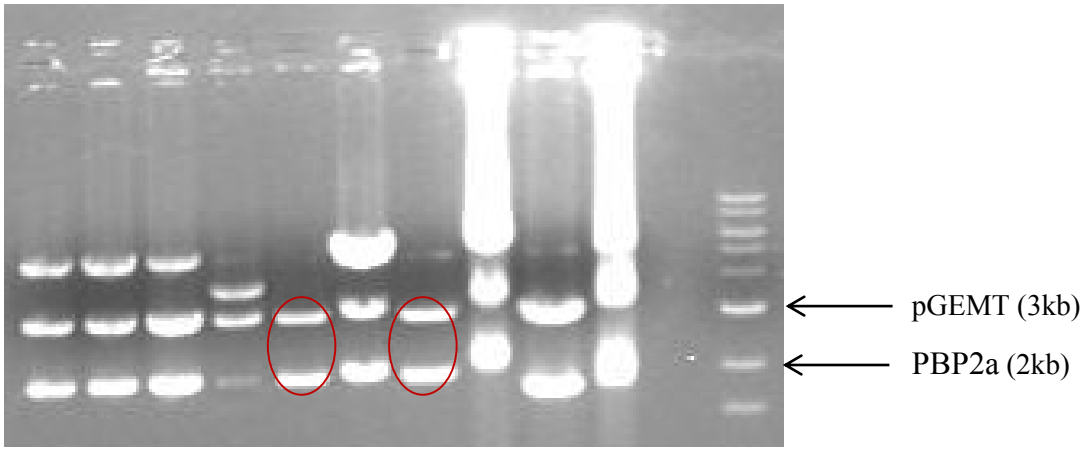

Figure 42: Double digestion results of different pGEMT-PBP2a clones with *Eco*R1 and *Xho*I. 1 kb ladder is shown at extreme right. The sizes of pGEMT (3kb) and PBP2a (2kb) are also shown. The recombinant vectors selected for subsequent cloning into pGEX-4T1 are circled.

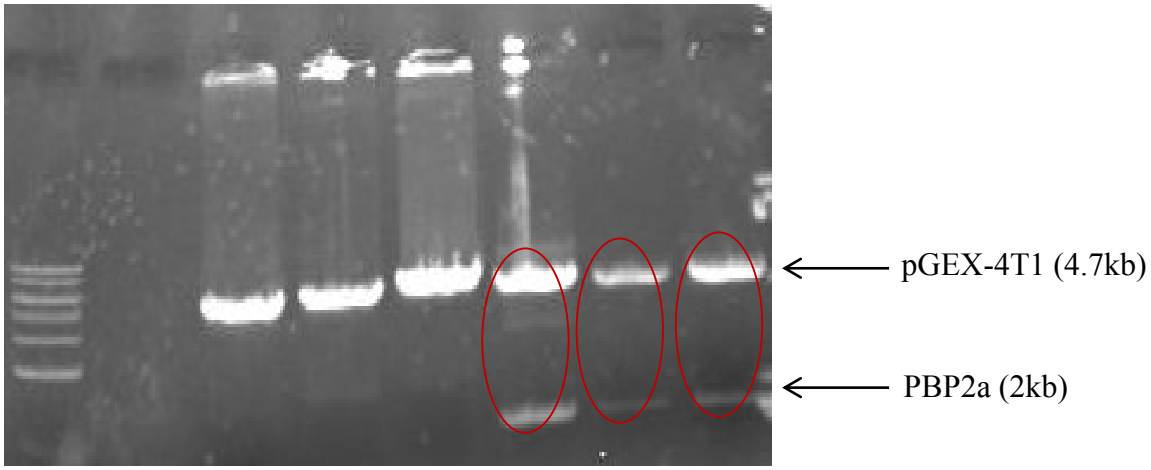

Figure 43: Double digestion results of different pGEX-4T1-PBP2a clones with *Eco*R1 and *Xho*I. 1 kb ladder is shown at extreme left. The sizes of pGEX-4T1 (4.7kb) and PBP2a (2kb) are also shown. The recombinant vectors selected for subsequent transformation into *E. coli* BL21 (DE3) for protein expression are circled.

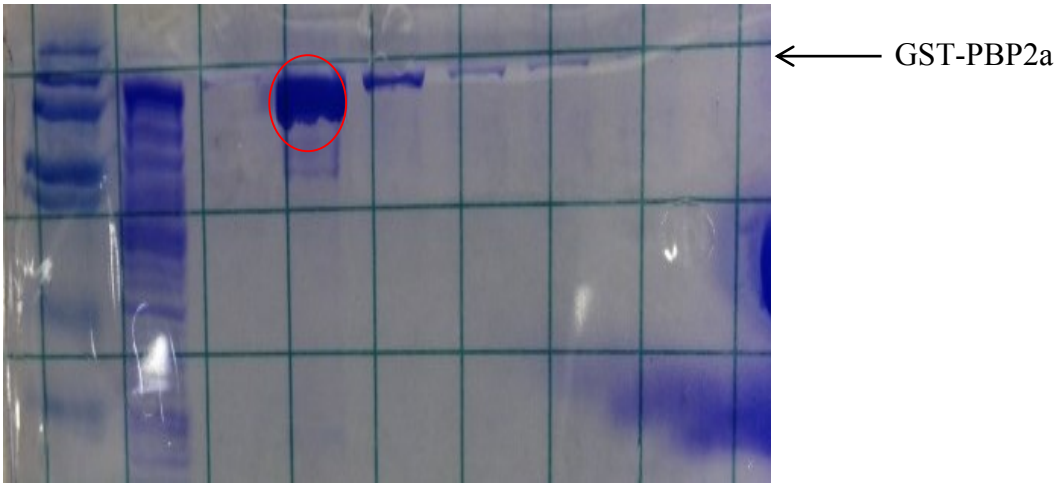

Figure 44: GST-PBP2a protein expression in *E. coli* BL21 (DE3) as described in materials and methods. Protein ladder is shown at extreme left. GST-PBP2a (~100 kDa) is circled.

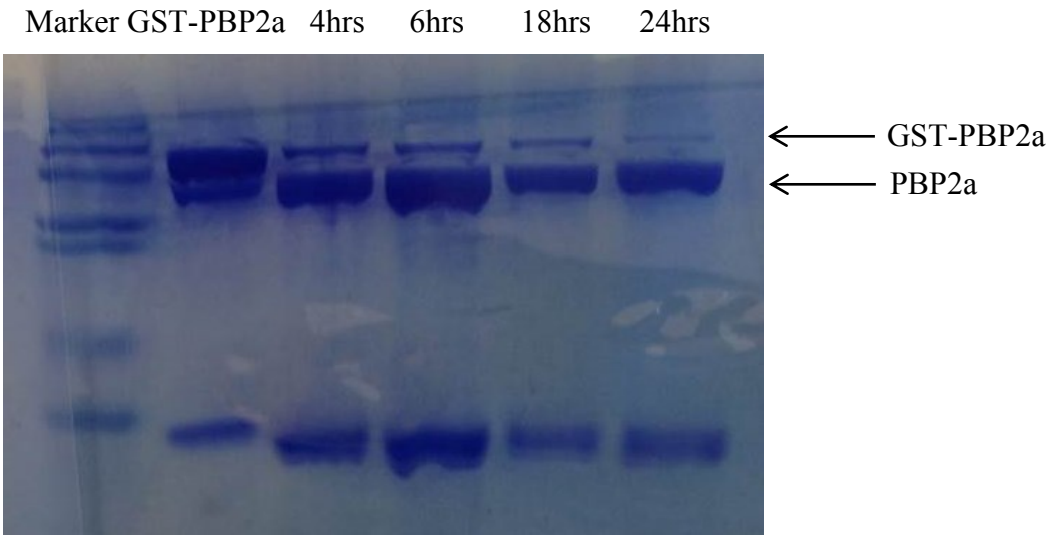

Figure 45: Cleavage of GST tag using thrombin as described in materials and methods. Protein ladder is shown at extreme left. GST-PBP2a (~100 kDa) and PBP2a (~76 kDa) are labeled. Different incubation time points of GST-PBP2a with thrombin are shown at the top of the figure.

Biotinylated ampicillin (Bio-Amp) and biotinylated cephalexin (Bio-Ceph) preparation

The identity and purity of both Bio-Amp and Bio-Ceph were confirmed by LC-MS analysis and both the reagents were greater than 95% pure. (Figures 37 and 46).

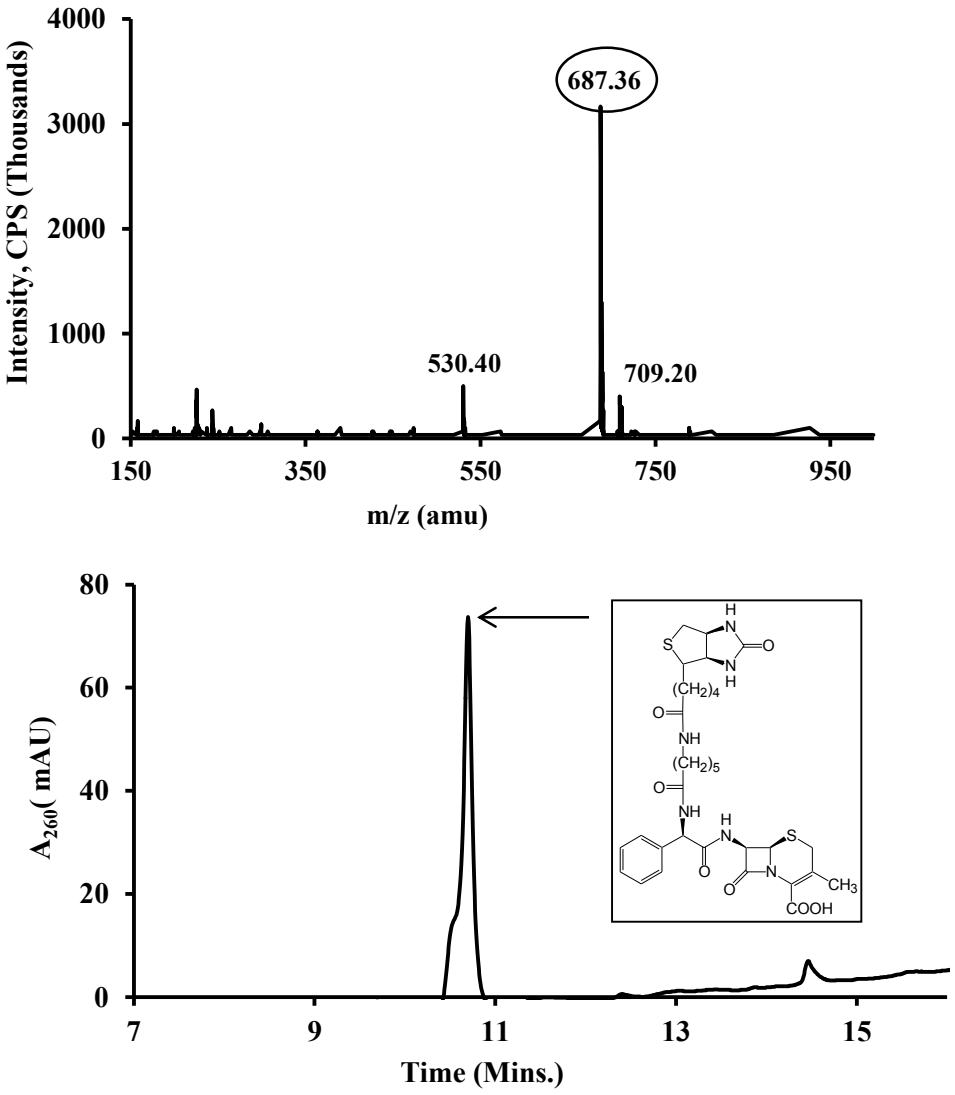

Figure 46: LC-MS spectra of Bio-Ceph prepared as described in materials and methods. (Top panel) Mass spectral signal showing $[M+H]^+$ peak for Bio-Ceph (m/z 687.36). (Bottom panel) UV absorption spectra at 260nm showing the purity of the Bio-Ceph. Structure of Bio-Ceph shown in inset.

General procedure for GST-PBP2a loading onto microtiter plates, labeling, and detection

As an initial proof of concept experiment, GST-PBP2a was loaded on to a microtiter plate, labeled with Bio-Amp and Bio-Ceph (100 μM), and detected with horse radish peroxide using amplex red as the substrate. GST-PBP2a was readily detectible under the assay conditions using both the reagents (Bio-Amp and Bio-Ceph) (Figure 47).

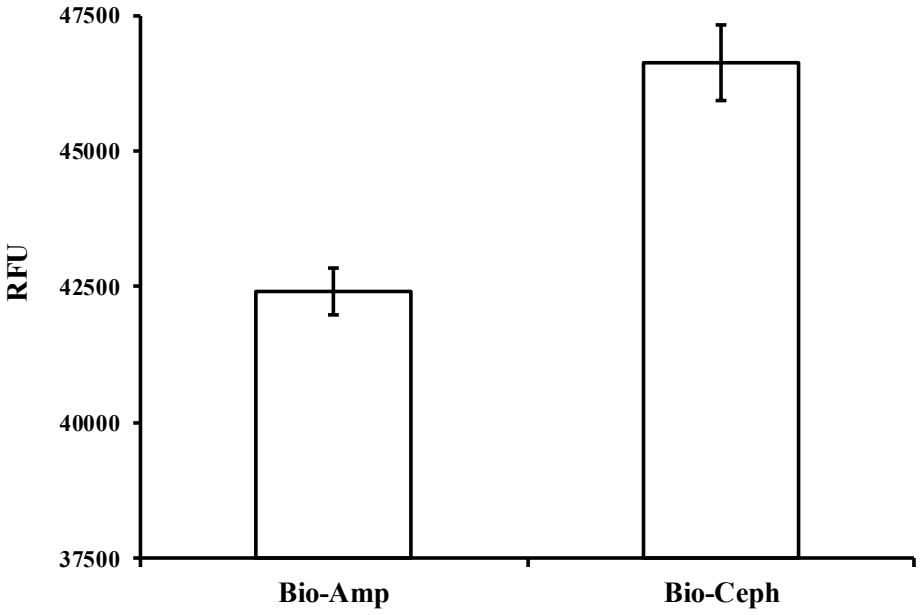

Figure 47: Proof of concept experiment showing labeling of GST-PBP2a with fixed concentration of Bio-Amp and Bio-Ceph (100 μM).

Determination of Bio-Amp and Bio-Ceph K_m for binding to GST-PBP2a

Bio-Amp and Bio-Ceph at varying concentration were titrated against GST-PBP2a to determine the binding constants. Both Bio-Amp and Bio-Ceph gave good saturation binding curves and fit perfectly for michaelis-menten kinetic equation (Figure 48). The apparent binding constants estimated by fitting to Eq. 18 using IBM SPSS under non-linear regression were 1.6 μM and 13.6 μM for Bio-Amp and Bio-Ceph respectively. Optimum incubation time of GST-PBP2a with Bio-Amp was tested at two time points (15 min and 30 min) to observe any change in signal intensity (relative fluorescence units and apparent binding constant). The observed apparent binding constants (K_m) obtained by fitting the data to Eq. 18 were virtually identical for 15 min (1.6 μM) and 30 min (1.7 μM) (Figure 48, Top panel). Based on this data, we chose the short incubation time of 15 min for all the subsequent experiments. Control experiments were conducted without the substrate (Bio-Amp) and without the enzymes and the experimental data were corrected to account for the background fluorescence.

Solution-phase SDS-PAGE-based Bio-Amp binding assay to confirm untagged PBP2a Bio-Amp binding activity, and to provide a solution phase K_m for Bio-Amp

As described further below in discussion section, GST-PBP2a gave good signals in the above described assay, but untagged PBP2a failed to give any detectible signal, even when the amount of PBP2a loaded into each well was increased up to 8 μg/well. This observation suggested that either untagged PBP2a was unable to bind Bio-Amp (e.g., it was inactive), or that untagged PBP2a was unable to bind to the microtiter plate wells. It was also desirable to determine if the affinity of GST-PBP2a for Bio-Amp in solution was the same as

in the microtiter plate-based assay, and also if GST-PBP2a (in solution) had the same affinity as PBP2a (in solution, and also if active). To address these issues, GST-PBP2a and untagged PBP2a were labeled in solution with Bio-Amp, the complex denatured and resolved by SDS-PAGE, and Bio-Amp labeled proteins detected using a procedure similar to that described by Dargis and Malouin[74]. The results from solution-phase SDS-PAGE analysis indicated that both GST-PBP2a and PBP2a were able to bind to Bio-Amp, and that binding to the proteins increased with increasing concentration of Bio-Amp (Figure 49). We also observed some untagged PBP2a present in the GST-PBP2a preparation due to the presence of endogenous proteases during GST-PBP2a purification.

Characterization of inhibition of PBP2a using a one step approach

For inhibitor screening and characterization the concentration of Bio-Amp was used at a fixed concentration equal to the determined K_m for PBP2a. This was selected since it is high enough to give ½ of the maximum possible assay signal and low enough to still allow inhibition to be readily detected. Ceftobiprole –a new β-lactam designed to inhibit PBP2a was characterized using this one step approach, incubating at 15 min and 30 min. Ceftobiprole showed a classic inhibition curve, with a decrease in signal intensity with an increase in concentration of ceftobiprole and the data fit well to the competitive binding equation. Both gave identical results with apparent K_m's of 6 and 7 μM respectively for 15 and 30 min (Figure 50) indicating steady state was reached within 15 min.

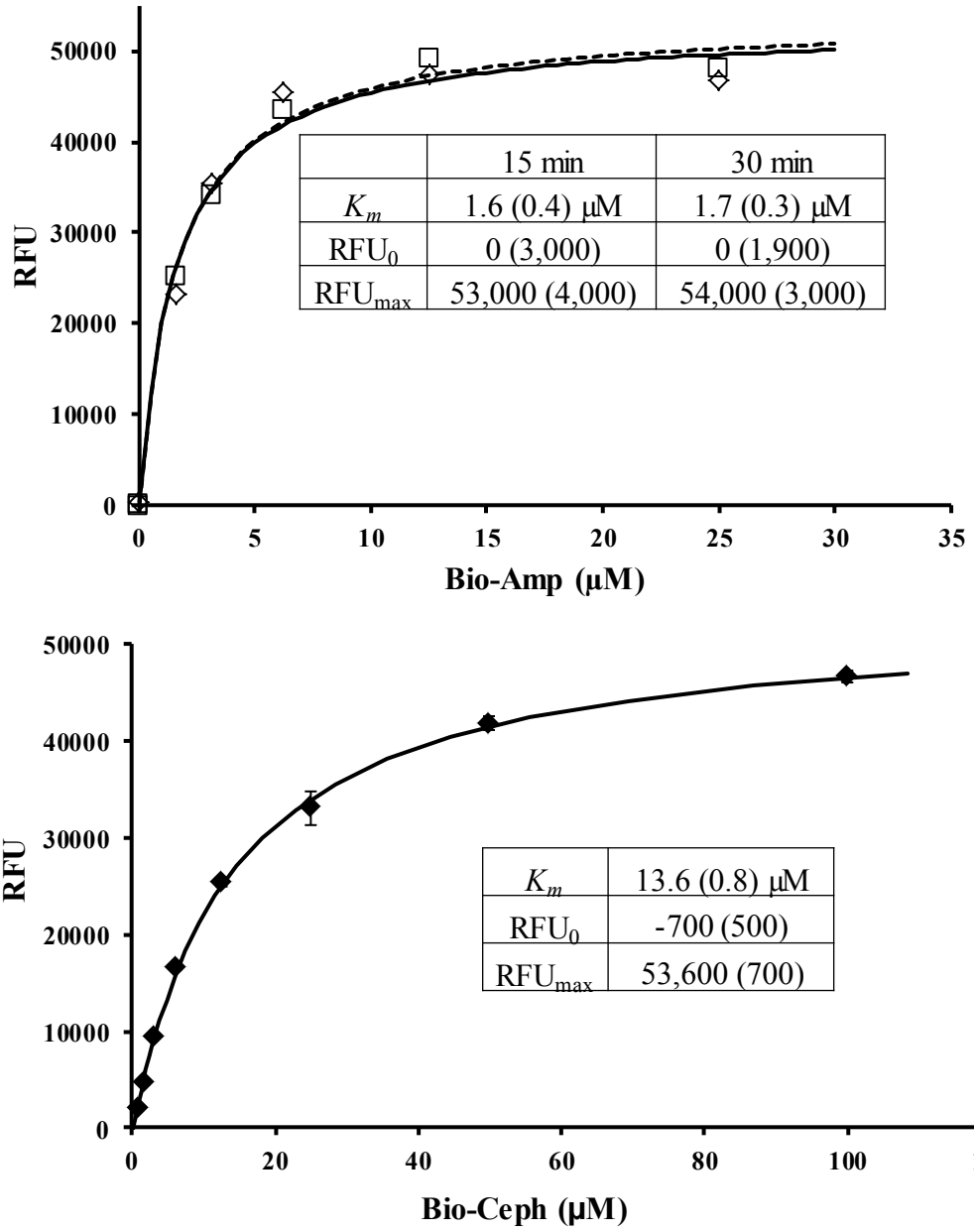

Figure 48: Top panel; Data, best fit curves, and best fit parameter values for titration of GST-PBP2a with Bio-Amp with 15 min and 30 min incubations. Data points obtained after 15 min incubations are denoted by diamonds (◊), and those after 30 min incubations are denoted by boxes (□). The best fit curve through data points obtained after 15 min incubation is denoted by the solid line, and after 30 min incubation is denoted by the dashed line. Bottom panel; Data and results for Bio-Ceph with a 15 min incubation. For all values standard errors are given in parentheses.

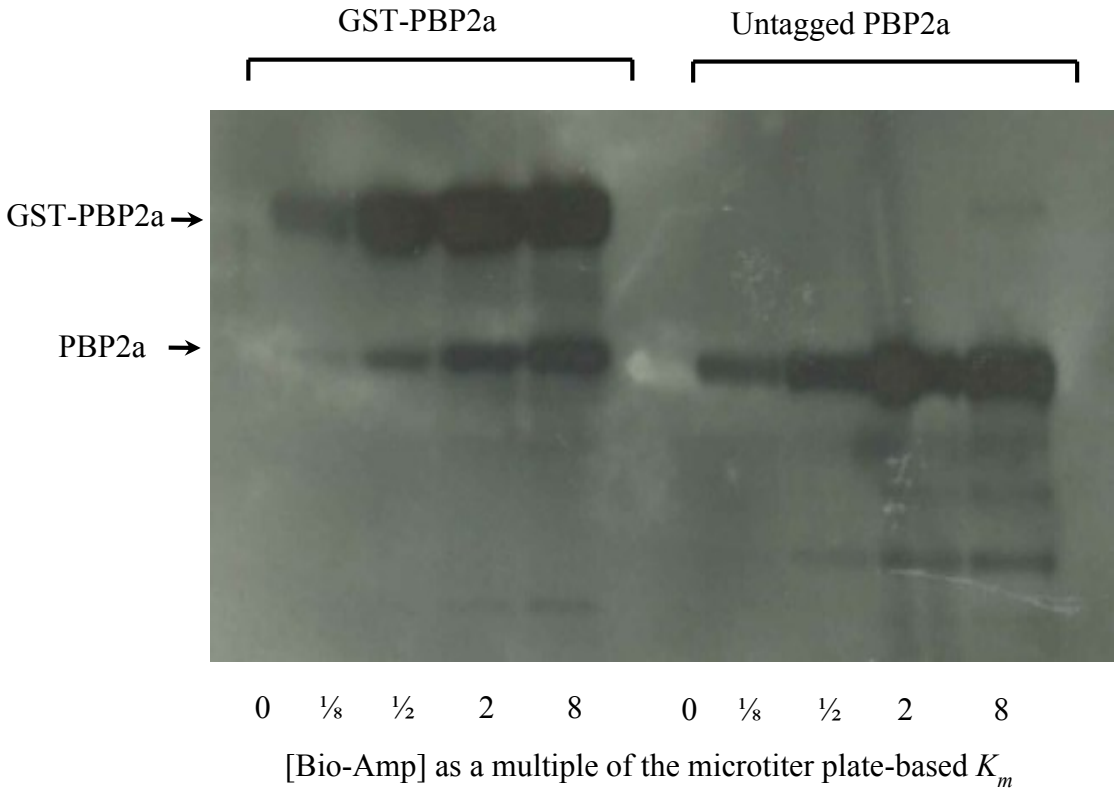

Figure 49: SDS-PAGE gel of Bio-Amp labeled GST-PBP2a (left) and untagged PBP2a (right), as a function of the Bio-Amp concentration relative to the K_m for Bio-Amp (as determined against GST-PBP2a in the microtiter plate based assay). Some untagged PBP2a was present in the GST-PBP2a preparation due to the presence of endogenous proteases during GST-PBP2a purification.

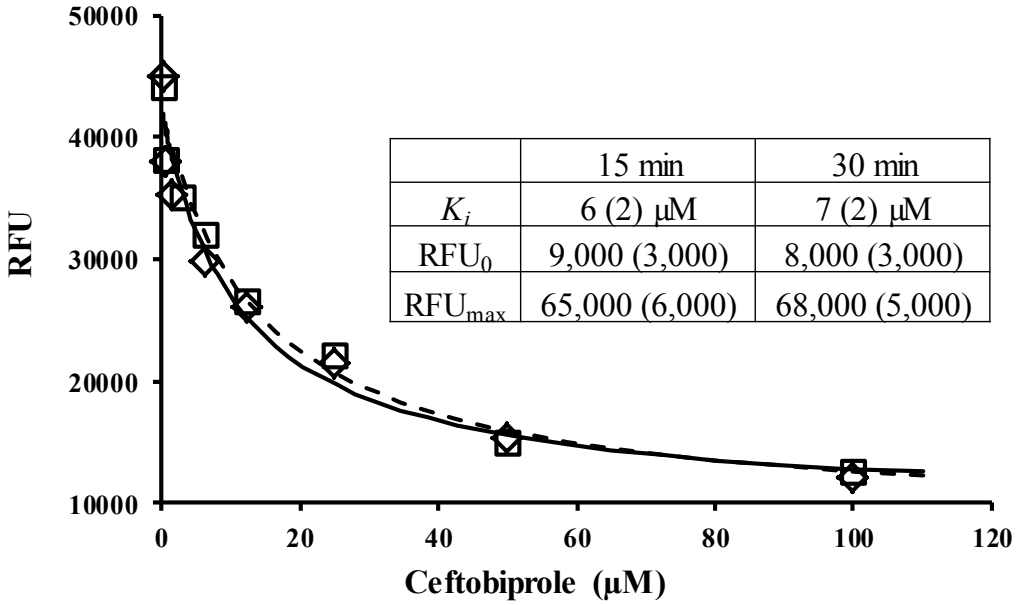

Figure 50: Competitive titration of GST-PBP2a by ceftobiprole in the presence of a fixed concentration (K_m = 1.6 µM) of Bio-Amp. including data points, error bars, best fit line and best fit parameter values. Data points obtained after 15 min incubation are denoted by diamonds (◊), and those after 30 min incubation are denoted by boxes (□). Best fit curve through data points obtained after 15 min incubation is denoted by the solid line, and after 30 min incubation is denoted by the dashed line. Standard errors are given in parentheses.

Application to screening of potential PBP2a inhibitors using a one step approach and inhibitor characterization

To assess the feasibility of screening of potential PBP2a inhibitors using a one step approach, 13 randomly selected β-lactam antibiotics were tested at 750 μM with Bio-Amp concentration fixed at its K_m (Table 13). Meropenem was selected for further characterization and subsequently, was titrated against GST-PBP2a to determine the apparent inhibitory constant. Both 15 min and 30 min incubation time points were tested to determine the steady state kinetics. The K_is were similar for both 15 min and 30 min (550 μM and 480 μM respectively), showing that equilibrium was reached within 15 min (Figure 51). Meropenem also showed a classic inhibition curve and the data fit well to the competitive binding equation (Eq. 19).

Characterization of inhibition of PBP2a using a two step assay approach

In order to compare our one step assay approach with the widely used two step approach, a two step assay was also performed by adding the inhibitor (ceftobiprole) first followed by incubation and addition of tagging reagent (Bio-Amp) at concentration 16 fold higher than the K_m for Bio-Amp. Using this approach, ceftobiprole gave good binding curve with apparent inhibitory binding constant of 2.9 μM (Figure 52).

Table 13:
Screening results in terms of percent inhibition of Bio-Amp binding in order of increasing potency. Given as value ± standard error.

β-Lactam (750 μM)	% Inhibition
Penicillin G	0 ± 2
Cefoxitin	0 ± 10
Cefuroxime	0 ± 8
Carbenicillin	0 ± 5
Cephaloridine	0 ± 2
Cefotaxime	0 ± 7
Aztreonam	0 ± 6
Ceftriaxone	0 ± 6
Ampicillin	8 ± 2
Cephalexin	15 ± 1
Cefoperazone	39 ± 1
Amoxicillin	48 ± 4
Meropenem	80 ± 2
Ceftobiprole	100 ± 3

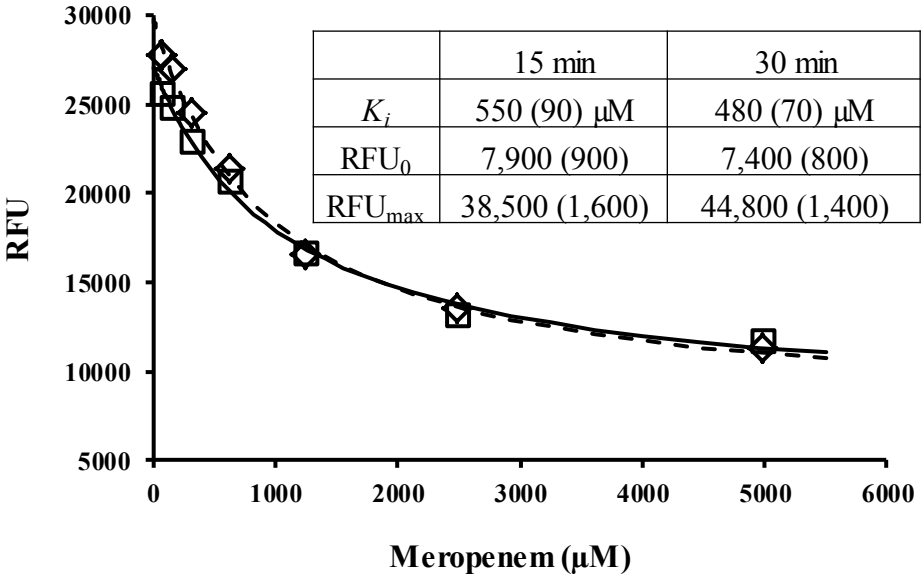

Figure 51: Competitive titration of GST-PBP2a by meropenem in the presence of a fixed concentration (K_m = 1.6 μM) of Bio-Amp. including data points, error bars, best fit line and best fit parameter values. Data points obtained after 15 min and 30 min incubations are denoted by diamonds (◊) and boxes (□) respectively. Best fit curve through data points obtained after 15 min and 30 min incubations are denoted by the solid line and dashed line respectively. Standard errors are given in parentheses.

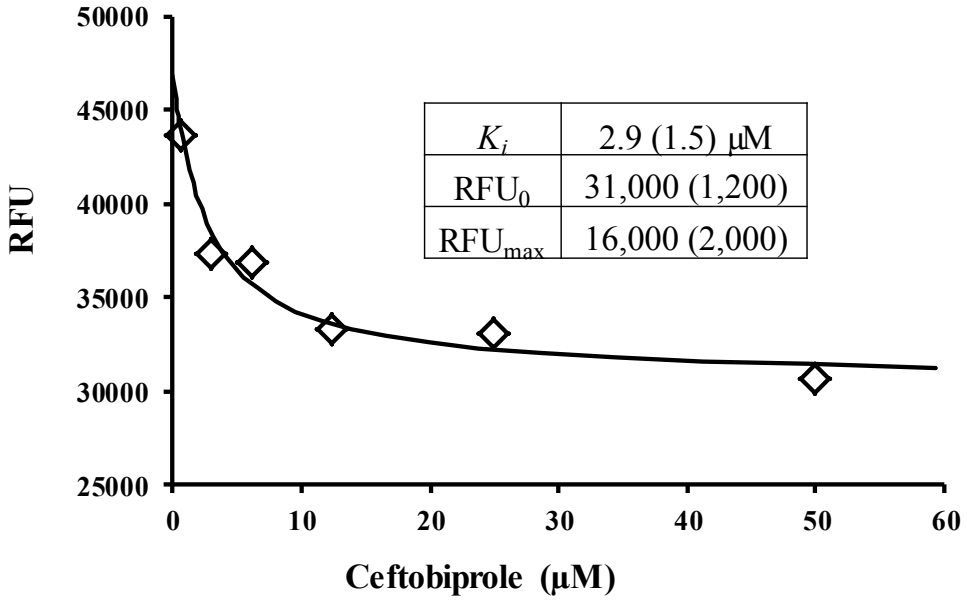

Figure 52: Results from two step (kinetic) binding assay result for ceftobiprole vs GST-PBP2a.

Virtual screening compound selection, PBP2a inhibition assay, and anti-MRSA testing

Several compounds were identified as potential PBP2a inhibitors by virtual screening against 1MWS.pdb structure of PBP2a. Based on ranking, cost, and commercial availability top ten candidates were chosen and evaluated for PBP2a inhibition ((I)- Boc-L-HomoPhe, (II)- 4-Phenylthiosemicarbazide, (III)- 5-(4-Chlorophenyl)-2,4-dihydro-[1,2,4]-triazole-3-thione, (IV)- Sulfaquinoxaline, (V)- 5-Phenyl-1,3,3-oxadiazole-2-thiol, (VI)- 3-Amino-2-(4-chlorobenzoyl)-6-nitrobenzofuran, (VII)- Naphthol, (VIII)- Fenoxaprop-ethyl racemate, (IX)- Coumarin 7, (X)- (-)-Riboflavin). All the compounds tested showed PBP2a inhibition (Figure 53).

Based on the inhibition data and the nature of the compound, four compounds (I-IV) were chosen and subsequently characterized. Compound I did not show any activity in MIC determinations, likely due to the high frequency of resistance apparent in the filter disc assays (Figure 54), but did show good PBP2a inhibitory activity. Compound II gave an MIC of 64 μg/mL vs MRSA+cefoxitin. Compound III gave an MIC of 16 μg/mL against MRSA+cefoxitin, and a low K_i of 1 μM, and also showed some activity against MRSA in the absence of cefoxitin, suggesting activity against one other lethal PBP target in MRSA (Table 14). A sample binding curve of Compund IV (Sulfaquinoxaline) is shown in Figure 55. Compund IV gave good MIC against MRSA (4 μg/ml) followed by compound III (64 μg/ml) and compound II (256 μg/ml).

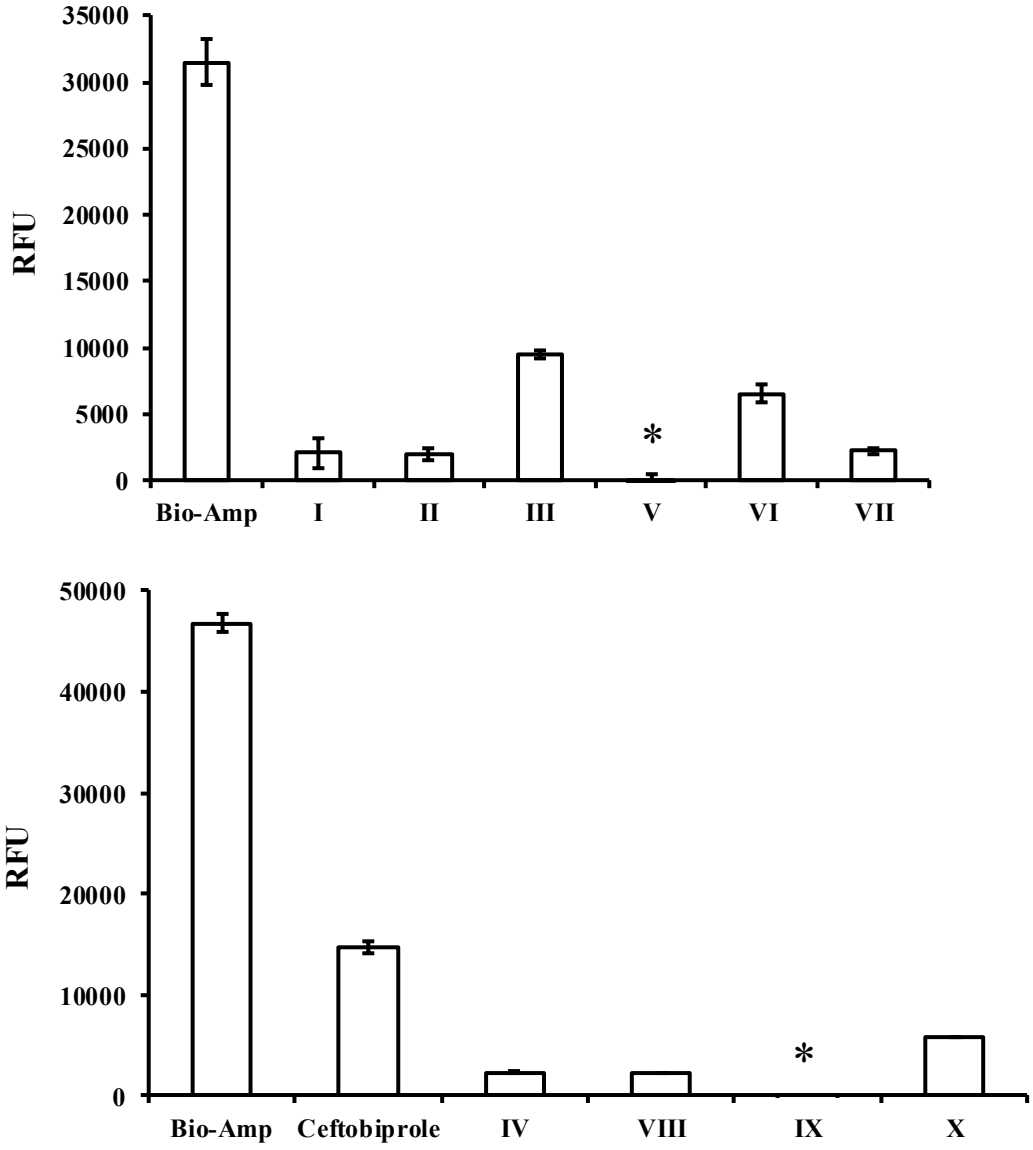

Figure 53: PBP2a inhibition assay for screening of top 10 virtual screening hits from MOE. All the compounds screened were at 750 μM.

Name of the compounds: (I)- Boc-L-HomoPhe, (II)- 4-Phenylthiosemicarbazide, (III)- 5-(4-Chlorophenyl)-2,4-dihydro-[1,2,4]-triazole-3-thione, (IV)- Sulfaquinoxaline, (V)- 5-Phenyl-1,3,3-oxadiazole-2-thiol, (VI)- 3-Amino-2-(4-chlorobenzoyl)-6-nitrobenzofuran, (VII)- Naphthol, (VIII)- Fenoxaprop-ethyl racemate, (IX)- Coumarin 7, (X)- (-)-Riboflavin.

* Compounds V and IX gave negative RFU values.

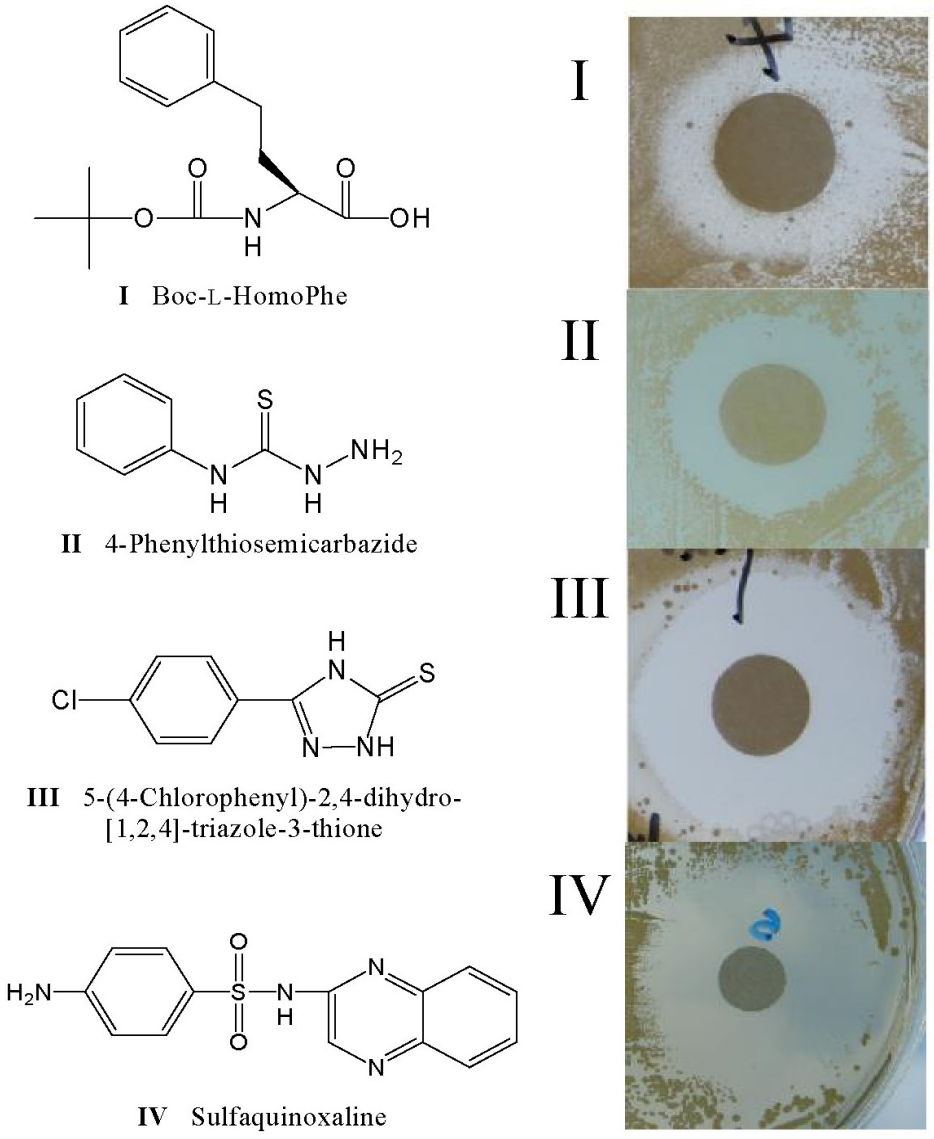

I Boc-L-HomoPhe

II 4-Phenylthiosemicarbazide

III 5-(4-Chlorophenyl)-2,4-dihydro-[1,2,4]-triazole-3-thione

IV Sulfaquinoxaline

Figure 54: Structures (left) and filter disc assay results (right) for four hits. 0.75 µmol of each test compound was spotted onto 0.5 cm filter discs and dried. Discs were placed onto Mueller-Hinton +16 µg/mL cefoxitin plates freshly spread with MRSA (ATCC # 43300), and incubated overnight.

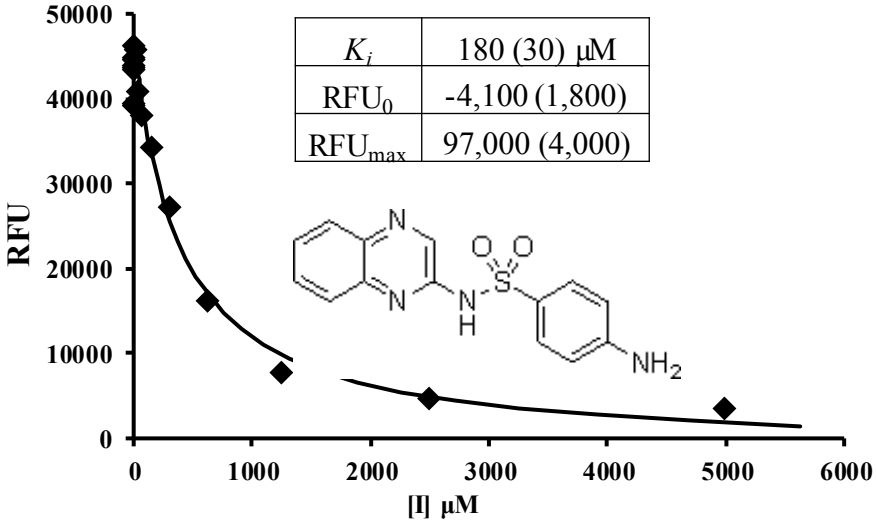

Figure 55: Competitive inhibition titration curve of GST-PBP2a by Compound IV in the presence of a fixed concentration (K_m = 1.6 µM) of Bio-Amp. Data points and best fit curve also shown.

Table 14:
MICs and K_i s for compounds I-IV, and for Bio-Amp and Bio-Ceph

	MICs (µg/mL)			K_i vs PBP2a
	MSSA	MRSA	MRSA + Cefoxitin	
I	NA[a] (High Frequency of Resistance)			37 µM (10 µg/mL)
II	256	128	64	160 µM (26 µg/mL)
III	64	64	16	1 µM (0.2 µg/mL)
IV[b]	2	4	2	180 µM (50 µg/mL)
Bio-Amp	ND	64	32	8 µM (4.6 µg/mL)
Bio-Ceph	ND	256	32	13 µM (7.4 µg/mL)

[a] NA – No activity. ND – Not determined.
[b] Compound IV is a known folate biosynthesis inhibitor, which might account for its observed antibacterial activity.

DISCUSSION

Assay development

Given the intrinsic resistance of PBP2a to most β-lactam antibiotics, it was uncertain at the outset if Bio-Amp and/or Bio-Ceph would bind to PBP2a. PBP2a was therefore over expressed as a GST fusion protein, and the potential of a Bio-Amp - or Bio-Ceph-based assay approach tested. In initial tests, strong signals were obtained with either 100 μM Bio-Amp or Bio-Ceph as the detection reagent, demonstrating the feasibility of this approach.

GST-PBP2a was next titrated with both Bio-Amp and Bio-Ceph to determine their respective apparent binding constants (K_ms). Both gave classic saturation binding curves (Figure 48). Analysis of these curves demonstrated binding constants of 1.6 μM for Bio-Amp and 13.6 μM for Bio-Ceph. These are both surprisingly good binding constants, and demonstrate that the biotinyl group can apparently form favorable interactions within the active site of PBP2a. That these two biotinylated β-lactams can effectively bind to PBP2a provides a foundation for their use in characterizing other inhibitors of PBP2a in competitive binding experiments.

The same effort using untagged PBP2a (obtained by cleaving the GST tag using thrombin) gave no signals. At first, it was suspected that the untagged PBP2a sample had lost its ability to bind Bio-Amp. However, a follow-up solution phase binding experiment using the Bio-Amp reagent followed by SDS-PAGE, blotting, and detection revealed that both the GST-PBP2a and untagged PBP were capable of binding to Bio-Amp (Figure 49). This experimental observation indicates that GST-PBP2a can bind efficiently to microtiter plate, whereas untagged PBP2a appears unable to bind to microtiter plate under the assay conditions used here. As also illustrated in Figure 49, the midpoint for the affinity of Bio-

Amp to GST-PBP2a and untagged PBP2a in solution is similar to the K_m as determined for GST-PBP2a as determined in the microtiter plate-based assay (Figure 48 (Top panel)). The one step assay is very precise. For the Bio-Amp titration with 15 min incubation (Figure 48 (Top panel)), the standard deviation for a set of replicate (n=3) samples averaged 4% of the total signal change over the titration (a standard deviation of 2000 RFU on average for each set of replicates, and with a total RFU change over the entire Bio-Amp titration RFU change of 53000 RFU).

Steady-state binding isotherm for Bio-Amp and lack of time dependence

To determine if the reaction of Bio-Amp with PBP2a was reaching steady-state under the conditions used here, the results of Bio-Amp + PBP2a incubations for 15 min and 30 min were determined and compared, and the data and analysis results are shown in Figure 48 (Top panel). It is clear that both the 15 min and 30 min incubations gave virtually identical results, and demonstrate that the reaction of Bio-Amp and PBP2a reached steady-state within 15 min. This is consistent with the time course for approach to steady-state for β-lactam binding in solution phase as reported by Graves-Woodward and Pratt[183]. The excellent Michaelis-Menten saturation binding curves observed for both Bio-Amp and Bio-Ceph (Figure 48) are also consistent with a steady-state reaction system.

Competitive one step binding assay for characterization of ceftobiprole binding to PBP2a

To demonstrate the utility of the one step microtiter plate-based assay described here for the characterization of inhibitors of PBP2a, it was used to characterize PBP2a inhibition by ceftobiprole (Figure 50) –a new β-lactam designed to inhibit PBP2a and provide a β-

lactam based treatment option for MRSA infections[180,181,186]. The results from the assay of variable concentrations of ceftobiprole vs. a fixed concentration of Bio-Amp are shown in Figure 50. Both 15 min and 30 min incubations were used in the PBP2a labeling reaction to determine if equilibrium was being achieved. Analysis of this competitive binding data by fitting with Eq. 19 gave a K_i of 6 μM after 15 min incubation, and 7 μM after 30 min incubation. The close similarity in K_i values at the two different incubation times indicates that a steady-state was reached within 15 min. Also, the competitive binding data fits very well to competitive binding equation (Eq. 19), further supporting this conclusion.

This K_i of 6 μM is above the MIC of ceftobiprole against MRSA of 1 μg/mL[186] (equal to 1.9 μM). This value is also slightly higher than range of IC_{50}s reported for ceftobiprole binding to PBP2a in membrane extracts of from 0.6 - 1.7 μM[187,188].

Comparison of one step and two step assays for ceftobiprole binding to PBP2a

In order to compare the results from a microtiter plate-based two step assay for characterizing ceftobiprole binding to PBP2a to those form the one step (equilibrium) binding assay described above, a microtiter plate-based two step assay was performed. The results from this two step microtiter plate-based assay are shown in Figure 52. Several features are notable. First, the K_i is lower than that determined using the one step assay, but the observed difference is not significant at the $P<0.05$ level. However, the lower K_i obtained with the two step assay is more consistent with the MIC of ceftobiprole against MRSA of 1 μg/mL[186](equal to 1.9 μM). This value is also more consistent with the range of IC_{50}s reported for ceftobiprole binding to PBP2a in membrane extracts of 0.6 - 1.7 μM[187,188].

Demonstration of inhibitor screening and follow-up inhibitor characterization

This assay (one step) was then tested for its utility in screening for PBP2a inhibitors. A random set of 13 β-lactams was selected, and screened for inhibition of PBP2a at 750 μM. This provided a ranked list of inhibitors (Table 13). As expected given PBP2a's intrinsic resistance to β-lactams, most of these β-lactams did not inhibit even at the relatively high concentration of 750 μM – only meropenem and ceftobiprole (positive control) gave greater that 50% inhibition (Table 13). As a follow-up, the K_i for meropenem inhibition was determined using the one step assay as described above for ceftobiprole, including with both 15 min and 30 min incubations, which gave K_i s of 550 (15 min incubation) and 480 μM (30 min incubation) for meropenem (Figure 51). This value of meropenem is approximately twice the IC_{50} value of 260 μM determined in membrane extracts[172], approximately a two-fold difference.

Virtual screening compound selection, PBP2a inhibition assays, and anti-MRSA testing

Four candidates (compounds I-IV) were chosen and further characterized for K_i and minimum inhibitor concentration (MIC). All the compounds tested (Boc-L-HomoPhe (I), 4-Phenylthiosemicarbazide (II), 5-(4-Chlorophenyl)-2,4-dihydro-[1,2,4]-triazole-3-thione (III), Sulfaquinoxaline (IV) showed antibacterial activity (MRSA) using filter disc assay (Figure 54). Compound I showed a substantial number of satellite colonies within the inhibition halo (Figure 54, top right), indicative of a possible high frequency of resistance. The filter disc assay results along with the structure of the compounds is shown in Figure 54. Two other compounds (compounds II and III) showed clear halos without any apparent resistance.

Compound IV is a sulfanilamide and has antibacterial activity against MRSA due to its anti-folate activity. The results of MICs and K_i's against PBP2a are given in Table 14.

However, since compound IV has antibacterial activity as a folate biosynthesis inhibitor, its observed anti-MRSA activity may not be due to PBP2a inhibition, nonetheless showed PBP2a inhibition at high concentration (Figure 55 and Table 14). Compound IV is still of significance since; 1) it demonstrates clear PBP2a inhibitory activity. 2) It suggests that suitably designed sulfonamides, a well established and readily accessible drug class, could provide effective new inhibitors of PBP2a. 3) It demonstrates that the virtual screening can identify interesting PBP2a inhibitors without chemical reactivity or other issues. Also included in Table 14 are results from Bio-Amp and Bio-Ceph for comparison. Both Bio-Amp and Bio-Ceph show activity against MRSA+Cefoxitin, and good binding to PBP2a in the *in vitro* assay.

Figure 56 shows the docked poses of compounds I-IV in the active site of PBP2a. Compounds I-III show a hydrogen bond to the catalytic Serine residue at the bottom of the PBP2a active site, and have a negative charge in this same area of the active site. This small set of lead compounds provides a preliminary pharmacophore for binding to the catalytic core of PBP2a, and demonstrates the potential of a virtual screening effort to identify new inhibitor chemotypes for PBP2a.

In conclusion, this study demonstrates a sensitive and convenient microtiter plate-based assay approach for the screening and characterization of inhibitors for PBP2a. The primary focus was on using a single step assay with a relatively short incubation time of 15 min. This approach was validated against a solution phase β-lactam assay detected by SDS-

PAGE, which demonstrated that GST-tagged PBP2a, necessary for binding to microtiter plates, bound Bio-Amp with the same affinity as untagged PBP2a, and that the solution phase and microtiter plate assays gave the same apparent binding constants within the resolution of these different approaches. The one step assay was further validated by using a longer (30 min) incubation time to demonstrate that the results using this assay were the same with the 15 min incubation time. Finally, a two step assay protocol was also implemented in the microtiter plate format. The K_i for ceftobiprole with the two step approach (2.9 μM) was lower that with the one step protocol (6 μM) but not by a substantial factor. The value for ceftobiprole binding obtained with the two step microtiter plate-based approach was similar to other studies using a two step SDS-PAGE-based approach as cited in the text. The one step approach gave more precise results that the two step approach, but the two step approach may provide a more accurate estimate, or at least an estimate more consistent with previous studies. For inhibitors (β-lactams) which reveal particularly slow acylation kinetics, a two step assay with inhibitor binding in the absence of competing probe may be preferable. For rapid screening and characterization of prospective new inhibitors the one step protocol will likely be preferred. Also, for the discovery and characterization of novel non-covalent PBP2a inhibitors, a slow off rate is not expected and the one step assay will be required for such efforts (a comparison of reaction kinetics of covalent vs non-covalent inhibitors is given in Figure 41). To demonstrate the applicability of one step approach for novel non-covalent PBP2a inhibitors, virtual screenings using MOE was used to identify potential non-β-lactam PBP2a inhibitors, and were screened and characterized using the one step assay. Given that PBP2a is a key molecular determinant for high-level β-lactam resistance in MRSA, and that new inhibitors for PBP2a could provide new agents effective against MRSA, the microtiter

plate-based assay approach described here is expected to facilitate the discovery, development, and characterization of new inhibitors against this important drug target.

Figure 56: Overlay of compounds I (magenta carbons), II (green carbons), III (cyan carbons), and IV (orange carbons) in their docked poses. Other atoms shown in their standard colors. This view is perpendicular to the long deep active site cleft in PBP2a, with the catalytic Ser shown at the bottom.

CHAPTER 6

QUANTITATIVE ANALYSIS OF CYTOPLASMIC UDP-PEPTIDOGLYCAN INTERMEDIATES IN S. AUREUS USING LC-ESI-MS/MS

INTRODUCTION AND RATIONALE

Bacterial peptidoglycan is a complex macromolecule that forms the bacterial cell wall and preserves cell integrity[189,190] Peptidoglycan is composed of alternating chains of *N*-acetylglucosamine and *N*-acetylmuramic acid linked by β-(1→4) linkages[27]. The biosynthesis of peptidoglycan is a multi-step process that can be divided into three stages. In Gram-positive bacteria, the first stage involves the formation of UDP-Mur-L-Ala-D-Glu- L-Lys-D-Ala-D-Ala through a series of steps initiated from UDP-*N*-acetyl glucosamine (UDP-NAG) in the cytoplasm. The first and the committed step of bacterial cell wall biosynthetic pathway is catalyzed by the MurA enzyme and catalyzes the conversion of UDP-NAG to UDP-NAG-enolpyruvate. The second step is catalyzed by MurB enzyme that reduces the pyruvate of UDP-NAG-enolpyruvate to lactyl yielding UDP-*N*-acetyl muramicacid (UDP-NAM). The subsequent steps involve a sequential addition of five amino acids. These addition steps are catalyzed by ATP driven amide bond ligases. In Gram-positive bacteria, MurC, MurD, MurE, and MurF enzymes catalyze the addition of L-Ala, D-Glu, L-Lys and D-Ala-D-Ala respectively. Cytoplasmic reactions catalyzed by Mur enzymes are shown in Figure 57. All the four Mur ligases (MurC, MurD, MurE, and MurF) have a similar enzymatic mechanism that involves the activation of carboxyl group by ATP, forming an acyl phosphate intermediate and subsequent formation of amide bond with the incoming amino acid. Even though the overall structural identity is low (15-22%), a number of specific motifs with high

degree of conserved structural features have been observed[3]. The second stage enzymatic reactions are catalyzed by enzymes MraY and MurG on the inner leaflet of the cell membrane. The peptidoglycan polymer (lipid II) formed in the second stage is translocated across the membrane and is incorporated into the growing peptidoglycan layer by transglycosylases and penicillin-binding proteins (PBPs) in the third stage[3,4].

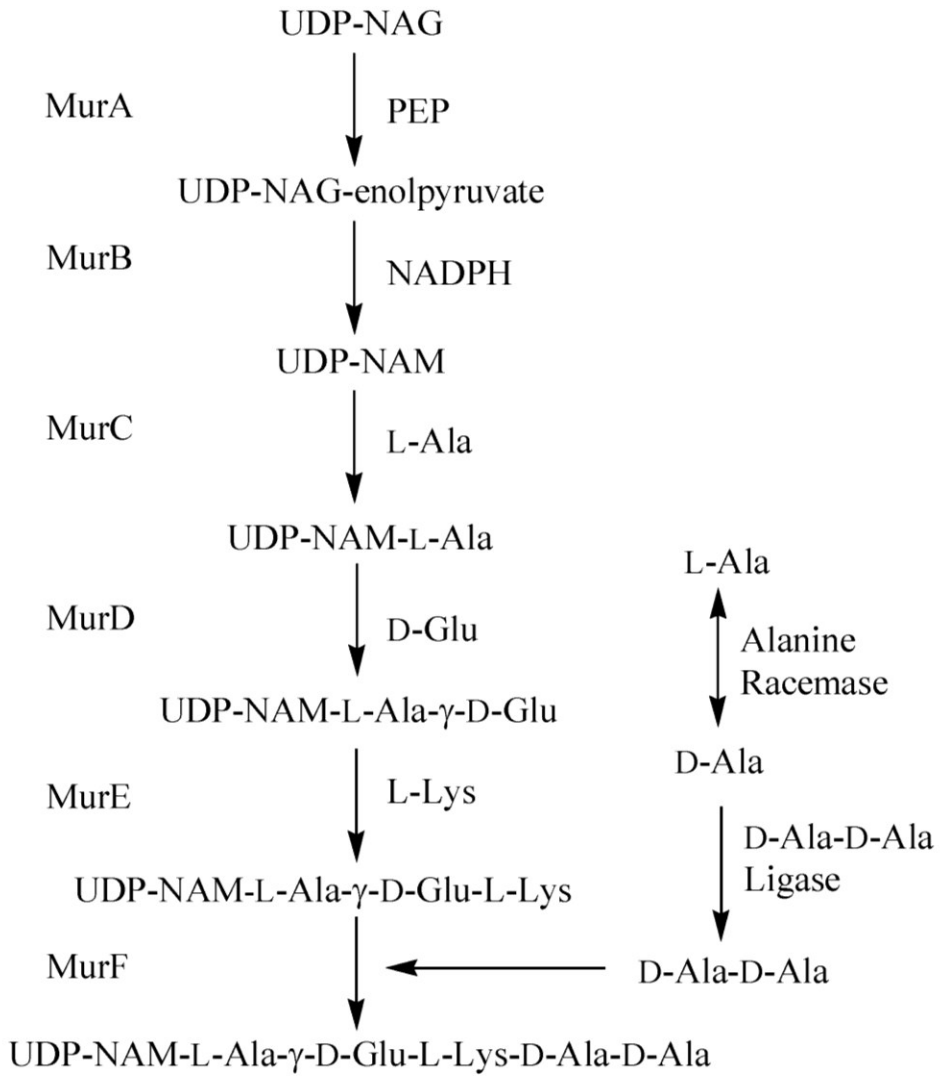

Figure 57: Cytoplasmic steps in cell wall biosynthetic pathway of *S. aureus.*
Abbreviations: PEP: phosphoenolpyruvate

The peptidoglycan biosynthetic pathway is the target of many antibiotics including phosphomycin, cycloserine, glycopeptides, and, β-lactams. The development of resistance due to extensive antibiotic use has become a major public health problem. Methicillin-resistant *Staphylococcus aureus* (MRSA) and vancomycin resistant *enterococci* (VRE) are of particular concern[75,144,160,191-193]. Further heightening concern is the fact that, although a number of new antibacterial agents from known antibacterial classes are under development, only two new classes of antibacterial agents, the oxazolidinones (e.g., Linezolid) and lipopeptides (e.g., Daptomycin), have been introduced into clinical practice in the last 40 years[144,194-196]. Therefore, there is a dire need for timely development of new antibacterial compounds.

Mur enzymes share a remarkable topological structural similarity, are unique to bacteria and are non-existent in eukaryotes[197]. Recently there has been an increase in interest in developing new antibacterial compounds targeting these enzymes, but so far phosphomycin is the only commercially available antibiotic targeting this pathway [3,198]. The Mur pathway is an important pathway and is of high interest as an inhibitor/drug development target due to increasing drug resistance to popular antibiotics. Mur enzymes have been the target of many novel inhibitors and much of the inhibitors have come from substrate structural analogs or transitional state analogs or from virtual screening[71,199-212].

A sensitive analytical method to quantify UDP-intermediates in the Mur pathway would be very useful for drug discovery and development efforts targeting this pathway. In light of growing accessibility to liquid chromatography-tandem mass spectrometry (LC-MS/MS) technology - with its benefits of sensitivity, selectivity, and relative ease of use - an LC-MS/MS assay for detection and quantitation of UDP-intermediates would meet this need.

The ability to quantitate *in vivo* levels of these cytoplasmic UDP-precursors is not only useful in drug development efforts, but would also provide insight into understanding the biochemistry of the Mur enzymes.

Detection and quantification of metabolic intermediates is always a challenge in complex biological extracts. The chromatographic separation of UDP-intermediates by reverse phase chromatography is especially challenging due to their polar nature. So far, reverse phase or ion exchange high performance liquid chromatography (HPLC) -based assays with optical spectrophotometry (UV/vis) have been employed to study and characterize these intermediates[198,211,213-222]. Some labs (especially Jean Van Heijenoort) have pioneered in this work[198,206,215,217-221,223]. However, these approaches suffer from labor intense sample preparation, limited sensitivity, and poor chromatographic resolution. Current sample preparation requires growing large scale bacterial cultures followed by preliminary purification with gel filtration and HPLC analysis. Another concern is the use of special columns and buffers for chromatographic separation of hydrophilic UDP-intermediates, as opposed to the widely used reverse phase columns and solvents. Currently, to our knowledge, characterization and quantitation of the cytoplasmic UDP-intermediates by LC-MS/MS has not been described. In the present study, the pool levels of cytoplasmic UDP-intermediates in *S. aureus* treated with phosphomycin, cycloserine, D-boroAla, vancomycin and ampicillin were quantified by LC-MS/MS. N, N-dimethyl hexylamine was used as an ion pair reagent for improved chromatographic resolution of the intermediates using reverse phase chromatography. Standard curves for UDP-NAM, UDP-Mur-L-Ala (UDP-Mono), UDP-Mur-L-Ala-D-Glu-L-Lys (UDP-Tri), and UDP-Mur-L-Ala-D-Glu-L-Lys-D-Ala-D-Ala (UDP-Penta) were generated from *S. aureus* treated with cycloserine and vancomycin. This assay

demonstrated that *in vivo* detection and quantitation of cytoplasmic peptidoglycan precursors by LC-MS/MS is feasible, opening the door for an improved understanding of the biochemistry of the Mur pathway and aiding drug discovery efforts targeting Mur enzymes.

MATERIALS AND METHODS

General

UDP-NAG and UDP-glucose were purchased from Sigma-Aldrich (St. Louis, MO). LC-MS/MS was performed on an AB Sciex 3200 QTrap LC-MS/MS mass spectrometer (Foster City, CA) in negative mode interfaced with a Shimadzu UFLC HPLC system (Columbia, MD) by electrospray ionization (ESI), and run using Analyst® v. 1.4.2. All chromatographic separations were performed on a Nucleodur 100-5 C_{18} 125 x 3 mm column (Macherey–Nagel, Bethlehem, PA) unless otherwise stated. M9 minimal media - consisting of Na_2HPO_4 (30g/L), KH_2PO_4 (15g/L), NH_4Cl (5g/L), and NaCl (2.5g/L) - was prepared following standard microbiology procedures. All centrifuge operations were performed on a Sorvall RT6000 refrigerated centrifuge unless otherwise stated. Klett measurements of *S. aureus* cultures were performed at 600 nm using a Biomate 3 Thermospectronic spectrophotometer (Waltham, MA).

Growth and preparation of bacterial extracts

A 10 mL saturated overnight (14hrs) culture of *S. aureus* grown in an incubator-shaker at 37°C was used as inoculum. After 14h, 400 mL of LB broth, Miller media (Luria-Bertani) with inoculum was transferred to baffled flasks and incubated with good agitation at 37°C. Cell growth was monitored by absorbance at 600 nm, with an observed doubling time of ~30 min. When the culture reached 0.5 to 0.6 OD_{600}, 60 mL portions were transferred to six 250 mL culture flasks. Antibiotics (phosphomycin, cycloserine, D-boroAla, vancomycin and ampicillin) were added at 10X of minimum inhibitory concentration (MIC) (MIC = 4 μg/mL for phosphomycin, 8 μg/mL for cycloserine and D-boroAla, 2 μg/mL for vancomycin, and 32μg/mL for ampicillin) in individual culture flasks. One control culture without antibiotic was prepared. After ~3 doubling times the cultures were rapidly cooled in an ice-water bath, 3 samples of 15 mL were removed from each flask into ice cold 15 mL centrifuge tubes, and the cells were pelleted by centrifugation at 4000 rpm for 15 min at 4°C. The cells were washed by re-suspending the pellet in 300 μL of ice-cold M9 minimal media and then centrifuged. The washing step was repeated. After washing, the cell pellet was re-suspended in 100 μL of ice-cold M9 minimal media, 100 μL of 25 μM UDP-Glucose was added as an internal standard (IS) and the sample was treated with 300 μL ice cold acetone (80% v/v). After mixing, the cells were lysed by snap freezing the tubes in liquid nitrogen. After thawing, the samples were centrifuged and supernatants were collected. The cell pellet was re-extracted by re-suspending the pellet in 200 μL of M9 minimal media and 300 μL acetone (80% v/v). The samples were centrifuged as described and the resultant supernatant fraction was transferred and pooled with the first supernatant. The samples were lyophilized, made up

to 200 μL with 0.1% formic acid in water (v/v) and filtered using Millex-GV filters (Millipore, MA). Samples were analyzed by LC-MS.

Growth and preparation of bacterial extracts for preparative HPLC

Sample preparation was as described above with the exceptions that 500 ml cultures were prepared and the antibiotics tested were cycloserine and vancomycin.

Preparative HPLC

The samples were purified by HPLC to identify and obtain the pure samples of UDP-intermediates. A Hewlett Packard-Ti series 1050 HPLC (Santa Clara, CA) was used with an Alltech-Econosil (250 x 22 mm) column. Chromatographic elution was performed at a flow rate of 5 ml/min with 3.2 mM of ion pair reagent (N, N dimethyl hexylamine) using a linear gradient. Mobile phase A was 0.1% (v/v) formic acid in water while mobile phase B was 0.1% formic acid (v/v) in 70/30 acetonitrile/water (v/v). Mobile phase B was ramped from zero percent to 50% over 70 min. 1 min fractions were collected using a Gilson 203 fraction collector (Middleton, WI). The fractions were analyzed by LC-MS to confirm the purity and identity of UDP-intermediates. The pure fractions were used to optimize the mass spectral parameters.

Mass spectral parameter optimization

Mass spectral parameter optimization was performed using the HPLC purified UDP-NAM, UDP-Mono, UDP-Tri, and UDP-Penta samples. For UDP-NAG, a commercially obtained standard purchased from Sigma-Aldrich (St. Louis, MO) was used. The

optimization was performed by automated quantitative optimization routine in Analyst® and the optimal parameters obtained are presented in Table 15.

Chromatographic conditions

Analytical scale chromatographic elution was performed at a flow rate of 300 µL/min. The solvents used were mobile phase A (0.1% (v/v) formic acid in water), mobile phase B (0.1% formic acid (v/v) in 70/30 acetonitrile/water (v/v)), mobile phase C (0.1% formic acid (v/v) in acetonitrile) and mobile phase D (160mM N, N dimethyl hexylamine). The chromatographic conditions used were with 8mM of ion pair (N, N dimethyl hexylamine) along with a linear gradient of 85% mobile phase A and 15% mobile phase B to 80% mobile phase A and 20% mobile phase B for 10 min.

Accurate mass spectral acquisition

The extracted HPLC-purified UDP-intermediates were diluted in 49/49/2 water/acetonitrile/formic acid (v/v/v) and infused directly into the ESI source of a high-resolution mass spectrometer at a flow rate of 10 µl/min. Accurate mass measurements were made on a Waters Synapt G2 High-definition mass spectrometry system (Milford, MA) in negative, full scan MS^E or MSMS resolution mode. Data were acquired over the *m/z* range 50 – 1200 using a capillary voltage of 3.5 kV, sampling cone voltage of 20 V, source temperature of 120°C and desolvation temperature of 350°C. For the high energy scan function of the MS^E scan type and the MS/MS data acquisition, a collision energy ramp of 15 – 45 eV was applied at the Trap traveling wave ion guide (TWIG). No additional energy was applied at the Trap TWIG for the low energy scan function of the MS^E scan type. A

continuous lock spray reference compound (fexofenadine) was sampled at 10 second intervals for centroid data mass correction.

Determination of response linearity, lower limit of detection (LLOD, lower limit of quantitation (LLOQ), possible matrix effects in bacterial extract, and carryover

For linearity, LLOD, and LLOQ determination, serial dilutions of UDP-NAG were prepared in bacterial extract. To assess matrix (bacterial extract) interference, a log phase *S. aureus* culture extract was prepared (using the procedure described above to test the effect of antibiotics on analyte levels), and serial dilutions of UDP-NAG, analogous to the serial dilutions in water, were prepared in this extract. Carryover was assessed by alternately analyzing blank samples and the UDP-NAG standard at the upper limit of quantitation (ULOQ, 2000 pmoles).

Sample preparation

Five different extraction procedures were assessed to determine the optimal approach in terms of recovery and practicality.

Trichloroacetic acid extraction: A 10 mL culture at 0.6 $O.D_{600}$ was collected and centrifuged. The pellet was suspended in 1 mL of M9 minimal media. An equal volume of ether and then trichloroacetic acid (TCA) at a final concentration of 5% (v/v) were added. The sample was centrifuged and the aqueous layer collected. The aqueous layer was extracted three times with ether to minimize the TCA, dried down and reconstituted in 200 μL of 0.1% formic acid in water (v/v).

Boiling water extraction: This extraction procedure was adapted from Mengin-lecreulx et.,al 1982[198]. Briefly, 10 mL culture in log phase (0.6 $O.D_{600}$) was harvested and the bacteria were suspended in 1 mL boiling water and heated up to 100ºC for 20 min. The extract was cooled on ice and a final concentration of 5% (v/v) trichloroacetic acid (TCA) was added. The suspension was centrifuged, and the supernatant was collected and extracted three times with ether, dried down and reconstituted in 200 µL of 0.1% formic acid in water (v/v).

Liquid nitrogen extraction: A 10 mL culture at 0.6 $O.D_{600}$ was harvested and centrifuged. The pellet was suspended in 1 mL of M9 minimal media and trichloroacetic acid (TCA) at a final concentration of 5% (v/v) was added. The cells were lysed by snap freezing the tubes in liquid nitrogen. The frozen solid was thawed at room temperature, centrifuged and supernatant was collected. The aqueous layer was extracted three times with ether, dried down and reconstituted in 200 µL of 0.1% formic acid in water (v/v).

Liquid nitrogen and acetone extraction: A 10 mL culture at 0.6 $O.D_{600}$ was harvested and centrifuged. The pellet was suspended in 1 mL of M9 minimal media and 2 mL of 80% (v/v) acetone. The cells were lysed by snap freezing the tubes in liquid nitrogen. The frozen sample was thawed, centrifuged and the supernatant was collected, dried down and reconstituted in 200 µL of 0.1% formic acid in water (v/v).

Acetone extraction: The procedure was as described above with the exception of snap freezing using liquid nitrogen.

RESULTS

Method development

Mass spectral parameters were optimized with commercially available UDP-NAG and HPLC purified UDP-intermediates in negative mode. The Analyst software (AB Sciex, Foster City, CA) quantitative optimization wizard was used to optimize LC-MS/MS parameters for the analytes of interest. For most of the UDP-intermediates, product ions of m/z 403.0 and 385.0 were observed and those ions were used for further analysis. The optimized mass spectral parameters are given in Table 15. Chromatographic separation on a C_{18} column was achieved by using an ion pair reagent (N, N-dimethyl hexylamine) to resolve all the UDP-intermediates. Optimum chromatographic resolution of the UDP-intermediates was observed with 8 mM ion pair reagent and subsequently used for all the analysis (Figure 58).

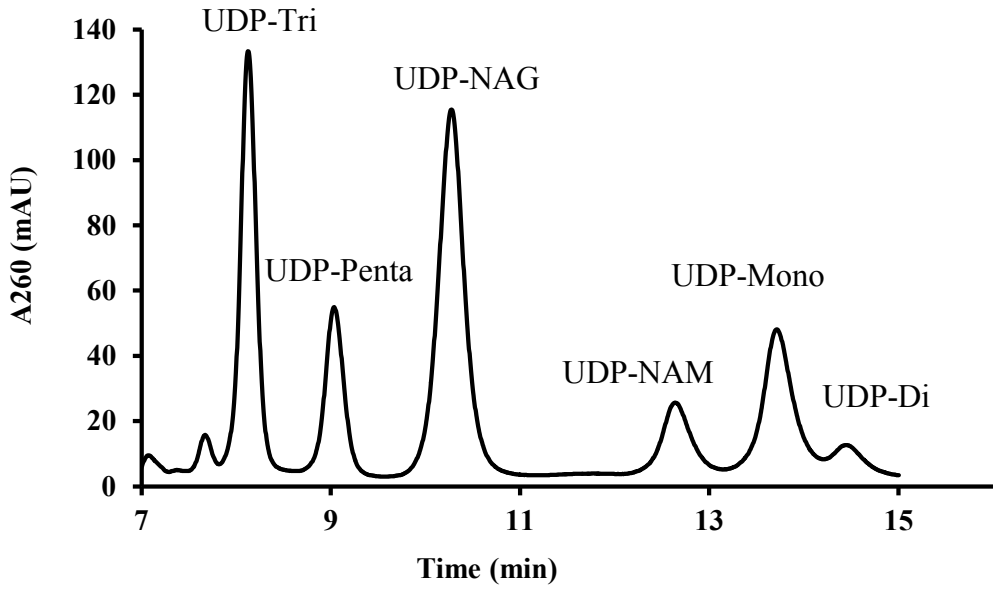

Figure 58: UV chromatogram of UDP-intermediates analyzed using ion pair reagent as described in materials and methods.

Validation

Sample preparation, assessment of analyte recovery and stability: Five different cell lysis and extraction procedures were assessed to determine the best extraction procedure. TCA, boiling water, liquid nitrogen, liquid nitrogen with 80% acetone, and 80% acetone (v/v) were tested for efficiency. Out of these, liquid nitrogen with 80% acetone was chosen based on practicability, ease, and efficiency, and subsequently used for all the extractions (Figure 59).

The above-mentioned extraction procedure was used to assess analyte recovery. To evaluate extraction procedure recovery, the *S. aureus* cell pellet was spiked with UDP-Glucose as an internal standard (I.S) and UDP-NAG (std) and extracted using liquid nitrogen and 80% acetone. The resulting pellet was re-extracted using the above procedure. 10 µL injections were analyzed by LC-MS. The recovery of the std and I.S was determined to be greater than 95% demonstrating a good recovery of the samples using this extraction procedure.

To evaluate the stability of the std and I.S.in bacterial extract, a stability time course study (up to 12 hrs) was performed by incubating the bacterial extract (prepared as described in the extraction procedure section) spiked with std and I.S at room temperature and analyzing by LC-MS (Figure 60). Samples frozen for up to four weeks were also analyzed by LC-MS following one freeze/thaw cycle. No significant decrease in the levels of either std or I.S (%CV < 5%) was observed, consistent with good stability under storage at -20°C and through the freeze/thaw cycle. This shows that the extraction procedure used effectively stopped the metabolism of UDP-intermediates.

Table 15:

Summary of optimized parameters for negative mode MS/MS detection of UDP-linked intermediates (precursor ion/product ion) [1,2]

	UDP-NAG		UDP-NAM		UDP-Mono		UDP-Di		UDP-Tri		UDP-Penta	
MS Parameters												
Q1	605.8		678.1		749.2		878.3		1006.3		1148.5	
DP (V)	-70		-90		-90		-105		-130		-140	
EP (V)	-5		-10		-10		-9.5		-12		-10	
CEP (V)	-26		-28		-26		-30		-38		-40	
MS/MS Parameters												
Q1/ Q3	605.8/ 158.9	605.8/ 385.0	678.1/ 385.0	678.1/ 403.0	749.2/ 385.0	749.2/ 403.0	878.3/ 385.0	878.3/ 403.0	1006.3/ 385.0	1006.3/ 403.0	1148.5/ 385.0	1148.5/ 403.0
CE (eV)	-62	-36	-38	-38	-46	-54	-56	-48	-60	-54	-80	-60

[1] Arb, arbitrary units; CAD, collisionally activated dissociation gas level; CE, collision energy; CEP, collision cell entrance potential; CUR, curtain gas setting; CXP, collision cell exit potential; EP, entrance potential; DP, declustering potential; GS1 and GS2, gas flow 1 and 2 settings, respectively; IS, internal standard; TEM, source temperature.

[2] For all ions: CXP (V) -8 (instrument default); CAD (Arb) medium; TEM (°C) 400; CUR (psi) 30; GS1 (psi) 70; GS2 (psi) 20.

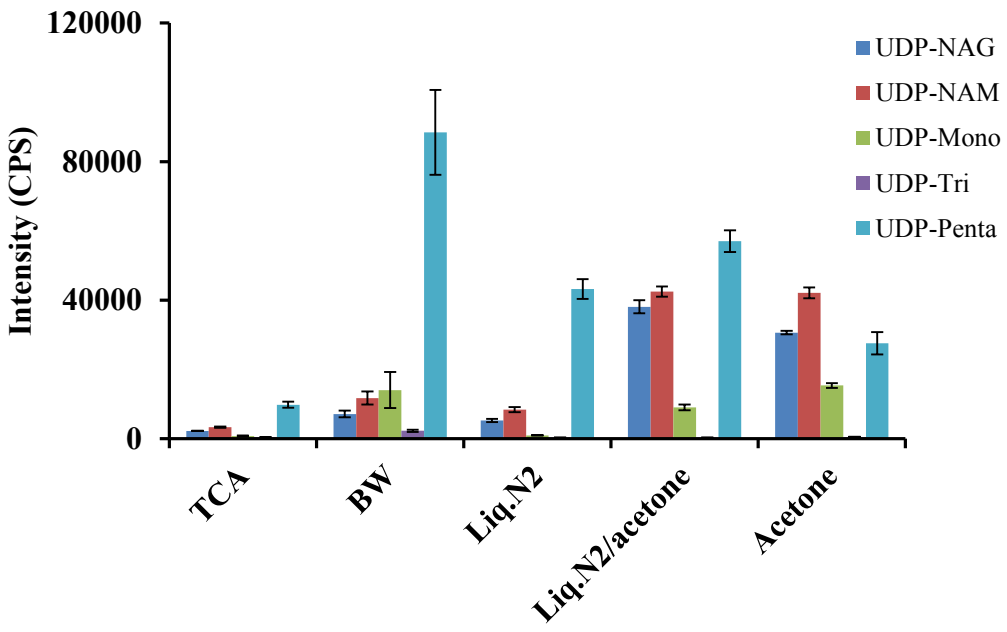

Figure 59: Extraction efficiencies of UDP-intermediates using difference sample preparation techniques.

Abbreviations: TCA: Trichloroacetic acid, BW: Boiling water, Liq. N2: liquid nitrogen.

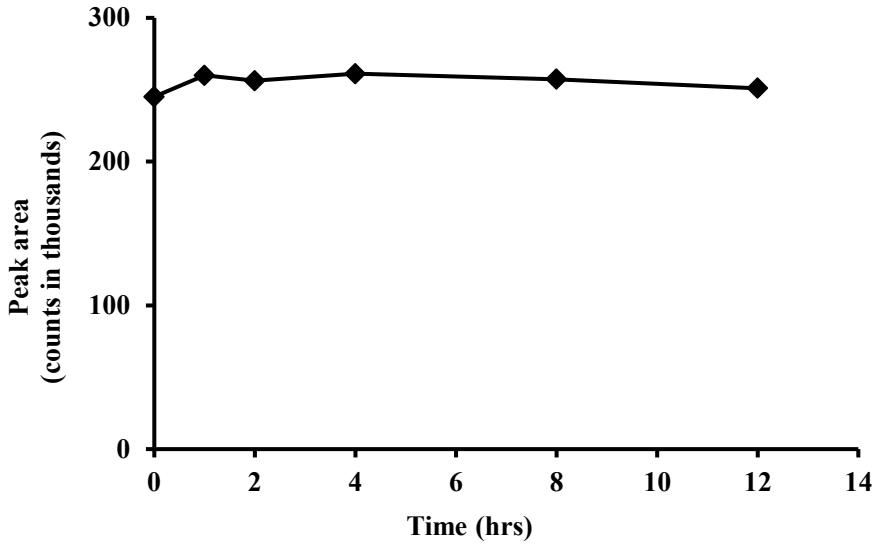

Figure 60: Stability of UDP-NAG in acetone/water bacterial extract at room temperature.

Assessment of linearity, and matrix effects for UDP-NAG: To assess linearity in acetone/water bacterial extract, serially diluted samples of UDP-NAG were prepared in matrix and analyzed. To determine the matrix effect on the quantitation of analyte, serially diluted samples of UDP-NAG were prepared in matrix analogous to the water dilutions. Analysis of these samples showed good linearity (r^2>0.999) over the range 0.64 to 2000 pmoles. Samples diluted in matrix gave a small higher signal than samples diluted in water, probably due to the background levels of UDP-NAG in the bacterial extract (Figure 61).

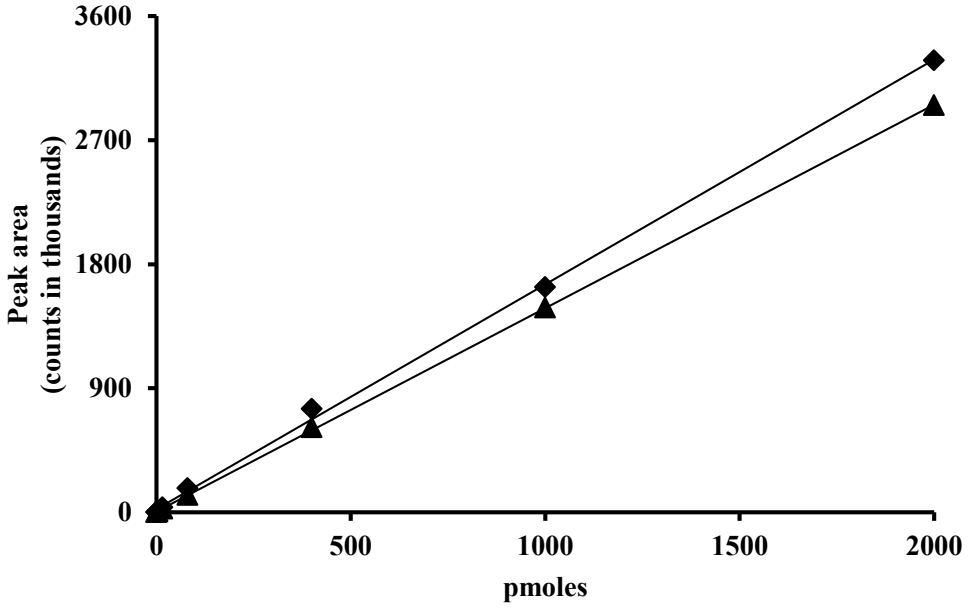

Figure 61: Standard curve of UDP-NAG serially diluted in water and bacterial extract quantitated by LC-MS/MS using (Precursor ion/Product ion)= 605.8/158.9. ▲UDP-NAG in water. ♦ UDP-NAG in acetone/water bacterial extract.

Calibration curves for UDP-intermediates: The calibration curve for UDP-NAG (commercially available) was prepared with serially diluted samples of matrix. Bacterial samples treated with cycloserine and vancomycin were used to prepare the calibration curves of UDP-NAM, UDP-Mono, UDP-Tri, and UDP-Penta. Absolute quantitation of UDP-NAM, UDP-Mono, UDP-Tri, and UDP-Penta was performed by UV against a calibration curve prepared from the UDP-NAG reference standard (All of the UDP-intermediates contain only uridine as the UV absorbing chromophore (Abs_{260})). The mass spectral calibration curves (UDP-NAM, UDP-Mono, UDP-Tri, and UDP-Penta) were re-constructed from the UV estimated quantities and the corresponding mass spectral signal. The slope of the calibration curve is directly proportional to sensitivity and the slopes of mass spectral calibration curves were more than 300 fold higher than the UV curves giving some approximation of the sensitivity improvements gained through implementation of the LC-MS method. The validated liquid chromatography tandem mass spectrometry method and the mass spectral calibration curves were then used to quantitate the UDP-intermediates from the bacterial samples. The calibration curves for UDP-NAM, UDP-Mono, and UDP-Penta were generated from vancomycin treated *S. aureus* and UDP-Tri from cycloserine treated *S. aureus*.

Sensitivity and carryover: The LC-MS method LLOD for UDP-NAG was determined to be 0.128 pmoles (using the criteria of $S/N \geq 3$) and the LLOQ was determined to be 0.64 pmoles (using the criteria of $S/N \geq 10$). There was no detectable carryover observed between samples even at the highest concentration (2000 pmoles) of UDP-NAG tested.

Selectivity: Selectivity for each of the UDP-intermediates was established by the combination of LC retention time and the mass spectral multiple reaction monitoring (MRM) transitions used. Two product ions were selected for each analyte of interest for the MRM method. The following product ions were used for each analyte: UDP-Glucose (158.6, 323.2), UDP-NAG (158.9, 385.0), UDP-NAM (385.0, 403.0), UDP-Mono (385.0, 403.0), UDP-Di (385.0, 403.0), UDP-Tri (385.0, 403.0), and UDP-Penta (385.0, 403.0).

Accuracy and precision: The accuracy and precision of the method were determined by analyzing UDP-NAG standard samples at concentrations of 0.64 pmoles (LLOQ), 80 pmoles (mid-LOQ), and 2000 pmoles (ULOQ). Samples were analyzed in triplicates intraday and interday (Table 16). The average percent coefficient of variation (%CV) for UDP-NAG at the ULOQ and mid-level was less than 4%, supporting the precision of the assay. The average deviation of the %nominal determined UDP-NAG for ULOQ and mid-LOQ intraday samples was within 83-120% supporting the accuracy of the assay.

Elemental analysis and identification of UDP-intermediates and fragments by high resolution mass spectrometry

The elemental composition of HPLC purified fractions of UDP-intermediates was determined by high-resolution mass spectrometry, further confirming the identity of the UDP-intermediates quantitated in the present study. The ppm errors determined for the compounds were less than 5 (Table 17) and those having error greater than 5 ppm (UDP-Di, UDP-Tri, and UDP-Penta) were analyzed as doubly charged species, which gave ppm errors less than 5 (data not shown). One observation of particular interest was that most of the

fragments observed for the UDP-intermediates were part of UDP structure (e.g. m/z 403 (UDP), m/z 385 (UDP-H_2O), m/z 323 (UMP), m/z 159 (diphosphate) (Table 17).

Quantitation of UDP-intermediates in bacterial samples

Different antibiotics acting at different stages of bacterial cell wall biosynthetic pathway were chosen (phosphomycin, cycloserine, D-boroAla, vancomycin, and ampicillin) to demonstrate the *in vivo* mechanism of action and the change in the pool levels of UDP-intermediates. The results are presented in Tables 18 and 19.

Table 16:
Intra- and inter-day precision and accuracy of UDP-NAG samples in bacterial extract.

	ULOQ	Mid LOQ	LLOQ
Quantity	2000	80	0.64
Intraday mean	1794	90	0.8
Intraday SD	41.8	4.9	0.3
Intraday %CV	1.0	2.5	17.2
Intraday %nominal	89.6	112.4	118.4
Interday mean	1924	84.3	0.8
Interday SD	160.8	9.8	0.2
Interday %CV	3.4	4.7	14.6
Interday %nominal	96.2	105.3	117.7

SD, standard deviation, CV, coefficient of variation.

Table 17:
HRMS data of all the UDP-intermediates analyzed, predicted fragment structures and the m/z values used for quantitation

Compound	Precursor $[M-H]^-$ m/z Theoretical	Practical	Error (ppm)
UDP-NAG	606.0737	606.0732	1
UDP-NAM	678.0949	678.0934	2
UDP-Mono	749.132	749.1291	4
UDP-Di	878.1746	878.1658	10
UDP-Tri	1006.2695	1006.2625	7
UDP-Penta	1148.3438	1148.333	9

Fragment structure	Fragment m/z Theoretical	Practical	Error (ppm)
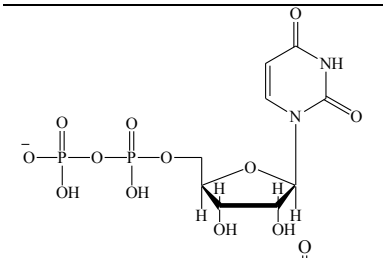	402.9949	402.9948	0.2
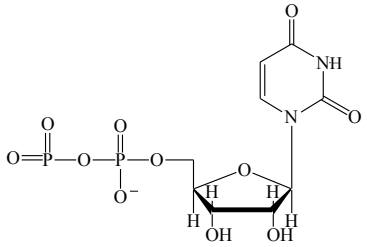	384.9838	384.9847	2
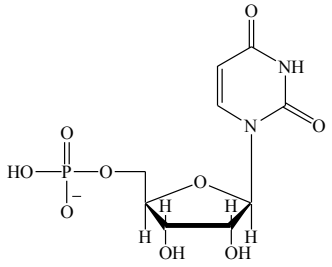	323.0286	323.0317	9
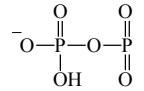	158.9253	158.9281	17

Table 18:
UDP-intermediates in nmol/g dry weight of *S. aureus*[a]

	nmol/g dry weight					
	Control	Phos	CYC	DBA	Vm	Amp
UDP-NAG	8.70	800	13.5	230	2.8	3.0
UDP-NAM	49.2	1.3	810	1870	3200	282
UDP-Mono	1.62	0.71	300	1700	3000	51
UDP-Di	ND[b]	ND	50	600	ND	ND
UDP-Tri	2.5	0.485	3700	11200	13.3	2.11
UDP-Penta	50	2.04	220	3.724	9000	430

Arrows indicate the step blocked by the antibiotic.
[a] Values reported to last significant digit. [b] ND; Not detected
Abbreviations: Phos: phosphomycin, CYC: cycloserine, DBA: D-boroAla, Vm: vancomycin, Amp: ampicillin.

Table 19:
UDP-intermediates expressed as % total of UDP-precursor content

% Total	Control	Phos	CYC	DBA	Vm	Amp
UDP-NAG	7.6	99.4	<0.1	1.5	<0.1	0.4
UDP-NAM	43.0	0.2	19.0	12.0	21.2	36.6
UDP-Mono	1.4	0.1	18.0	10.9	19.5	6.6
UDP-Di	ND	ND	0.3	3.8	ND	ND
UDP-Tri	2.2	0.1	62.5	71.8	0.1	0.3
UDP-Penta	45.8	0.3	<0.1	<0.1	59.2	56.2

ND: Not detected

DISCUSSION

Method development

Direct infusion of the bacterial extracts treated with cycloserine and vancomycin gave no mass spectral signal for the peptidoglycan precursors in negative mode, not even for UDP-Tri and UDP-Penta that accumulate during treatment with these antibiotics[213,224]. The lack of signal was presumably due to suppression by matrix interferences. The samples were subsequently analyzed by LC-MS with an ion pair reagent (N, N-dimethyl hexylamine) in negative mode. Although a good signal was observed by LC with UV detection, the mass spectral signal at this point was weak but the signal was strong enough to enable preliminary identification of the UDP-intermediates. The samples were consequently HPLC purified to obtain pure and desalted samples of UDP-peptidoglycan precursors. The purity and identity of the UDP-intermediate fractions were determined by LC-MS. The pure fractions were then used for mass spectral parameter optimization.

UDP-intermediates (commercially obtained UDP-NAG and the other intermediates prepared from *S. aureus* culture by HPLC purification) were infused into mass spectrometer, which gave readily observable precursor $[M-H]^-$ and product ions and the Analyst software quantitative optimization wizard was used to optimize for LC-MS/MS transitions for the analytes of interest (Table 15).

For optimization of the chromatographic separation conditions, a standard mixture of UDP-intermediates was prepared by combining HPLC purified fractions containing different UDP-intermediates. N, N dimethyl hexylamine was used as an ion pair reagent and was tested at different concentrations (1.6 mM, 3.2 mM, 8 mM, and 16 mM). Optimum

chromatographic resolution of the UDP-intermediates was observed with 8 mM ion pair reagent and the same was used for subsequent separations (Figure 58).

The UDP-intermediates were all chromatographically well resolved with the exception of UDP-NAG and UDP-glucose using N, N dimethyl hexylamine as an ion pair reagent. The ion pair reagent masks the negative charges of UDP-intermediates thus increasing the hydrophobicity, which results in optimal separation. Sample representative UV chromatogram is shown in Figure 58.

Validation

The LC-MS/MS method was validated for analyte recovery, stability, matrix effects, linearity, sensitivity, carryover, selectivity, accuracy and precision using the commercially available standard UDP-NAG. The calibration curves for UDP-NAM, UDP-Mono, and UDP-Penta were generated from vancomycin treated *S. aureus* and UDP-Tri from cycloserine treated *S. aureus*.

Quantitation of UDP-intermediates in bacterial samples

Five different antibiotics with different modes of action (phosphomycin, cycloserine, D-boroAla, vancomycin, and ampicillin) were evaluated. The group was selected as each antibiotic act at different stage of the cell wall biosynthetic pathway, with the exception of cycloserine and D-boroAla that act on the same D-Ala-D-Ala pathway.

Antibiotic effects on peptidoglycan precursors:

Phosphomycin: Phosphomycin is a commercially available broad-spectrum antibiotic, which acts by inhibiting the MurA enzyme[4]. Changes in peptidoglycan precursor levels of *S. aureus* when treated with 10X MIC of phosphomycin were investigated. A 66-fold increase in the UDP-NAG level was observed when compared to the control, consistent with the mechanism of action of phosphomycin (Table 18 and 19). Inhibition of the MurA enzyme, the initial and the first committed step of the Mur pathway, leads to the accumulation of UDP-NAG and depletion of the downstream products[218].

Cycloserine and D-boroAla: Cycloserine and D-boroAla are broad-spectrum antibacterial agents, which act by inhibiting alanine racemase and D-Ala-D-Ala ligase involved in the D-Ala-D-Ala pathway[144,225]. Changes in peptidoglycan precursor levels of *S. aureus* treated with 10X MIC of cycloserine and D-boroAla were explored. Owing to cycloserine and D-boroAla action on the D-Ala-D-Ala pathway, treatment with these antibiotics resulted in a 1480- and 2800-fold increase in UDP-Tri levels, respectively (Table 18 and 19),consistent with what others have observed[218,224,226]. In addition to UDP-Tri accumulation, 185-fold and a 660-fold increase in UDP-Mono was observed with cycloserine and D-boroAla, respectively. Interestingly, UDP-Di, which was not detected in control, was detected in these samples. Other researchers have described UDP-Di accumulation in *E. coli* treated with cycloserine[224].

Vancomycin: Vancomycin is a glycopeptide used to treat Gram-positive bacterial infections and acts by binding to the precursor peptidoglycan peptide terminus D-Ala-D-Ala thus preventing the bacterial cell wall crosslinking[193,227]. At 10X MIC of vancomycin, a 140-fold increase in UDP-Penta was observed in *S. aureus* when compared to the control (Table

18 and 19), consistent with earlier observations confirming the mode of action of vancomycin[213,215]. Due to the bidirectional nature of the reaction catalyzed by MraY, saturation of the downstream lipid pool when treated with vancomycin leads to a rapid rise in the levels of UDP-Penta[214]. An interesting observation was that of a significant accumulation of UDP-NAM and UDP-Mono upon vancomycin treatment.

Ampicillin: Ampicillin is a broad-spectrum β-lactam antibiotic, which acts by deactivating penicillin-binding proteins (PBPs), which catalyze the final step of cell wall biosynthesis[75,166,195]. No drastic changes in the UDP-intermediate levels were observed when *S. aureus* was treated with 10X MIC of ampicillin. A 22-fold increase in the UDP-Mono level, and a 6-fold increase in the UDP-Penta levels were observed when compared to the control (Table 18 and 19). The small changes observed in the peptidoglycan precursor levels are consistent with the fact that ampicillin acts far down the cell wall biosynthetic pathway[213,216,222] that it has little effect on the initial cytoplasmic UDP-precursors.

In summary, the UDP-intermediates in *S. aureus* have been successfully quantitated using LC-MS/MS assay. N, N dimethyl hexyl amine ion pair reagent yielded improved chromatographic resolution of the hydrophilic peptidoglycan precursors and resulted in the development of a convenient method for peptidoglycan precursor analysis and quantitation. This is the first method so far for quantitating UDP-intermediates using LC-MS/MS. Observed changes in the levels of peptidoglycan precursors when treated with different antibiotics, determined with the LC-MS/MS method, were similar to those previously reported in the literature with the exception of a substantial increase in the UDP-Mono levels following treatment with cycloserine, D-boroAla and vancomycin. The present data also

confirms the initial observation of the accumulation of UDP-Tri and UDP-Penta after treatment with cycloserine and vancomycin, respectively. The developed assay has the potential for use in many applications. The LC-MS/MS method could be used for characterizing the Mur enzyme pathway, which can serve as an alternate target pathway to address increasing resistance to commonly prescribed antibiotics. It could be used in drug discovery and development efforts for characterizing prospective compounds targeting Mur enzymes and to demonstrate their *in vivo* mechanism of action. The assay also has potential for characterizing cell wall differences between bacterial species and cell wall composition changes due to antibacterial treatment. The ion pair method used to resolve the peptidoglycan precursors also has potential to be used as a general approach for the separation of nucleotides. Finally, the changes in peptidoglycan precursor levels could also be used to characterize the resistance mechanism in bacteria, especially vancomycin resistant *enterococci* (VRE). In future, the assay could be modified to enable determination of changes in the levels of UDP-Mur-L-Ala-D-Glu-L-Lys-D-Ala-D-Lac, and UDP-Mur-L-Ala-D-Glu-L-Lys-D-Ala-D-Ser, which are responsible for resistance in *enterococci*.

CHAPTER 7

PART II: LIQUID CHROMATOGRAPHY–TANDEM MASS SPECTROMETRY ASSAY FOR DETECTION AND QUANTITATION OF ENDOGENOUS BIOACTIVE PEPTIDES IN RAT BRAIN[228]

INTRODUCTION AND RATIONALE

The opioid β-endorphin is one of many influences on voluntary ethanol consumption in rats. Two cleavage products of β-endorphin$_{1-31}$ – β-endorphin$_{1-27}$ and Gly-Gln (β-endorphin$_{30-31}$) – are implicated in reduction of ethanol intake[229-234]. β-endorphin$_{1-27}$ and Gly-Gln act in different ways. The 27 residue peptide and classical opioid antagonists act by blocking mu and delta receptors, whereas Gly-Gln does not significantly bind to opioid receptors, does not displace naltrexone bound to mu or delta receptors, and does not bind to other known neurotransmitter receptors or transporters[235]. It apparently acts by a unique and as yet undefined mechanism[231,232]. Along with inhibition of voluntary alcohol consumption activity, Gly-Gln has also been shown to inhibit the reward benefiting effects of morphine and nicotine[236-238]. All these findings corroborate the fact that Gly-Gln has an interesting and potentially useful pharmacological activity. Gly-Gln has previously been quantitated in sheep and pig pituitary gland using radioimmunoassay (RIA)[229,230]. Given the widespread availability LC-MS/MS technology, and its relative ease of use and lack of requirement for radiolabeled analytes, we felt it would be beneficial to develop an LC-MS/MS assay for detection and quantification of Gly-Gln in the brain. The ability to quantitatively determine *in vivo* levels of Gly-Gln is fundamentally important to understanding its biochemistry, physiological function, and for the development of active analogs and derivatives.

Detection and quantification of small amines in complex biological samples is a challenge, and generally requires precolumn derivatization for retention and separation by reverse-phase HPLC. Ninhydrin and o-phthaladehyde (OPA) have been the most widely used derivatization reagents for UV-vis detected analyses, however the instability of their adducts is a significant limitation[239,240]. Marfey's reagent is a chiral analog of Sanger's reagent, which is used to derivatize chiral amino acid mixtures prior to separation on achiral media to determine chiral purity[241-243]. In a recent study we reported the use of LC-MS/MS detection and quantitation for Marfey's derivatives of the racemic amino acids L-Ala and D-Ala, and the dipeptide D-Ala-D-Ala[225]. LC-MS/MS detection of Marfey's derivatives of low molecular mass hydrophilic amines appears to be a potentially general approach to the stereospecific detection and quantitation of this otherwise challenging class of biomolecules. Given our interest in Gly-Gln, the present effort was directed towards expanding the application of Marfey's derivatization and LC-MS/MS analysis to the difficult analytical problem of detecting and quantitating of Gly-Gln in rat brain extracts. This assay demonstrated that *in vivo* detection and quantification of Gly-Gln in brain extracts by LC-MS/MS is feasible, which opens the door for an improved understanding of how Gly-Gln works to reduce addictive behavior, and for the development and characterization new anti-addictive Gly-Gln analogs and derivatives in a similar fashion.

MATERIALS AND METHODS

General

Gly-Gln was purchased from Bachem (Torrance, CA) and Gly-Asn from Sigma-Aldrich (St. Louis, MO). C_{18}-silica gel was obtained from Sep-Pak Cartridges (Waters Co, Milford MA). Marfey's reagent (1-fluoro-2,4-dinitripheny-L-5-alanine amide) was purchased from Novabiochem (a division of EMD Chemicals, Gibbstown, NJ). LC-MS/MS was performed on an Applied Biosystems Sciex 3200 QTrap LC-MS/MS mass spectrometer equipped with a Shimadzu UFLC HPLC system using an electrospray ionization (ESI) source in positive mode, and run using Analyst® v. 1.4.2. All chromatographic separations were performed on Nucleodur 100-3 C_8 125 x 2.0 mm column (Macherey–Nagel, Bethlehem, PA).

Animals

Two strains of rats were used in this work. Male alcohol preferring (P) rats (Center for Alcohol Studies, Indiana University Medical Center, Indianapolis, IN) and male Sprague–Dawley rats (SD) (Charles River), weighing 300–350 g. Rats were maintained with food and water ad libitum under an established 12/12 h photoperiod (lights on: 0700 h). Each rat was handled daily and maintained in individual cages in accordance with the National Institutes of Health Guide for the Care and Use of Laboratory Animals (publication No. 80-23, revised 1996), with all experimental protocols approved by the UMKC Animal Care and Use Committee. All rats were alcohol naive. Fresh frozen pig brain was obtained from a local butcher shop (Biedermyers, Kansas City, MO).

Marfey's Gly-Gln derivatization reaction

A standard solution of the Marfey's adduct of Gly-Gln (Mar-Gly-Gln) was prepared by diluting 1.5 μL of 5 mM Gly-Gln to 150 μL with H_2O to give a 50 μM sample. A 20 μL aliquot of this sample (1 nmol) was added to 20 μL of 10 mM Marfey's reagent in acetone, and then 5 μL of 1 M triethylamine was added to this mixture to initiate the reaction. The contents were mixed well and kept in an incubator at 37ºC for 120 minutes. The derivatization reaction was quenched by acidifying with 5 μL 1 M HCl, and the sample diluted with 150 μL of 70% H_2O/30% acetonitrile/0.1 % formic acid (final Mar-Gly-Gln concentration of 5 μM). This provided a standard solution of Mar-Gly-Gln suitable for use in initial experiments to optimize separation and quantitation parameters.

MS and MS/MS optimization

Salts interfere with MS detection of Marfey's derivatives. To remove salts prior to infusion for MS and MS/MS optimization, a 100 μL sample of the Mar-Gly-Gln standard solution was purified on 200 mg of C_{18}-silica packed in a 1 mL syringe. C_{18}-silica was prepared by first washing with MeOH (1 mL), and then pre-equilibrated with 1 mL of H_2O/0.1% formic acid. After adding the Marfey's derivatized sample, the C_{18}-silica was washed with 100% H_2O/0.1% formic acid. Marfey's adducts were then eluted with 75% MeCN/25% H_2O/0.1% formic acid to provide a sample free of salts. MS, MS/MS and flow (LC-MS/MS) parameter optimization were performed using the desalted Marfey's adduct sample and the automated quantitative optimization routine in Analyst®. This optimization process resulted in the MS/MS settings given in Table 20.

Standard chromatographic conditions

Chromatographic elution was performed at a flow rate of 300 µL/min, with a gradient of 85% solvent A (100% H_2O/0.1% formic acid) and 15% solvent B (70% MeCN/30% H_2O/0.1% formic acid) for 1 minute, followed by a 22 minute linear gradient to 75% solvent A and 25% solvent B.

Table 20:
Summary of optimized parameters for MS/MS detection of Marfey's adducts of Gly-Gln and Gly-Asn.

	Mar-Gly-Gln m/z Precursor ion $[M+H]^+$/ Product ion			Mar-Gly-Asn (IS) m/z Precursor ion $[M+H]^+$/ Product ion		
MS parameters	456.2 / 366.2	456.2 / 237.2	456.2 / 147.0	442.2 / 352.5	442.2 / 425.2	442.2 / 396.1
DP (V)	–– 51 ––			–– 51 ––		
EP (V)	–– 5.5 ––			–– 5.5 ––		
CEP (V)	–– 22 ––			–– 22 ––		
MS/MS parameters						
CE (eV)	20	40	57	23	19	17
CXP (V)	6	6	4	6	4	6
CAD (Arb)	–– 5 ––			–– 5 ––		
ESI parameters						
TEM (ºC)	–– 400 ––			–– 400 ––		
CUR (psi)	–– 26 ––			–– 26 ––		
GS1 (psi)	–– 60 ––			–– 60 ––		
GS2 (psi)	–– 60 ––			–– 60 ––		

Arb, arbitrary instrument-based setting; CAD, collisionally activated dissociation gas level; CE, collision energy; CEP, collision cell exit potential; CUR, curtain gas setting; CXP, collision cell exit potential; EP, entrance potential; DP, declustering potential; GS1 and GS2, gas flow 1 and 2 settings, respectively; IS, internal standard; TEM, ion spray temperature.

Validation:

Determination of response linearity, lower limit of detection (LLOD), lower limit of quantitation (LLOQ), possible matrix effects in pig brain samples, and carryover: For linearity, LLOD, and LLOQ determination, serial dilutions of Gly-Gln were prepared in water containing 0.45 μM Gly-Asn as an internal standard. To determine if matrix (brain extract) would interfere with analyte detection, a pig brain extract was prepared (using the same procedure as described below for rat brain samples), and an identical serial dilution was prepared in this extract with 0.45 μM Gly-Asn added to all samples as an internal standard. These serially diluted samples were derivatized with Marfey's reagent as described above, and LC-MS/MS analysis was performed using the MS/MS settings given in Table 20. Carryover was analyzed by alternately analyzing blank samples and Gly-Gln standard at upper limit of quantitation (ULOQ, 500 pmoles).

Assessment of analyte recovery and stability: To assess analyte recovery using our extraction procedure, rat brain samples were processed as described above to obtain extracts. The resulting pellets were re-extracted by re-suspending in five volumes of acetone/water with internal standard, incubated on ice for 10 min, and the supernatant recovered. The supernatant was derivatized with Marfey's reagent and analyzed by LC-MS/MS. To assess the recovery of internal standard, Gly-Asn was added to a concentration of 0.45 μM to a fresh crude homogenate of rat brain in five volumes of acetone/water (80/20), supernatant recovered and derivatized with Marfey's reagent.

Stability of the analyte in the extract was assessed by performing a stability time course by incubating an acetone/water rat brain homogenate spiked with Gly-Gln on ice (i.e.,

as generated and handled as described during the extraction process), taking samples periodically over 4 hours for immediate derivatization with Marfey's reagent.

Accuracy and precision: The accuracy and precision were determined by analyzing Mar-Gly-Gln samples (n=6) at concentrations at LLOQ, Mid LOQ and ULOQ. Samples and standards were run intraday (same day) and interday (two weeks).

Preparation of rat brain samples for analysis

The nucleus accumbens (NAC) samples were isolated from rat brain using the following coordinates. NAC: anterior-posterior +2 to -4.8 mm from bregma; -5 mm from dorsal surface to base of brain; +/- 1.5 mm lateral to the midline. The cortex sample was taken from above the NAC from above the corpus callosum[244]. Samples weighed between 200-400 mg, and to these were added five volumes (v/w) of ice cold acetone/water (80/20) containing internal standard (Gly-Asn) at 0.45 μM. The mixture was homogenized for 10-20 seconds on ice, centrifuged at 14,000xg at 4ºC for 5 minutes, and 200 μL of the supernatant taken and dried under vacuum. Dried samples were reconstituted with 100 μL of 70% water/30% acetonitrile/0.1% formic acid. This was followed by addition of 20 μL of 10 mM Marfey's reagent in acetone, 5 μL of 1M triethylamine (dissolved in water), incubated at 37°C for 120 min and then the mixture was neutralized with 5 μL 1M HCl. This was again dried down under high vacuum and made up to a final volume of 60 μL with 70% water/30% acetonitrile/0.1% formic acid. 20 μL of this mixture was injected for LC-MS/MS analysis.

Peak shifting and MRM channel ratio normalization

Peak shifting was performed using the standard chromatographic conditions described above with a constant admixture of 0-20 % of channel D (25% methanol) in place of that percentage of solvent A. Raw data (collected at 3.6 sec time intervals sequentially in each channel) were smoothed by seven point moving average. Then the data were then normalized to the MRM peak ratios obtained from a pure standard sample of Mar-Gly-Gln under identical conditions. The normalized peak ratios were calculated relative to the most intense peak (456.2/336.2). The other peak ratios for the Mar-Gly-Gln standard for 456.2/237.2 and 466.2/147.0 were 0.41 and 0.21 respectively (1:0.41:0.21). Normalizing the three channels for sample MRM chromatograms based on this ratio had the effect of making all three MRM channels of equal intensity for pure Mar-Gly-Gln.

RESULTS

Marfey's Gly-Gln derivatization reaction

The concentration of Marfey's reagent used was at least 200 fold in excess to the concentration of Gly-Gln to drive the reaction towards completion. The completion of the reaction was checked by ninhydrin test to detect the presence of free amine group of Gly-Gln.

Method development

A desalted sample of Mar-Gly-Gln was used to optimize the chromatographic conditions and mass spectral parameters. Three most intense fragment ions were used to build an LC-MS/MS-based quantitation method. Figure 62 shows the molecular $[M+H]^+$ ion

of Mar-Gly-Gln and possible fragment ion structures. Analyst® optimization routine was used for parameter optimization of sensitivity and detection of Mar-Gly-Gln and this process gave the parameters listed in Table 20. To determine if this method could be used to detect Gly-Gln in rat brain extracts. A portion of the rat brain containing the nucleus accumbens (NAC) was isolated, homogenized, derivatized with Marfey's reagent, and analyzed by LC-MS/MS. A signal for Mar-Gly-Gln was observed, but was weak. The extraction procedure was altered to concentrate the analyte before injection, revealing a readily detectible peak for Mar-Gly-Gln (Figure 63).

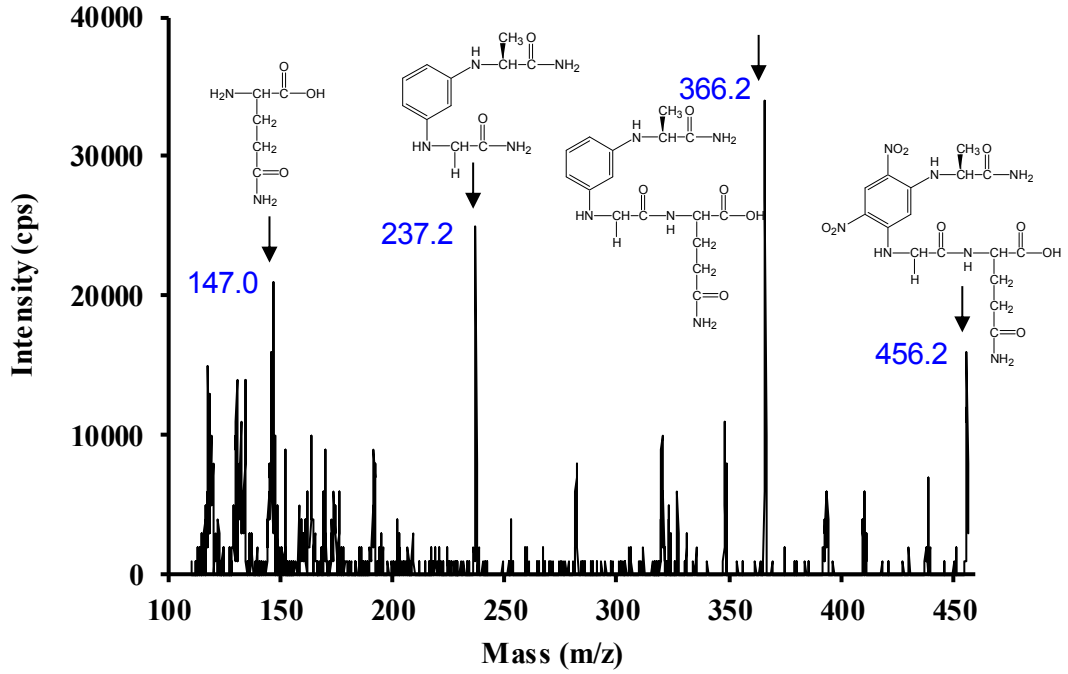

Figure 62: MS/MS spectrum of Mar-Gly-Gln with the possible fragment ions (M of $[M+H]^+$).

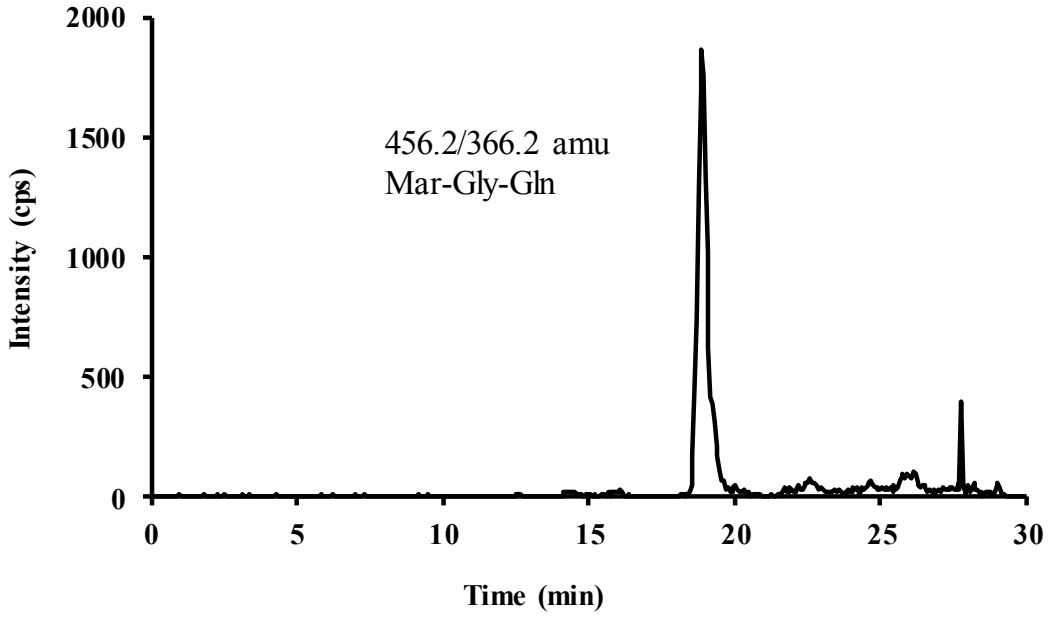

Figure 63: LC-MS/MS chromatogram of Marfey's derivatized rat brain nucleus accumbens extract detected in positive mode at m/z 456.2/366.2 (Precursor ion/Product ion).

Validation:

Determination of response linearity, lower limit of detection (LLOD), lower limit of quantitation (LLOQ), possible matrix effects in pig brain samples, and carryover: In order to determine the linearity and sensitivity of this assay for Gly-Gln, serially diluted samples were prepared, derivatized with Marfey's reagent, and analyzed with this method. Using this assay the lower limit of detection (LLOD) was determined to be 1 pmole (1.5 pmoles/mg of brain) (by the criteria of signal: noise ratio of ≥ 3:1) and the lower limit of quantitation (LLOQ) was 4 pmoles (5.8 pmoles/mg of brain) (by the criteria of signal: noise ratio of ≥ 10:1). The biological matrix (brain extract) could have a substantial interference or matrix suppression in the detection and quantitation of Gly-Gln. Serial dilutions of Gly-Gln prepared in pig brain extract and water followed by Marfey's derivatization were used to determine matrix effects. Analysis of these samples demonstrated good linearity, with $R^2 > 0.99$ and little matrix effects (Figure 64). Samples diluted in water gave a small but significantly higher signal than samples diluted in matrix (pig brain extract), with matrix giving 90% of the signal observed in water. The %CV of a given analyte level ranged from 4% at the ULOQ to 15% at the LLOQ. Error bars are not shown in Figure 64 due to crowding. The response curve therefore has good dynamic range and good quantitative (linear response) characteristics. There was no detectible carryover observed between samples even at the highest concentration (500 pmoles) of Mar-Gly-Gln.

Assessment of analyte recovery and stability: The analyte recovered from the second extraction averaged 15% of the amount of the analyte recovered in the first extraction, demonstrating an 85% recovery in the one step extraction process used in this study. Gly-Asn

was chosen as internal standard as it is structurally similar to Gly-Gln, and initial results did not show any detectable levels of Gly-Asn nor interfering isobars in rat or pig brain samples. The recovery of Gly-Asn in the brain extract sample was determined to be 95% relative to the water extract sample.

Marfey's adducts were stable for at least 48 hr at room temperature and for at least 3 months at -20^{o}C and are stable in an auto sampler at room temperature during analysis or in a freezer for long term storage. A final concern was the stability of the analyte in the crude rat brain extract in acetone/water. Stability time course experiment was performed for 4 hr as described in materials and methods and no significant decrease in measured Gly-Gln levels (e.g. <3% decrease) were observed over the 4 hr incubation period. This demonstrates that the ice cold acetone extraction process effectively stops metabolism of Gly-Gln (Figure 65).

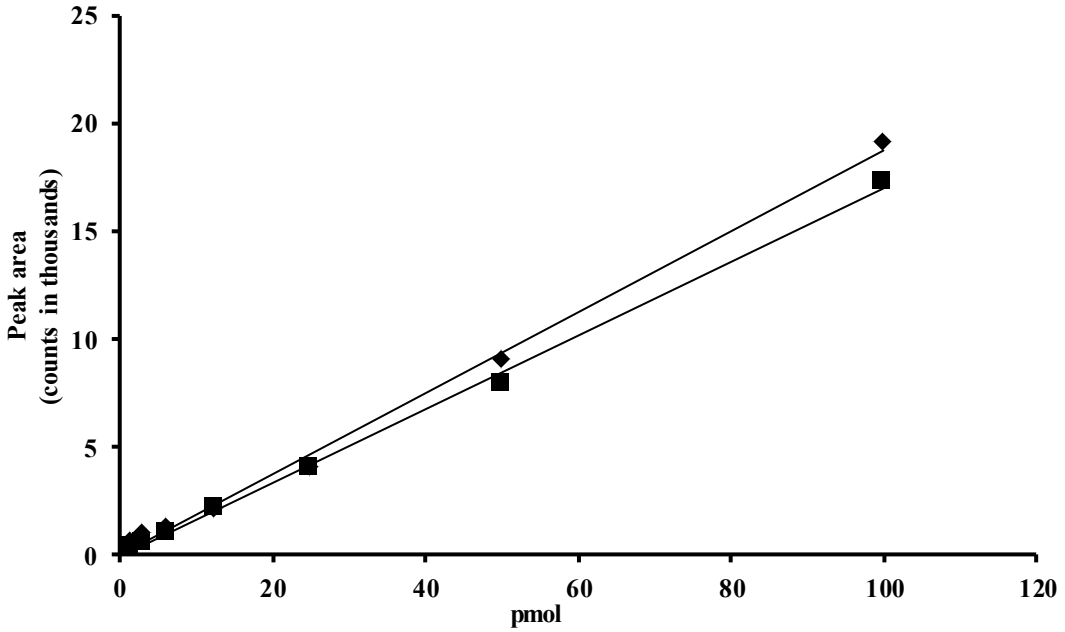

Figure 64: Standard curve of Gly-Gln serially diluted in water and pig brain extract, derivatized with Marfey's reagent, and quantitated by LC-MS/MS using (Precursor ion/Product ion)= 456.2/366.2. ♦ Gly-Gln diluted in water. ■ Gly-Gln diluted in pig brain.

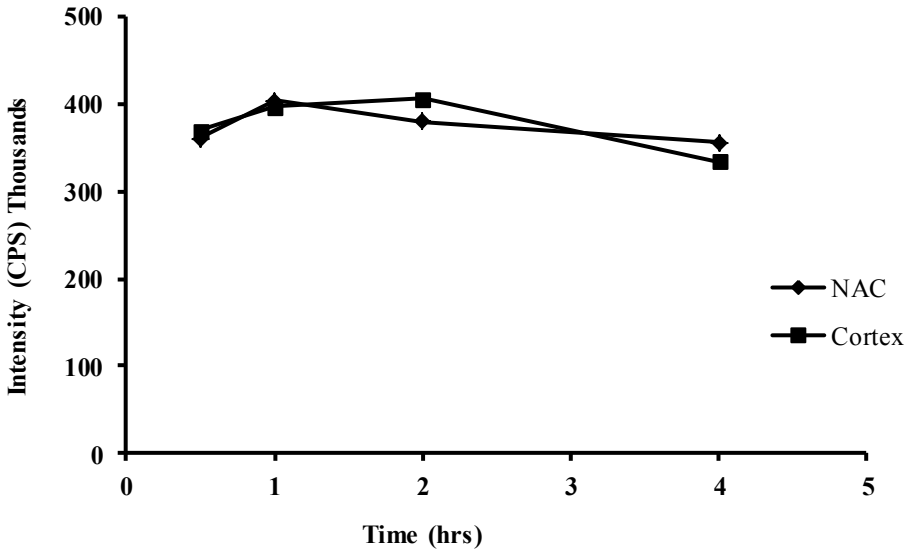

Figure 65: Stability of Gly-Gln in crude rat brain extracts (nucleus accumbens (NAC) and cortex) in acetone/water.

Accuracy and precision: The accuracy and precision were determined by analyzing Mar-Gly-Gln samples (n=6) at concentrations at LLOQ, Mid LOQ and ULOQ. Samples and standards were run intraday (same day) and interday (two weeks) (Table 21). The average percent coefficient of variation (% CV) for Mar-Gly-Gln at the ULOQ and Mid LOQ was 4%, which is a measure of the precision of the assay. The average deviation of the % nominal determined for Mar-Gly-Gln at ULOQ and Mid LOQ intraday samples was 2.5%, which is a measure of the accuracy of the assay.

Table 21:
Intra- and inter-day (2 weeks) precision and accuracy of Mar-Gly-Gln samples (n=6) in pig brain homogenate.

	ULOQ	Mid LOQ	LLOQ
Quantity (pmoles)	500	62.5	3.9
Intraday mean	490	60	4.3
Intraday SD	20	4	1.5
Intraday %CV	3.8	6.1	15.2
Intraday %nominal	99	96	110
Interday mean	500	58.5	4.1
Interday SD	20	0.5	2.0
Interday %CV	2.9	0.9	14.2
Interday %nominal	100	94	106

Note: Intraday values from first day samples and standards, and interday values from the same samples and standards run after two weeks. SD, standard deviation.

Selectivity: Peak shifting and MRM channel ratio normalization: Examination of rat brain extract MRM chromatograms for Mar-Gly-Gln revealed several spurious (isobar) signals in some of the MRM channels. To determine if any possible interfering isobars were co-eluting with Mar-Gly-Gln, a combination of peak shifting and MRM channel ratio normalization was performed according to the method described in materials and methods section. Introduction of methanol to the chromatographic conditions decreased the retention time of the Mar-Gly-Gln peak with increasing concentration of methanol (Figure 66). The shift in the sample's (rat brain extract) retention time of Mar-Gly-Gln was compared and correlated with that of standard Mar-Gly-Gln, revealing the identity of the peak. Normalization of MRM channels was also done to address the selectivity of Mar-Gly-Gln. The normalized peak ratios were calculated relative to the most intense peak (456.2/336.2). The peak ratios of Mar-Gly-Gln standard and sample should be the same for a pure peak and different for isobaric peak interferences. Normalization of peak 456.2/336.2, 456.2/237.2 and 466.2/147.0 with ratios of 1, 0.41 and 0.21 respectively (1:0.41:0.21) gave all the three MRM channels of equal intensity for pure Mar-Gly-Gln (Figure 66). As a further test of selectivity, a blank and LLOQ spiked pig brain extract were also analyzed. (Pig brain showed undetectable levels of Gly-Gln (Figure 67), in contrast to rat brain, which showed readily detectible levels (Figure 63).

Quantitation of Gly-Gln in rat brain samples

The *in vivo* levels of Gly-Gln in alcohol preferring P rats and alcohol naïve SD rats were determined in different rat brain regions (cortex and NAC). The measured levels of Gly-Gln in NAC and cortex were around 5 and 20 pmol/mg of brain respectively in both the

rat strains (Figure 68). The estimated quantities of Gly-Gln in SD and P rats were statistically the same ($p < 0.05$, *t* test).

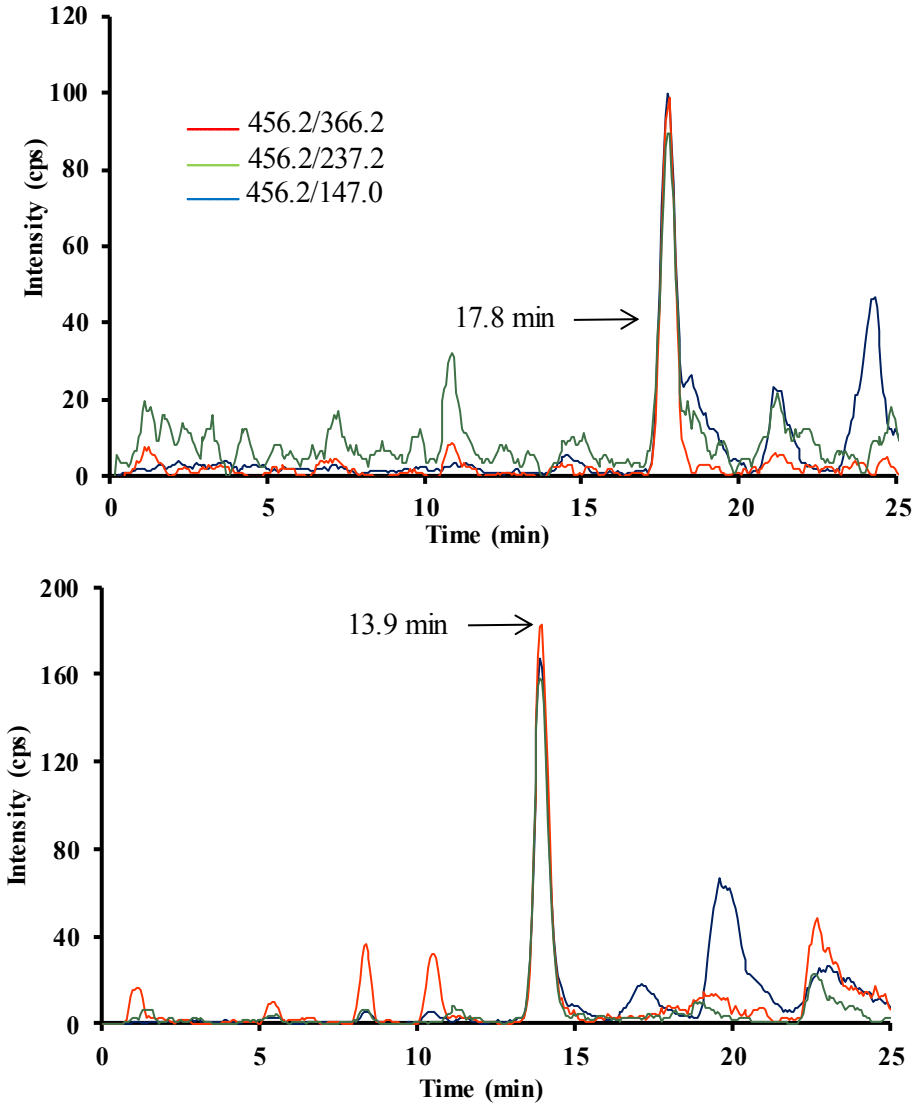

Figure 66: Results from MRM channel normalization and chromatographic peak shifting for Mar-Gly-Gln in rat brain nucleus accumbens extract. Top: normalized MRM chromatogram with the standard chromatographic (0% methanol) solvent system. Bottom: normalized MRM chromatogram peak shifted with 10% channel D (25% methanol) admixture into the standard chromatographic solvent system. MRM channels: Blue - 456.2/336.2; Green - 456.2/237.2; and Red- 147.0/456.2.

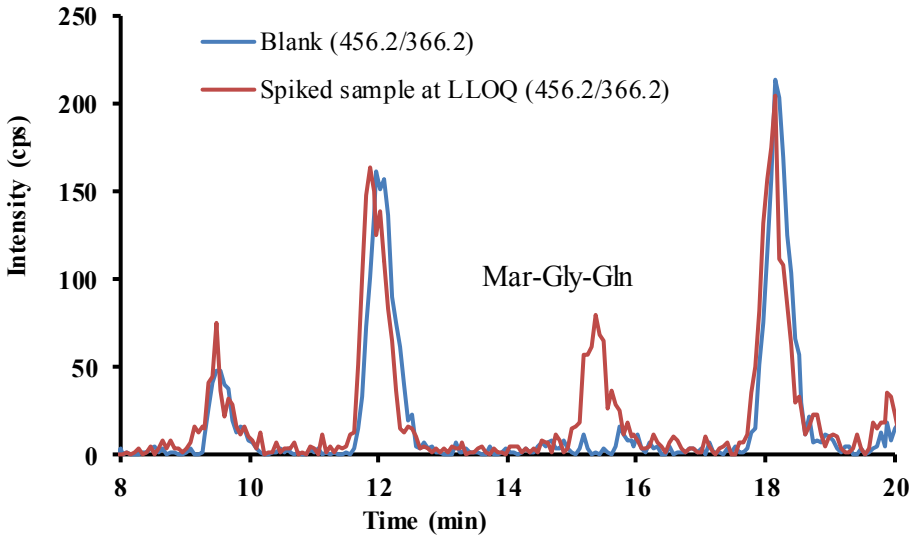

Figure 67: Results from analysis of pig brain extract with (red line) and without (blue line) the addition of Gly-Gln at LLOQ. Pig brain extract has undetectable levels of Gly-Gln present, in contrast to rat brain which has readily detectible levels (Figure 63).

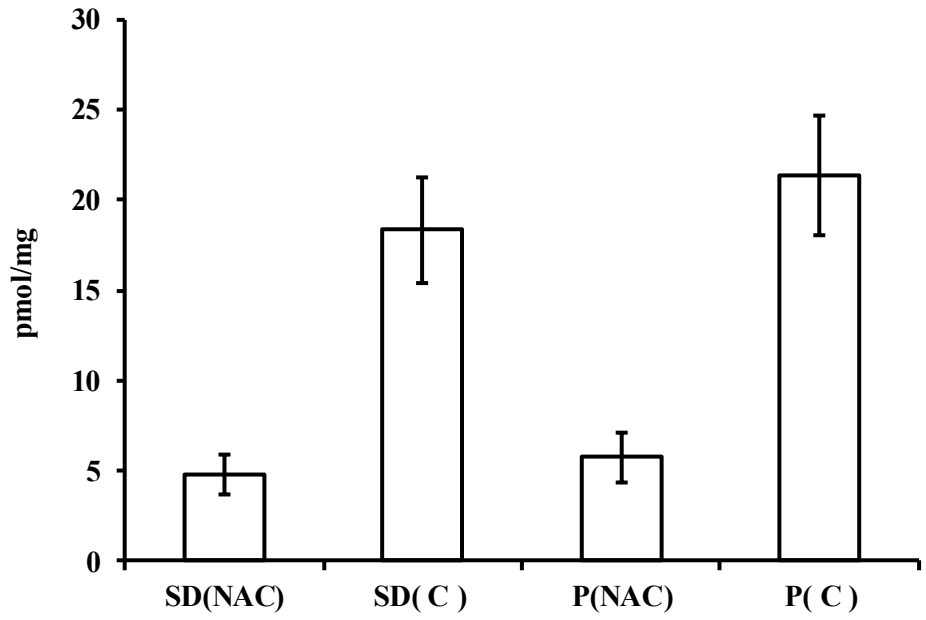

Figure 68: Measured levels of Gly-Gln in rat brain extracts. Each individual analyte represented the Gly-Gln extracted from 2.8 mg of brain. Error bars represent the standard error (n = 4) for each measurement. SD(NAC), Sprague-Dawley (nucleus accumbens); SD(C), Sprague-Dawley (cortex); P(NAC), Alcohol preferring (nucleus accumbens); P(C), Alcohol preferring (cortex).

DISCUSSION

Method development

To optimize the mass spectral parameters for detection and quantitation of the Marfey's adducts of Gly-Gln, diluted solutions of the Marfey's derivative reaction mixtures were infused into the MS instrument. The infused samples demonstrated no signals, or very weak signals, from the precursor $[M+H]^+$ ions, indicating that the presence of salts strongly suppressed ionization of Marfey's adducts. This problem was circumvented by running crude Marfey's derivative mixtures onto C_{18} silica, washing the salts away with a water–formic acid mixture, and eluting the Marfey's adducts with water–acetonitrile–formic acid mixtures. Derivatized products were easily tracked because of intense yellow color of Marfey's reagent and adducts. A desalted sample of Mar-Gly-Gln was prepared and infused into the MS instrument, and a good signal for the precursor $[M+H]^+$ ion was observed. Analyst® software quantitative optimization algorithms were used to optimize for LC-MS/MS-based quantitation on the three most intense parent ion fragment peaks (Figure 62). This process gave the parameters listed in Table 20 for optimum sensitivity for detection of Mar-Gly-Gln. The same procedure was followed to develop a method for quantitation of Mar-Gly-Asn for use as an internal standard.

Validation

The developed LC-MS/MS method was validated for analyte recovery, stability, matrix effects, linearity, sensitivity, carryover, selectivity, accuracy and precision using a Mar-Gly-Gln standard. The lower limit of detection (LLOD) was determined to be 1 pmole (1.5 pmoles/mg of brain) and the lower limit of quantitation (LLOQ) was 4 pmoles (5.8

pmoles/mg of brain). Isobar peaks were observed in the MRM chromatogram of rat brain extract. To exclude the possibility of isobar interference and to address the issue of selectivity in the detection and quantitation of Mar-Gly-Gln, a combination of peak shifting and MRM channel ratio normalization were used (Figure 66). Different MRM channels have different intensities for a given compound of interest according to the fragmentation of the compound and sensitivity of the instrument. Signals from the three MRM channels were overlaid after normalizing their intensity to the MRM peak intensities observed for a Mar-Gly-Gln standard run under identical conditions. Such a normalized MRM chromatogram will show equal MRM channel peak heights for Mar-Gly-Gln, but isobars will be unlikely to show identical MRM peak ratios. Peak shifting was performed with a fixed level of Channel D (25% methanol) added to the gradient. In general, different compounds will be shifted in the chromatogram to different degrees. This combined MRM peak ratio normalization and chromatographic peak shifting analysis demonstrated that Mar-Gly-Gln is well resolved and free from possible isobar interference (Figure 66). Selectivity was also addressed by spiking the Gly-Gln at LLOQ to pig brain extract, derivatized with Marfey's and analyzed, which demonstrated that this analytical method has a high degree of selectivity for Mar-Gly-Gln (Figure 67).

Quantitation of Gly-Gln in rat brain samples

This method was then applied for the *in vivo* detection and quantification of Gly-Gln in different rat strains (SD and P) and in different parts of the rat brain (cortex and nucleus accumbens). All samples were analyzed in quadruplicates (Figure 68), and the quantity of Gly-Gln measured was standardized to the amount of rat brain initially extracted (pmoles

Gly-Gln/mg of brain). The measured levels of Gly-Gln in SD and P rats were statistically the same, whereas the levels in different parts of rat brain were higher in cortex compared to nucleus accumbens in both SD and P rats ($P < 0.05$, t-test).

In summary, we have demonstrated a quick and easy LC-MS/MS assay for detection and quantitation of Gly-Gln in rat brain. Gly-Gln is a known inhibitor of voluntary ethanol drinking in rats acting within the nucleus accumbens, and has also been shown to inhibit the reward benefiting effects of morphine and nicotine[231-235,237,238]. An assay for Gly-Gln would be of great utility for further investigation of this effect and in efforts to exploit this effect for the development of novel anti-addictive agents. The hydrophilic nature and low molecular weight of Gly-Gln precludes direct analysis by LC-MS/MS. To address this analytical problem a Marfey's derivatization based strategy was explored, which we have previously demonstrated for quantitation of L-Ala, D-Ala, and D-Ala-D-Ala from bacterial extracts[225]. Good linearity between 1 and 500 pmol was observed, with a LLOQ of 4 pmol. MRM peak ratio normalization and chromatographic peak shifting were used to demonstrate this specificity of this method, and finally demonstrated for detection of Gly-Gln in rat brain samples.

CHAPTER 8

SUMMARY AND CONCLUSIONS

PBPs are ubiquitous and essential bacterial enzymes necessary for bacteria survival and catalyze the final steps in cell wall biosynthesis. The PBPs are therefore of high interest for their important role in bacterial cell wall biosynthesis, and are mechanistically interesting enzymes that can catalyze different reaction pathways using the same catalytic machinery. HMM PBPs catalyze transpeptidation reactions, whereas LMM PBPs generally catalyze carboxypeptidase and endopeptidase reactions. A particularly enigmatic feature of the PBPs is that, while LMM PBPs give readily detectible activity against peptide substrates, purified HMM PBPs give either low or undetectable activity against natural or synthetic cell wall-related peptide substrates. The intricate nature of these enzymes and the emergence of resistance to the commonly used antibiotics have impeded the efforts in new antibacterial drug development. Thus, there is an unmet need for the development of new antibacterial agents.

This dissertation was aimed at understanding the structural and mechanistic differences between bacterial cell wall enzymes especially PBPs using statistical, biochemical and analytical tools. In the first part of my graduate research, to understand the structural differences among PBPs, a global catalytic residue comparison was performed for all the PBPs available in the protein data bank, and analyzed using univariate and multivariate statistical methods. This study demonstrated a novel multivariate global comparison of geometrical relationships between key active site residues in the PBPs. A number of significant observations and insights were made in this study. The distances

between some of the key catalytic residues were highly conserved, suggesting importance for PBP function along with the distribution of the dihedral angle for the SXXK-motif Lys side chain that was bimodal, and strongly correlated with HMM/transpeptidase vs LMM/hydrolase classification.

In later parts of my dissertation, we developed a quick and easy assay for the essential HMM PBPs. This assay is the first microtiter-plate based assay for characterizing HMM PBPs and inhibitor screening. The assay was based on Bio-Amp as a tagging agent, detected and quantitated using a streptavidin horseradish peroxidase conjugate. The assay was validated and used for inhibitor screening and characterization. This assay provided us the platform to expand it to other important HMM PBPs (e.g., PBP2a, PBP2x) and more importantly to high throughput screening (HTS) for rapid screening of potential inhibitors. The microtiter HMM PBP assay was then used to characterize PPB2a - PBP responsible for β-lactam resistance in MRSA. Given the high intrinsic resistance of PBP2a to β-lactams, it was uncertain whether a microtiter plate β-lactam binding assay described earlier for HMM PBPs, e.g., based on biotinylated β-lactams, would work with PBP2a. Both the tagging agents Bio-Amp and for Bio-Ceph bound well to PBP2a and gave good binding constants in low micro molar range, which was very surprising given the intrinsic resistance to β-lactams. The assay was developed and validated predominantly to screen and characterize non β-lactam inhibitors (non-covalent) using a quick and easy one step assay protocol over the conventional two step approach typically used for screening β-lactam inhibitors.

In final chapter of part I of my dissertation, an LC-MS/MS assay was developed and validated to quantitate key cytoplasmic intermediates in bacterial cell wall biosynthesis. This assay is the first LC-MS/MS assay to quantitate UDP-intermediates. N, N-dimethyl

hexylamine was used as an ion pair reagent for improved chromatographic resolution of the UDP-intermediates using reverse phase chromatography. Different antibiotics acting at different stages of bacterial cell wall biosynthetic pathway were tested (phosphomycin, cycloserine, D-boroAla, vancomycin, and ampicillin) to demonstrate the *in vivo* mechanism of action and to quantitate the change in the pool levels of UDP-intermediates.

In summary, the studies discussed in this dissertation are useful for characterizing bacterial cell wall enzymes especially PBPs. The assays developed could be used for development of potential and novel antibacterial agents.

Future directions:

- The tripeptide and pentapeptide substrates could be used to study the substrate specificity of *Haemophilus influenzae* PBP 4 and PBP 5, which have never been characterized for substrate specificity studies
- UDP-Tri, UDP-Penta, their hydrolysis products NAM-Tri, NAM-Penta and the corresponding acylated compounds could be used to further establish the substrate specificity of *Actinomadura* R39
- Since HMM PBPs do not show any activity with synthetic or natural substrates, UDP-Tri, UDP-Penta could be used to study the transpeptidase activity of HMM PBPs
- The microtiter plate based PBP2a assay could be expanded to high through put screening of novel and potential non β-lactam inhibitors
- The LC-MS/MS assay for UDP-intermediates could be expanded to study changes in peptidoglycan precursor levels to characterize the resistance mechanism in bacteria, especially vancomycin resistant *enterococci* (VRE). In future, the assay could be

modified to enable determination of changes in the levels of UDP-Mur-L-Ala-D-Glu-L-Lys-D-Ala-D-Lac, and UDP-Mur-L-Ala-D-Glu-L-Lys-D-Ala-D-Ser, which are responsible for resistance in *enterococci*

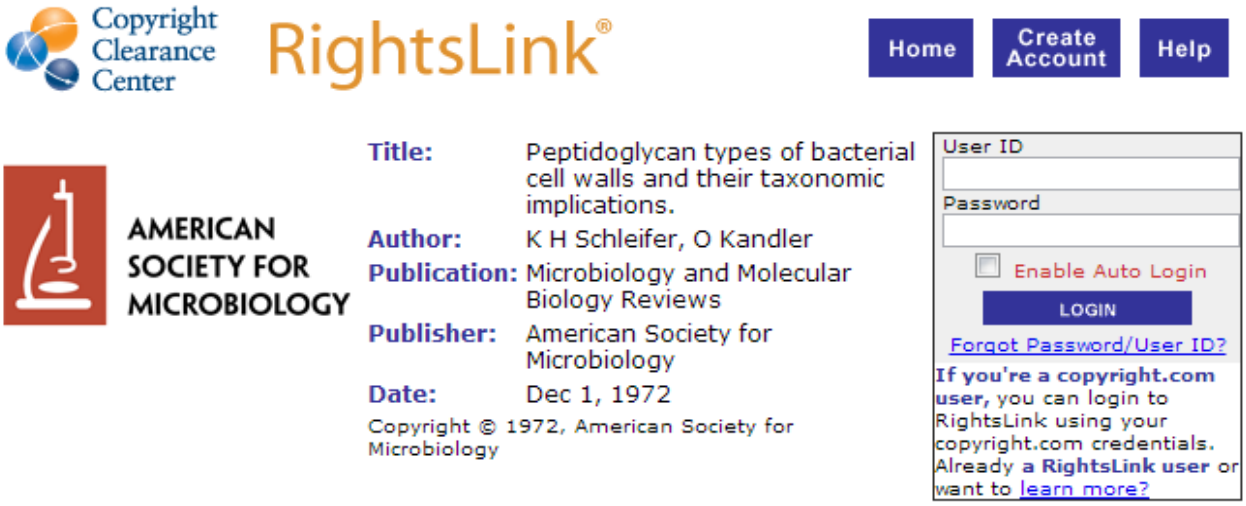

Permissions Request

ASM authorizes an advanced degree candidate to republish the requested material in his/her doctoral thesis or dissertation. If your thesis, or dissertation, is to be published commercially, then you must reapply for permission.

BACK CLOSE WINDOW

Springer

April 26, 2013

Springer reference
Antibiotics
Containing the Beta-Lactam Structure Part II
Series: Handbook of Experimental Pharmacology, Part 67 / 2
Subseries: Antibiotics
ISBN 978-3-540-12131-2
One figure pp 1-77

Your thesis:
University:
Title:

With reference to your request to reuse material in which Springer Science+Business Media controls the copyright, our permission is granted free of charge under the following conditions:

Springer material

- represents original material which does not carry references to other sources (if material in question refers with a credit to another source, authorization from that source is required as well);
- requires full credit (book title, year of publication, page, chapter title, name(s) of author(s), original copyright notice) is given to the publication in which the material was originally published by adding: "With kind permission of Springer Science+Business Media";
- may not be altered in any manner. Any other abbreviations, additions, deletions and/or any other alterations shall be made only with prior written authorization of the author and/or Springer Science+Business Media.

This permission

- is non-exclusive;
- is valid for one-time use only for the purpose of defending your thesis and with a maximum of 100 extra copies in paper.
- includes use in an electronic form, provided it is an author-created version of the thesis on his/her own website and his/her university's repository, including UMI (according to the definition on the Sherpa website: http://www.sherpa.ac.uk/romeo/);
- is subject to courtesy information to the corresponding author;
- is personal to you and may not be sublicensed, assigned, or transferred by you to any other person without Springer's written permission;
- is valid only when the conditions noted above are met.

Permission free of charge does not prejudice any rights we might have to charge for reproduction of our copyrighted material in the future.

Best regards,

Rights and Permissions
Springer-Verlag GmbH
Tiergartenstr. 17
69121 Heidelberg
Germany
E-mail: permissions.heidelberg@springer.com

Copyright Clearance Center RightsLink®

Home | Account Info | Help

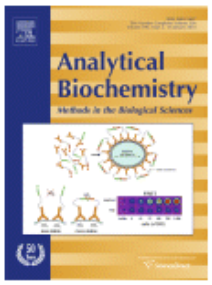

Title: A liquid chromatography–tandem mass spectrometry assay for detection and quantitation of the dipeptide Gly-Gln in rat brain

Author: Sudheer Bobba,Garth E. Resch,William G. Gutheil

Publication: Analytical Biochemistry

Publisher: Elsevier

Date: 15 June 2012

Logged in as:
sudheer bobba

LOGOUT

Order Completed

Thank you very much for your order.

This is a License Agreement between sudheer bobba ("You") and Elsevier ("Elsevier"). The license consists of your order details, the terms and conditions provided by Elsevier, and the payment terms and conditions.

Get the printable license.

License Number	3117261474997
License date	Mar 27, 2013
Licensed content publisher	Elsevier
Licensed content publication	Analytical Biochemistry
Licensed content title	A liquid chromatography–tandem mass spectrometry assay for detection and quantitation of the dipeptide Gly-Gln in rat brain
Licensed content author	Sudheer Bobba,Garth E. Resch,William G. Gutheil
Licensed content date	15 June 2012
Licensed content volume number	425
Licensed content issue number	2
Number of pages	6
Type of Use	reuse in a thesis/dissertation
Portion	full article
Format	both print and electronic
Are you the author of this Elsevier article?	Yes
Will you be translating?	No
Order reference number	
Title of your thesis/dissertation	STRUCTURAL AND ENZYMATIC CHARACTERIZATION OF BACTERIAL CELL WALL ENZYMES: FOCUS ON PENICILLIN BINDING PROTEINS
Expected completion date	May 2013
Estimated size (number of pages)	180
Elsevier VAT number	GB 494 6272 12
Permissions price	0.00 USD
VAT/Local Sales Tax	0.00 USD
Total	0.00 USD

ORDER MORE... | CLOSE WINDOW

Copyright Clearance Center RightsLink®

Home | Account Info | Help

Title: Multivariate geometrical analysis of catalytic residues in the penicillin-binding proteins

Author: Sudheer Bobba,William G. Gutheil

Publication: The International Journal of Biochemistry & Cell Biology

Publisher: Elsevier

Date: October 2011

Logged in as:
sudheer bobba
LOGOUT

Order Completed

Thank you very much for your order.

This is a License Agreement between sudheer bobba ("You") and Elsevier ("Elsevier"). The license consists of your order details, the terms and conditions provided by Elsevier, and the payment terms and conditions.

Get the printable license.

License Number	3117270088748
License date	Mar 27, 2013
Licensed content publisher	Elsevier
Licensed content publication	The International Journal of Biochemistry & Cell Biology
Licensed content title	Multivariate geometrical analysis of catalytic residues in the penicillin-binding proteins
Licensed content author	Sudheer Bobba,William G. Gutheil
Licensed content date	October 2011
Licensed content volume number	43
Licensed content issue number	10
Number of pages	10
Type of Use	reuse in a thesis/dissertation
Portion	full article
Format	both print and electronic
Are you the author of this Elsevier article?	Yes
Will you be translating?	No
Order reference number	
Title of your thesis/dissertation	STRUCTURAL AND ENZYMATIC CHARACTERIZATION OF BACTERIAL CELL WALL ENZYMES: FOCUS ON PENICILLIN BINDING PROTEINS
Expected completion date	May 2013
Estimated size (number of pages)	180
Elsevier VAT number	GB 494 6272 12
Permissions price	0.00 USD
VAT/Local Sales Tax	0.00 USD
Total	0.00 USD

ORDER MORE... | CLOSE WINDOW

Copyright Clearance Center RightsLink®

Home | Account Info | Help

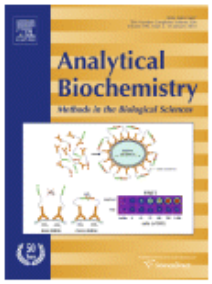

Title: A microtiter plate-based β-lactam binding assay for inhibitors of high-molecular-mass penicillin-binding proteins

Author: Miglena Stefanova,Sudheer Bobba,William G. Gutheil

Publication: Analytical Biochemistry

Publisher: Elsevier

Date: 1 January 2010

Logged in as:
sudheer bobba

LOGOUT

Order Completed

Thank you very much for your order.

This is a License Agreement between sudheer bobba ("You") and Elsevier ("Elsevier"). The license consists of your order details, the terms and conditions provided by Elsevier, and the payment terms and conditions.

Get the printable license.

License Number	3117270249122
License date	Mar 27, 2013
Licensed content publisher	Elsevier
Licensed content publication	Analytical Biochemistry
Licensed content title	A microtiter plate-based β-lactam binding assay for inhibitors of high-molecular-mass penicillin-binding proteins
Licensed content author	Miglena Stefanova,Sudheer Bobba,William G. Gutheil
Licensed content date	1 January 2010
Licensed content volume number	396
Licensed content issue number	1
Number of pages	3
Type of Use	reuse in a thesis/dissertation
Portion	full article
Format	both print and electronic
Are you the author of this Elsevier article?	Yes
Will you be translating?	No
Order reference number	
Title of your thesis/dissertation	STRUCTURAL AND ENZYMATIC CHARACTERIZATION OF BACTERIAL CELL WALL ENZYMES: FOCUS ON PENICILLIN BINDING PROTEINS
Expected completion date	May 2013
Estimated size (number of pages)	180
Elsevier VAT number	GB 494 6272 12
Permissions price	0.00 USD
VAT/Local Sales Tax	0.00 USD
Total	0.00 USD

ORDER MORE... | CLOSE WINDOW

REFERENCES

1. Schleifer KH, Kandler O 1972. Peptidoglycan types of bacterial cell walls and their taxinomic implications. Bacteriol Rev 36:407-477.

2. Vollmer W, Bertsche U 2008. Murein (peptidoglycan) structure, architecture and biosynthesis in Escherichia coli. Biochim Biophys Acta 1778(9):1714-1734.

3. Smith CA 2006. Structure, function and dynamics in the mur family of bacterial cell wall ligases. J Mol Biol 362(4):640-655.

4. El Zoeiby A, Sanschagrin F, Levesque RC 2003. Structure and function of the Mur enzymes: development of novel inhibitors. Mol Microbiol 47(1):1-12.

5. van Heijenoort J 2001. Recent advances in the formation of the bacterial peptidoglycan monomer unit. Nat Prod Rep 18(5):503-519.

6. Waxman DJ, Strominger JL 1983. Penicillin-binding proteins and the mechanism of action of b-lactam antibiotics. Annu Rev Biochem 52:825-869.

7. Georgopapadakou N, Sykes B 1983. Bacterial enzymes interacting with b-lactam antibiotics. Handb Exp Pharmacol 67(2):1-77.

8. Ghuysen JM 1991. Serine beta-lactamases and penicillin-binding proteins. Annu Rev Microbiol 45:37-67.

9. Macheboeuf P, Contreras-Martel C, Job V, Dideberg O, Dessen A 2006. Penicillin binding proteins: key players in bacterial cell cycle and drug resistance processes. FEMS Microbiol Rev 30(5):673-691.

10. Goffin C, Ghuysen JM 1998. Multimodular penicillin-binding proteins: an enigmatic family of orthologs and paralogs. Microbiol Mol Biol Rev 62(4):1079-1093.

11. Massova I, Mobashery S 1998. Kinship and diversification of bacterial penicillin-binding proteins and beta-lactamases. Antimicrob Agents Chemother 42(1):1-17.

12. Sauvage E, Kerff F, Terrak M, Ayala JA, Charlier P 2008. The penicillin-binding proteins: structure and role in peptidoglycan biosynthesis. FEMS Microbiol Rev 32(2):234-258.

13. Schiffer G, Holtje JV 1999. Cloning and characterization of PBP 1C, a third member of the multimodular class A penicillin-binding proteins of Escherichia coli. The Journal of biological chemistry 274(45):32031-32039.

14. Goffin C, Ghuysen JM 2002. Biochemistry and comparative genomics of SxxK superfamily acyltransferases offer a clue to the mycobacterial paradox: presence of penicillin-susceptible target proteins versus lack of efficiency of penicillin as therapeutic agent. Microbiol Mol Biol Rev 66(4):702-738, table of contents.

15. Denome SA, Elf PK, Henderson TA, Nelson DE, Young KD 1999. Escherichia coli mutants lacking all possible combinations of eight penicillin binding proteins: viability, characteristics, and implications for peptidoglycan synthesis. J Bacteriol 181(13):3981-3993.

16. Waxman DJ, Yocum RR, Strominger JL 1980. Penicillins and cephalosporins are active site-directed acylating agents: evidence in support of the substrate analogue hypothesis. Philos Trans R Soc Lond B Biol Sci 289(1036):257-271.

17. Holtje JV 1998. Growth of the stress-bearing and shape-maintaining murein sacculus of Escherichia coli. Microbiol Mol Biol Rev 62(1):181-203.

18. Ghosh AS, Chowdhury C, Nelson DE 2008. Physiological functions of D-alanine carboxypeptidases in Escherichia coli. Trends Microbiol 16(7):309-317.

19. Ghuysen JM, Frere JM, Leyh-Bouille M, Coyette J, Dusart J, Nguyen-Disteche M 1979. Use of model enzymes in the determination of the mode of action of penicillins and delta 3-cephalosporins. Annu Rev Biochem 48:73-101.

20. Young KD 2001. Approaching the physiological functions of penicillin-binding proteins in Escherichia coli. Biochimie 83(1):99-102.

21. Pratt RF 2008. Substrate specificity of bacterial DD-peptidases (penicillin-binding proteins). Cell Mol Life Sci 65(14):2138-2155.

22. Tamura T, Imae Y, Strominger JL 1976. Purification to homogeneity and properties of two D-alanine carboxypeptidases I From Escherichia coli. The Journal of biological chemistry 251(2):414-423.

23. Korat B, Mottl H, Keck W 1991. Penicillin-binding protein 4 of Escherichia coli: molecular cloning of the dacB gene, controlled overexpression, and alterations in murein composition. Mol Microbiol 5(3):675-684.

24. Meberg BM, Paulson AL, Priyadarshini R, Young KD 2004. Endopeptidase penicillin-binding proteins 4 and 7 play auxiliary roles in determining uniform morphology of Escherichia coli. J Bacteriol 186(24):8326-8336.

25. Kishida H, Unzai S, Roper DI, Lloyd A, Park SY, Tame JR 2006. Crystal structure of penicillin binding protein 4 (dacB) from Escherichia coli, both in the native form and covalently linked to various antibiotics. Biochemistry 45(3):783-792.

26. Nguyen-Disteche M, Leyh-Bouille M, Ghuysen JM 1982. Isolation of the membrane-bound 26 000-Mr penicillin-binding protein of Streptomyces strain K15 in the form of a penicillin-sensitive D-alanyl-D-alanine-cleaving transpeptidase. The Biochemical journal 207(1):109-115.

27. van Heijenoort J 2001. Formation of the glycan chains in the synthesis of bacterial peptidoglycan. Glycobiology 11(3):25R-36R.

28. Born P, Breukink E, Vollmer W 2006. In vitro synthesis of cross-linked murein and its attachment to sacculi by PBP1A from Escherichia coli. The Journal of biological chemistry 281(37):26985-26993.

29. Bertsche U, Breukink E, Kast T, Vollmer W 2005. In vitro murein peptidoglycan synthesis by dimers of the bifunctional transglycosylase-transpeptidase PBP1B from Escherichia coli. The Journal of biological chemistry 280(45):38096-38101.

30. Bertsche U, Kast T, Wolf B, Fraipont C, Aarsman ME, Kannenberg K, von Rechenberg M, Nguyen-Disteche M, den Blaauwen T, Holtje JV, Vollmer W 2006. Interaction between two murein (peptidoglycan) synthases, PBP3 and PBP1B, in Escherichia coli. Mol Microbiol 61(3):675-690.

31. Scheffers DJ, Pinho MG 2005. Bacterial cell wall synthesis: new insights from localization studies. Microbiol Mol Biol Rev 69(4):585-607.

32. Josephine HR, Charlier P, Davies C, Nicholas RA, Pratt RF 2006. Reactivity of Penicillin-Binding Proteins with Peptidoglycan-Mimetic beta-Lactams: What's Wrong with These Enzymes? Biochemistry 45(51):15873-15883.

33. Popham DL, Young KD 2003. Role of penicillin-binding proteins in bacterial cell morphogenesis. Curr Opin Microbiol 6(6):594-599.

34. Spratt BG, Pardee AB 1975. Penicillin-binding proteins and cell shape in E. coli. Nature 254(5500):516-517.

35. Duez C, Vanhove M, Gallet X, Bouillenne F, Docquier J, Brans A, Frere J 2001. Purification and characterization of PBP4a, a new low-molecular-weight penicillin-binding protein from Bacillus subtilis. J Bacteriol 183(5):1595-1599.

36. Schuster C, Dobrinski B, Hakenbeck R 1990. Unusual septum formation in Streptococcus pneumoniae mutants with an alteration in the D,D-carboxypeptidase penicillin-binding protein 3. J Bacteriol 172(11):6499-6505.

37. Morlot C, Noirclerc-Savoye M, Zapun A, Dideberg O, Vernet T 2004. The D,D-carboxypeptidase PBP3 organizes the division process of Streptococcus pneumoniae. Mol Microbiol 51(6):1641-1648.

38. Henze UU, Roos M, Berger-Bachi B 1996. Effects of penicillin-binding protein 4 overproduction in Staphylococcus aureus. Microb Drug Resist 2(2):193-199.

39. Nelson DE, Young KD 2000. Penicillin binding protein 5 affects cell diameter, contour, and morphology of Escherichia coli. J Bacteriol 182(6):1714-1721.

40. Nelson DE, Young KD 2001. Contributions of PBP 5 and DD-carboxypeptidase penicillin binding proteins to maintenance of cell shape in Escherichia coli. J Bacteriol 183(10):3055-3064.

41. Nelson DE, Ghosh AS, Paulson AL, Young KD 2002. Contribution of Membrane-Binding and Enzymatic Domains of Penicillin Binding Protein 5 to Maintenance of Uniform Cellular Morphology of Escherichia coli. J Bacteriol 184(13):3630-3639.

42. Ghosh AS, Young KD 2003. Sequences near the active site in chimeric penicillin binding proteins 5 and 6 affect uniform morphology of Escherichia coli. J Bacteriol 185(7):2178-2186.

43. Stefanova ME, Tomberg J, Olesky M, Holtje JV, Gutheil WG, Nicholas RA 2003. Neisseria gonorrhoeae penicillin-binding protein 3 exhibits exceptionally high carboxypeptidase and beta-lactam binding activities. Biochemistry 42(49):14614-14625.

44. Arthur M, Molinas C, Bugg TD, Wright GD, Walsh CT, Courvalin P 1992. Evidence for in vivo incorporation of D-lactate into peptidoglycan precursors of vancomycin-resistant enterococci. Antimicrob Agents Chemother 36(4):867-869.

45. Nemmara VV, Dzhekieva L, Sarkar KS, Adediran SA, Duez C, Nicholas RA, Pratt RF 2011. Substrate specificity of low-molecular mass bacterial DD-peptidases. Biochemistry 50(46):10091-10101.

46. Peddi S 2002. Substrate and inhibitor specificity studies on low molecular weight penicillin-binding proteins. University of Missouri-Kansas City.

47. Rhazi N, Delmarcelle M, Sauvage E, Jacquemotte F, Devriendt K, Tallon V, Ghosez L, Frere JM 2005. Specificity and reversibility of the transpeptidation reaction catalyzed by the Streptomyces R61 D-Ala-D-Ala peptidase. Protein Sci 14(11):2922-2928.

48. Anderson JW, Pratt RF 2000. Dipeptide binding to the extended active site of the Streptomyces R61 D-alanyl-D-alanine-peptidase: the path to a specific substrate. Biochemistry 39(40):12200-12209.

49. Peddi S, Nicholas RA, Gutheil WG 2009. Neisseria gonorrhoeae penicillin-binding protein 3 demonstrates a pronounced preference for N(epsilon)-acylated substrates. Biochemistry 48(24):5731-5737.

50. Jamin M, Adam M, Damblon C, Christiaens L, Frere JM 1991. Accumulation of acyl-enzyme in DD-peptidase-catalysed reactions with analogues of peptide substrates. The Biochemical journal 280 (Pt 2):499-506.

51. Adam M, Damblon C, Plaitin B, Christiaens L, Frere JM 1990. Chromogenic depsipeptide substrates for beta-lactamases and penicillin-sensitive DD-peptidases. The Biochemical journal 270(2):525-529.

52. Granier B, Jamin M, Adam M, Galleni M, Lakaye B, Zorzi W, Grandchamps J, Wilkin JM, Fraipont C, Joris B, et al. 1994. Serine-type D-Ala-D-Ala peptidases and penicillin-binding proteins. Methods Enzymol 244:249-266.

53. Nakagawa J, Matsuhashi S 1982. Molecular divergence of a major peptidoglycan synthase with transglycosylase-transpeptidase activities in Eschericia coli. Biochem Biophys Res Commun 105(1546-1553).

54. Schwartz B, Markwalder JA, Wang Y 2001. Lipid II: total synthesis of the bacterial cell wall precursor and utilization as a substrate for glycosyltransfer and transpeptidation by penicillin binding protein (PBP) 1b of Escherichia coli. J Am Chem Soc 123(47):11638-11643.

55. Taku A, Stuckey M, Fan DP 1982. Purification of the peptidoglycan transglycosylase of Bacillus megaterium. The Journal of biological chemistry 257(9):5018-5022.

56. Adam M, Fraipont C, Rhazi N, Nguyen-Disteche M, Lakaye B, Frere JM, Devreese B, Van Beeumen J, van Heijenoort Y, van Heijenoort J, Ghuysen JM 1997. The bimodular G57-V577 polypeptide chain of the class B penicillin-binding protein 3 of Escherichia coli catalyzes peptide bond formation from thiolesters and does not catalyze glycan chain polymerization from the lipid II intermediate. J Bacteriol 179(19):6005-6009.

57. Adam M, Damblon C, Jamin M, Zorzi W, Dusart V, Galleni M, el Kharroubi A, Piras G, Spratt BG, Keck W, et al. 1991. Acyltransferase activities of the high-molecular-mass essential penicillin-binding proteins. The Biochemical journal 279 (Pt 2):601-604.

58. Macheboeuf P, Fischer DS, Brown T, Jr., Zervosen A, Luxen A, Joris B, Dessen A, Schofield CJ 2007. Structural and mechanistic basis of penicillin-binding protein inhibition by lactivicins. Nat Chem Biol 3(9):565-569.

59. Macheboeuf P, Di Guilmi AM, Job V, Vernet T, Dideberg O, Dessen A 2005. Active site restructuring regulates ligand recognition in class A penicillin-binding proteins. Proc Natl Acad Sci U S A 102(3):577-582.

60. Lim D, Strynadka NC 2002. Structural basis for the beta lactam resistance of PBP2a from methicillin-resistant Staphylococcus aureus. Nat Struct Biol 9(11):870-876.

61. Thomas B, Wang Y, Stein RL 2001. Kinetic and mechanistic studies of penicillin-binding protein 2x from Streptococcus pneumoniae. Biochemistry 40(51):15811-15823.

62. Damblon C, Zhao GH, Jamin M, Ledent P, Dubus A, Vanhove M, Raquet X, Christiaens L, Frere JM 1995. Breakdown of the stereospecificity of DD-peptidases and beta-lactamases with thiolester substrates. The Biochemical journal 309 (Pt 2):431-436.

63. Preston DA, Wu CY, Blaszczak LC, Seitz DE, Halligan NG 1990. Biological characterization of a new radioactive labeling reagent for bacterial penicillin-binding proteins. Antimicrob Agents Chemother 34(5):718-721.

64. Spratt BG 1977. Properties of the penicillin-binding proteins of Escherichia coli K12. European journal of biochemistry / FEBS 72(2):341-352.

65. Zhao G, Meier TI, Kahl SD, Gee KR, Blaszczak LC 1999. BOCILLIN FL, a sensitive and commercially available reagent for detection of penicillin-binding proteins. Antimicrob Agents Chemother 43(5):1124-1128.

66. Fedarovich A, Djordjevic KA, Swanson SM, Peterson YK, Nicholas RA, Davies C 2012. High-throughput screening for novel inhibitors of Neisseria gonorrhoeae penicillin-binding protein 2. PLoS One 7(9):e44918.

67. Inglis SR, Strieker M, Rydzik AM, Dessen A, Schofield CJ 2012. A boronic-acid-based probe for fluorescence polarization assays with penicillin binding proteins and beta-lactamases. Anal Biochem 420(1):41-47.

68. Kocaoglu O, Calvo RA, Sham LT, Cozy LM, Lanning BR, Francis S, Winkler ME, Kearns DB, Carlson EE 2012. Selective penicillin-binding protein imaging probes reveal substructure in bacterial cell division. ACS Chem Biol 7(10):1746-1753.

69. Daniel RA, Errington J 2003. Control of cell morphogenesis in bacteria: two distinct ways to make a rod-shaped cell. Cell 113(6):767-776.

70. Zervosen A, Bouillez A, Herman A, Amoroso A, Joris B, Sauvage E, Charlier P, Luxen A 2012. Synthesis and evaluation of boronic acids as inhibitors of Penicillin Binding Proteins of classes A, B and C. Biorg Med Chem 20(12):3915-3924.

71. Tomasic T, Kovac A, Klebe G, Blanot D, Gobec S, Kikelj D, Masic LP 2012. Virtual screening for potential inhibitors of bacterial MurC and MurD ligases. J Mol Model 18(3):1063-1072.

72. Maurer P, Todorova K, Sauerbier J, Hakenbeck R 2012. Mutations in Streptococcus pneumoniae penicillin-binding protein 2x: importance of the C-terminal penicillin-binding protein and serine/threonine kinase-associated domains for beta-lactam binding. Microb Drug Resist 18(3):314-321.

73. Dzhekieva L, Kumar I, Pratt RF 2012. Inhibition of bacterial DD-peptidases (penicillin-binding proteins) in membranes and in vivo by peptidoglycan-mimetic boronic acids. Biochemistry 51(13):2804-2811.

74. Dargis M, Malouin F 1994. Use of biotinylated beta-lactams and chemiluminescence for study and purification of penicillin-binding proteins in bacteria. Antimicrob Agents Chemother 38(5):973-980.

75. Bobba S, Ponnaluri VK, Mukherji M, Gutheil WG 2011. Microtiter plate-based assay for inhibitors of penicillin-binding protein 2a from methicillin-resistant Staphylococcus aureus. Antimicrob Agents Chemother 55(6):2783-2787.

76. Stefanova M, Bobba S, Gutheil WG 2010. A microtiter plate-based beta-lactam binding assay for inhibitors of high-molecular-mass penicillin-binding proteins. Anal Biochem 396(1):164-166.

77. Tiyanont K, Doan T, Lazarus MB, Fang X, Rudner DZ, Walker S 2006. Imaging peptidoglycan biosynthesis in Bacillus subtilis with fluorescent antibiotics. Proceedings of the National Academy of Sciences of the United States of America 103(29):11033-11038.

78. Kalan L, Perry J, Koteva K, Thaker M, Wright G 2013. Glycopeptide sulfation evades resistance. J Bacteriol 195(1):167-171.

79. Bobba S, Gutheil WG 2011. Multivariate geometrical analysis of catalytic residues in the penicillin-binding proteins. The international journal of biochemistry & cell biology 43(10):1490-1499.

80. Suzuki H, van Heijenoort Y, Tamura T, Mizoguchi J, Hirota Y, van Heijenoort J 1980. In vitro peptidoglycan polymerization catalysed by penicillin binding protein 1b of Escherichia coli K-12. FEBS Lett 110(2):245-249.

81. Nakagawa J, Tamaki S, Tomioka S, Matsuhashi M 1984. Functional biosynthesis of cell wall peptidoglycan by polymorphic bifunctional polypeptides. Penicillin-binding protein 1Bs of Escherichia coli with activities of transglycosylase and transpeptidase. The Journal of biological chemistry 259(22):13937-13946.

82. den Blaauwen T, Aarsman M, Nanninga N 1990. Interaction of monoclonal antibodies with the enzymatic domains of penicillin-binding protein 1b of Escherichia coli. J Bacteriol 172(1):63-70.

83. Terrak M, Ghosh TK, van Heijenoort J, Van Beeumen J, Lampilas M, Aszodi J, Ayala JA, Ghuysen JM, Nguyen-Disteche M 1999. The catalytic, glycosyl transferase and acyl transferase modules of the cell wall peptidoglycan-polymerizing penicillin-binding protein 1b of Escherichia coli. Mol Microbiol 34(2):350-364.

84. Pechenov A, Stefanova ME, Nicholas RA, Peddi S, Gutheil WG 2003. Potential transition state analogue inhibitors for the penicillin-binding proteins. Biochemistry 42(2):579-588.

85. Sauvage E, Herman R, Petrella S, Duez C, Bouillenne F, Frere JM, Charlier P 2005. Crystal structure of the Actinomadura R39 DD-peptidase reveals new domains in penicillin-binding proteins. The Journal of biological chemistry 280(35):31249-31256.

86. Sauvage E, Powell AJ, Heilemann J, Josephine HR, Charlier P, Davies C, Pratt RF 2008. Crystal structures of complexes of bacterial DD-peptidases with peptidoglycan-mimetic ligands: the substrate specificity puzzle. J Mol Biol 381(2):383-393.

87. Sauvage E, Zervosen A, Dive G, Herman R, Amoroso A, Joris B, Fonze E, Pratt RF, Luxen A, Charlier P, Kerff F 2009. Structural basis of the inhibition of class A beta-

lactamases and penicillin-binding proteins by 6-beta-iodopenicillanate. J Am Chem Soc 131(42):15262-15269.

88. Sauvage E, Duez C, Herman R, Kerff F, Petrella S, Anderson JW, Adediran SA, Pratt RF, Frere JM, Charlier P 2007. Crystal structure of the Bacillus subtilis penicillin-binding protein 4a, and its complex with a peptidoglycan mimetic peptide. J Mol Biol 371(2):528-539.

89. Davies C, White SW, Nicholas RA 2001. Crystal structure of a deacylation-defective mutant of penicillin-binding protein 5 at 2.3-A resolution. The Journal of biological chemistry 276(1):616-623.

90. Nicholas RA, Krings S, Tomberg J, Nicola G, Davies C 2003. Crystal structure of wild-type penicillin-binding protein 5 from Escherichia coli: implications for deacylation of the acyl-enzyme complex. The Journal of biological chemistry 278(52):52826-52833.

91. Nicola G, Fedarovich A, Nicholas RA, Davies C 2005. A large displacement of the SXN motif of Cys115-modified penicillin-binding protein 5 from Escherichia coli. The Biochemical journal 392(Pt 1):55-63.

92. Nicola G, Peddi S, Stefanova M, Nicholas RA, Gutheil WG, Davies C 2005. Crystal Structure of Escherichia coli Penicillin-Binding Protein 5 Bound to a Tripeptide Boronic Acid Inhibitor: A Role for Ser-110 in Deacylation. Biochemistry 44(23):8207-8217.

93. Chen Y, Zhang W, Shi Q, Hesek D, Lee M, Mobashery S, Shoichet BK 2009. Crystal structures of penicillin-binding protein 6 from Escherichia coli. J Am Chem Soc 131(40):14345-14354.

94. Kawai F, Clarke TB, Roper DI, Han GJ, Hwang KY, Unzai S, Obayashi E, Park SY, Tame JR 2009. Crystal structures of penicillin-binding proteins 4 and 5 from Haemophilus influenzae. J Mol Biol 396(3):634-645.

95. Navratna V, Nadig S, Sood V, Prasad K, Arakere G, Gopal B 2010. Molecular basis for the role of Staphylococcus aureus penicillin binding protein 4 in antimicrobial resistance. J Bacteriol 192(1):134-144.

96. Rhazi N, Charlier P, Dehareng D, Engher D, Vermeire M, Frere JM, Nguyen-Disteche M, Fonze E 2003. Catalytic mechanism of the Streptomyces K15 DD-transpeptidase/penicillin-binding protein probed by site-directed mutagenesis and structural analysis. Biochemistry 42(10):2895-2906.

97. Fonze E, Vermeire M, Nguyen-Disteche M, Brasseur R, Charlier P 1999. The crystal structure of a penicilloyl-serine transferase of intermediate penicillin sensitivity. The DD-transpeptidase of streptomyces K15. The Journal of biological chemistry 274(31):21853-21860.

98. Sung MT, Lai YT, Huang CY, Chou LY, Shih HW, Cheng WC, Wong CH, Ma C 2009. Crystal structure of the membrane-bound bifunctional transglycosylase PBP1b from Escherichia coli. Proc Natl Acad Sci U S A 106(22):8824-8829.

99. Powell AJ, Tomberg J, Deacon AM, Nicholas RA, Davies C 2009. Crystal structures of penicillin-binding protein 2 from penicillin-susceptible and -resistant strains of Neisseria gonorrhoeae reveal an unexpectedly subtle mechanism for antibiotic resistance. The Journal of biological chemistry 284(2):1202-1212.

100. Lovering AL, de Castro LH, Lim D, Strynadka NC 2007. Structural insight into the transglycosylation step of bacterial cell-wall biosynthesis. Science 315(5817):1402-1405.

101. Lovering AL, De Castro L, Strynadka NC 2008. Identification of dynamic structural motifs involved in peptidoglycan glycosyltransfer. J Mol Biol 383(1):167-177.

102. Contreras-Martel C, Job V, Di Guilmi AM, Vernet T, Dideberg O, Dessen A 2006. Crystal structure of penicillin-binding protein 1a (PBP1a) reveals a mutational hotspot implicated in beta-lactam resistance in Streptococcus pneumoniae. J Mol Biol 355(4):684-696.

103. Job V, Carapito R, Vernet T, Dessen A, Zapun A 2008. Common alterations in PBP1a from resistant Streptococcus pneumoniae decrease its reactivity toward beta-lactams: structural insights. The Journal of biological chemistry 283(8):4886-4894.

104. Yamada M, Watanabe T, Baba N, Takeuchi Y, Ohsawa F, Gomi S 2008. Crystal structures of biapenem and tebipenem complexed with penicillin-binding proteins 2X and 1A from Streptococcus pneumoniae. Antimicrob Agents Chemother 52(6):2053-2060.

105. Macheboeuf P, Lemaire D, Teller N, Martins Ados S, Luxen A, Dideberg O, Jamin M, Dessen A 2008. Trapping of an acyl-enzyme intermediate in a penicillin-binding protein (PBP)-catalyzed reaction. J Mol Biol 376(2):405-413.

106. Contreras-Martel C, Dahout-Gonzalez C, Martins Ados S, Kotnik M, Dessen A 2009. PBP active site flexibility as the key mechanism for beta-lactam resistance in pneumococci. J Mol Biol 387(4):899-909.

107. Dessen A, Mouz N, Gordon E, Hopkins J, Dideberg O 2001. Crystal structure of PBP2x from a highly penicillin-resistant Streptococcus pneumoniae clinical isolate: a mosaic framework containing 83 mutations. The Journal of biological chemistry 276(48):45106-45112.

108. Chesnel L, Pernot L, Lemaire D, Champelovier D, Croize J, Dideberg O, Vernet T, Zapun A 2003. The structural modifications induced by the M339F substitution in PBP2x from Streptococcus pneumoniae further decreases the susceptibility to beta-lactams of resistant strains. The Journal of biological chemistry 278(45):44448-44456.

109. Gordon E, Mouz N, Duee E, Dideberg O 2000. The crystal structure of the penicillin-binding protein 2x from Streptococcus pneumoniae and its acyl-enzyme form: implication in drug resistance. J Mol Biol 299(2):477-485.

110. Pernot L, Chesnel L, Le Gouellec A, Croize J, Vernet T, Dideberg O, Dessen A 2004. A PBP2x from a clinical isolate of Streptococcus pneumoniae exhibits an alternative mechanism for reduction of susceptibility to beta-lactam antibiotics. The Journal of biological chemistry 279(16):16463-16470.

111. Yamada M, Watanabe T, Miyara T, Baba N, Saito J, Takeuchi Y, Ohsawa F 2007. Crystal structure of cefditoren complexed with Streptococcus pneumoniae penicillin-binding protein 2X: structural basis for its high antimicrobial activity. Antimicrob Agents Chemother 51(11):3902-3907.

112. Kelly JA, Kuzin AP 1995. The refined crystallographic structure of a DD-peptidase penicillin-target enzyme at 1.6 A resolution. J Mol Biol 254(2):223-236.

113. Kuzin AP, Liu H, Kelly JA, Knox JR 1995. Binding of cephalothin and cefotaxime to D-ala-D-ala-peptidase reveals a functional basis of a natural mutation in a low-affinity penicillin-binding protein and in extended-spectrum beta-lactamases. Biochemistry 34(29):9532-9540.

114. Lee W, McDonough MA, Kotra L, Li ZH, Silvaggi NR, Takeda Y, Kelly JA, Mobashery S 2001. A 1.2-A snapshot of the final step of bacterial cell wall biosynthesis. Proc Natl Acad Sci U S A 98(4):1427-1431.

115. McDonough MA, Anderson JW, Silvaggi NR, Pratt RF, Knox JR, Kelly JA 2002. Structures of two kinetic intermediates reveal species specificity of penicillin-binding proteins. J Mol Biol 322(1):111-122.

116. Silvaggi NR, Anderson JW, Brinsmade SR, Pratt RF, Kelly JA 2003. The Crystal Structure of Phosphonate-Inhibited d-Ala-d-Ala Peptidase Reveals an Analogue of a Tetrahedral Transition State. Biochemistry 42(5):1199-1208.

117. Silvaggi NR, Josephine HR, Kuzin AP, Nagarajan R, Pratt RF, Kelly JA 2005. Crystal structures of complexes between the R61 DD-peptidase and peptidoglycan-mimetic beta-lactams: a non-covalent complex with a "perfect penicillin". J Mol Biol 345(3):521-533.

118. Silvaggi NR, Kaur K, Adediran SA, Pratt RF, Kelly JA 2004. Toward better antibiotics: crystallographic studies of a novel class of DD-peptidase/beta-lactamase inhibitors. Biochemistry 43(22):7046-7053.

119. Leyh-Bouille M, Nakel M, Frere JM, Johnson K, Ghuysen JM, Nieto M, Perkins HR 1972. Penicillin-sensitive DD-carboxypeptidases from Streptomyces strains R39 and K11. Biochemistry 11(7):1290-1298.

120. Ghuysen JM, Leyh-Bouille M, Campbell JN, Moreno R, Frere JM, Duez C, Nieto M, Perkins HR 1973. Structure of the wall peptidoglycan of Streptomyces R39 and the specificity profile of its exocellular DD-carboxypeptidase--transpeptidase for peptide acceptors. Biochemistry 12(7):1243-1251.

121. Clarke TB, Kawai F, Park SY, Tame JR, Dowson CG, Roper DI 2009. Mutational analysis of the substrate specificity of Escherichia coli penicillin binding protein 4. Biochemistry 48(12):2675-2683.

122. Amanuma H, Strominger JL 1980. Purification and properties of penicillin-binding proteins 5 and 6 from Escherichia coli membranes. The Journal of biological chemistry 255(23):11173-11180.

123. Matsuhashi M, Tamaki S, Curtis SJ, Strominger JL 1979. Mutational evidence for identity of penicillin-binding protein 5 in Escherichia coli with the major D-alanine carboxypeptidase IA activity. J Bacteriol 137(1):644-647.

124. van der Linden MP, de Haan L, Hoyer MA, Keck W 1992. Possible role of Escherichia coli penicillin-binding protein 6 in stabilization of stationary-phase peptidoglycan. J Bacteriol 174(23):7572-7578.

125. Kozarich JW, Strominger JL 1978. A membrane enzyme from Staphylococcus aureus which catalyzes transpeptidase, carboxypeptidase, and penicillinase activities. The Journal of biological chemistry 253(4):1272-1278.

126. Leyh-Bouille M, Coyette J, Ghuysen JM, Idczak J, Perkins HR, Nieto M 1971. Penicillin-sensitive DD-carboxypeptidase from Streptomyces strain R 61. Biochemistry 10(11):2163-2170.

127. Perkins HR, Nieto M, Frere JM, Leyh-Bouille M, Ghuysen JM 1973. Streptomyces DD-carboxypeptidases as transpeptidases. The specificity for amino compounds acting as carboxyl acceptors. The Biochemical journal 131(4):707-718.

128. Pettersen EF, Goddard TD, Huang CC, Couch GS, Greenblatt DM, Meng EC, Ferrin TE 2004. UCSF chimera - A visualization system for exploratory research and analysis. J Comput Chem 25(13):1605-1612.

129. Jolliffe IT. 2002. Principal component analysis. 2nd ed., New York: Springer. p xxix, 487 p.

130. Malhotra KT, Nicholas RA 1992. Substitution of lysine 213 with arginine in penicillin-binding protein 5 of Escherichia coli abolishes D-alanine carboxypeptidase activity without affecting penicillin binding. The Journal of biological chemistry 267(16):11386-11391.

131. Zhao GH, Duez C, Lepage S, Forceille C, Rhazi N, Klein D, Ghuysen JM, Frere JM 1997. Site-directed mutagenesis of the Actinomadura R39 DD-peptidase. The Biochemical journal 327 (Pt 2):377-381.

132. Zhang W, Shi Q, Meroueh SO, Vakulenko SB, Mobashery S 2007. Catalytic mechanism of penicillin-binding protein 5 of Escherichia coli. Biochemistry 46(35):10113-10121.

133. Stefanova ME, Tomberg J, Davies C, Nicholas RA, Gutheil WG 2004. Overexpression and enzymatic characterization of Neisseria gonorrhoeae penicillin-binding protein 4. European journal of biochemistry / FEBS 271(1):23-32.

134. Stefanova ME, Davies C, Nicholas RA, Gutheil WG 2002. pH, inhibitor, and substrate specificity studies on Escherichia coli penicillin-binding protein 5. Biochim Biophys Acta 1597(2):292-300.

135. Gutheil WG, Stefanova ME, Nicholas RA 2000. Fluorescent coupled enzyme assays for D-alanine: application to penicillin-binding protein and vancomycin activity assays. Anal Biochem 287(2):196-202.

136. Adediran SA, Kumar I, Nagarajan R, Sauvage E, Pratt RF 2011. Kinetics of reactions of the Actinomadura R39 DD-peptidase with specific substrates. Biochemistry 50(3):376-387.

137. Nemmara VV, Adediran SA, Dave K, Duez C, Pratt RF 2013. Dual Substrate Specificity of Bacillus subtilis PBP4a. Biochemistry 52(15):2627-2637.

138. Dzhekieva L, Rocaboy M, Kerff F, Charlier P, Sauvage E, Pratt RF 2010. Crystal structure of a complex between the Actinomadura R39 DD-peptidase and a peptidoglycan-mimetic boronate inhibitor: interpretation of a transition state analogue in terms of catalytic mechanism. Biochemistry 49(30):6411-6419.

139. Anderson JW, Adediran SA, Charlier P, Nguyen-Disteche M, Frere JM, Nicholas RA, Pratt RF 2003. On the substrate specificity of bacterial DD-peptidases: evidence from two series of peptidoglycan-mimetic peptides. The Biochemical journal 373(Pt 3):949-955.

140. Zervosen A, Herman R, Kerff F, Herman A, Bouillez A, Prati F, Pratt RF, Frere JM, Joris B, Luxen A, Charlier P, Sauvage E 2011. Unexpected tricovalent binding mode of boronic acids within the active site of a penicillin-binding protein. J Am Chem Soc 133(28):10839-10848.

141. Radzicka A, Wolfenden R 1995. Transition state and multisubstrate analog inhibitors. Methods Enzymol 249:284-312.

142. Arvind A, Kumar V, Saravanan P, Mohan CG 2012. Homology modeling, molecular dynamics and inhibitor binding study on MurD ligase of Mycobacterium tuberculosis. Interdiscip Sci 4(3):223-238.

143. Zervosen A, Sauvage E, Frere JM, Charlier P, Luxen A 2012. Development of new drugs for an old target: the penicillin binding proteins. Molecules 17(11):12478-12505.

144. Putty S, Rai A, Jamindar D, Pagano P, Quinn CL, Mima T, Schweizer HP, Gutheil WG 2011. Characterization of d-boroAla as a novel broad-spectrum antibacterial agent targeting d-Ala-d-Ala ligase. Chem Biol Drug Des 78(5):757-763.

145. Tipton KF, Dixon HB 1979. Effects of pH on enzymes. Methods Enzymol 63:183-234.

146. Lee SD, Jeong HS 2006. Actinomadura hallensis sp. nov., a novel actinomycete isolated from Mt. Halla in Korea. Int J Syst Evol Microbiol 56(Pt 1):259-264.

147. Ye XY, Lo MC, Brunner L, Walker D, Kahne D, Walker S 2001. Better substrates for bacterial transglycosylases. J Am Chem Soc 123(13):3155-3156.

148. van Heijenoort Y, Gomez M, Derrien M, Ayala J, van Heijenoort J 1992. Membrane intermediates in the peptidoglycan metabolism of Escherichia coli: possible roles of PBP 1b and PBP 3. J Bacteriol 174(11):3549-3557.

149. Chandrakala B, Elias BC, Mehra U, Umapathy NS, Dwarakanath P, Balganesh TS, deSousa SM 2001. Novel scintillation proximity assay for measuring membrane-associated steps of peptidoglycan biosynthesis in Escherichia coli. Antimicrob Agents Chemother 45(3):768-775.

150. Chandrakala B, Shandil RK, Mehra U, Ravishankar S, Kaur P, Usha V, Joe B, deSousa SM 2004. High-throughput screen for inhibitors of transglycosylase and/or

transpeptidase activities of Escherichia coli penicillin binding protein 1b. Antimicrob Agents Chemother 48(1):30-40.

151. Jha RK, de Sousa SM 2006. Microplate assay for inhibitors of the transpeptidase activity of PBP1b of Escherichia coli. J Biomol Screen 11(8):1005-1014.

152. DeLoney CR, Schiller NL 1999. Competition of various beta-lactam antibiotics for the major penicillin-binding proteins of Helicobacter pylori: antibacterial activity and effects on bacterial morphology. Antimicrob Agents Chemother 43(11):2702-2709.

153. Bamberger DM, Herndon BL, Fitch J, Florkowski A, Parkhurst V 2002. Effects of neutrophils on cefazolin activity and penicillin-binding proteins in Staphylococcus aureus abscesses. Antimicrob Agents Chemother 46(9):2878-2884.

154. Tamura T, Suzuki H, Nishimura Y, Mizoguchi J, Hirota Y 1980. On the process of cellular division in Escherichia coli: isolation and characterization of penicillin-binding proteins 1a, 1b, and 3. Proc Natl Acad Sci U S A 77(8):4499-4503.

155. Nicholas RA, Strominger JL, Suzuki H, Hirota Y 1985. Identification of the active site in penicillin-binding protein 3 of Escherichia coli. J Bacteriol 164(1):456-460.

156. Ropp PA, Nicholas RA 1997. Cloning and characterization of the ponA gene encoding penicillin-binding protein 1 from Neisseria gonorrhoeae and Neisseria meningitidis. J Bacteriol 179(8):2783-2787.

157. Schultz DE, Spratt BG, Nicholas RA 1991. Expression and purification of a soluble form of penicillin-binding protein 2 from both penicillin-susceptible and penicillin-resistant Neisseria gonorrhoeae. Protein Expr Purif 2(5-6):339-349.

158. Amanuma H, Strominger JL 1984. Purification and properties of penicillin-binding proteins 5 and 6 from the dacA mutant strain of Escherichia coli (JE 11191). The Journal of biological chemistry 259(2):1294-1298.

159. Fajardo A, Martinez JL 2008. Antibiotics as signals that trigger specific bacterial responses. Curr Opin Microbiol 11(2):161-167.

160. Antignac A, Tomasz A 2009. Reconstruction of the phenotypes of methicillin-resistant Staphylococcus aureus by replacement of the staphylococcal cassette chromosome mec with a plasmid-borne copy of Staphylococcus sciuri pbpD gene. Antimicrob Agents Chemother 53(2):435-441.

161. Llarrull LI, Fisher JF, Mobashery S 2009. Molecular basis and phenotype of methicillin resistance in Staphylococcus aureus and insights into new beta-lactams that meet the challenge. Antimicrob Agents Chemother 53(10):4051-4063.

162. Russo TA, MacDonald U, Beanan JM, Olson R, MacDonald IJ, Sauberan SL, Luke NR, Schultz LW, Umland TC 2009. Penicillin-binding protein 7/8 contributes to the survival of Acinetobacter baumannii in vitro and in vivo. J Infect Dis 199(4):513-521.

163. Moya B, Dotsch A, Juan C, Blazquez J, Zamorano L, Haussler S, Oliver A 2009. Beta-lactam resistance response triggered by inactivation of a nonessential penicillin-binding protein. PLoS Pathog 5(3):e1000353.

164. Kishii K, Chiba N, Morozumi M, Hamano-Hasegawa K, Kurokawa I, Masaki J, Ubukata K 2010. Diverse mutations in the ftsI gene in ampicillin-resistant Haemophilus influenzae isolates from pediatric patients with acute otitis media. J Infect Chemother 16(2):87-93.

165. Fisher J, Belasco JG, Khosla S, Knowles JR 1980. beta-Lactamase proceeds via an acyl-enzyme intermediate. Interaction of the Escherichia coli RTEM enzyme with cefoxitin. Biochemistry 19(13):2895-2901.

166. Llarrull LI, Testero SA, Fisher JF, Mobashery S 2010. The future of the beta-lactams. Curr Opin Microbiol 13(5):551-557.

167. Appelbaum PC 2007. Reduced glycopeptide susceptibility in methicillin-resistant Staphylococcus aureus (MRSA). Int J Antimicrob Agents 30(5):398-408.

168. Fischbach MA, Walsh CT 2009. Antibiotics for emerging pathogens. Science 325(5944):1089-1093.

169. Mertens R, Seyler L, Lacor P, Denis O 2012. Community associated methicillin-resistant Staphylococcus aureus. Acta Clin Belg 67(4):235-240.

170. Hartman BJ, Tomasz A 1984. Low-affinity penicillin-binding protein associated with beta-lactam resistance in Staphylococcus aureus. J Bacteriol 158(2):513-516.

171. Mainardi JL, Villet R, Bugg TD, Mayer C, Arthur M 2008. Evolution of peptidoglycan biosynthesis under the selective pressure of antibiotics in Gram-positive bacteria. FEMS Microbiol Rev 32(2):386-408.

172. Sumita Y, Fukasawa M, Mitsuhashi S, Inoue M 1995. Binding affinities of beta-lactam antibodies for penicillin-binding protein 2' in methicillin-resistant staphylococcus aureus. The Journal of antimicrobial chemotherapy 35(4):473-481.

173. Zapun A, Contreras-Martel C, Vernet T 2008. Penicillin-binding proteins and beta-lactam resistance. FEMS Microbiol Rev 32(2):361-385.

174. Appelbaum PC 2006. MRSA--the tip of the iceberg. Clin Microbiol Infect 12 Suppl 2:3-10.

175. Klevens RM, Morrison MA, Nadle J, Petit S, Gershman K, Ray S, Harrison LH, Lynfield R, Dumyati G, Townes JM, Craig AS, Zell ER, Fosheim GE, McDougal LK, Carey RB, Fridkin SK 2007. Invasive methicillin-resistant Staphylococcus aureus infections in the United States. Jama 298(15):1763-1771.

176. Taubes G 2008. The bacteria fight back. Science 321(5887):356-361.

177. Lu WP, Sun Y, Bauer MD, Paule S, Koenigs PM, Kraft WG 1999. Penicillin-binding protein 2a from methicillin-resistant Staphylococcus aureus: kinetic characterization of its interactions with beta-lactams using electrospray mass spectrometry. Biochemistry 38(20):6537-6546.

178. Fuda C, Suvorov M, Vakulenko SB, Mobashery S 2004. The basis for resistance to beta-lactam antibiotics by penicillin-binding protein 2a of methicillin-resistant Staphylococcus aureus. The Journal of biological chemistry 279(39):40802-40806.

179. Fuda C, Hesek D, Lee M, Heilmayer W, Novak R, Vakulenko SB, Mobashery S 2006. Mechanistic basis for the action of new cephalosporin antibiotics effective against methicillin- and vancomycin-resistant Staphylococcus aureus. The Journal of biological chemistry 281(15):10035-10041.

180. Lodise TP, Patel N, Renaud-Mutart A, Gorodecky E, Fritsche TR, Jones RN 2008. Pharmacokinetic and pharmacodynamic profile of ceftobiprole. Diagn Microbiol Infect Dis 61(1):96-102.

181. Bazan JA, Martin SI, Kaye KM 2009. Newer beta-lactam antibiotics: doripenem, ceftobiprole, ceftaroline, and cefepime. Infect Dis Clin North Am 23(4):983-996, ix.

182. Katayama Y, Zhang HZ, Chambers HF 2004. PBP 2a mutations producing very-high-level resistance to beta-lactams. Antimicrob Agents Chemother 48(2):453-459.

183. Graves-Woodward K, Pratt RF 1998. Reaction of soluble penicillin-binding protein 2a of methicillin-resistant Staphylococcus aureus with beta-lactams and acyclic substrates: kinetics in homogeneous solution. The Biochemical journal 332 (Pt 3):755-761.

184. Bush K, Smith SA, Ohringer S, Tanaka SK, Bonner DP 1987. Improved sensitivity in assays for binding of novel beta-lactam antibiotics to penicillin-binding proteins of Escherichia coli. Antimicrob Agents Chemother 31(8):1271-1273.

185. Wayne 2010. Clinical and Laboratory Standards Institute. Performance Standards for Antimicrobial Susceptibility Testing. TIS 30(1):M100-S120.

186. Vidaillac C, Rybak MJ 2009. Ceftobiprole: first cephalosporin with activity against methicillin-resistant Staphylococcus aureus. Pharmacotherapy 29(5):511-525.

187. Entenza JM, Hohl P, Heinze-Krauss I, Glauser MP, Moreillon P 2002. BAL9141, a novel extended-spectrum cephalosporin active against methicillin-resistant Staphylococcus aureus in treatment of experimental endocarditis. Antimicrob Agents Chemother 46(1):171-177.

188. Davies TA, Page MG, Shang W, Andrew T, Kania M, Bush K 2007. Binding of ceftobiprole and comparators to the penicillin-binding proteins of Escherichia coli, Pseudomonas aeruginosa, Staphylococcus aureus, and Streptococcus pneumoniae. Antimicrob Agents Chemother 51(7):2621-2624.

189. Johnson JW, Fisher JF, Mobashery S 2013. Bacterial cell-wall recycling. Ann NY Acad Sci 1277:54-75.

190. Yount NY, Yeaman MR 2013. Peptide antimicrobials: cell wall as a bacterial target. Ann NY Acad Sci 1277:127-138.

191. Jovetic S, Zhu Y, Marcone GL, Marinelli F, Tramper J 2010. beta-Lactam and glycopeptide antibiotics: first and last line of defense? Trends Biotechnol 28(12):596-604.

192. Moisan H, Pruneau M, Malouin F 2010. Binding of ceftaroline to penicillin-binding proteins of Staphylococcus aureus and Streptococcus pneumoniae. J Antimicrob Chemother 65(4):713-716.

193. Courvalin P 2006. Vancomycin resistance in gram-positive cocci. Clin Infect Dis 42 Suppl 1:S25-34.

194. Barrett CT, Barrett JF 2003. Antibacterials: are the new entries enough to deal with the emerging resistance problems? Curr Opin Biotechnol 14(6):621-626.

195. Abbanat D, Morrow B, Bush K 2008. New agents in development for the treatment of bacterial infections. Curr Opin Pharmacol 8(5):582-592.

196. Baltz RH 2009. Daptomycin: mechanisms of action and resistance, and biosynthetic engineering. Curr Opin Chem Biol 13(2):144-151.

197. Klein CD, Bachelier A 2006. Molecular modeling and bioinformatical analysis of the antibacterial target enzyme MurA from a drug design perspective. J Comput Aided Mol Des 20(10-11):621-628.

198. Mengin-Lecreulx D, Flouret B, van Heijenoort J 1982. Cytoplasmic steps of peptidoglycan synthesis in Escherichia coli. J Bacteriol 151(3):1109-1117.

199. Eschenburg S, Priestman MA, Abdul-Latif FA, Delachaume C, Fassy F, Schonbrunn E 2005. A novel inhibitor that suspends the induced fit mechanism of UDP-N-acetylglucosamine enolpyruvyl transferase (MurA). The Journal of biological chemistry 280(14):14070-14075.

200. Baum EZ, Montenegro DA, Licata L, Turchi I, Webb GC, Foleno BD, Bush K 2001. Identification and characterization of new inhibitors of the Escherichia coli MurA enzyme. Antimicrob Agents Chemother 45(11):3182-3188.

201. Andres CJ, Bronson JJ, D'Andrea SV, Deshpande MS, Falk PJ, Grant-Young KA, Harte WE, Ho HT, Misco PF, Robertson JG, Stock D, Sun Y, Walsh AW 2000. 4-Thiazolidinones: novel inhibitors of the bacterial enzyme MurB. Bioorg Med Chem Lett 10(8):715-717.

202. Emanuele JJ, Jr., Jin H, Jacobson BL, Chang CY, Einspahr HM, Villafranca JJ 1996. Kinetic and crystallographic studies of Escherichia coli UDP-N-acetylmuramate:L-alanine ligase. Protein Sci 5(12):2566-2574.

203. Liger D, Masson A, Blanot D, van Heijenoort J, Parquet C 1995. Over-production, purification and properties of the uridine-diphosphate-N-acetylmuramate:L-alanine ligase from Escherichia coli. European journal of biochemistry / FEBS 230(1):80-87.

204. Liger D, Blanot D, van Heijenoort J 1991. Effect of various alanine analogues on the L-alanine-adding enzyme from Escherichia coli. FEMS Microbiol Lett 64(1):111-115.

205. Gegnas LD, Waddell ST, Chabin RM, Reddy S, Wong KK 1998. Inhibitors of the bacterial cell wall biosynthesis enzyme MurD. Bioorg Med Chem Lett 8(13):1643-1648.

206. Tanner ME, Vaganay S, van Heijenoort J, Blanot D 1996. Phosphinate Inhibitors of the D-Glutamic Acid-Adding Enzyme of Peptidoglycan Biosynthesis. J Org Chem 61(5):1756-1760.

207. Zeng B, Wong, K.K., Pompliano, D.L., Reddy, S., and Tanner, M.E. 1998. A phosphinate inhibitor of the meso-diaminopimelic acid-adding enzyme (MurE) of peptidoglycan biosynthesis. J Org Chem 63:10081–10086.

208. Miller DJ, Hammond, S.M., Anderluzzi, D., and Bugg, T.D. 1998. Aminoalkylphosphinate inhibitors of D-Ala-D-Ala adding enzyme. J Chem Soc Perkin Trans 1:131-142.

209. Tomasic T, Zidar N, Sink R, Kovac A, Blanot D, Contreras-Martel C, Dessen A, Muller-Premru M, Zega A, Gobec S, Kikelj D, Masic LP 2011. Structure-based design of a new series of D-glutamic acid based inhibitors of bacterial UDP-N-acetylmuramoyl-L-alanine:D-glutamate ligase (MurD). J Med Chem 54(13):4600-4610.

210. Zidar N, Tomasic T, Sink R, Kovac A, Patin D, Blanot D, Contreras-Martel C, Dessen A, Premru MM, Zega A, Gobec S, Masic LP, Kikelj D 2011. New 5-benzylidenethiazolidin-4-one inhibitors of bacterial MurD ligase: design, synthesis, crystal structures, and biological evaluation. Eur J Med Chem 46(11):5512-5523.

211. Baum EZ, Crespo-Carbone SM, Foleno BD, Simon LD, Guillemont J, Macielag M, Bush K 2009. MurF inhibitors with antibacterial activity: effect on muropeptide levels. Antimicrob Agents Chemother 53(8):3240-3247.

212. Baum EZ, Crespo-Carbone SM, Klinger A, Foleno BD, Turchi I, Macielag M, Bush K 2007. A MurF inhibitor that disrupts cell wall biosynthesis in Escherichia coli. Antimicrob Agents Chemother 51(12):4420-4426.

213. Lara B, Mengin-Lecreulx D, Ayala JA, van Heijenoort J 2005. Peptidoglycan precursor pools associated with MraY and FtsW deficiencies or antibiotic treatments. FEMS Microbiol Lett 250(2):195-200.

214. Billot-Klein D, Shlaes D, Bryant D, Bell D, Legrand R, Gutmann L, van Heijenoort J 1997. Presence of UDP-N-acetylmuramyl-hexapeptides and -heptapeptides in enterococci

and staphylococci after treatment with ramoplanin, tunicamycin, or vancomycin. J Bacteriol 179(15):4684-4688.

215. Billot-Klein D, Gutmann L, Collatz E, van Heijenoort J 1992. Analysis of peptidoglycan precursors in vancomycin-resistant enterococci. Antimicrob Agents Chemother 36(7):1487-1490.

216. Kohlrausch U, Holtje JV 1991. Analysis of murein and murein precursors during antibiotic-induced lysis of Escherichia coli. J Bacteriol 173(11):3425-3431.

217. Michaud C, Mengin-Lecreulx D, van Heijenoort J, Blanot D 1990. Over-production, purification and properties of the uridine-diphosphate-N-acetylmuramoyl-L-alanyl-D-glutamate: meso-2,6-diaminopimelate ligase from Escherichia coli. European journal of biochemistry / FEBS 194(3):853-861.

218. Mengin-Lecreulx D, van Heijenoort J 1990. Correlation between the effects of fosfomycin and chloramphenicol on Escherichia coli. FEMS Microbiol Lett 54(1-3):129-133.

219. Mengin-Lecreulx D, Siegel E, van Heijenoort J 1989. Variations in UDP-N-acetylglucosamine and UDP-N-acetylmuramyl-pentapeptide pools in Escherichia coli after inhibition of protein synthesis. J Bacteriol 171(6):3282-3287.

220. Mengin-Lecreulx D, Flouret B, van Heijenoort J 1983. Pool levels of UDP N-acetylglucosamine and UDP N-acetylglucosamine-enolpyruvate in Escherichia coli and correlation with peptidoglycan synthesis. J Bacteriol 154(3):1284-1290.

221. Flouret B, Mengin-Lecreulx D, van Heijenoort J 1981. Reverse-phase high-pressure liquid chromatography of uridine diphosphate N-acetylmuramyl peptide precursors of bacterial cell wall peptidoglycan. Anal Biochem 114(1):59-63.

222. Lugtenberg EJ, v Schijndel-van Dam A, van Bellegem TH 1971. In vivo and in vitro action of new antibiotics interfering with the utilization of N-acetyl-glucosamine-N-acetyl-muramyl-pentapeptide. J Bacteriol 108(1):20-29.

223. Mengin-Lecreulx D, van Heijenoort J 1985. Effect of growth conditions on peptidoglycan content and cytoplasmic steps of its biosynthesis in Escherichia coli. J Bacteriol 163(1):208-212.

224. de Roubin MR, Mengin-Lecreulx D, van Heijenoort J 1992. Peptidoglycan biosynthesis in Escherichia coli: variations in the metabolism of alanine and D-alanyl-D-alanine. J Gen Microbiol 138 Pt 8:1751-1757.

225. Jamindar D, Gutheil WG 2010. A liquid chromatography-tandem mass spectrometry assay for Marfey's derivatives of L-Ala, D-Ala, and D-Ala-D-Ala: application to the in vivo confirmation of alanine racemase as the target of cycloserine in Escherichia coli. Anal Biochem 396(1):1-7.

226. Ishiguro EE, Ramey WD 1978. Involvement of the relA gene product and feedback inhibition in the regulation of DUP-N-acetylmuramyl-peptide synthesis in Escherichia coli. J Bacteriol 135(3):766-774.

227. Lowy FD 2003. Antimicrobial resistance: the example of Staphylococcus aureus. J Clin Invest 111(9):1265-1273.

228. Bobba S, Resch GE, Gutheil WG 2012. A liquid chromatography-tandem mass spectrometry assay for detection and quantitation of the dipeptide Gly-Gln in rat brain. Anal Biochem 425(2):145-150.

229. Smyth DG, Parish DC, Normanton JR, Wolstencroft JH 1983. The C-terminal dipeptide of beta-endorphin: a neuropeptide with inhibitory activity. Life Sci 33 Suppl 1:575-578.

230. Parish DC, Smyth DG, Normanton JR, Wolstencroft JH 1983. Glycyl glutamine, an inhibitory neuropeptide derived from beta-endorphin. Nature 306(5940):267-270.

231. Resch GE, Simpson CW 2008. Cyclo-glycyl-glutamine inhibits ethanol intake in P and Sprague-Dawley rats. Peptides 29(3):430-439.

232. Resch GE, Simpson CW 2008. Glycyl-glutamine reduces ethanol intake at three reward sites in P rats. Alcohol 42(2):99-106.

233. Resch GE, Shridharani S, Millington WR, Garris DR, Simpson CW 2005. Glycyl-glutamine in nucleus accumbens reduces ethanol intake in alcohol preferring (P) rats. Brain Res 1058(1-2):73-81.

234. Simpson CW, Resch GE, Millington WR, Myers RD 1998. Glycyl-L-glutamine injected centrally suppresses alcohol drinking in P rats. Alcohol 16(2):101-107.

235. Unal CB, Owen MD, Millington WR 1994. Beta-endorphin-induced cardiorespiratory depression is inhibited by glycyl-L-glutamine, a dipeptide derived from beta-endorphin processing. J Pharmacol Exp Ther 271(2):952-958.

236. Basaran NF, Buyukuysal RL, Millington WR, Cavun S 2010. Glycyl-glutamine (beta-endorphin(30-31)) inhibits morphine-induced dopamine efflux in the nucleus accumbens. Naunyn-Schmiedeberg's Arch Pharmacol 381(5):467-475.

237. Goktalay G, Cavun S, Levendusky MC, Hamilton JR, Millington WR 2006. Glycyl-glutamine inhibits nicotine conditioned place preference and withdrawal. Eur J Pharmacol 530(1-2):95-102.

238. Cavun S, Goktalay G, Millington WR 2005. Glycyl-glutamine, an endogenous beta-endorphin-derived peptide, inhibits morphine-induced conditioned place preference, tolerance, dependence, and withdrawal. J Pharmacol Exp Ther 315(2):949-958.

239. Kaspar H, Dettmer K, Gronwald W, Oefner PJ 2009. Advances in amino acid analysis. Anal Bioanal Chem 393(2):445-452.

240. Chan SW, Lin G, Yamamoto K, Yew DT, Rudd JA Simultaneous determination of amino acids in discrete brain areas in Suncus murinus by high performance liquid chromatography with electrochemical detection. J Pharm Biomed Anal 53(3):705-709.

241. Adamson JG, Hoang T, Crivici A, Lajoie GA 1992. Use of Marfey's reagent to quantitate racemization upon anchoring of amino acids to solid supports for peptide synthesis. Anal Biochem 202(1):210-214.

242. Bhushan R, Bruckner H 2004. Marfey's reagent for chiral amino acid analysis: a review. Amino Acids 27(3-4):231-247.

243. Marfey P 1984. Determination of D-amino acids: II. Use of a bifunctional reagent, 1,5-difluoro-2,4-dinitrobenzene. Calsberg Res Commun 49:591-596.

244. Paxinos G WC. 1998. The Rat Brain in Stereotaxic Coordinates. 4th ed., New York: Academic Press.

VITA

Sudheer Bobba was born on January 4, 1986, in the town of Gannavaram, Andhra Pradesh, India. He completed his education from Aditya High School, Gannavaram. He later obtained his Bachelor of Pharmacy degree from K.V.S.R. Siddhartha College of Pharmaceutical Sciences (SCOPS), Vijayawada, which is affiliated to Nagarjuna University, Guntur in April 2007.

Sudheer Bobba joined University of Missouri-Kansas City in Spring-2008 in pursuit of an interdisciplinary doctorate degree in Pharmaceutical Sciences and Chemistry.

He was awarded the prestigious preparing future faculty fellowship for the academic years 2011-2014. He completed his doctoral studies in May 2013 under the guidance of Dr. William Gutheil.

Mr. Bobba has done summer internships at Johnson and Johnson (J&J), Vertex Pharmaceuticals, and Stowers Institute for Medical Research. He has authored/co-authored several peer reviewed research articles in reputed international journals. He is also a member of American Association of Pharmaceutical Scientists (AAPS) and American Society for Mass Spectrometry (ASMS).